INTERACTIONS BETWEEN MACROBIOTA (WILD AND AQUACULTURED) AND THE PHYSICAL-PLANKTONIC ENVIRONMENT: INSIGHTS FROM A NEW 3-D END-TO-END MODELLING FRAMEWORK

by

Diego A. Ibarra

Submitted in partial fulfilment of the requirements
for the degree of Doctor of Philosophy

at

Dalhousie University
Halifax, Nova Scotia
December 2011

DALHOUSIE UNIVERSITY

DEPARTMENT OF OCEANOGRAPHY

The undersigned hereby certify that they have read and recommend to the Faculty of Graduate Studies for acceptance a thesis entitled "INTERACTIONS BETWEEN MACROBIOTA (WILD AND AQUACULTURED) AND THE PHYSICAL-PLANKTONIC ENVIRONMENT: INSIGHTS FROM A NEW 3-D END-TO-END MODELLING FRAMEWORK" by Diego A. Ibarra in partial fulfilment of the requirements for the degree of Doctor of Philosophy.

Dated: December 6, 2011

External Examiner: _____

Co-Supervisors: _____

_____

Examining Committee: _____

_____

Departmental Representative: _____

DALHOUSIE UNIVERSITY

DATE: December 6, 2011

AUTHOR: Diego A. Ibarra

TITLE: INTERACTIONS BETWEEN MACROBIOTA (WILD AND AQUACULTURED) AND THE PHYSICAL-PLANKTONIC ENVIRONMENT: INSIGHTS FROM A NEW 3-D END-TO-END MODELLING FRAMEWORK

DEPARTMENT OR SCHOOL: Department of Oceanography

DEGREE: PhD CONVOCATION: May YEAR: 2012

_____

Signature of Author

To Allison,

...for enduring this degree by my side.

Table of Contents

List of Tables

List of Figures

Abstract

Marine ecosystem-based management requires end-to-end models, which are models capable of representing the entire ecosystem including physical, chemical and biological processes, anthropogenic activities, and multiple species with different sizes, life histories and from different trophic levels. To adequately represent ecosystem dynamics in shallow coastal regions, end-to-end models may need to include macrobiota species (wild and aquacultured) and may have to allow feedbacks (i.e. two-way coupling) between macrobiota and planktonic ecosystem dynamics. This is because the biomass of macrobiota can locally exceed the biomass of plankton, thus influencing the distribution of planktonic ecosystem tracers and altering the overall food web structure. Here, I describe a hybrid (Eulerian/Individual-Based) ecosystem framework, implemented in the Regional Ocean Modeling System (ROMS), a state-of-the-art 3-D ocean circulation model. The framework was applied to a model of a synthetic embayment containing seagrass, rockweed and kelp beds, a wild oyster reef, a mussel ranch and a fish farm. I found that two-way coupling is essential to reproduce expected spatial patterns of all variables and to conserve mass in the system. I also developed a shellfish ecophysiology model (SHELL-E) and compared its results against water samples collected over 5 years in Ship Harbour, a fjord with mussel aquaculture in Nova Scotia, Eastern Canada. Also, from a high-resolution bio-optical survey of the fjord, I found that mussels decrease phytoplankton biomass inside the farm, but also cause a bloom of phytoplankton outside the farm. Using ROMS/SHELL-E, I determined that the increase of phytoplankton around the farm is caused by the waste products of the farmed bivalves, which have a fertilization effect, enhancing phytoplankton production outside the farm during nutrient-limited and light-replete conditions (i.e. late spring to late fall in Ship Harbour). The main conclusion of this thesis is that—in shallow coastal regions—ecosystem models must represent bilateral interactions between macrobiota and physical-planktonic dynamics, in a spatially-explicit setting, to adequately represent mass flows and ecosystem dynamics. The hybrid end-to-end modelling system provides a computationally efficient framework for describing these interactions and, through careful comparisons against observations, can be a powerful tool to test hypotheses and generate insights into coastal ecosystems.

List of Abbreviations and Symbols Used

Abbreviations used in this thesis.

Abbr.	Description
0-D	Zero-dimensional (i.e. model space is described by a single box)
1-D	One-dimensional
2-D	Two-dimensional
3-D	Three-dimensional
CPU	Central Processing Unit (i.e. a computer's processor)
CDOM	Coloured Dissolved Organic Matter
IBM	Individual-Based Model
GPS	Global Positioning System
NEMO	Nucleus for European Modelling of the Ocean
PSU	Practical Salinity Units (dimensionless)
ROMS	Regional Ocean Modeling System

Symbols used in this thesis.

Symbol	Units	Description
Chl	mg Chl m^{-3}	Local concentration of chlorophyll
LDet	mmol N m^{-3}	Local concentration of large detritus
NO3	mmol N m^{-3}	Local concentration of nitrate
NH4	mmol N m^{-3}	Local concentration of ammonium
Oxy	mmol O_2 m^{-3}	Local concentration of oxygen (SHELL-E model)
Phy	mmol N m^{-3}	Local concentration of phytoplankton
Sed	g m^{-3}	Local concentration of inorganic sediments
SDet	mmol N m^{-3}	Local concentration of small detritus
Zoo	mmol N m^{-3}	Local concentration of zooplankton
Salt	dimensionless (referred to as Practical Salinity Units, PSU)	Local salinity (SHELL-E model)
Temp	°C	Local temperature (SHELL-E model)
AE_D	dimensionless	Absorption efficiency on small detritus of an individual bivalve in Culture Unit *k* (SHELL-E model)
AE_P	dimensionless	Absorption efficiency on phytoplankton of an individ-

		ual bivalve in Culture Unit *k* (SHELL-E model)
AE_Z	dimensionless	Absorption efficiency on zooplankton of an individual bivalve in Culture Unit *k* (SHELL-E model)
$AE_F^{A,i}$	dimensionless	Absorption efficiency on artificial food of an individual aquacultured fish of species *i*
$AE_P^{F,i}$	dimensionless	Absorption efficiency on phytoplankton of an individual filter-feeder of species *i*
$AE_Z^{F,i}$	dimensionless	Absorption efficiency on zooplankton of an individual filter-feeder of species *i*
$AE_D^{F,i}$	dimensionless	Absorption efficiency on detritus of an individual filter-feeder of species *i*
Fae_k	mmol N ind^{-1} d^{-1}	Faeces production rate of an individual bivalve in Culture Unit *k* (SHELL-E model)
$Fae_k^{F,i}$	mmol N ind^{-1} d^{-1}	Faeces production rate of an individual filter-feeder of species *i*
$Fae_k^{A,i}$	mmol N ind^{-1} d^{-1}	Faeces production rate of an individual aquacultured fish of species *i*
$Food_k^{A,i}$	mmol N ind^{-1}	Amount of feed delivered to an individual aquacultured fish of species *i*
$Gonad_k$	mmol N ind^{-1}	Structural biomass of an individual bivalve in Culture Unit *k* (SHELL-E model)
$Harvest_k$	ind d^{-1}	Number of individual bivalves removed from Culture Unit *k* in a time step through harvesting (SHELL-E model)
$IE_F^{A,i}$	dimensionless	Absorption efficiency on artificial food of an individual aquacultured fish of species *i*
Oxy_L	mmol O_2 m^{-3}	Lower tolerance range for oxygen (SHELL-E model)
$PsFae_k$	mg m^{-3}	Pseudofaeces production rate of an individual bivalve in Culture Unit *k* (SHELL-E model)
$Salt_L$	PSU	Lower limit of tolerance range for salinity (SHELL-E model)
$Soma_k$	mmol N ind^{-1}	Reproductive biomass of an individual bivalve in Culture Unit *k* (SHELL-E model)
$Spawning_k$	mmol N ind^{-1} d^{-1}	Loss term representing the gamete biomass expelled during reproduction by an individual bivalve in Culture Unit *k* (SHELL-E model)
$Temp_H$	°C	Upper limit of tolerance range for temperature (SHELL-E model)
$Temp_L$	°C	Lower limit of tolerance range for temperature (SHELL-E model)
$upNO3_k^{M,i}$	mmol N ind^{-1} d^{-1}	Uptake rate of nitrate of an individual macroalga of species *i*
$upNO3_k^{S,i}$	mmol N ind^{-1} d^{-1}	Uptake rate of nitrate of an individual seagrass shoot of species *i*
$upNH4_k^{M,i}$	mmol N ind^{-1} d^{-1}	Uptake rate of ammonium of an individual macroalga of species *i*

$upNH4_k^{S,i}$	mmol N ind^{-1} d^{-1}	Uptake rate of ammonium of an individual seagrass shoot of species *s*
A_k	mmol N ind^{-1} d^{-1}	Assimilation rate of an individual bivalve in Culture Unit *k* (SHELL-E model)
$A_k^{F,i}$	mmol N ind^{-1} d^{-1}	Assimilation rate of an individual in super-individual *k* from species *i* and the filter-feeder functional group
$A_k^{A,i}$	mmol N ind^{-1} d^{-1}	Assimilation rate of an individual in super-individual *k* from species *i* and the aquacultured fish functional group
B_k	mmol N ind^{-1}	Biomass of an individual bivalve in Culture Unit *k* (SHELL-E model)
B_{Pub}	mmol N ind^{-1}	Biomass of bivalve at puberty (SHELL-E model)
B_{ref}	mmol N ind^{-1}	Biomass of reference bivalve (SHELL-E model)
C_{Eul}^j	mmol N m^{-3} s^{-1}	Eulerian source/sink terms for tracer *j*
C_{IBM}^j	mmol N m^{-3} s^{-1}	Individual-based source/sink terms for tracer *j*
D_Ψ	mmol N m^{-3} s^{-1}	Horizontal diffusive terms
F_k	m^3 ind^{-1} d^{-1}	Filtration rate of an individual bivalve in Culture Unit *k* (SHELL-E model)
$F_k^{\max}$	m^3 ind^{-1} d^{-1}	Maximum filtration rate achievable by an individual bivalve in Culture Unit *k* (SHELL-E model)
$F_{ref}^{\max}$	m^3 ind^{-1} d^{-1}	Filtration rate exhibited by a reference bivalve when evaluated in ideal conditions (SHELL-E model)
$F^{F,i}$	m^3 ind^{-1} d^{-1}	Filtration rate of an individual filter-feeder of species *i*
G	-	A set of all super-individuals of species *i* and functional group φ that occur within the target grid cell
H	m	Total water depth
H_z	m	Thickness of the grid cell
I	W m^{-2}	Photosynthetically available radiation
K_Ψ	m^2 s^{-1}	Vertical eddy diffusivity coefficient
$K_{NO3}^{M,i}$	mmol N m^{-3}	Half-saturation constants for the uptake of *NO3*
$K_{NO3}^{M,i}$	mmol N m^{-3}	Half-saturation constants for the uptake of *NH4*
K_P	(mmol N m^{-3}) ^{2}	Half-saturation concentration of phytoplankton ingestion by zooplankton
K_{Temp}^H	(°C) $^{-1}$	Decreasing coefficient for limitation due to temperature at upper boundary (SHELL-E model)
K_{Temp}^L	(°C) $^{-1}$	Decreasing coefficient for limitation due to temperature at lower boundary (SHELL-E model)
K_{Salt}^L	(PSU) $^{-1}$	Decreasing coefficient for limitation due to salinity at lower boundary (SHELL-E model)
K_{Oxy}^L	(mmol O_2 m^{-3}) $^{-1}$	Decreasing coefficient for limitation due to oxygen at lower boundary (SHELL-E model)
K_{Food}	mmol N m^{-3}	Half-saturation food concentration for bivalve filtration

		(SHELL-E model)
K_{RE}	mmol N ind^{-1}	Half-saturation constant for *RE* (SHELL-E model)
$M^{F,i}$	mmol N ind^{-1} d^{-1}	Weight-specific maintenance respiration rate of an individual from species *i* and the filter-feeder functional group
$M^{A,i}$	mmol N ind^{-1} d^{-1}	Weight-specific maintenance respiration rate of an individual from species *i* and the aquacultured fish functional group
NOQ	mol N (mol O_2) $^{-1}$	Nitrogen:oxygen quotient for bivalve respiration (SHELL-E model)
$P_{\max}^{M,i}$	units can vary, but common units are µmol O_2 (g Fresh Weight)$^{-1}$ h^{-1}	Maximum photosynthesis rate of an individual macroalga of species *i*
$P_{\max}^{S,i}$	units can vary, but common units are µmol O_2 (g Fresh Weight)$^{-1}$ h^{-1}	Maximum photosynthesis rate of an individual seagrass shoot of species *i*
R_k	mmol N ind^{-1} d^{-1}	Respiration rate of an individual bivalve in Culture Unit *k* (SHELL-E model)
$R_k^{F,i}$	mmol N ind^{-1} d^{-1}	Respiration rate of an individual in super-individual *k* from species *i* and the filter-feeder functional group
R_m^{Ai}	d^{-1}	Weight-specific maintenance respiration rate of an individual aquacultured fish of species *i*
RE_k	dimensionless	Reproductive effort (i.e. fraction of production allocated to reproduction) of an individual bivalve in Culture Unit *k* (SHELL-E model)
T	dimensionless	Threshold fraction (i.e. $Gonad_k/B_k$) triggering spawning (SHELL-E model)
V	m^3	Volume of grid cell
g	-	Column index representing properties in the individual-based matrix
h	m	Mean water depth
i	-	Index representing individual-based species of the φ functional group
j	-	Index representing Eulerian tracer variables
k	-	Row index representing super-individuals (or Culture Units in SHELL-E) in the individual-based matrix
$m_k^{A,i}$	mmol N ind^{-1}	Biomass of an individual in super-individual *k* from species *i* and the aquacultured fish functional group
$m_k^{F,i}$	mmol N ind^{-1}	Biomass of an individual in super-individual *k* from species *i* and the filter-feeder functional group
$m_k^{M,i}$	mmol N ind^{-1}	Biomass of an individual in super-individual *k* from species *i* and the macroalgae functional group
$m_k^{S,i}$	mmol N ind^{-1}	Biomass of an individual in super-individual *k* from species *i* and the seagrass functional group
$m_k^{\varphi,i}$	mmol N ind^{-1}	Biomass of an individual in super-individual *k* from species *i* and the φ functional group
n_k	ind	Number of identical individuals forming the Culture Unit *k* (SHELL-E)

$n_k^{A,i}$	ind	Number of identical individuals forming super-individual k from species i and the aquacultured fish functional group
$n_k^{F,i}$	ind	Number of identical individuals forming super-individual k from species i and the filter-feeder functional group
$n_k^{M,i}$	ind	Number of identical individuals forming super-individual k from species i and the macroalgae functional group
$n_k^{S,i}$	ind	Number of identical individuals forming super-individual k from species i and the seagrass functional group
$n_k^{\varphi,i}$	ind	Number of identical individuals forming super-individual k from species i and the φ functional group
p	-	Number of super-individuals (i.e. rows) in the individual-based matrix for species i and functional group φ
q	-	Number of properties (i.e. columns) in the individual-based matrix for species i and functional group φ
r	-	Number of Eulerian tracers forming the state Ψ
s	-	Number of individual-based species of the φ functional group
t	d	Time
u	m s^{-1}	Mean component of the velocity in the horizontal (x) direction
v	m s^{-1}	Mean component of the velocity in the horizontal (y) direction
x	m	Horizontal coordinate in the North-South direction
y	m	Horizontal coordinate in the East-West direction
z	m	Vertical coordinate
$x_k^{\varphi,i}$	m	x location of super-individual k of species i and functional group φ
$y_k^{\varphi,i}$	m	y location of super-individual k of species i and functional group φ
$z_k^{\varphi,i}$	m	Depth of super-individual k of species i and functional group φ
Θ	s^{-1}	Mean component of the velocity in the vertical (σ) direction
Ψ^j	Vary according to tracer	State representing the concentration of the j^{th} Eulerian tracer in the gridded field
$\Omega^{\varphi,i}$	Vary according to property	State of species i and functional group φ in the individual-based framework
$\Phi^{M,i}$	d^{-1}	Specific erosion rate of an individual macroalga of species i
$\Phi^{S,i}$	d^{-1}	Specific erosion rate of an individual seagrass shoot of species i

$X^{\varphi,i}$	unit · m^{-3}	Grid-based equivalent of $\chi_k^{\varphi,i}$ representing the concentration variable for all super-individuals of species *i* and functional group φ in the grid cell
$\alpha^{M,i}$	units of P_{max} divided by W m^{-2}	Initial slope of photosynthesis *vs.* irradiance curve of an individual macroalga of species *i*
$\alpha^{S,i}$	units of P_{max} divided by W m^{-2}	Initial slope of photosynthesis *vs.* irradiance curve of an individual seagrass shoot of species *i*
β	dimensionless	Cost of growth coefficient of an individual bivalve (SHELL-E model)
$\beta^{F,i}$	dimensionless	Cost of growth coefficient of an individual filter-feeder of species *i*
$\beta^{A,i}$	dimensionless	Cost of growth coefficient of an individual aquacultured fish of species *i*
φ	-	Index representing functional groups
ε_D	dimensionless	Feeding efficiency on small detritus of an individual bivalve in Culture Unit *i* (SHELL-E model)
ε_P	dimensionless	Feeding efficiency on phytoplankton of an individual bivalve in Culture Unit *i* (SHELL-E model)
ε_Z	dimensionless	Feeding efficiency on zooplankton of an individual bivalve in Culture Unit *i* (SHELL-E model)
$\varepsilon_F^{A,i}$	dimensionless	Feeding efficiency on artificial food of an individual aquacultured fish of species *i*
$\varepsilon_D^{F,i}$	dimensionless	Feeding efficiency on detritus of an individual filter-feeder of species *i*
$\varepsilon_P^{F,i}$	dimensionless	Feeding efficiency on phytoplankton of an individual filter-feeder of species *i*
$\varepsilon_Z^{F,i}$	dimensionless	Feeding efficiency on zooplankton of an individual filter-feeder of species *i*
η	m	Wave-averaged free surface elevation
κ_{CDOM}	m^{-1}	Diffuse attenuation coefficient of PAR downwelling irradiance due to CDOM
κ_{TOTAL}	m^{-1}	Diffuse attenuation coefficient of PAR downwelling irradiance due to water plus chlorophyll plus CDOM
λ^{Nat}	d^{-1}	Natural mortality rate of bivalves in Culture Unit *k* (SHELL-E model)
λ^{Harv}	d^{-1}	Harvesting rate (SHELL-E model)
$\lambda^{M,i}$	d^{-1}	Constant mortality rate of an individual macroalga of species *i*
$\lambda^{S,i}$	d^{-1}	Constant mortality rate of an individual seagrass shoot of species *i*
$\lambda^{F,i}$	d^{-1}	Constant mortality rate of an individual filter-feeder of species *i*
$\lambda^{A,i}$	d^{-1}	Constant mortality rate of an individual aquacultured fish of species *i*
$\mu_k^{M,i}$	d^{-1}	Specific rate of increase in biomass (after accounting for respiration) of an individual macroalga of species *i*

$\mu_k^{S,i}$	d^{-1}	Specific rate of increase in biomass (after accounting for respiration) of an individual seagrass shoot of species *i*
$\mu_{\max}^{M,i}$	d^{-1}	Maximum growth rate of an individual macroalga of species *i*
$\mu_{\max}^{S,i}$	d^{-1}	Maximum growth rate of an individual seagrass shoot of species *i*
ν_θ	$m^2\ s^{-1}$	Tracer kinematic diffusivity
σ	dimensionless	Vertical sigma coordinate
τ	-	Number of functional groups forming the state Ω
$\chi_k^{\varphi i}$	unit · ind^{-1}	Any variable of an individual in super-individual *k* of functional group φ and of species *i*
$\zeta^{A,i}$	d^{-1}	Artificial food delivery rate (feeding) of an individual aquacultured fish of species *i*
ω	Vary according to property	Element of matrix $\Omega^{\varphi,i}$

Acknowledgements

If I have seen further, it is because giants grilled me with math, stats, parameter validation, skill assessment and scientific skepticism... before lifting me onto their shoulders. And for that, I am very thankful.

First and foremost, I would like to thank my supervisors John Cullen and Katja Fennel for their guidance and support throughout this PhD. It was a pleasure to be directed by them. I also want to thank the other members of my committee, Marlon Lewis and Mike Dowd, for their insightful comments and their constructive criticism. Over the last decade all of them have become not only mentors, but also friends. I would also like to thank my external examiner, Cédric Bacher, for taking the time to read my thesis, for crossing the Atlantic Ocean to be in my thesis defence, and for his insightful comments.

Besides my committee, many others had an influence in my thesis. Thus, for provoking innovative ideas through insightful conversations, I am very grateful to Arnaud Laurent, Daisuke Hasegawa, Chris Jones, Adam Comeau, Stéphane Kirchhoff, and to all previous and present members of the Phytoplankton Lab (www.ceotr.ca) and the Marine Environmental Modelling Group (memg.ocean.dal.ca), and also to Keith Thompson, Bob Fournier, Bruce Johnson, Jinyu Sheng, Dan Kelly, Alex Hay, Ransom (RAM) Myers, Bob Scheibling, Heike Lotze, Boris Worm, Marta Coll, Colin Minto and Allison Schmidt. This thesis, in one way or another, reflects conversation that we once had.

I want to give special thanks to the wonderful crew of AquaPrime Mussel Ranch Ltd., particularly John Stairs, Darlene, Kiaja and Steve, for all the support during the field campaign. Also for their invaluable help during field work and sample processing, I would like to thank Stéphane Kirchhoff, Allison Schmidt, Adam Comeau, Dave Bowen, Arnaud Laurent, Daisuke Hasegawa, Anadiuska Rondon, Cathy Ryan, Claire Normandeau, Richard Davis, and also Lyndsey, Cait and Maud.

I particularly want to thank Katja Fennel for adopting me and my project, for providing the cluster computer to run my models, for teaching me ROMS, and for the weekly meetings that kept me on track. All were instrumental contributions to the successful accomplishment of my thesis.

Although not all the research I did made its way into this thesis, the learned experiences are invaluable. I would like to thank Allan Cembella (AWI, Germany), Jorge Diogene and Margarita Fernandez (IRTA, Spain), Penny Barnes (Centre for Shellfish Research, Nanaimo, BC), Toby Balch (Nova Scotia Dept. of Agriculture and Fisheries) and Marlon Lewis and Sean Nutter (Satlantic Inc.). It was a pleasure to work with you.

Many others helped me through this degree, and for that I am very grateful. I would like to give thanks to Chris Jones (Stats Wizard), Jon Pye, Sean Hartwell, Daniel Morrison and Balagopal Pillai (Computer Jedi Knights), Bruce Johnson (Instrument Oracle), Mark Merrimen and Walter Judge (Workshop Superheroes), Wes Paul (Electronic Guru), Moritz Lehmann, Paul Mattern, Jinyu Sheng, Laura Bianucci, Daisuke, Arnaud and Katja (Modelling Virtuosos), Adam Comeau (Bio-optics Maverick), Susanne Craig (Bio-optics Muse), Richard Davis (MATLAB Extraordinaire), Dave Ciochetto (Encouragement Tzar), Audrey Barnett, Cathy Ryan and Flavienne Bruyant (Phytoplankton Goddesses), Hugh MacIntyre (Phytoplankton Maestro), John Cullen (Good-science Sensei and Phytoplankton Illuminato), Cheryl Rafuse, Joe Cullen and Matt Beck (Bio-fuel Black-belts), Gerry Hammer, Pamela Larivee, Tamara Cantrill, Dianne Crouse and Sharon Earl (Administration Divas) and Fabian (The Building's Almighty Wizard).

Finally, I would like to thank my parents and my family for their continuous support, my friends for all the good moments, and Allison for her love, her unconditional support and her infinite patience.

Funding was provided by AquaNet - Canada's Network of Centres of Excellence in Aquaculture, Office of Naval Research, NSERC Discovery, NSERC Research Partnerships, CFCAS and Dalhousie University.

CHAPTER 1

Introduction

Coastal ecosystems are among the most dynamic ecosystems on earth (Haslett, 2008; Leon et al., 2011). In these fast-changing environments, trying to answer the seemingly simplest ecological question challenges the ingenuity of coastal ecologists, who are continuously developing new techniques to be able to discern patterns in the apparent turmoil. The interdisciplinary nature of coastal systems has pushed modern coastal ecologists to explore tools from disciplines like physical oceanography, sediment dynamics, ocean optics, etc. While these tools are powerful, their "instruction manuals" are often written in a language foreign to ecologists. Therefore, the role of ecologists is increasingly not only to answer ecological questions, but also to bridge the gap between ecology and these other disciplines. This thesis attempts to narrows the gap between macrobiota and planktonic ecology, aquaculture and hydrodynamic modelling, through the development of new tools, but also through the thorough description of their application, so they can be used more broadly in future ecological research.

This thesis is about assessing interactions between macrobiota and the hydrodynamic and planktonic environment. To this end, I need a modelling framework that allows the simultaneous representation of both, macrobiota (e.g. fish, shellfish and macroalgae) and planktonic ecosystem variables (i.e. plankton, detritus and nutrients), in a 3-D hydrodynamic environment. However, modelling a large number of state variables in a three-dimensional space is computationally intensive and, in shallow coastal applications—where hydrodynamic constrains demand small grid cells (~100 × 100 m) and a fast time-step (approx. a few seconds)—modelling a large number of state variables truly exceeds the limits of even today's high-performance computer clusters. Therefore, in this thesis, the first step is to develop a modelling framework capable of overcoming this computer limitation; that is, a hybrid (Eulerian/Individual-based) framework optimized for repre-

senting two-way feedbacks among a large number of variables in a three-dimensional space. Below I describe some key concepts and pertinent history, before I further introduce the chapters of this thesis.

1.1. Eulerian vs. Lagrangian Frameworks

The terms Eulerian and Lagrangian are used in fluid dynamics to distinguish between the two alternative kinds of specification of the flow field (Batchelor, 2000). In the Eulerian specification, flow quantities are defined as functions of position in space, thus flow quantities can be thought of as records of a current meter that is moored at a fixed location. In the Lagrangian specification, flow quantities are defined as functions of a particle within the fluid. This can be thought as records of position from a GPS onboard a drifting buoy, from which flow quantities can be calculated.

The vast majority of ocean circulation models describe flow using an Eulerian framework (e.g. ROMS, Haidvogel et al., 2008; NEMO, Madec, 2008). That is, the model domain is divided into a gridded field, and the model tracks the flow characteristics inside every single grid cell. However, some models describe flow using a Lagrangian framework, where many particles are released within the model domain and then the model tracks the trajectory of each of the particles (e.g. Thompson et al., 1998). There are advantages and disadvantages to both frameworks, and therefore, most modern Eulerian circulation models also include a Lagrangian or particle-tracking sub-model (e.g. ROMS, Haidvogel et al., 2008) to exploit the advantages of both modelling frameworks. These Eulerian/Lagrangian models simultaneously (1) estimate flow characteristics in every grid cell, and (2) use the predicted Eulerian flow to transport particles, whose locations are tracked.

Strictly speaking, the terms Eulerian and Lagrangian frameworks are only applicable to physical models describing flow fields. However, the concept of tracking properties associated with grid cells or with particles is also widely applied in biology, biogeochemistry,

population dynamics, etc. (see examples in Table 1-1), and therefore, the terms Eulerian and Lagrangian are also used sometimes to describe the frameworks use by these models. However, in this study I will use the terms grid-based framework (for Eulerian) and particle-based or individual-based framework. I will not use the term Lagrangian because it applies exclusively to particles passively drifting with the flow, and thus should not be used to describe particles displaying any kind of swimming or sinking behaviour or particles that are not transported by the flow. See Table 1-1 for a detailed comparison of these modelling frameworks, Figure 1-1 for a graphical representation, and Chapter 2 for the equations describing these modelling systems.

1.2. History of Marine Ecosystem Modelling

Today's ecosystem models utilize a very diverse range of approaches and techniques, and therefore it is not easy to draw a generalized description of their evolution. However, the following trends can be loosely sketched: (1) ecosystem models often adopt techniques earlier developed for physical oceanography, (2) the spatial resolution of models increases over time, and (3) simpler models get coupled into increasingly more complex models. Below I give a brief history of the evolution of models using different frameworks, which I also show in a graphical representation in Figure 1-2.

1.2.1. Grid-based (Eulerian) Models

Eulerian or grid-based models were first used in physical oceanography to study exchanges of temperature and salinity between a few box compartments to understand basic ocean circulation (e.g. Seiwell, 1938). About a decade later, the same principles were applied to nutrient, phytoplankton and zooplankton to understand the dynamics of planktonic ecosystems (Riley, 1946). Faster computers permitted tracking of tracers like temperature and salinity in dense 3-dimensional grids for detailed studies of ocean currents and circulation (e.g. Bryan, 1969; Hess, 1976). Some time later, the same principles were used to track not only temperature and salinity, but also nutrients and plankton. That is,

Table 1-1. Comparison between modelling frameworks in ecosystem models.

Grid-based (Eulerian) models	Particle-based or individual-based models	Hybrid models
Model domain is divided into grid cells (i.e. gridded field). Within each cell, the model tracks the concentration of a many tracers.	Model domain is not divided (i.e. continuous field). The model tracks many properties (e.g. location, mass, etc.) for many individuals.	Model tracks tracers in a gridded field AND particles in a continuous field. At every time step, individuals are projected onto the Eulerian grid for coupling with tracers.
Outputs one time-series for every tracer and grid cell. Each series represent the system from the point of view of the observer (e.g. from a moored instrument).	Outputs one time-series for every property and individual. Each series representing the system from the point of view of an individual.	Outputs one time-series for every tracer and grid cell, AND one time-series for every property and individual.
Tracer concentrations act as bulk property variables. That is, a mean value describes ecophysiological traits of all individuals in a cell. Information on individuals is not retained.	Variability among individuals is allowed and recorded. Average values are computed *a posteriori* using recorded fields.	Grid-based species are described with a single (bulk property) variable. Individual-based species allow individual variability and average values to be computed from recorded fields.
Difficult to represent processes requiring a history of the conditions experienced by an individual.	Natural way to represent processes requiring a history of the conditions experienced by an individual.	Individual-based variables have access to a history of conditions experienced by each individual. grid-based variables do not.
Abundant and ubiquitous species (i.e. found in all cells at all times) are represented efficiently. Details from many organisms within one cell are condensed into one bulk calculation.	Abundant and ubiquitous species are represented inefficiently, because the number of required individuals is many times larger than the number of grid cells in a grid-based model.	Abundant and ubiquitous species are efficiently represented as tracers, while rare species are efficiently represented as individuals.
Rare species (i.e. found in only a few cells), are represented inefficiently, because the model has to calculate the species concentration in all grid cells, even if the species is absent in most of those cells.	Rare species are handled very efficiently. Especially in cases where number of individuals of a species is a lot smaller than the number of grid cells in a grid-based model.	
Other names: Eulerian models, field models (Woods and Onken, 1982), bulk property models (Lande and Lewis, 1989) and community- or population-based models (Neuheimer et al., 2010), biogeochemically-based approach (Fulton, 2010).	Other names: Agent-based models, multi-agent models, Lagrangian models. However, the term Lagrangian is not accurate if individuals display any movement (or lack of movement) that deviates from passive advection by currents.	Other names: Two-way coupled biological-physical individual-based model
Examples—Lower-trophic models: Fasham et al, (1990), Franks and Chen (2001), Fennel et al. (2006). Aquaculture models: Grant et al. (2008), Guyondet et al. (2010). End-to-end models: NEMURO (Kishi et al. 2007), Ecospace (spatial version of Ecopath, Christensen and Walters, 2004), ATLANTIS (Fulton et al. 2005), SEAPODYM (Lehodey et al. 2008), APECOSM (Maury, 2010), ERSEM (Baretta-Bekker et al., 1997)	Examples—Saunders et al. (2010), Neuheimer et al. (2010). IBMs forced with output from an Eulerian model: LTRANS (North et al., 2008), models in review by Miller (2007). Aquaculture models: Nunes et al. (2003), Nobre et al. (2010), Brigolin et al. (2009) End-to-end models where IBM is forced with output from an Eulerian model: OSMOSE (Shin and Cury, 2004), North et al. (2010).	Examples— Woods and Onken (1982), only for nutrients and plankton. Aquaculture models: SHELL-E (Chapter 3) End-to-end models: Chapter 2

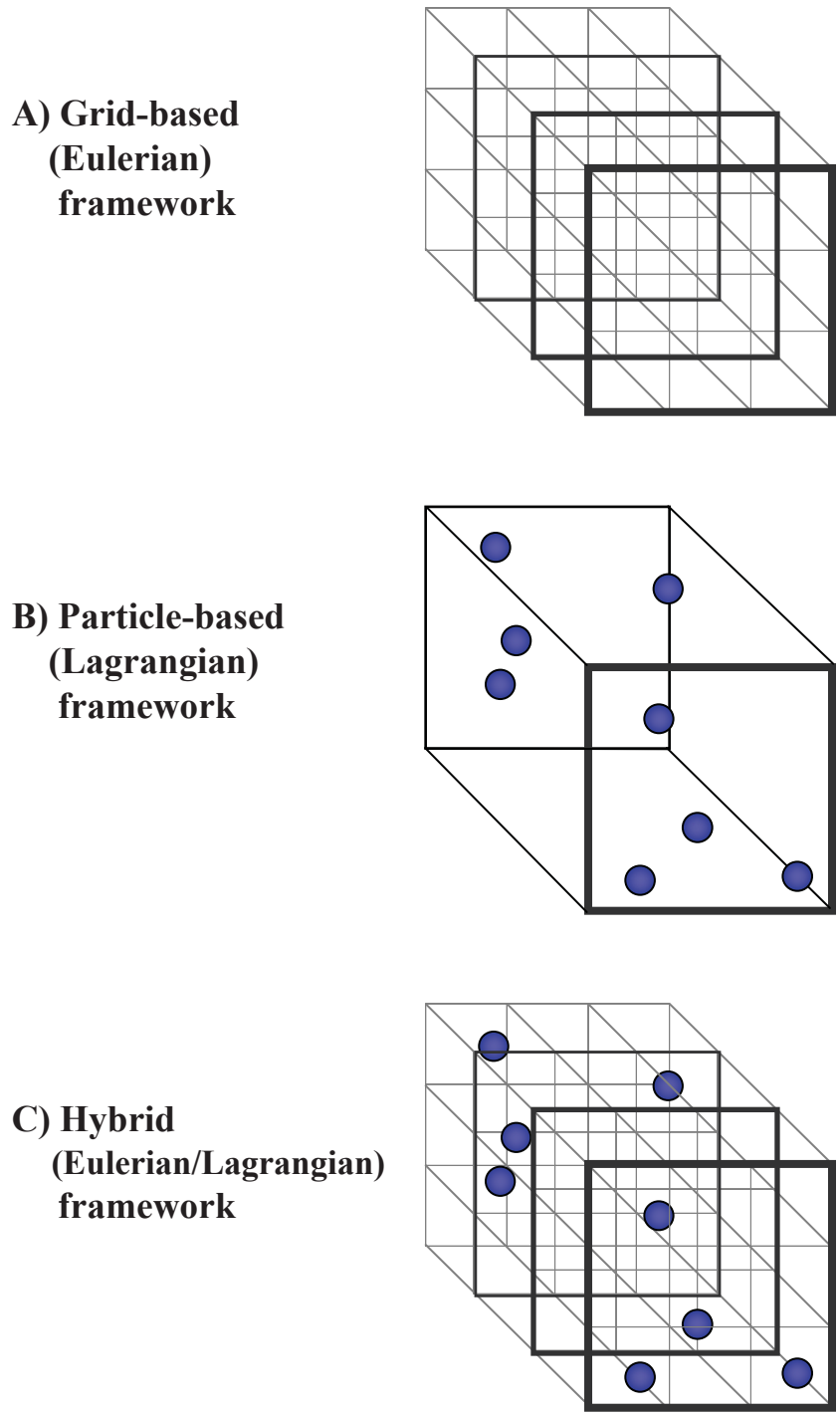

Figure 1-1. Conceptual diagram showing the three kinds of modelling frameworks. (A) In the grid-based or Eulerian framework, the model domain is divided into a gridded field and the model tracks state variables in every grid cell. (B) In the particle-based framework, the model (defined in continuous space) tracks the location and other properties of every particles. (C) In the hybrid framework, two models (i.e. one grid-based and one particle-based) work simultaneously; some state variables are tracked in every grid cell and some by every particle.

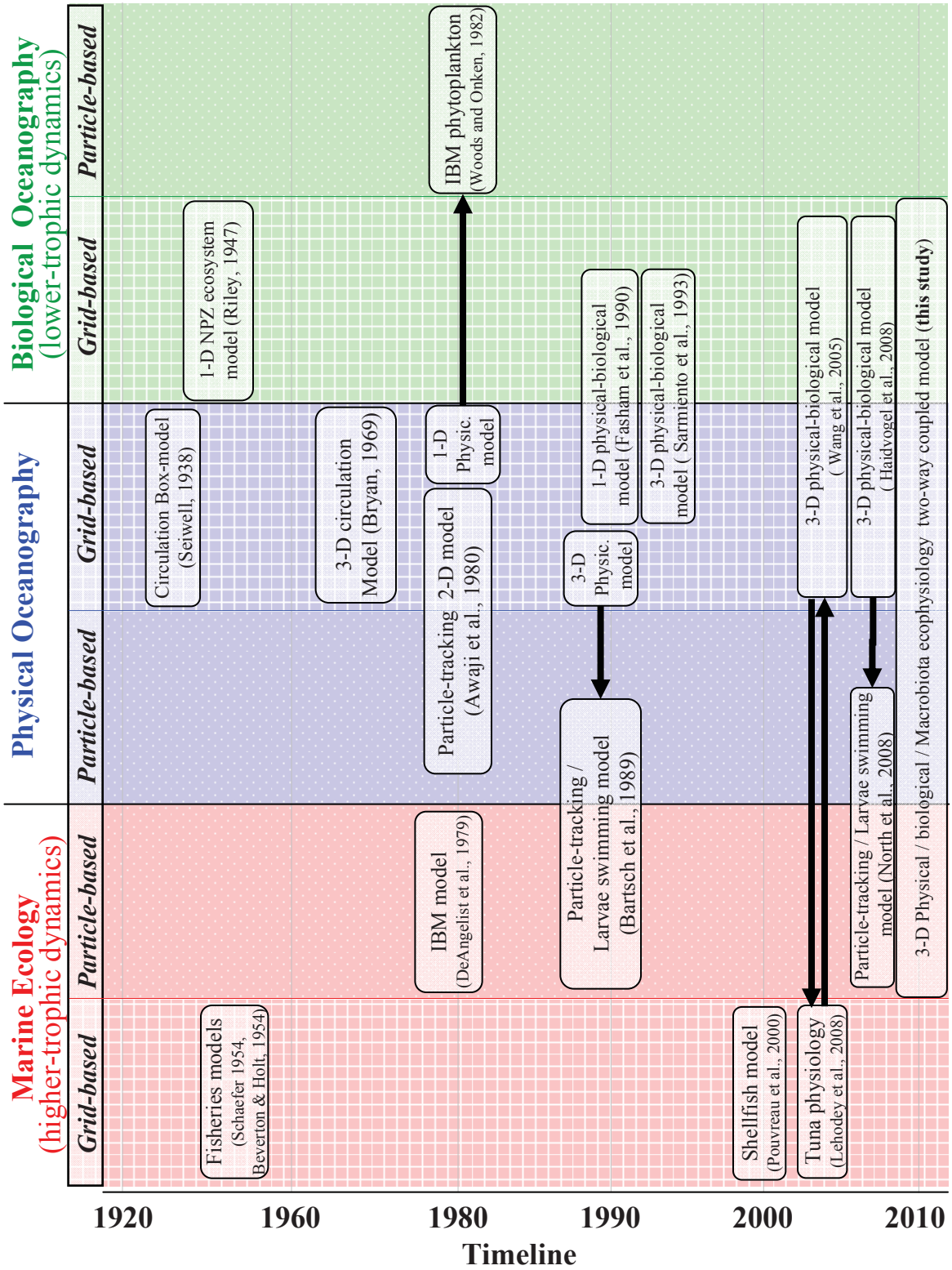

Figure 1-2. History and evolution of marine ecosystem models. Background colour represents main discipline and background texture represents modelling framework. One-way coupling between models is shown with single arrow, while two-way coupling is shown with two arrows or simply by extending the model box over two or more disciplines or frameworks. At the farthest right, we show the model developed in this study (Chapters 2 and 3). Note: timeline is not linear.

biological oceanographers piggybacked on the infrastructure of circulation models by adding new tracers capable of representing biological dynamics. These models are often called physical-biological coupled models (e.g. Fasham et al., 1990; Sarmiento et al., 1993; Baretta-Bekker et al., 1997; Fennel et al., 2006) or, when applied to the study of global ocean cycles, they are sometimes referred to as biogeochemical ocean general circulation models (Friedrichs et al., 2009). These models are currently the standard for planktonic ecosystem modelling.

The modelling of higher-trophic levels, such as tuna and other carnivorous fish, diverged early on from the modelling of lower-trophic levels (i.e. plankton). Kremer and Nixon (1978) suggested that—in the absence of computers—ecosystem modellers from the late 40's and early 50's had to choose between two paths: (1) if one wanted to assess the dynamics of populations over time, then it was necessary to use simple equations with very general coefficients that one could solve by hand; or (2) if one wanted to use more complex equations and parameters with significant biological meaning, then one was limited to solve the equations only for steady-state conditions and under various limiting assumptions. The former path was followed by fisheries scientists and population ecologists studying higher-trophic level species (e.g. Beverton and Holt, 1957), while the later path was followed by scientists studying lower-trophic levels like plankton dynamics (Kremer and Nixon, 1978). These two branches of marine ecology have been separated for the last 50 years, partially because they have their own separate funding bodies, scientific journals and scientific meetings, and partially because they focus of different scientific questions (Moloney et al., 2011). However, it has been recently recognized that the higher- and lower-trophic levels should not be studied in isolation from each other, thus a large initiative has begun to bring these two disciplines together (DeYoung et al., 2004; Travers et al., 2009; Moloney et al., 2011).

1.2.2. Particle-based or Individual-based Models

Although Eulerian models are certainly favoured in physical oceanography, particle-tracking models have been implemented to aid in the study of circulation in complex sys-

tems, like tidal exchange through a narrow strait (Awaji et al., 1980; Thompson et al., 1998). As mentioned above, most modern Eulerian circulation models have particle-based sub-models that allow users to insert and track particles through the model domain (e.g. Sheng et al., 2009). As particle-tracking models become more popular, biologists have started to figure out ways to piggyback in the infrastructure of these physical particle-based models, just as they did with the physical Eulerian models. The aim of biologists is to add enough biological dynamics to convert those initially "inert" particles into virtual biological entities, like larvae, fish, etc., for example by allowing them to sink or swim as influenced by various environmental factors. So far, most biological particle-based models are one-way coupled to an Eulerian physical-biological model. That is, the output from a physical-biological model simulation is used to force the particle-based model (see reviews by Werner et al., 2001; Miller, 2007). Therefore, the grid-based biological variables can modify the behaviour and the physiology of the biological particles; however the reverse is not possible. Part of the mass of the system is tracked as grid-based tracers, and the other part is tracked as biological particles; however because particles and tracers are not dynamically linked, mass is not conserved in the system. For example, particle-based fish larvae may grow faster in grid cells with high concentration of phytoplankton, but in one-way coupled models, phytoplankton will not be reduced by the corresponding amount taken by the larvae, thus mass is not conserved. In this thesis, I developed a three-dimensional Eulerian/particle-based two-way coupled model, which, as I describe in detail later, is of key importance for coastal applications.

The use of particle-based models in not restricted to the research of ocean circulation. Therefore, the so called individual-based models (IBMs) evolved from another kind of particle-based models. The history of individual-based models is somewhat difficult to piece together since there is a wide range of applications: Early individual-based models were used to model plasma properties from individual electrons (Buneman et al., 1980), flock properties from individual birds (e.g. Thompson et al., 1974), phytoplankton dynamics (Woods and Onken, 1982), etc. In recent years, most individual-based models applied to marine ecology are used to study the dynamics of fish larvae (see reviews by Werner et al., 2001; Miller, 2007), where an Eulerian circulation model is used to predict

currents which are used (online or offline) to transport particles that simulate larvae. However, the particles can be used to represent just about anything; for example, Kohlmeier and Ebenhöh (2007) also used output from an Eulerian circulation model to transport particles, but in this case the particles represented parcels of water, each simulating a pelagic mesocosm (with nutrients, plankton, detritus, etc.). Other individual-based model have been applied to study zooplankton (Neuheimer et al., 2010), impacts of climate change on lobsters (Chang et al., 2010), elk population management (Kindall et al., 2011), transmission of human diseases (Guzzetta et al., 2011), etc.

In physics, the relationship of flow quantities between the grid-based and particle-based frameworks has been known since the early 1930's (i.e. Fokker-Planck equation; Kadanoff, 2000). However, in ecology, it has been difficult for IBM modellers to define the differences between their individual-based models and the more traditional models (i.e. Eulerian models), which they have referred to as state-variable models (Huston et al., 1988; Grimm, 1999) or equation-based models (Nguyen et al., 2008), thus implying that IBM models do not have state variables or equations. In practice, individual-based models are described using a set of rules or a brief description of what the model code does (e.g. Grimm and Railsback, 2005). However, I argue that this is not because individual-based models cannot be described by state variables and equations, but rather because it is very hard to extend the notation used in a grid-based framework to describe a problem in a particle-based framework. In Chapter 2, I tackled the task of developing a set of equations, and a notation based on state variables, to describe individual-based systems. The new notation shows the relationships between the two modelling frameworks explicitly and should be useful for future IBM modelling work.

Individual-based models have been defined as models where the properties of an entire ecosystem "emerge" from the properties of the individuals constituting it (Grimm and Railsback, 2005). Woods and Onken (1982) suggested that tracking individual phytoplankters yields more accurate results that computing the dynamics of a bulk property representing the average state inside a grid cell. However, Lande and Lewis (1989) compared the two approaches and found negligible differences on the predicted results for

phytoplankton. However, DeYoung et al. (2004) emphasised that modelling individual variability and life-history details (rather than bulk properties) becomes increasingly important with distance up the food-web, thus individual-based models are needed to represent organisms from higher-trophic levels.

1.3. Outline of the Thesis

Besides the general introduction (Chapter 1) and the general conclusions (Chapter 5), the main content of this thesis is divided into three chapters (Chapters 2, 3 and 4), each written to be a self-contained entity.

In Chapter 2, I present a hybrid (Eulerian/IBM) modelling framework and I demonstrate its applicability by simulating two-way interactions between five species of macrobiota (i.e. rockweed, kelp, seagrass, wild oysters, aquacultured mussels and farmed fish) and planktonic ecosystem variables (i.e. nutrients, plankton and detritus), in an idealized embayment. I also show how the two-way coupled model produces mass-balanced results that are fundamentally different from results of (commonly used) one-way coupled models, which can spuriously increase mass in the system. Finally, I show how the hybrid framework is an adequate alternative for tackling the high computational demands of integrating a large number of species in a 3-D space: ubiquitous species (e.g. plankton) are handled in the grid-based system, while rarer species (e.g. shellfish) are represented in the particle-based system. The objective of this chapter is to develop a hybrid (Eulerian/IBM) modelling framework and to demonstrate its applicability.

In Chapter 3, I present a hydrodynamic model capable of representing interactions between the planktonic ecosystem and aquacultured bivalves. This model operates under the hybrid (Eulerian/IBM) framework that I developed in Chapter 2. Here, I also apply this model to a fjord with a mussel farm and I compare model results against water samples collected over 5 years. Finally, I use the model to estimate the carrying capacity of the mussel farm. The objective of this chapter is to develop a coupled hydrodynamic,

planktonic and bivalve ecophysiology model and to apply it to estimated the carrying capacity of an embayment with bivalve aquaculture.

In Chapter 4, I use data from a high resolution survey in the fjord with mussel aquaculture, and the model developed in Chapter 3, to assess the effects of mussel aquaculture on the spatial distribution of phytoplankton. In this chapter I show that, as expected, mussels locally decreased phytoplankton biomass inside the mussel farm. However, unexpectedly, mussels also increased phytoplankton biomass in areas outside and around the farm. Here, I use the model to determine that the outside-farm increase in phytoplankton biomass is a result of enhanced phytoplankton production caused by the farm wastes during nutrient-limited and light-replete conditions. I also show that bivalve-induced spatial gradients in the concentration of planktonic ecosystem variables have the potential to drastically bias the results of 0-D bivalve-environment models, which assume a uniform concentration of all variables within the model domain. The objective of this chapter is to determine the effect of mussel aquaculture on the spatial distribution of phytoplankton in an embayment in Eastern Canada.

In Chapter 5, I present general conclusions about the interactions between macrobiota and its hydrodynamic and planktonic environment, and about the significance of this work. I end this thesis with recommendations for future work.

CHAPTER 2

Two-way Coupling of Macrobiota and Planktonic Dynamics in Shallow Embayments Using a Hybrid (IBM/Eulerian) End-to-End Model

2.1. Introduction

There is a growing consensus that the management of marine resources must encompass whole ecosystems (Pikitch et al., 2004; Soto et al., 2008). Consequently, there has been an accelerating effort towards the development of so called end-to-end models, which integrate physical dynamics with biological processes that span from lower-trophic levels (e.g. plankton) to higher-trophic levels (e.g. large fish), including human activities (Travers et al., 2007; Cury et al., 2008; Huse and Fiksen, 2010). Perhaps the greatest challenge in the development of end-to-end models is the coupling of models of different trophic levels (DeYoung et al., 2004), especially if the coupling allows feedbacks (i.e. two-way coupling; Travers et al., 2009). This is because, until recently, lower- and higher-trophic levels of marine ecosystems have been studied by different research communities that utilize fundamentally different modelling tools (Latour et al., 2003; Cury et al., 2008; Fennel, 2008; Shin et al., 2010; Moloney et al., 2011). That is, planktonic or lower-trophic levels are commonly studied with grid-based (or Eulerian) models that track organisms as concentrations of tracers in a gridded field (see details in Table 1-1

[*] This chapter comprises a co-authored manuscript by D. A. Ibarra, K. Fennel, J. J. Cullen. The contribution of the author of this thesis to this manuscript includes the development of a modelling framework and macrobiota ecophysiological models, and all the analysis and writing of this manuscript. Other authors contributed with guidance and multiple rounds of corrections.

and section 2.2.2.1). These grid-based models—commonly referred to as physical-biological coupled models—typically focus on the dynamics of nutrients, plankton and detritus, but do not explicitly describe the effects of organisms bigger than zooplankton (e.g. Fasham et al., 1990; Fennel et al., 2006). In contrast, higher-tropic levels are often studied with individual-based models (also known as particle-based) that track species as a collection of individuals, from which emerging properties of the ecosystem are computed *a posteriori* (see more details in Table 1-1 and section 2.2.2.2). These individual-based models often focus on commercially-valuable fish and only utilize plankton as forcing (e.g. Jennings et al., 2008); that is, the modelled fish do not affect plankton dynamics. Commercially valuable species are also the focus of aquaculture models, which are designed to assess the carrying capacity and/or environmental impacts of farming operations. Aquaculture models can be either grid-based (e.g. Dowd, 2003) or individual-based (e.g. Brigolin et al., 2009) and tend to focus on a single farmed species from either a lower- or higher-trophic level. Aquaculture models sometimes include plankton (usually as forcing), but rarely take wild macrobiota into consideration.

The importance of two-way coupling of multiple trophic levels has been highlighted in recent studies. Feedback loops among multiple trophic levels were found to be a fundamental requirement for the stability of complex food webs (Rooney et al., 2006; Neutel et al., 2007) and an essential component for the prediction of ecosystem dynamics beyond the near term (Hannah et al., 2010). Also, feedbacks between lower- and higher-trophic levels may provide insight on the combined effects of fishing and climate change on fish populations (Travers et al., 2009). It is not surprising that many modelling approaches for integrating multiple species of different sizes and trophic levels are under development (e.g. Travers et al., 2007; Fennel, 2008; Grant et al., 2008; Libralato and Solidoro, 2009; Fulton, 2010; Nobre et al., 2010; Shin et al., 2010).

In this paper we focus on embayments and other shallow coastal regions where the need for integration of multiple species may be greater than anywhere else. Unlike the open ocean, where most of the ecosystem biomass resides in plankton, in shallow coastal regions the planktonic biomass per unit area can be locally exceeded by the biomass of wild

and aquacultured macrobiota*. Therefore, aggregations of macrobiota species can influence (and sometimes even control) the variability of planktonic ecosystem variables (i.e. nutrients, plankton and detritus) in coastal ecosystems. For example, corals in the Red Sea (Yahel et al., 1998), wild oysters in Chesapeake Bay (Newell, 1988) and aquacultured mussels in Prince Edward Island (Grant et al., 2008) filter ecologically significant amounts of phytoplankton. In addition, production of wild seaweeds in St. Margaret's Bay (Eastern Canada) is three times the production of phytoplankton (Mann, 1973). Consequently, ecosystem models applied to shallow coastal areas may need to include not only plankton, but also wild and aquacultured macrobiota, in order to adequately represent mass flows and trophic dynamics.

The aquaculture sector also needs ecosystem models capable of representing multiple species from different trophic levels. In particular, these models are of interest in Integrated Multi-Trophic Aquaculture (Barrington et al., 2009), where multiple species of different trophic levels (e.g. salmon, mussels and kelp) are farmed in proximity of each other with the purpose of maximising growth of aquacultured species while minimising environmental impacts. Ecosystem models designed to help farmers and regulators in the planning and management of aquaculture farms will have to account not only for the different aquacultured species, but also for plankton and nearby wild macrobiota.

In shallow coastal applications, ecosystem models may need to represent interactions among species in a 3-D or spatially-explicit framework to be able to reproduce ecologically relevant spatial patterns of planktonic ecosystem variables. Miyajima et al. (2007) conducted fine-scale sampling in a coastal lagoon with wild seagrass beds and coral reefs. They found that nutrients decreased above seagrass beds and chlorophyll decreased over coral reefs, effectively forming persistent small-scale spatial patterns. Moreover, aquaculture operations can also cause patterns in the distributions of water column properties. For example, a decrease in chlorophyll has been observed inside and around shellfish

* For example, in a mussel farm in Ship Harbour (Nova Scotia, Canada), for a water column of 8 m, the biomass of farmed mussels (~134 mmol N m^{-2}) is much larger than the biomass of phytoplankton (~16 mmol N m^{-2}).

farms (e.g. Grant et al., 2008), and high ammonia has been observed inside and around fish farms (e.g. Sanderson et al., 2008). In Integrated Multi-Trophic Aquaculture, quantitative and spatially-explicit information about these water column spatial patterns is necessary when deciding where and how far apart to rear one species with respect to the others (e.g. Reid et al., 2010).

Two-way coupling may be particularly important in ecosystem models applied to coastal regions. In the open ocean, most fish larvae models (see review by Miller, 2007) and small fish models (e.g. Politikos et al., 2011) utilize a one-way coupling scheme that allows phytoplankton and other water properties to modify the physiology and behaviour of fish, but do not account for feeding, excretion and defecation of fish, implicitly assuming a negligible effect of fish on water properties. However, in coastal ecosystems the biomass of macrobiota (wild or aquacultured) can be large enough to influence food web structure and the variability of the planktonic ecosystem (e.g. Cranford et al., 2007; Guyondet et al., 2010). In this case, ignoring dynamic feedbacks between macrobiota and planktonic ecosystem variables (i.e. two-way coupling) would cause spurious losses or gains of mass, which would disrupt the inferred mass balance of the system.

In this study, we assessed the importance of two-way coupling in the estimation of interactions among multiple species of macrofauna (wild and aquacultured) and water column biogeochemistry (i.e. plankton, nutrients and detritus) in shallow coastal regions. We did not intend to assess the quantitative effect of any one species on the others—which is site- and case dependent. Instead we focused on demonstrating that modelling planktonic and macrobiota species simultaneously produces fundamentally different results than modelling them separately. In other words, we tested the following working hypothesis:

In a shallow coastal embayment, the coupling of planktonic ecosystem dynamics with realistic densities of wild and farmed macrobiota species performing known physiological activities, will (a) significantly alter the planktonic food web structure, and (b) create spatial gradients in biomass of the macrobiota species, if and only if, coupling between macrobiota and planktonic ecosystem variables is two-way and mass-balanced.

To test the above hypothesis, we developed a spatially-explicit model capable of accounting for two-way trophic interactions among multiple species. We applied the two-way coupled model to an idealized embayment with wild and aquacultured species, and we compared the model results against results from a one-way coupled version of the same model.

During the development of the two-way coupled model, we found that neither of the two basic modelling approaches (i.e. grid-based or individual-based) can efficiently represent a wide range of species from different sizes, abundances and trophic levels: Eulerian models are inefficient at representing rare species (i.e. species found only in a few cells) because they have to solve ecosystem equations in all cells, even if the species is absent in most of those cells. Individual-based models are inefficient at representing abundant and ubiquitous species (i.e. species found in all cells at all times), where the number of individuals needed to represent a system is many times larger than the number of grid cells in the domain. Therefore we developed a hybrid (Eulerian/IBM) ecosystem framework for the Regional Ocean Modeling System (ROMS), that simultaneously operates a grid-based model for the planktonic ecosystem (Fennel et al., 2006) and a new individual-based model for six wild and aquacultured macrobiota species.

In this study we (1) presented and described a hybrid modelling framework; (2) applied the hybrid model to an idealized embayment with wild and aquacultured species; (3) assessed the fidelity of our hybrid model by comparing model results against published data from different laboratory and field studies; and (4) tested the working hypothesis by comparing results from the two-way coupled hybrid model against results from a one-way coupled version of the same model.

2.2. Materials and Methods

2.2.1. The Regional Ocean Modeling System (ROMS)

ROMS is a state-of-the-art, open-source, 3-D ocean circulation model that is particularly suited for coastal applications (Haidvogel et al., 2008; http://myroms.org). ROMS operates under a collaborative framework, which has resulted in the inclusion of modules of, for example, sea ice (Budgell, 2005), sediment transport (Warner et al., 2008), planktonic biological processes (e.g. Fennel et al., 2006) and individual-based biological processes (this study). Each module can be included or excluded in the executable file, therefore maximizing applicability and minimizing memory use. Also, ROMS can be spatially optimized by using non-uniform grids with smaller grid cells in regions of interest (i.e. inside and around a bivalve farm) and nested grids to allow for finer grids in regions of interest (e.g. close to the coast). ROMS is widely used in the ocean and planktonic ecosystem modelling communities.

2.2.2. Hybrid Ecosystem Modelling Framework

In this study we utilized the ROMS conventional Eulerian framework to represent abundant and ubiquitous species like plankton (also nutrients and detritus), and we used a newly implemented individual-based framework for ROMS (described below) to represent rare species like benthic macrobiota and aquacultured species.

2.2.2.1. Grid-based (Eulerian) Framework

ROMS is an Eulerian circulation model, which means that the model domain is divided into a grid and—within every grid cell—the model keeps track of r number of tracers, each representing a scalar quantity like temperature or zooplankton concentration. Some tracers (i.e. temperature and salinity) influence physical dynamics and are always calculated, while other tracers (e.g. suspended sediments or plankton) do not affect circulation,

and therefore are modelled only if the sediment or ecosystem modules are activated. The state of the grid-based system is defined by:

2-1 $$\Psi^{j}(x,y,z,t) \qquad \text{for tracer } j = 1, \ldots, r$$

where x, y and z are the used Cartesian coordinates, t is time and j is the tracer index. For a complete list of symbols, see the list of abbreviations and symbols at the beginning of this thesis.

The time-rate of change of any tracer, Ψ^{j}, is estimated using the following scalar transport equation (adapted from Haidvogel et al., 2008; Warner et al., 2008).

Eq. 2-2

$$\frac{\partial \Psi^{j}}{\partial t}(x,y,\sigma,t) = -u\frac{\partial \Psi^{j}}{\partial x} - v\frac{\partial \Psi^{j}}{\partial y} - \Theta\frac{\partial \Psi^{j}}{\partial \sigma} + \frac{\partial}{H_z \partial \sigma}\left(K_\Psi \frac{\partial \Psi^{j}}{H_z \partial \sigma} + v_\theta \frac{\partial \Psi^{j}}{H_z \partial \sigma}\right) + D_\Psi + C^{j}_{Eul} + C^{j}_{IBM}$$

where u, v (m s^{-1}) and Θ (s^{-1}) are the mean components of the velocity in the horizontal (x and y) and vertical (σ) directions, respectively. The vertical sigma coordinate (σ, dimensionless) ranges from $\sigma = -1$ at the bottom to $\sigma = 0$ at the free surface, and is calculated with $\sigma = (z-\eta)/H$, where z is the vertical coordinate (positive upwards, $z = 0$ at the mean sea level), η is the wave-averaged free-surface elevation and H is the total water depth, $H = h + \eta$, where h is the mean water depth. Also, H_z (m) is the thickness of the grid cell, K_Ψ (m^2 s^{-1}) is the vertical eddy diffusivity coefficient, v_θ (m^2 s^{-1}) is the tracer kinematic diffusivity, D_Ψ represents the horizontal diffusive terms, C^{j}_{Eul} are the Eulerian source/sink terms for tracer j, and C^{j}_{IBM} are the individual-based source/sink terms for tracer j.

For biologically active tracers, such as nutrients, plankton and detritus, the C^{j}_{Eul} terms are solved using the ROMS grid-based biology module. Several planktonic ecosystem models are included in the grid-based biology module (Bissett et al., 1999; Lima and Doney,

2004; Fennel et al., 2006; Powell et al., 2006); however only one model can be used during each simulation (Haidvogel et al., 2008). Currently, the hybrid-ecosystem framework can be used only with the Fennel et al. (2006) ecosystem model. The C^{j}_{IBM} terms are solved using ROMS individual-based biology module described below.

2.2.2.2. Individual-based (Particle-based) Framework

The individual-based biology module allows ROMS to track properties of an array of particles. Here, each particle represents a group of identical individuals of species *i* and functional group φ. Each functional group (e.g. Macroalgae or Filter-feeders) refers to a collection of species whose dynamics are simulated using the same ecophysiological model. Different species within a functional group (e.g. kelp vs. rockweed, or oysters vs. mussels) differ only in the value of the parameters used by the ecophysiological model. Following established terminology (Scheffer et al., 1995), we herein use the term super-individual to refer to each group of identical individuals (i.e. each particle). For each super-individual *k* of species *i* and functional group φ, the individual-based module tracks a *q* number of properties, like position ($x_k^{\varphi,i}$, $y_k^{\varphi,i}$, $z_k^{\varphi,i}$), biomass ($m_k^{\varphi,i}$), number of identical individuals in the super-individual ($n_k^{\varphi,i}$), nitrate uptake ($upNO3_k^{\varphi,i}$), etc. Therefore, the state of the individual-based system is defined by:

$$\Omega^{\varphi,i}(k,g,t) \qquad \begin{array}{ll} \text{for functional groups} & \varphi = 1,\ldots,\tau \\ \text{for species} & i = 1,\ldots,s \\ \text{for super - individuals} & k = 1,\ldots,p \\ \text{for properties} & g = 1,\ldots,q \end{array} \tag{2-3}$$

where the state of species *i* and functional group φ, $\Omega^{\varphi,i}$, is represented (at any given time) by a separate $p \times q$ matrix with rows corresponding to super-individuals and columns to properties:

Eq. 2-4

$$\Omega^{\varphi,i}(t) = \begin{bmatrix} x_1^{\varphi,i} & y_1^{\varphi,i} & z_1^{\varphi,i} & m_1^{\varphi,i} & n_1^{\varphi,i} & (\omega_{1,6})^{\varphi,i} & \cdots & (\omega_{1,g})^{\varphi,i} & \cdots & (\omega_{1,q})^{\varphi,i} \\ x_2^{\varphi,i} & y_2^{\varphi,i} & z_2^{\varphi,i} & m_2^{\varphi,i} & n_2^{\varphi,i} & (\omega_{2,6})^{\varphi,i} & \cdots & (\omega_{2,g})^{\varphi,i} & \cdots & (\omega_{2,q})^{\varphi,i} \\ \vdots & \vdots & \vdots & \vdots & \vdots & \vdots & \vdots & \vdots & \vdots & \vdots \\ x_k^{\varphi,i} & y_k^{\varphi,i} & z_k^{\varphi,i} & m_k^{\varphi,i} & n_k^{\varphi,i} & (\omega_{k,6})^{\varphi,i} & \cdots & (\omega_{k,g})^{\varphi,i} & \cdots & (\omega_{k,q})^{\varphi,i} \\ \vdots & \vdots & \vdots & \vdots & \vdots & \vdots & \vdots & \vdots & \vdots & \vdots \\ x_p^{\varphi,i} & y_p^{\varphi,i} & z_p^{\varphi,i} & m_p^{\varphi,i} & n_p^{\varphi,i} & (\omega_{p,6})^{\varphi,i} & \cdots & (\omega_{p,g})^{\varphi,i} & \cdots & (\omega_{p,q})^{\varphi,i} \end{bmatrix}$$

where $(\omega_{k,g})^{\varphi,i}$ are elements of the $\Omega^{\varphi,i}$ matrix, each representing the property g of super-individual k of species i and functional group φ. Note that, in the first 5 columns, we utilized a simplified notation by substituting the element symbol ω for the specific symbol used to describe the property g (e.g. $(\omega_{1,1})^{\varphi,i} = x_1^{\varphi,i}$). Also, for simplicity, we eliminated the parentheses, however note that the subscripts k and p are different for different $\Omega^{\varphi,i}$ matrices and should be referred to as $k^{\varphi,i}$ and $p^{\varphi,i}$ if not accompanied by a superscript φ,i. We used this simplified notation hereinafter.

In this nitrogen-based model, the biomass of each super-individual is defined by the product of the biomass of a single individual, $m_k^{\varphi,i}$ (mmol N ind^{-1}) and the number of identical individuals in the super-individual, $n_k^{\varphi,i}$ (ind). The ecophysiological dynamics of each super-individual are defined by the following two generic equations: the first (Eq. 2-5) is a physiology equation determining the time rate of change of the biomass of an individual, and the second (Eq. 2-6) is a population dynamics equation controlling the time rate of change of the number of individuals forming the super-individual.

Eq. 2-5

$$\frac{dm_k^{\varphi,i}}{dt} = \text{production}_k^{\varphi,i} - \text{respiration}_k^{\varphi,i} - \text{other losses}_k^{\varphi,i}$$

Eq. 2-6

$$\frac{dn_k^{\varphi,i}}{dt} = \text{recruitment}_k^{\varphi,i} - \text{mortality}_k^{\varphi,i} - \text{other losses}_k^{\varphi,i}$$

At every time-step, individual-based variables that interact with the Eulerian model have to be converted into their grid-based equivalents (in units of concentration) to allow reactions among all involved variables (see section 2.2.2.3 for details on the coupling of tracers and individuals). The conversion from the individual-based framework to the grid-based framework is implemented using the following generic formula:

Eq. 2-7
$$X^{\varphi,i}(x,y,\sigma,t) = \sum_{k^{\varphi,i} \in G} \left(\chi_k^{\varphi,i}(x,y,\sigma,t) \cdot \frac{n_k^{\varphi,i}(x,y,\sigma,t)}{V(x,y,\sigma,t)} \right)$$

where G is a set of all super-individuals of species i and functional group φ that occur, at time t, within a target grid cell—which is defined by the coordinates x, y, σ. Then, $\chi_k^{\varphi,i}$ (unit · ind^{-1}) is any individual-based variable of the super-individuals of G, and $X^{\varphi,i}$ (unit · m^{-3}) is the grid-based equivalent of $\chi_k^{\varphi,i}$, which represents the concentration variable accounting for all super-individuals of species i and functional group φ in the target grid cell. Note that the volume of the target grid cell, V (m^3), changes over time due to variations in the free surface and its representation in the sigma coordinate system used by ROMS.

The individual-based module currently has five ecophysiology models. The first four (Figure 2-1) are generic models to simulate the ecophysiology of different functional groups (i.e. macroalgae, seagrass, filter-feeders and aquacultured fish), and are described below. The fifth is a more elaborate model to simulate Shellfish Ecophysiology (SHELL-E), and is described in detail in Chapter 3. In the individual-based framework, all ecophysiology models can be used in the same simulation run. Note that we disable the ability of the particles to be transported by currents, therefore the individuals remain in the location of initial insertion throughout the model simulation. See Appendix A for more details on the functioning of the individual-based module.

Macroalgae Model: This model simulates photosynthetic macroalgae (e.g. kelp and rockweed), where the time rate of change of the biomass of a single macroalga is given by:

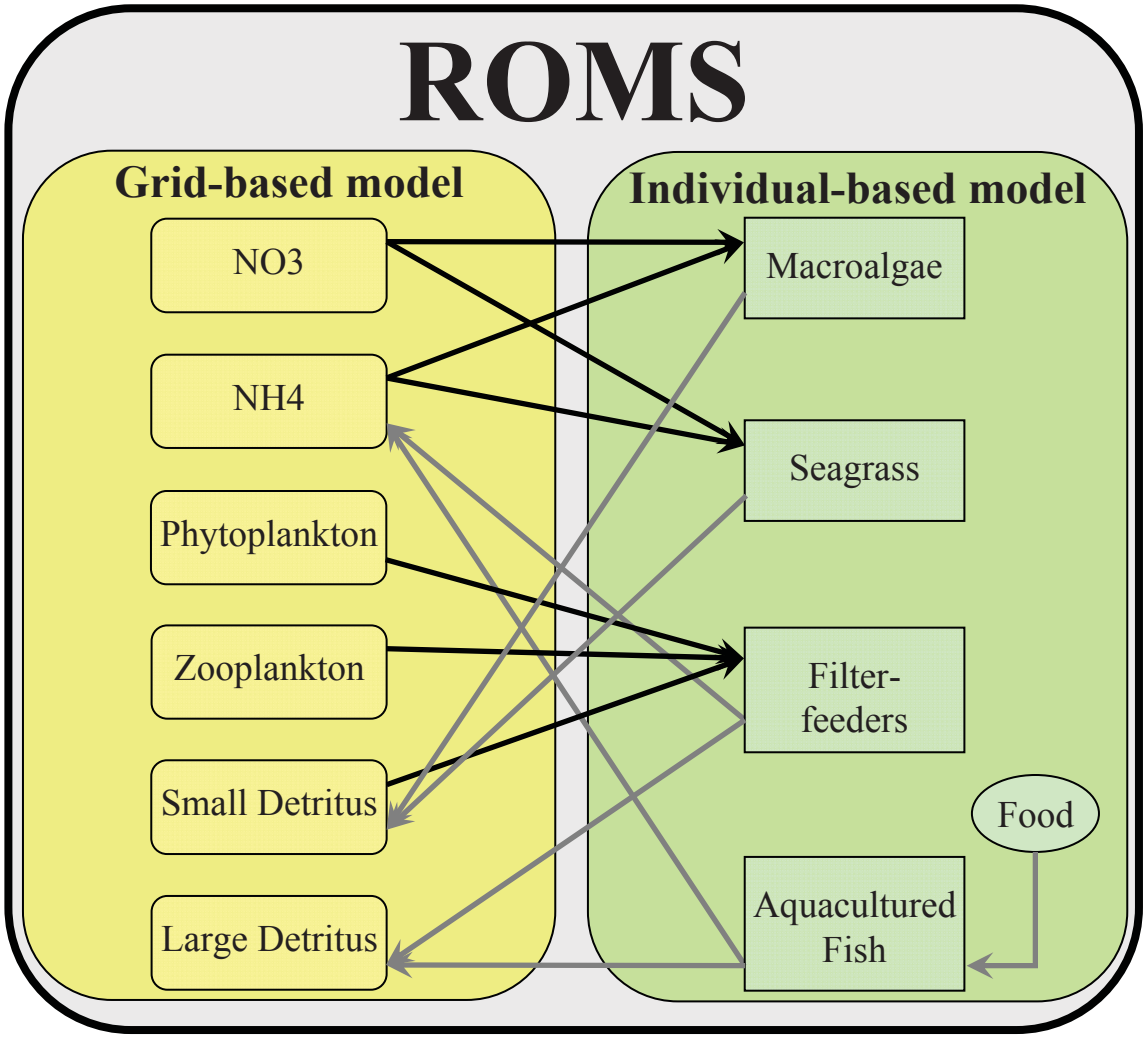

Figure 2-1. Conceptual diagram showing the coupling between all four generic ecophysiological models in this study (green squares) and the planktonic ecosystem model (yellow squares) from Fennel et al. (2006).

Eq. 2-8 $$\frac{\partial m_k^{M,i}}{\partial t} = \left(\mu_k^{M,i} \cdot m_k^{M,i}\right) - \left(\Phi^{M,i} \cdot m_k^{M,i}\right)$$

where the superscript *M,i* denotes any species *i* from the Macroalgae functional group (i.e. *M*); $m_k^{M,i}$ (mmol N ind^{-1}) is the biomass of an individual of species *M,i*. In turn, the term $\mu_k^{M,i}$ (d^{-1}) is the specific rate of increase in biomass after accounting for respiration and $\Phi^{M,i}$ (d^{-1}) is the specific erosion rate, which includes grazing and is assumed to be independent of location.

The specific rate of increase in biomass, $\mu_k^{M,i}$, depends on the maximum growth rate, $\mu_{\max}^{M,i}$ (d^{-1}), the local concentrations of nitrate, *NO3* (mmol N m^{-3}) and ammonium, *NH4* (mmol N m^{-3}), and the photosynthetically available radiation, *I* (W m^{-2}) which is attenuated throughout the water column using a constant attenuation coefficient for seawater plus a variable attenuation coefficient as a function of chlorophyll concentration, which is calculated in the Eulerian component of the model. Note that the Eulerian tracer quantities are evaluated at the specific location of the super-individual $k^{\varphi,i}$. However, for simplicity, we omitted the spatial dependency; for example, *NO3* instead of *NO3*($x_k^{\varphi,i}, y_k^{\varphi,i}, z_k^{\varphi,i}$).

Eq. 2-9 $$\mu_k^{M,i} = \mu_{\max}^{M,i} \cdot f^{M,i}(I) \cdot [f^{M,i}(NO3) + f^{M,i}(NH4)]$$

where

Eq. 2-10 $$f^{M,i}(I) = \frac{\alpha^{M,i} \cdot I}{\sqrt{(P_{\max}^{M,i})^2 + \left(\alpha^{M,i} \cdot I\right)^2}}$$

Eq. 2-11 $$f^{M,i}(NO3) = \frac{NO3}{K_{NO3}^{M,i} + NO3} \cdot \frac{1}{1 + (NH4 / K_{NH4}^{M,i})}$$

Eq. 2-12 $$f^{M,i}(NH4) = \frac{NH4}{K_{NH4}^{M,i} + NH4}$$

where $P_{\max}^{M,i}$ is the maximum photosynthesis rate for macroalgae of species *i* (units can vary, but common units are μmol O_2 (g Fresh Weight)$^{-1}$ h^{-1}), and $\alpha^{M,i}$ (units of $P_{\max}^{M,i}$ divided by W m^{-2}) is the initial slope of photosynthesis *vs* irradiance curve. Finally, $K_{NO3}^{M,i}$ and $K_{NH4}^{M,i}$ (mmol N m^{-3}) are the half-saturation constants for the uptake of *NO3* and *NH4*, respectively, for macroalgae of species *i*, with inhibition of nitrate uptake by ammonium as implemented for phytoplankton by Fennel et al. (2006).

We define the uptake rate of nitrate and ammonium (mmol N ind^{-1} d^{-1}) as:

Eq. 2-13 $$upNO3_k^{M,i} = \mu_{\max}^{M,i} \cdot f^{M,i}(I) \cdot f^{M,i}(NO3) \cdot m_k^{M,i}$$

and

Eq. 2-14 $$upNH4_k^{M,i} = \mu_{\max}^{M,i} \cdot f^{M,i}(I) \cdot f^{M,i}(NH4) \cdot m_k^{M,i}$$

Population dynamics in the super-individual are determined by the time evolution of the number of individuals of macroalgae of species *i*, $n^{M,i}$ (*ind*):

Eq. 2-15 $$\frac{\partial n_k^{M,i}}{\partial t} = -\lambda^{M,i} \cdot n_k^{M,i}$$

where $\lambda^{M,i}$ (d^{-1}) is a constant mortality rate for macroalgae of species *i*. Dead individuals are immediately decomposed and added to the ammonium pool (see Table 2-1).

Table 2-1. Summary of C_{IBM}^{j} terms added to the grid-based advection-diffusion equation (Eq. 2-2) to couple the different ecophysiology models currently included in the Individual-Based Module with the grid-based model

	Macroalgae	Seagrass	Filter-feeders	Aquacultured Fish
$C_{IBM}^{Phy} =$			$-\sum_{i=1}^{s}\sum_{k^{F,i}\in G}\left(\frac{F^{F,i}\cdot\varepsilon_{P}^{F,i}\cdot n_{k}^{F,i}\cdot Phy}{V}\right)$	
$C_{IBM}^{Zoo} =$			$-\sum_{i=1}^{s}\sum_{k^{F,i}\in G}\left(\frac{F^{F,i}\cdot\varepsilon_{Z}^{F,i}\cdot n_{k}^{F,i}\cdot Zoo}{V}\right)$	
$C_{IBM}^{SDet} =$	$+\sum_{i=1}^{s}\sum_{k^{S,i}\in G}\left(\frac{\Phi^{M,i}\cdot m_{k}^{M,i}\cdot n_{k}^{M,i}}{V}\right)$	$+\sum_{i=1}^{s}\sum_{k^{S,i}\in G}\left(\frac{\Phi^{S,i}\cdot m_{k}^{S,i}\cdot n_{k}^{S,i}}{V}\right)$	$-\sum_{i=1}^{s}\sum_{k^{F,i}\in G}\left(\frac{F^{F,i}\cdot\varepsilon_{D}^{F,i}\cdot n_{k}^{F,i}\cdot SDet}{V}\right)$	$+\sum_{i=1}^{s}\sum_{k^{A,i}\in G}\left(\frac{\varepsilon_{F}^{A,i}\cdot(1-IE^{A,i})\cdot Food_{k}^{A,i}\cdot n_{k}^{A,i}}{V}\right)$
$C_{IBM}^{LDet} =$			$+\sum_{i=1}^{s}\sum_{k^{F,i}\in G}\left(\frac{Fae_{k}^{F,i}\cdot n_{k}^{F,i}}{V}\right)$	$+\sum_{i=1}^{s}\sum_{k^{A,i}\in G}\left(\frac{\left\{Fae_{k}^{A,i}+\left[(1-\varepsilon_{F}^{A,i})\cdot Food_{k}^{A,i}\right]\right\}\cdot n_{k}^{A,i}}{V}\right)$
$C_{IBM}^{NH4} =$	$-\sum_{i=1}^{s}\sum_{k^{M,i}\in G}\left(\frac{\left[\left(\lambda^{M,i}\cdot m_{k}^{M,i}\right)-upNH4_{k}^{M,i}\right]\cdot n_{k}^{M,i}}{V}\right)$	$-\sum_{i=1}^{s}\sum_{k^{S,i}\in G}\left(\frac{upNH4_{k}^{S,i}\cdot n_{k}^{S,i}}{V}\right)$	$+\sum_{i=1}^{s}\sum_{k^{F,i}\in G}\left(\frac{\left[R_{k}^{F,i}+\left(\lambda^{F,i}\cdot m_{k}^{F,i}\right)\right]\cdot n_{k}^{F,i}}{V}\right)$	$+\sum_{i=1}^{s}\sum_{k^{A,i}\in G}\left(\frac{\left[R_{k}^{A,i}+\left(\lambda^{A,i}\cdot m_{k}^{A,i}\right)\right]\cdot n_{k}^{A,i}}{V}\right)$
$C_{IBM}^{NO3} =$	$-\sum_{i=1}^{s}\sum_{k^{M,i}\in G}\left(\frac{upNO3_{k}^{M,i}\cdot n_{k}^{M,i}}{V}\right)$	$-\sum_{i=1}^{s}\sum_{k^{S,i}\in G}\left(\frac{upNO3_{k}^{S,i}\cdot n_{k}^{S,i}}{V}\right)$		

Seagrass model: This model simulates photosynthetic macro-organisms that grow horizontally by creating new shoots, rather than by lengthening their shoots (e.g. seagrass; functional group *S*). In this case, the biomass of an individual shoot of seagrass of species *i* ($m_k^{S,i}$; mmol N ind^{-1}) is considered to remain constant at the initial biomass value defined at the beginning of the simulation (Table 2-1). Consequently, the time rate of change in an individual shoot biomass is zero. However, the number of individuals in the super-individual, and thus the total biomass of the super-individual, varies over time. The time evolution of the number of shoots in a super-individual, $n_k^{S,i}$, is calculated as:

Eq. 2-16
$$\frac{\partial n_k^{S,i}}{\partial t} = n_k^{S,i} \cdot \left(\mu_k^{S,i} - \Phi^{S,i}\right)$$

where $\Phi^{S,i}$ (d^{-1}) is the specific erosion rate for seagrass of species *i*, which is assumed to be spatially constant over the entire domain. The specific rate of increase in biomass, $\mu_k^{S,i}$ (d^{-1}), estimated similarly as $\mu_k^{M,i}$ in Eq. 2-9, but with parameters for species *S,i*. Our seagrass model is designed to evaluate the effect of seagrass on the planktonic ecosystem variables over short time scales (i.e. weeks), therefore we neglected to include processes like rhizome and shoot growth as well as the mass allocation among these compartments (Larkum et al., 2006). These process should not be neglected in longer simulations (i.e. months to years).

Filter-feeder model: This model simulates organisms that feed on particles suspended in the water column (e.g. oysters or sponges; functional group *F*) and is built upon earlier work (Dowd, 1997). The time rate of change of the biomass of an individual filter-feeder of species *i* is defined as:

Eq. 2-17
$$\frac{\partial m_k^{F,i}}{\partial t} = A_k^{F,i} - R_k^{F,i}$$

where the superscript *F,i* denotes any species *i* from the filter-feeder functional group, $m_k^{F,i}$ is the biomass of an individual filter-feeder (mmol N ind^{-1}), $A_k^{F,i}$ is the assimilation rate (mmol N ind^{-1} d^{-1}) and $R_k^{F,i}$ is the respiration rate (mmol N ind^{-1} d^{-1}) for an individual filter-feeder.

The assimilation rate represents the total amount of food absorbed per individual and per unit time, and is calculated as follows:

Eq. 2-18 $$A_k^{F,i} = F^{F,i} \cdot \left[\left(\varepsilon_P^{F,i} \cdot AE_P^{F,i} \cdot Phy\right) + \left(\varepsilon_Z^{F,i} \cdot AE_Z^{F,i} \cdot Zoo\right) + \left(\varepsilon_D^{F,i} \cdot AE_D^{F,i} \cdot SDet\right)\right]$$

where $F^{F,i}$ is the individual filtration rate (m^3 ind^{-1} d^{-1}), $\varepsilon^{F,i}$ and $AE^{F,i}$ are the dimensionless feeding and absorption efficiencies, and subscripts *P*, *Z* and *D* indicate phytoplankton, zooplankton and small detritus, respectively.

The respiration rate $R_k^{F,i}$, represents the biomass lost due to catabolic processes, and is estimated as follows:

Eq. 2-19 $$R_k^{F,i} = \left(M^{F,i} \cdot m_k^{F,i}\right) + \left(\beta^{F,i} \cdot A_k^{F,i}\right)$$

where $M^{F,i}$ (d^{-1}) is the weight-specific maintenance respiration rate (for now, assumed to be constant) and $\beta^{F,i}$ is the dimensionless cost of growth (see Dowd, 1997; Grant et al., 2007).

The production rate of faeces by one individual, $Fae_k^{F,i}$ (mmol N ind^{-1} d^{-1}), is determined as follows:

Eq. 2-20

$$Fae_k^{F,i} = F^{F,i} \cdot \left\{ \left[\varepsilon_P^{F,i} \cdot (1 - AE_P^{F,i}) \cdot Phy\right] + \left[\varepsilon_Z^{F,i} \cdot (1 - AE_Z^{F,i}) \cdot Zoo\right] + \left[\varepsilon_D^{F,i} \cdot (1 - AE_D^{F,i}) \cdot SDet\right] \right\}$$

Once faeces are produced, they are incorporated into the large detritus pool (Table 2-1), where they undergo sinking and decomposition. This model assumes negligible production of pseudofaeces, which are rejected particles that are packed into pellets and expelled before undergoing ingestion.

The number of individuals in a super-individual, $n_k^{F,i}$, is influenced only by a constant mortality rate, calculated in the same way as $n_k^{M,i}$ in Eq. 2-15. This generic filter-feeder is a simplification of the SHELL-E (Chapter 3) used for bivalve aquaculture.

Aquacultured fish model: This model simulates farmed fish (i.e. functional group *A*) that are fed by humans and remain in a fixed location because they are contained within net-cages. The time-rate of change of the biomass of an individual fish is defined as:

Eq. 2-21

$$\frac{\partial m_k^{A,i}}{\partial t} = A_k^{A,i} - R_k^{A,i}$$

where $m_k^{A,i}$ is the biomass of an individual aquacultured fish of species *i* (mmol N ind^{-1}), $A_k^{A,i}$ is the assimilation rate (mmol N ind^{-1} d^{-1}) and $R_k^{A,i}$ is the respiration rate (mmol N ind^{-1} d^{-1}). The assimilation rate represents the total amount of food absorbed per individual and per unit time, and is calculated as follows:

Eq. 2-22

$$A_k^{A,i} = \varepsilon_A^{A,i} \cdot IE_A^{A,i} \cdot AE_A^{A,i} \cdot Food_k^{A,i}$$

where $\varepsilon_A^{A,i}$ is the dimensionless feeding representing the fraction of food swallowed by the fish; however, part of the swallowed food is spit out as food crumbs (i.e. sloppy feed-

ing), thus the dimensionless ingestion efficiency, $IE_A^{A,i}$, represents the fraction of swallowed food that makes it to the stomach. The fraction of ingested food that is digestible is defined by the dimensionless absorption efficiency, $AE_A^{A,i}$ (subscripts *A* indicates Aquacultured fish). $Food_k^{A,i}$ (mmol N ind^{-1} d^{-1}) is the amount of feed delivered to an individual fish per day, and is estimated as follows:

Eq. 2-23 $$Food_k^{A,i} = \zeta^{A,i} \cdot m_k^{A,i}$$

where $\zeta^{A,i}$ (d^{-1}) is the artificial food delivery or feeding rate.

The respiration rate $R_k^{A,i}$, represents the biomass of an individual aquacultured fish of species *i* lost due to catabolic processes, and is estimated as follows:

Eq. 2-24 $$R_k^{A,i} = \left(M^{A,i} \cdot m_k^{A,i}\right) + \left(\beta^{A,i} \cdot A_k^{A,i}\right)$$

where $M^{A,i}$ (d^{-1}) is the weight-specific maintenance respiration rate and $\beta^{A,i}$ is the dimensionless cost of growth for an individual aquacultured fish of species *i*. Both parameters are assumed to remain constant.

The production rate of faeces by one individual fish ($Fae_k^{A,i}$, mmol N ind^{-1} d^{-1}) is determined as follows:

Eq. 2-25 $$Fae_k^{A,i} = \varepsilon_F^{A,i} \cdot IE_F^{A,i} \cdot (1 - AE_F^{A,i}) \cdot Food_k^{A,i}$$

Similar to filter-feeder faeces, fish faeces are incorporated into the large detritus pool (Table 2-1), where they undergo sinking, decomposition and ingestion by filter-feeders. Population dynamics are estimated by the time evolution of the number of individuals in a super-individual, affected only by a constant natural mortality term, similarly as in Eq.

2-15. A harvesting term can be easily incorporated, but for the purpose of this study, we did not include losses due to harvesting.

2.2.2.3. Coupling the Grid-based and the Individual-based Frameworks

The two-way coupling allowing bidirectional exchanges of mass between the grid-based variables (e.g. plankton and nutrients) and the individual-based variables (e.g. bivalves, fish) is achieved as follows: (1) the effect of tracers on individuals occurs in the eco-physiology equations, where source/sink terms are modulated by the local concentration of tracers; and (2) the effect of individuals on tracers is accomplished by the insertion, in Eq. 2-2, of the term C_{IBM}^{j} that represents individual-based source/sink terms for tracer j, and follows this functional form:

Eq. 2-26
$$C_{IBM}^{j} = \sum_{\varphi=1}^{\tau} \sum_{i=1}^{s} \sum_{k^{\varphi,i} \in G} \left[\frac{f^{\varphi,i}(\Psi, \Omega_{k^{\varphi,i}})}{V} \right]$$

where Ψ are grid-based variables and $\Omega_{k^{\varphi,i}}$ are individual-based variables. The specific C_{IBM}^{j} terms for each tracer j are shown in Table 2-1 and are represented graphically in Figure 2-1.

2.2.3. Example Application

To demonstrate the applicability of the hybrid ecosystem model and to test our working hypothesis, we set up ROMS for an idealized shallow bay, typical of Eastern Canada, containing wild aggregations of plants and oysters, and aquaculture farms of mussels and fish. We chose this region because wild and aquacultured species typical of this region have been studied extensively. To avoid adding more complexity, we did not account for influence of benthic microalgae, although they can account for a significant portion of the primary productivity in shallow environments (e.g. MacIntyre and Cullen, 1996; Guarini et al., 1998). We ran the simulation for 1 month.

Model domain and grid: The idealized bay is rectangular (4 km × 14 km) with three closed boundaries and an open boundary to the east (Figure 2-2). Depth increases linearly from 2.1 m in the western end to 6 m in the eastern end. The domain has 10 sigma layers resulting in a vertical spatial resolution that varies from approximately 20 cm in the shallow end to 60 cm in the deep end. The horizontal grid-size is uniform (200 m × 200 m) throughout the model domain. Also, we found that the boundary conditions have a strong influence on the concentration of tracers inside the bay. Therefore, we extended the model domain eastwards by 5 km. The added grid cells allowed tracers in the incoming water to mix with "bay water" before entering the region of interest. The buffer region is not shown in our results.

Forcing: We used synthetic tides and atmospheric variables to force the model. Sinusoidal functions were used to create M2 tides (amplitude 1.5 m), diurnal southerly winds (max 6.3 km h^{-1} or 1.75 m s^{-1}), seasonal air temperature (min 8°C, max 15°C), and diurnal short wave solar radiation (max 920 Watt m^{-2}). Surface air relative humidity (95%) and pressure (1015 mbar or 101500 Pa), cloud fraction (0.5 dimensionless) and rain fall rate (0 kg m^{-2} s^{-1}) were kept constant through the model simulation. We also included small random noise (i.e. ~10% of mean) to the time-series of winds and short wave solar radiation to produce more realistic forcing.

Initial and boundary conditions: At the beginning of the simulation, the concentration of all tracers was set constant throughout the model domain (values shown in Table 2-2). We initialize nitrate to relatively high initial concentration (5 mmol N m^{-3}) typically observed during upwelling events (e.g. Chapter 3), which are common in the region during the fall (Platt et al., 1972). Water entering the bay through the eastern boundary during flood tide was set to have constant concentrations of all biological tracers as given in Table 2-2.

Individual organisms: We inserted groups of identical individuals (i.e. super-individuals) as shown in Figure 2-2. Rockweed (*Ascophyllum nodosum*) was inserted on the bottom in

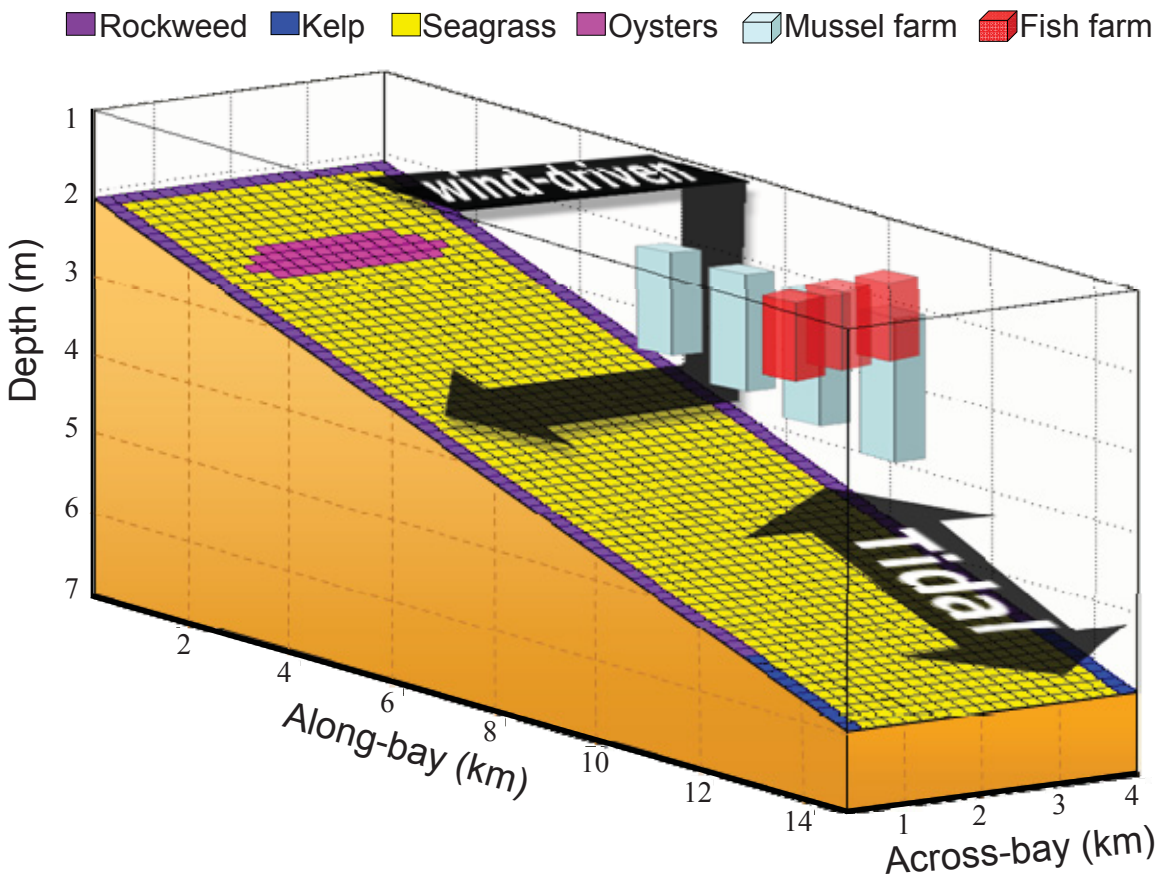

Figure 2-2. Diagram of the idealized embayment used for model simulations. Colors show the grid cells occupied by different species of macrofauna. The fish farm (red blocks) and the mussel farm (light blue blocks) are suspended in the water column. Black arrows give an idea of the physical circulation produced by tidal and wind forcing.

Table 2-2. Initial and boundary condition for biological tracers in the planktonic ecosystem model.

Variable	Units	Initial	Boundary
Chlorophyll	mg Chl m^{-3}	1	1
Phytoplankton	mmol N m^{-3}	1	1
Zooplankton	mmol N m^{-3}	0.2	0.2
Small detritus	mmol N m^{-3}	0.5	0.5
Large detritus	mmol N m^{-3}	0.1	0.1
Ammonium	mmol N m^{-3}	0.1	0.1
Nitrate	mmol N m^{-3}	5	0.5

all cells along the coast. Kelp (*Laminaria digitata*) was also added to the coast cells, but only close to the mouth of the bay where there are stronger currents. A natural oyster reef (*Crassostrea virginica*) was inserted on the bottom at the shallow end of the bay, and a mussel farm (*Mytilus edulis*) was inserted in middle water-column near the mouth of the bay. A fish farm with steelhead trout (*Oncorhynchus mykiss*) was also added at the mouth of the bay, but cages only occupied the upper water-column. Seagrass (*Zostera marina*) was inserted at the bottom throughout the model domain with exception of the cells occupied by rockweed or oysters. We utilized data from several field studies in Eastern Canada as initial conditions for our ecophysiological models, and we parameterize them using published physiological rates for the specific species used in our example application (see footnotes of Table 2-3). The initial densities of all species were realistic, yet leaning on the conservative (low) side. In total, 1854 super-individuals were inserted within the model domain.

2.2.4. Comparison of One-way and Two-way Coupled Models

To test our hypothesis and assess the effects that two-way coupling had on our modeling results, we also ran the application described above using a one-way coupled model. In the one-way coupled model, the feedback from the individual-based variables to the grid-based variables was disconnected. That is, the term C_{IBM}^{j} from Eq. 2-2 was eliminated.

Table 2-3. Parameters and initial conditions used in the example simulation.

Functional group:			Macroalgae		Seagrass	Filter-feeders		Fish
Symb.	Description	Units	$\varphi i = M1$ Kelp	$\varphi i = M2$ Rockweed	$\varphi i = S1$ Seagrass	$\varphi i = F1$ Oysters	$\varphi i = F2$ Mussels	$\varphi i = A1$ Steelhead trout
$\lambda^{\varphi,i}$	Mortality rate	d^{-1}	0	0	0	0	0	0
$\mu^{\varphi,i}_{\max}$	Maximum growth rate	d^{-1}	0.09[a]	0.14[b]	0.27[c]	-	-	-
$\Phi^{\varphi,i}$	Erosion rate	d^{-1}	0.006[d]	0.0001	0.0001	-	-	-
$P^{\varphi,i}_{\max}$	Maximum photosynthesis rate	see footnotes	45[e]	64[f]	0.25[g]	-	-	-
$\alpha^{\varphi,i}$	Initial slope	see footnotes	12.52[h]	1.03[i]	0.014[j]	-	-	-
$I^{\varphi,i}_k$	$P_{\max}$ / α	W m^{-2}	3.6	62	17	-	-	-
$K^{\varphi,i}_{NO3}$	Half-saturation for NO3	mmol N m^{-3}	5[k]	11[l]	9.2[m]	-	-	-
$K^{\varphi,i}_{NH4}$	Half-saturation for NH4	mmol N m^{-3}	12.7[n]	14[o]	9.2[p]	-	-	-
$F^{\varphi,i}$	Individual filtration rate	m^3 ind^{-1} d^{-1}	-	-	-	0.012[q]	0.048[r]	-
$M^{\varphi,i}$	Weight-specific maintenance respiration rate	d^{-1}	-	-	-	0.002	0.002[t]	0.001225[y]
$\zeta^{\varphi,i}$	Artificial food delivery rate (feeding)	d^{-1}	-	-	-	-	-	0.0085[u]
$\varepsilon^{\varphi,i}_A$	Feeding efficiency on artificial food	dimensionless	-	-	-	-	-	0.92[v]
$\varepsilon^{\varphi,i}_P$	Feeding efficiency on phytoplankton	dimensionless	-	-	-	1	1	-
$\varepsilon^{\varphi,i}_Z$	Feeding efficiency on zooplankton	dimensionless	-	-	-	0	0	-
$\varepsilon^{\varphi,i}_D$	Feeding efficiency on detritus	dimensionless	-	-	-	1	1	-
$IE^{\varphi,i}_A$	Ingestion efficiency on artificial food	dimensionless	-	-	-	-	-	0.95[u]
$AE^{\varphi,i}_A$	Absorption efficiency on artificial food	dimensionless	-	-	-	-	-	0.885[w]
$AE^{\varphi,i}_P$	Absorption efficiency on phytoplankton	dimensionless	-	-	-	0.9[s]	0.9[t]	-
$AE^{\varphi,i}_Z$	Absorption efficiency on zooplankton	dimensionless	-	-	-	0	0	-
$AE^{\varphi,i}_D$	Absorption efficiency on detritus	dimensionless	-	-	-	0.2[x]	0.2[t]	-
$\beta^{\varphi,i}$	Cost of growth coefficient	dimensionless	-	-	-	0.1	0.1[y]	0.44[z]
$n^{\varphi,i}(t=0)$	Initial number of individuals per grid cell	ind × 10^6	0.3[aa]	0.18[bb]	3.8[cc]	1.7[dd]	0.85[ee]	0.020642[f]
see footnotes	Initial biomass per individual	mmol N ind^{-1}	5[gg]	143[hh]	1.5[ii]	0.48[jj]	4.17[kk]	1104[ll]

[a] Gordillo et al. (2002).
[b] Nielsen and Sand-Jensen (1990).
[c] Dennison and Alberte (1982).
[d] Schmidt and Scheibling (2007) using biometric conversions from Gevaert et al. (2008).
[e] Units of µmol O_2 (g Fresh Weight)$^{-1}$ h^{-1}; Forster and Luning (1996).
[f] Units of µmol O_2 g dwt^{-1} h^{-1}; Peckol et al. (1988).
[g] Units of µmol O_2 g (mg Chl)$^{-1}$ min^{-1}; Dennison and Alberte (1982).
[h] Units of µmol O_2 (g Fresh Weight)$^{-1}$ h^{-1} (W m^{-2})$^{-1}$; Forster and Luning (1996).
[i] Units of µmol O_2 g dwt^{-1} h^{-1} (W m^{-2})$^{-1}$; Peckol et al. (1988).
[j] µmol O_2 g (mg Chl)$^{-1}$ min^{-1} (W m-2)$^{-1}$; Dennison and Alberte (1982).
[k] For a similar species in Nova Scotia: *Laminaria longicruris*; Harlin and Craigie (1978).
[l] For another brown algae: *Fucus vesiculosus*; Pedersen and Borum (1997).
[m] Zimmerman et al. (1987).
[n] For another *Laminaria* species; Korb and Gerald (2000).
[o] For another brown algae *Fucus vesiculosus*; Pedersen and Borum (1997).
[p] Thursby and Harlin (1984).
[q] 0.5 l h^{-1}; "low gear", Powell et al. (1992).
[r] 2 l h^{-1}; Carver and Mallet (1990).
[s] We assumed the same $AE_P^{\varphi,i}$ as mussels (see t).
[t] Dowd 1997.

[u] Estimated from Hall et al. (1990) where fish were grown from 300 g to 2000 g in 6 months (assuming a 3.45 food conversion ratio).

[v] Hall et al. (1992) found ~23% of food ends in particle sedimentation. We assumed 5, 8 and 10% ending as sloppy-feeding detritus, uneaten pellets and faeces, respectively.

[w] Calculated to yield 10% of food ending in faeces (see u).

[x] Langdon and Newell (1990).

[y] Grant et al. (2008).

[z] Assumed so that there is 48% of food ending in ammonia + urea and that 30% of that is due to maintenance respiration (Rodehutscord and Pfeffer, 1999).

[aa] 30 ind m^{-2} (Schmidt and Scheibling, 2007) × 50 m strip × 200 m grid cell length.

[bb] 45 ind m^{-2} (Schmidt et al., 2011) × 20 m strip × 200 m grid cell length.

[cc] 190 ind m^{-2} (Schmidt et al., 2011) × 40000 m^2 per grid cell × 0.5 (assuming patchy distribution thus only 50% of the cell has seagrass).

[dd] 217 ind m^{-2} (Grizzle et al., 2008) × 8000 m^2 (assumed only 20% of grid cell covered with reefs) per grid cell.

[ee] 80 gdw m^{-2} (Carver and Mallet, 1990) × 40000 m^2 (grid-column area) ÷ 5 grid cells.

[ff] 8.5 fish m^{-3} (Hall et al., 1990) × 4000 m^2 (only 10% of grid cell contains cages) × 0.2 m average cell depth.

[gg] $m_k^{M1}(t=0)$; 38 cm (Schmidt and Scheibling, 2007) and conversions biometrics from Gevaert et al. (2008).

[hh] $m_k^{M2}(t=0)$; 0.09 kg N m^{-2} (Schmidt et al. unpublished data).

[ii] $m_k^{S1}(t=0)$; 0.004 kg N m^{-2} (Schmidt et al. unpublished data).

[jj] $m_k^{F1}(t=0)$; 31.7 mm = 0.05 gdw (Grizzle et al., 2008) = 0.337 g wet weight (conversion from USDA, 2008) and 2% N content of fresh weigh (Boucher and Boucherrodoni, 1988).

[kk] $m_k^{F2}(t=0)$; 55 mm = 9.94 g wet weight = 0.75 gdw (Ibarra 2003) and 7.79% N content of dry weight (Smaal and Vonck, 1997).

[ll] $m_k^{A1}(t=0)$; 300 g wet weight (Hall et al. 1990) using conversions in Hall et al. (1992).

2.2.5. Comparison of Model Results against Published Data

We assessed the fidelity of the hybrid ROMS model and our IBM module by assessing its ability to reproduce expected patterns of tracer concentrations and patterns in the biomass of macrobiota species (i.e. pattern-oriented modelling; Grimm and Railsback, 2005). We used multiple field studies researching interactions between species similar to the ones modelled in this study (see references in the results section) to generate a matrix with a total of 40 expected patterns (Figure 2-3), where each species could decrease or increase the biomass of other species. For example, filter-feeders were expected to decrease phytoplankton through grazing, and aquacultured fish were expected to increase phytoplankton through fertilization by the farm wastes. Then we compared the expected patterns against modeled results.

To objectively assess whether the presence of our modelled macrobiota produced spatial patterns in all other modelled variables, we ran six hybrid model simulations, each without one macrobiota species. Then, for each modelled variable, we calculated the percent increase (positive difference) or percent decrease (negative difference) with respect to the standard simulation that included all macrobiota species (Figure 2-3). To evaluate the effect of each macrobiota species on itself (i.e. self-regulation), we ran an additional six two-way coupled hybrid simulations, and six one-way coupled simulations (see below), each with only one macrobiota species. Then, for each macrobiota species, we calculated the percent increase/decrease of the two-way coupled simulation with respect to the one-way coupled simulation (Figure 2-3). We did the above calculations in a pixel-per-pixel basis, thus resulting in a map for every pair of analysed variables (Figure 2-3). However, we also calculated the percent increase or decrease averaged over the entire bay after excluding data showing negligible difference (i.e. from -1% to +1% difference). We established that a modelled species had an overall increasing effect on another species (symbol ▲ in Figure 2-3) if the difference averaged over the entire bay was positive. Similarly, we established an overall decreasing effect (symbol ▼ in Figure 2-3) if the bay-averaged difference was negative, and no effect (symbol ▬ in Figure 2-3) if the bay-averaged difference was zero. We repeated the assessment using the one-way coupled model to test

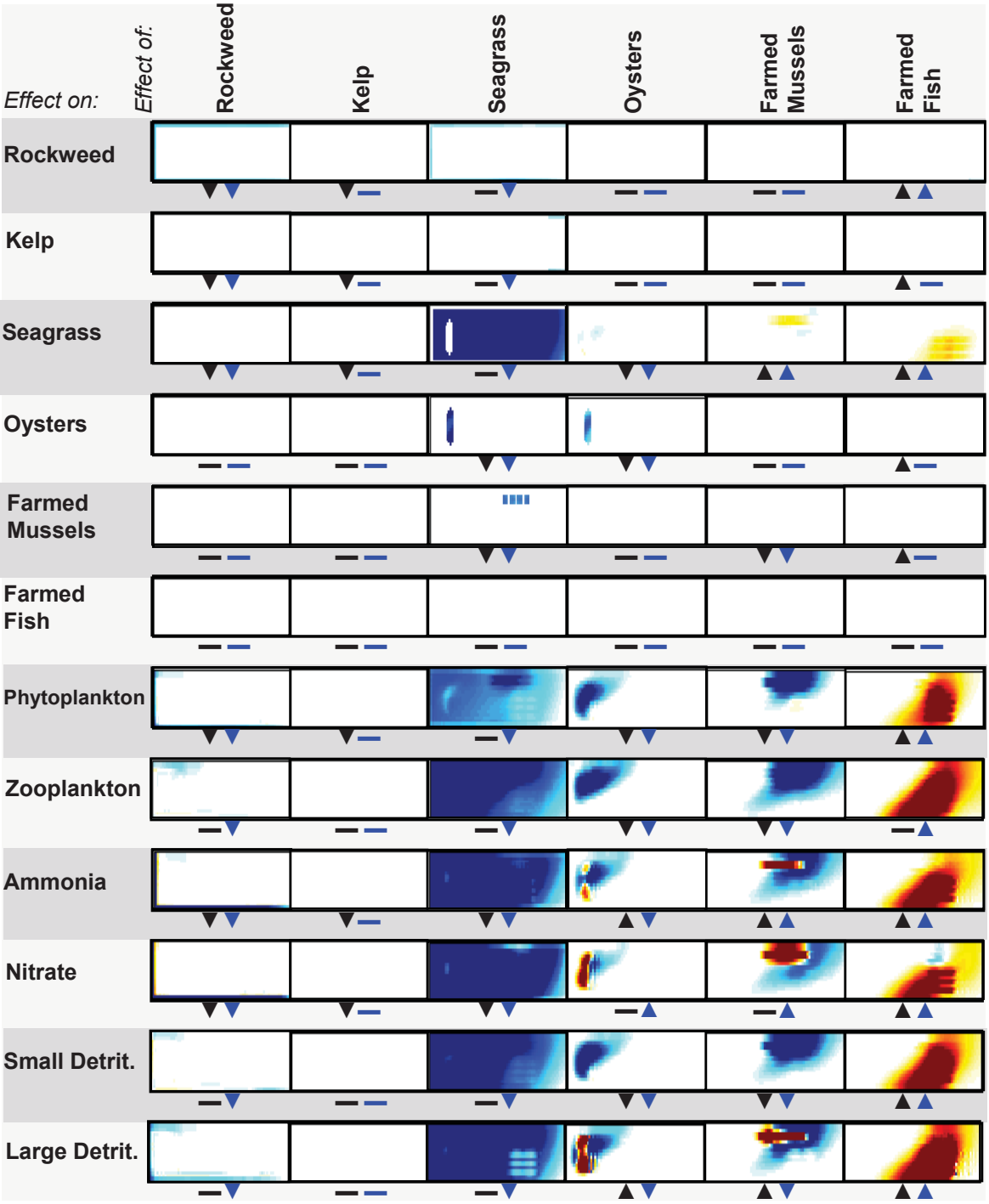

Figure 2-3. Expected vs. modelled patterns. Color plots are aerial views of the domain. Colours represent the enhancement (yellow to red) or depression (cyan to blue) effect that each macrobiota species had on all other biological variables. We also calculated the domain-averaged effect, which we represent using symbols for enhancement (▲), depression (▼) or no effect (▬). The first symbol of each pair (left) denotes the expected effect according to the literature (see results), and the second symbol (right) denotes the effect yielded by the two-way coupled (hybrid) model (see details in section 2.2.5 of the methods). The one-way coupled model did not produce any spatial patterns.

our hypothesis, and to demonstrate that none of the expected patterns can be reproduced using the one-way coupled model and thus emphasising that two-way coupling is essential in shallow water applications.

Finally, we utilize the procedure from Franks (2009) to assess the fidelity of the hybrid ROMS model, where we compared modeled rates of growth, assimilation, respiration and nutrient uptake, against published physiological rates for the specific species used in our application. Data used in validation was different from the data used in parameterization.

2.3. Results

2.3.1. Planktonic Ecosystem (Grid-based) Variables

After the one-month simulation with the two-way coupled ROMS hybrid model, the concentration of all the planktonic ecosystem tracers (i.e. nutrients, plankton and detritus) showed spatial gradients that resulted from interactions among macrofauna species, planktonic ecosystem variables and physical processes (Figure 2-4 and Figure 2-5, right panels). On the contrary, the concentrations of the planktonic ecosystem tracers from the one-way coupled model exhibited spatial variability that was solely caused by the influence of physical processes on the planktonic ecosystem (Figure 2-4 and Figure 2-5, left panels). The patterns in the spatial distribution of the planktonic ecosystem variables shown by the one-way coupled model are consistent with water entering the embayment through the open boundary, causing relatively strong gradients in all the planktonic ecosystem variables and resulting in the prominent feature at the seaward end of the embayment (Figure 2-4 and Figure 2-5, left panels). When we allowed the macrobiota to interact with the planktonic ecosystem variables (i.e. two-way coupled model), the spatial distribution of all of the planktonic ecosystem variables changed dramatically, yielding spatial features consistent with the presence of macrobiota.

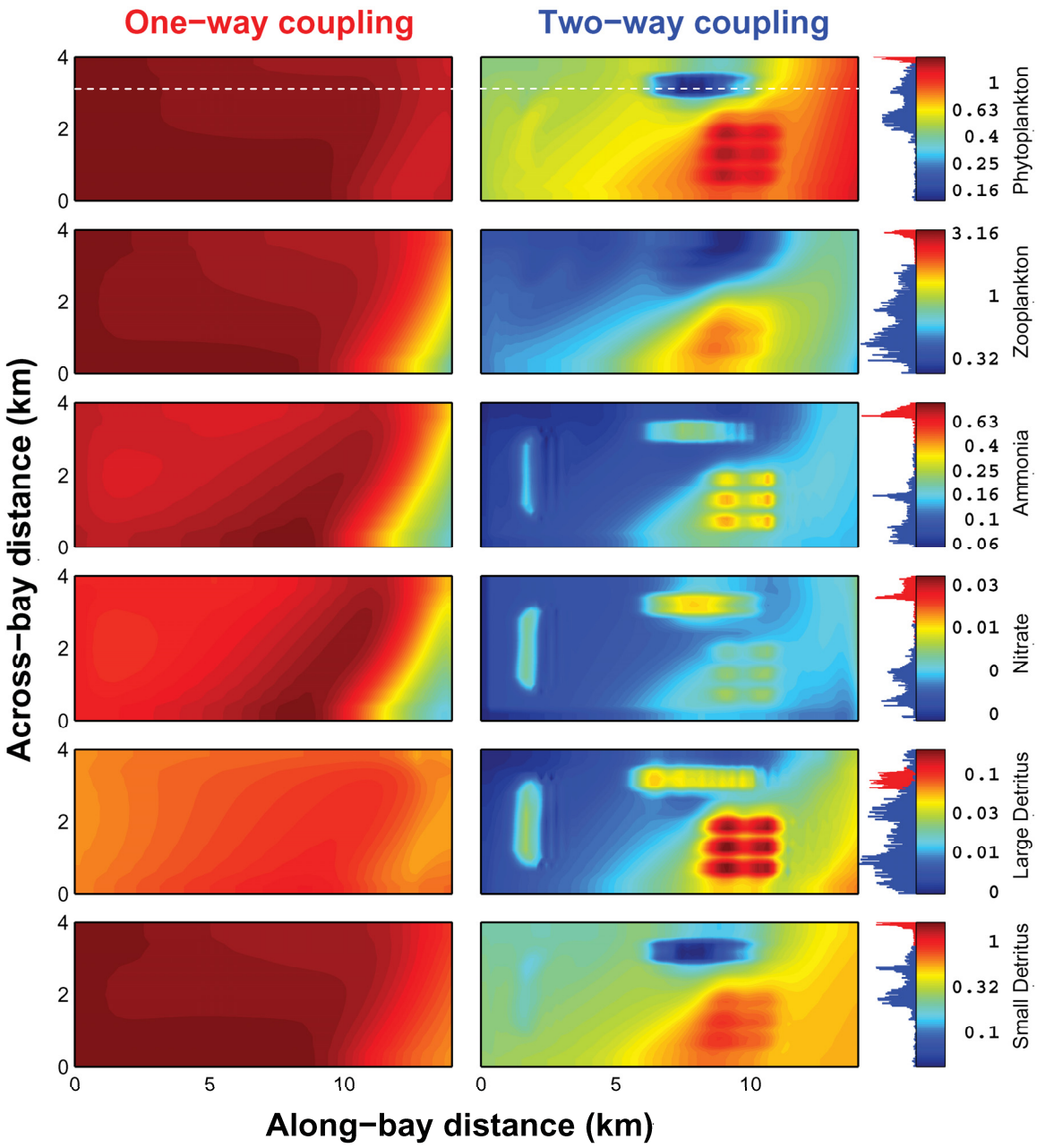

Figure 2-4. Color maps (top-view, middle of the water column) representing the concentration of different biological tracers (all units are in mmol N m^{-3}; note logarithmic scale). Left panels are results from the one-way coupled model and right panels are results form the two-way coupled (hybrid) model. On the color scale bars, there are histograms displaying the same data as in the color maps; one-way coupled model in red and two-way coupled (hybrid) in blue. The water dashed line represent the location of the transect shown in the next figure.

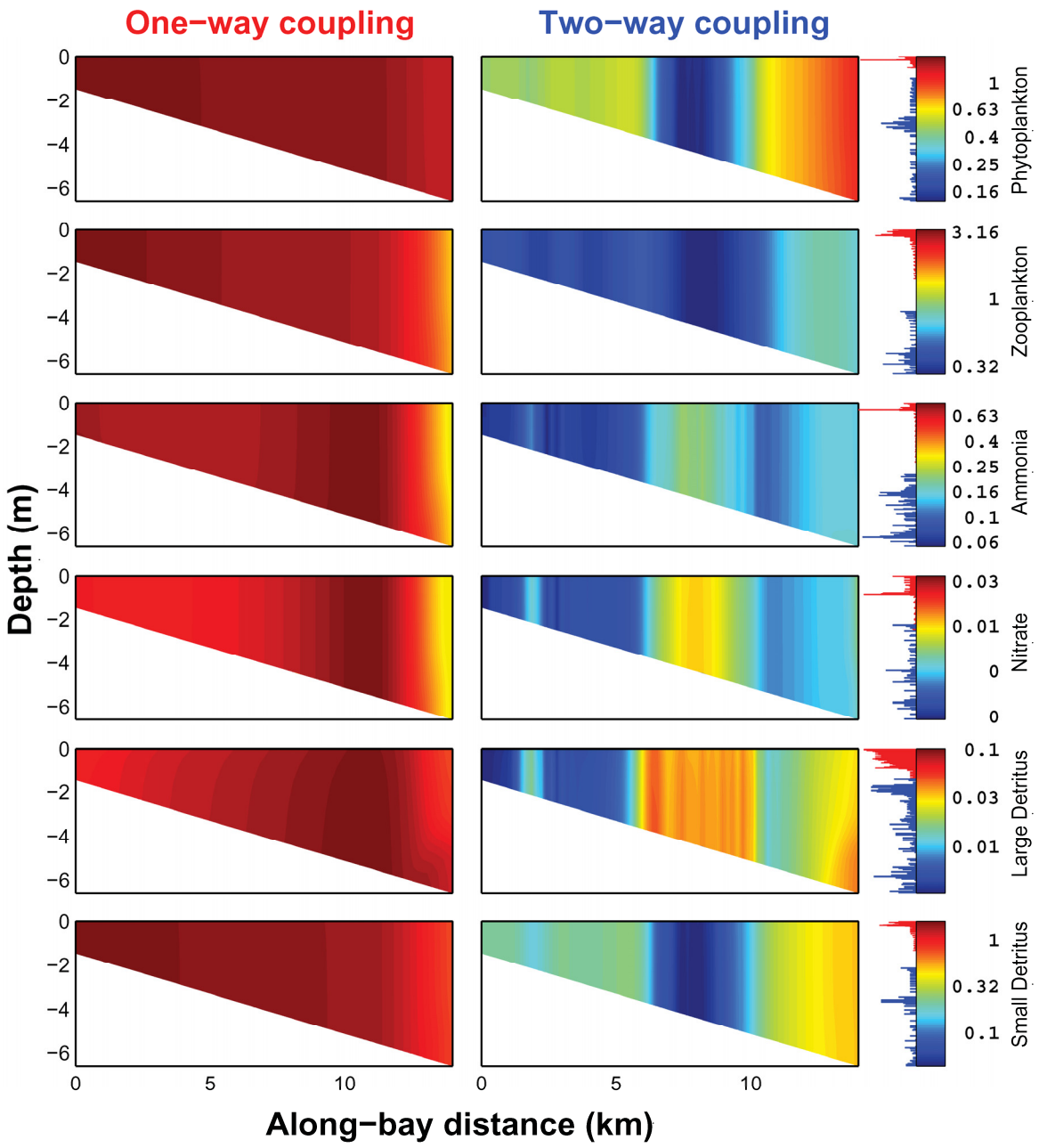

Figure 2-5. Caption is the same as in Figure 2-4, but from side-view.

The concentrations of biological tracers from the one-way coupled model were higher, but less variable, than the concentrations from the hybrid model (see histograms on the colour bars of Figure 2-4 and Figure 2-5). Most notably, the mean concentration of phytoplankton and large detritus from the one-way coupled model were doubled and tripled, respectively, compared to those from the two-way coupled model.

2.3.2. Macrobiota (Individual-based) Variables

The individual-based portion of our hybrid model tracked the biomass (and other properties) of each of the 1854 macrobiota super-individuals that we inserted throughout the domain for these simulations. Therefore, we were able to visualize the time-evolution of the biomass of each and all super-individuals of each macrobiota species (Figure 2-6, right panels), or to visualize the spatial distribution (at any given time) of their biomass (e.g. end of simulation, Figure 2-6, left panels), to assess the importance of location on the macrobiota dynamics. We also ran a one-way coupled version of our hybrid model, where we disabled the feedbacks between macrobiota and the planktonic ecosystem variables, to assess the differences between one-way and two-way coupling, and to establish the importance of these feedbacks. Both, the one-way and two-way coupled models, showed similar temporal dynamics (Figure 2-6, right panels), but the accumulation of biomass was greater in the one-way coupled model because food resources were never depleted.

In the simulation with the two-way coupled hybrid model, individual-based species (i.e. plants and most animals) grew at different rates creating spatial patterns in size (or density) among individuals of the same species (Figure 2-6, left panels). Aquacultured fish were the exception because all fish were fed equally and therefore grew at the same rate. All plants and animals (except farmed fish) showed high growth rates at the beginning of the simulation when nitrate concentration was high, and then rates decreased as nitrate was used up (Figure 2-6, right panels). Results from both, the two-way and the one-way coupled models, showed variability in growth among individual plants and animals (except farmed fish). Also, individuals of all species (except farmed fish) in the one-way

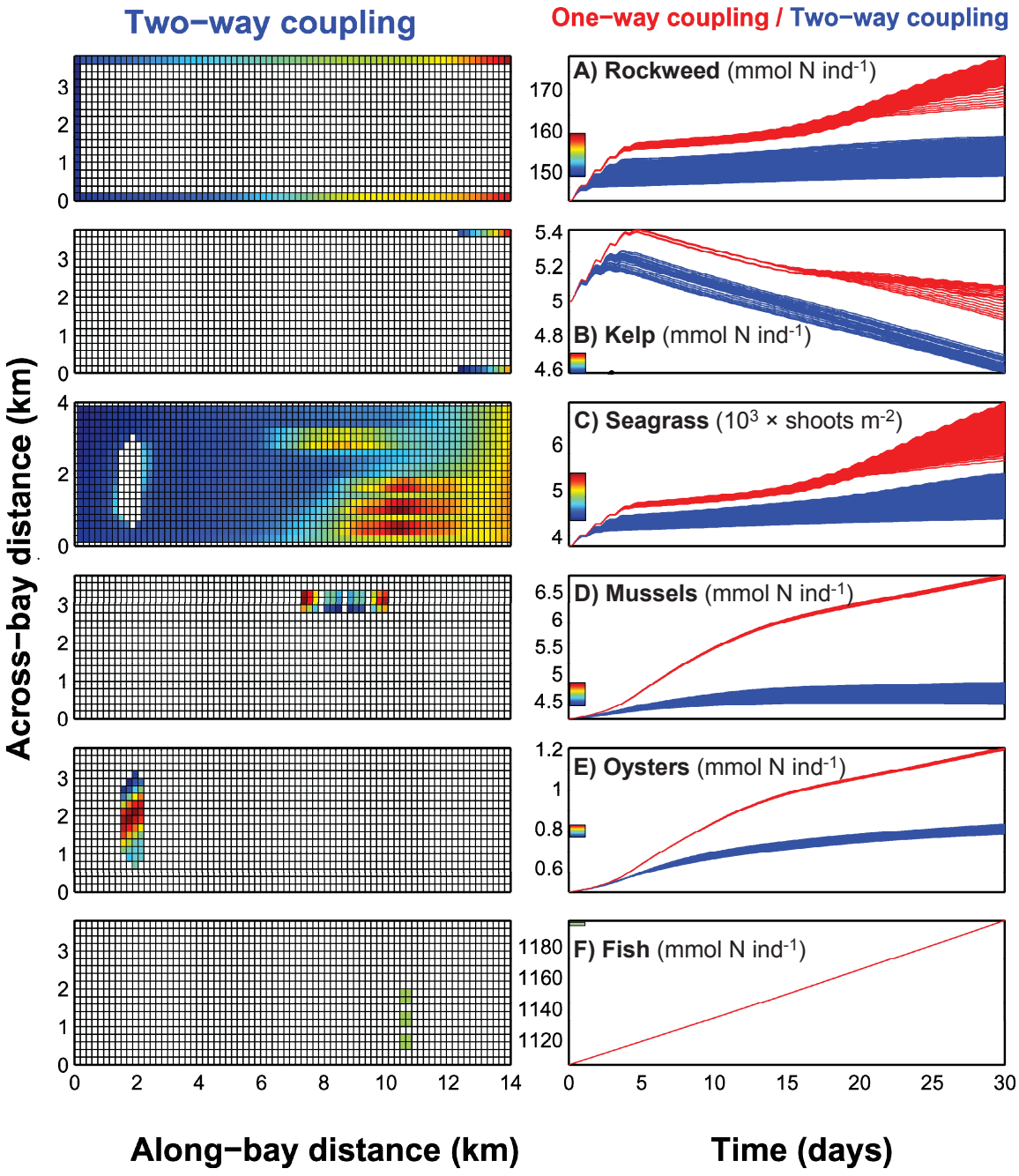

Figure 2-6. Right panels: Time-series of modeled biomass or density for different species (one-way coupled model in red and two-way coupled (hybrid) in blue). On each plot, each line represents the biomass trajectory of a single super-individual from the species ensemble. Left panels: Color maps (top view) of the biomass or density corresponding to the last time-step in the time-series produce with the two-way (hybrid) model. Respective colour bars are shown on the y-axis of the right panels.

coupled model grew to a total biomass 10 to 70% higher than those in the two-way coupled, during the same one-month simulation.

2.3.2.1. Rockweed and Kelp

In the hybrid simulation, rockweed individuals grew approximately three times faster towards the mouth of the bay than at the head of the bay because nitrate and ammonium concentration were higher at the mouth of the bay. The biomass of kelp only increased for a few days and then it decreased for the remainder of the simulation, losing about 10% of its biomass in less than one month (Figure 2-6). This is consistent with field measurements of kelp growth in Eastern Canada (Schmidt and Scheibling, 2007), where kelp erodes faster than it grows when nutrients are depleted (i.e. late spring and summer). Rockweed grew slightly faster (1%) on the area closest to the fish farm (Figure 2-3) due to higher ammonium concentrations produced by the fish (see section 2.3.2.4 Aquacultured fish).

In the two-way coupled model, rockweed locally reduced ammonium and nitrate concentrations (Figure 2-3), particularly along the southern shore. The reduction of nutrients due to uptake by rockweed and kelp also resulted in a local decrease in phytoplankton, zooplankton and detritus concentrations (Figure 2-3). Studies using mesocosms (Smith and Horne, 1988) and 3-D modelling (Trancoso et al., 2005) also found a decrease in phytoplankton biomass due to competition for nutrients by macroalgae. Rockweed also caused a slight decrease in the biomass of kelp and seagrass as a result of competition for nutrients (Figure 2-3). We are unaware of any field study assessing the competition for nutrients between rockweed and seagrass. However, it is known that in some places in Eastern Canada the macroalgae production is three times the production of phytoplankton (Mann, 1973), and therefore we suspect that the uptake of nutrients required to support such production of macroalgae may have some influence on the growth of adjacent seagrass.

In the one-way coupled model, rockweed and kelp achieved a higher biomass than in the hybrid model (approx. 13% and 10%, respectively); however spatial variability in bio-

mass was smaller than in the hybrid model. Because one-way coupling does not allow depletion of nutrients by rockweed, its growth did not cause any spatial patterns in any of the planktonic ecosystem or individual-based variables.

2.3.2.2. Seagrass

In the hybrid model, seagrass became denser around the mussel and fish farms and, to a lesser extent, around the natural oyster bed (Figure 2-6). We described the effect of bivalves and aquacultured fish in sections 2.3.2.3 and 2.3.2.4, respectively.

The presence of seagrass resulted in a decrease in the all the planktonic ecosystem variables as well as all individual-based species (except farmed fish). Seagrass beds are known to play an important role in controlling coastal biogeochemistry (Marbà et al., 2006), particularly because seagrass is very effective at removing nutrients from the water (Romero et al., 2006).

In the one-way coupled model, seagrass became 30% more dense than in the hybrid model after the one-month simulation. However, seagrass density was less spatially variable in the one-way model than in the hybrid model because of the inability of the model to represent feedbacks between macrobiota and tracers. Seagrass did not cause any spatial patterns in any of the planktonic ecosystem or individual-based variables in the simulations using the one-way coupled model.

2.3.2.3. Aquacultured Mussels and Wild Oysters

In the hybrid model, mussels grew twice as fast at the edges of the farm as in the farm center (Figure 2-6), because the middle of the farm became depleted in phytoplankton and small detritus due to extensive filter-feeding (Figure 2-3 and Figure 2-4). Similar gradients in mussel growth have been documented in field studies (e.g. Karayucel and Karayucel, 2000) and have been studied using models (Bacher et al., 2003; Grant et al., 2007). Since zooplankton feeds on phytoplankton, the local reduction in phytoplankton in

and around the farm (due to mussel feeding) resulted in a reduction in the concentration of zooplankton (Figure 2-3 and Figure 2-4). Similar to our results, Lonsdale et al. (2009) found in a shallow coastal embayment that resource competition between bivalves and zooplankton can result in periods when zooplankton biomass is regulated by bivalve filtration.

Mussels produced a local increase of ammonia inside the farm (Figure 2-3 and Figure 2-4) due to (1) excretion of ammonia by mussels, (2) benthic remineralization of mussel faeces, and (3) reduced uptake by phytoplankton resulting from the low phytoplankton abundance in the farm. However, surrounding the area of increased ammonia was a larger area where the effects of mussels reverted to a decrease in ammonia (Figure 2-3 and Figure 2-4). The decrease in ammonia in the far-field area (i.e. area surrounding the farm) was smaller than the increase in ammonia inside the mussel farm, therefore mussels overall increased ammonia in the system. The far-field decrease in ammonia (and all other planktonic ecosystem variables) is a result of the decreased zooplankton due to depleted phytoplankton, which in turn lowered detritus, and ultimately lowered ammonia. Field studies of nutrient dynamics in bays with mussel farming showed findings that are in agreement with our modelling results (Strain, 2002; Cranford et al., 2007).

Similarly to the patterns in ammonia, the concentration of large detritus was also increased inside and near the mussel farm, but was decreased in the far-field area surrounding the mussel farm (Figure 2-3 and Figure 2-4). Results from field and modelling studies (Grant et al., 2005; McKindsey et al., 2009) are in agreement with our findings.

Although nitrate was found at very low concentrations everywhere in the bay, nitrate was higher within the mussel farm due to the decreased uptake resulting from the lower phytoplankton concentration within the farm, and some inhibition of nitrate uptake by ammonium. To our knowledge, the effect of farmed mussels on nitrate has not been studied.

Similarly to the farmed mussels, the wild oyster reef caused a local increase of ammonia, nitrate and large detritus, a local decrease of phytoplankton, zooplankton and small detritus, and a far-field decrease in all planktonic ecosystem variables (Figure 2-3). When averaged over the entire bay, oysters caused an increase only in nitrate and a decrease in all other variables (Figure 2-3). However, the results from the hybrid model with all macrobiota species (Figure 2-4) showed a higher concentration of phytoplankton inside the oyster reef, which corresponded to a higher oyster growth in the center of the reef compared to the edges of the reef (Figure 2-6). We speculate that these patterns may have been caused by the absence of seagrass, rather than by the presence of oysters. That is, we think that the absence of nutrient uptake by seagrass inside the oyster reef resulted in higher phytoplankton growth inside the reef (i.e. compared to the area outside the reef, which was occupied by seagrass; Figure 2-6), which in turn resulted in higher oyster growth. Simulations with and without the feedback between oysters and tracers (Figure 2-3) showed that oysters had a decreasing effect on themselves (i.e. self-limitation) as well as on the surrounding seagrass.

The effect of bivalves on seagrass is not straightforward: In close proximity to the bivalves, we speculate that seagrass growth was enhanced (Figure 2-3) partially due to the increased light penetration resulting from the depletion of seston by filter-feeding, but mainly due to the increase in nutrient concentrations resulting from bivalve excretion and remineralization of faeces. However, a few hundred meters away from the bivalves, seagrass growth was depressed (Figure 2-3) because the water downstream and around the bivalve region was impoverished in ammonium and nitrate. Also note that our model did not account for epiphytes, which—in regions of increased nutrient concentrations—can grow to the point of limiting light availability to seagrass (Short et al., 1995).

Seagrass grew slightly denser immediately around the oysters (Figure 2-6). In agreement with our results, mesocosm studies found an enhancement of seagrass productivity associated with suspension-feeding bivalves (Wall et al., 2008), and Smith et al. (2009) modeled and showed a positive effect of oyster reefs on seagrass due to increased light penetration and decreased wave height (breakwater-effect); however, they did not include nu-

trient dynamics in their model. Contrarily to our results, transplant studies found that seagrass grew less dense close to oysters beds (Kelly and Volpe, 2007). In summary, the effect of bivalves on seagrass depends on the scale and location of interest. In our study, when averaging over the entire bay, mussels enhanced seagrass while oysters decrease it.

At the end of the one-way coupled simulation, mussels and oysters were remarkably larger (by approx. 50% and 70%, respectively) than those in the hybrid model (Figure 2-6); however the variability in individual biomass was smaller in the one-way coupled simulation. Both patterns can be related to the lack of seston depletion inside the mussel farms or oyster reefs. This reinforces the notion that two-way coupling between filter-feeders and their food is essential in aquaculture and ecosystem models in shallow regions (Grant et al., 2008).

2.3.2.4. Aquacultured Fish

Since all fish were subject to the same feeding regime, each grew at exactly the same rate. However, the external feeding inputs had visible effects on all biological tracer variables (Figure 2-4 and Figure 2-5) and on the growth of many species of individual organisms (Figure 2-6). The concentrations of all biological tracers were increased inside the fish farm and beyond farm boundaries, with visible effects over half of the embayment (Figure 2-3 and Figure 2-4). Concentrations of phytoplankton, ammonia, nitrate and detritus (large and small) were particularly increased in the water parcels located inside the farm during periods of minimal current speed at high and low tide stages (Figure 2-4). Sanderson et al. (2008) conducted a survey around salmon cages in Scotland and found spatial patterns in ammonia concentration similar to our model results; with higher concentrations close to shore and in shallower regions. In both, Sanderson et al. (2008) and here, the concentration of ammonia near the farm was about 5 times larger than the far-field concentration. Our results are also in agreement with other modelling studies showing spatial patterns of deposition of solids inside and around marine finfish farms (Cromey et al., 2002; Cromey et al., 2009). The effect of fish farms on zooplankton is currently poorly understood.

Phytoplankton, seagrass, and rockweed grew faster in areas enriched with ammonia and nitrate originating from fish feed. Field studies assessing the effect of fish farms on adjacent seagrass (e.g. Holmer et al., 2008; Apostolaki et al., 2009), showed that enrichment of organic matter in sediments and anoxia can harm nearby plants. However, our model does not account for oxygen limitation on plants and thus was unable to reproduce such effects. On the other hand, there is an increasing interest in the effect of fish farms on aquacultured macroalgae, where algae are grown around farms because of faster growth (i.e. increased profit), but also because it removes fish-produced nutrients (Chopin et al., 2001; Carmona et al., 2006; Abreu et al., 2009).

Since our ecophysiology model for aquaculture fish did not include dependencies of fish growth on any tracer variable, fish in the one-way coupled model grew at exactly the same rate as in the hybrid model. However, only the hybrid model was able to reproduce the impact of fish on water-column variables (Figure 2-4 and Figure 2-5).

2.3.3. Ecosystem Properties

Time-series of all biological tracer variables and of the total biomass of all individual-based species were calculated using the two-way coupled hybrid model and the one-way coupled model (Figure 2-7). In both models, tracer variables showed short-term variability (hours to days), while individual-based variables showed longer-term variability (days to weeks).

In the two-way coupled hybrid model, total nitrogen remained constant around 1.78×10^{10} mmol N, with small oscillations due to tides through the open boundary (Figure 2-7C). At the end of the simulation, 94% of total nitrogen in the bay was stored in individual-based species, while tracer variables accounted for only a small (6%) fraction of the total nitrogen.

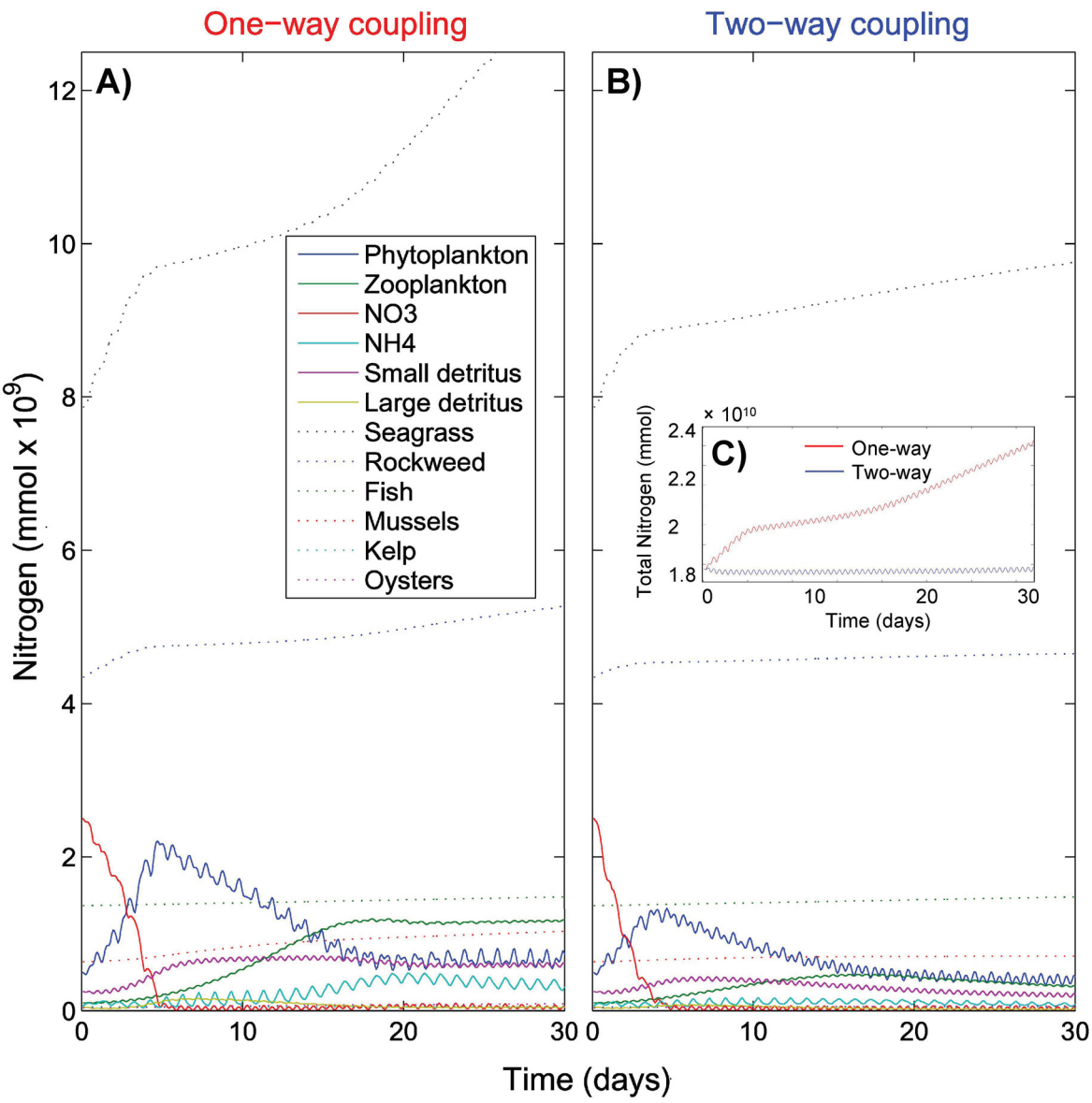

Figure 2-7. Time evolution of all ecosystem variables from one-way coupled model (panel A) and the two-way coupled (hybrid) model (panel B). Tracer variables (solid lines) describe the planktonic ecosystem and individual-based variables (dashed lined) describe macrobiota. Panel C (insert in right panel) shows the total nitrogen in the system (i.e. sum of all ecosystem variables). Note that total nitrogen is conserved with the two-way coupled model (blue) while the one-way couple model spuriously increases by 33% (red).

At the end of the one-month simulation with the one-way coupled model, all variables (individual-based and grid-based) were remarkably higher than those in the two-way coupled model. As a consequence of the lack of feedbacks between macrobiota and the planktonic variables, total nitrogen in the one-way coupled ecosystem spuriously increased throughout the one-month simulation from 1.78×10^{10} mmol N to 2.4×10^{10} mmol N (Figure 2-7C). At the end of the one-way coupled simulation, 88% of the total nitrogen in the bay was stored in individual-based species, while tracer variables accounted for 12% of the total nitrogen; however this results must be viewed with caution because nitrogen was not conserved. Our study exemplifies how models that use one-way coupling between biogeochemistry and macrobiota are not mass-conserving and could cause spurious results (Fennel, 2008), particularly when applied to shallow water environments.

2.3.4. Comparison of Model Results against Published Data

We compared diagnostic physiological rates calculated with ROMS against measured rates for the same species in comparable field scenarios. The model was able to resolve short-scale variability (hours to days) of physiological rates, which are a result of short-scale variability in solar irradiance, in the concentration of biological tracers, and in the degree of resource limitation experienced by each super-individual. Published rates were often calculated using much coarser temporal and spatial resolutions, and they are not expected to show the level of variability shown in the model. All physiological rates calculated with ROMS were within the range of measured rates (Figure 2-8).

We also assessed the model based on its capacity to match expert knowledge; that is, to reproduce patterns seen in field studies (i.e. expected patterns). Based on the literature, we expected to see 40 patterns resulting from the increasing or decreasing effect of macrobiota species on other individual-based or grid-based variables. Out of the 40 expected patterns, 9 modelled results showed negligible effects (i.e. between -1% and +1% difference) and 28 patterns were reproduced as expected. In three cases the model behaved opposite to the expectation: (1) oysters were expected to increase ammonia, which they did

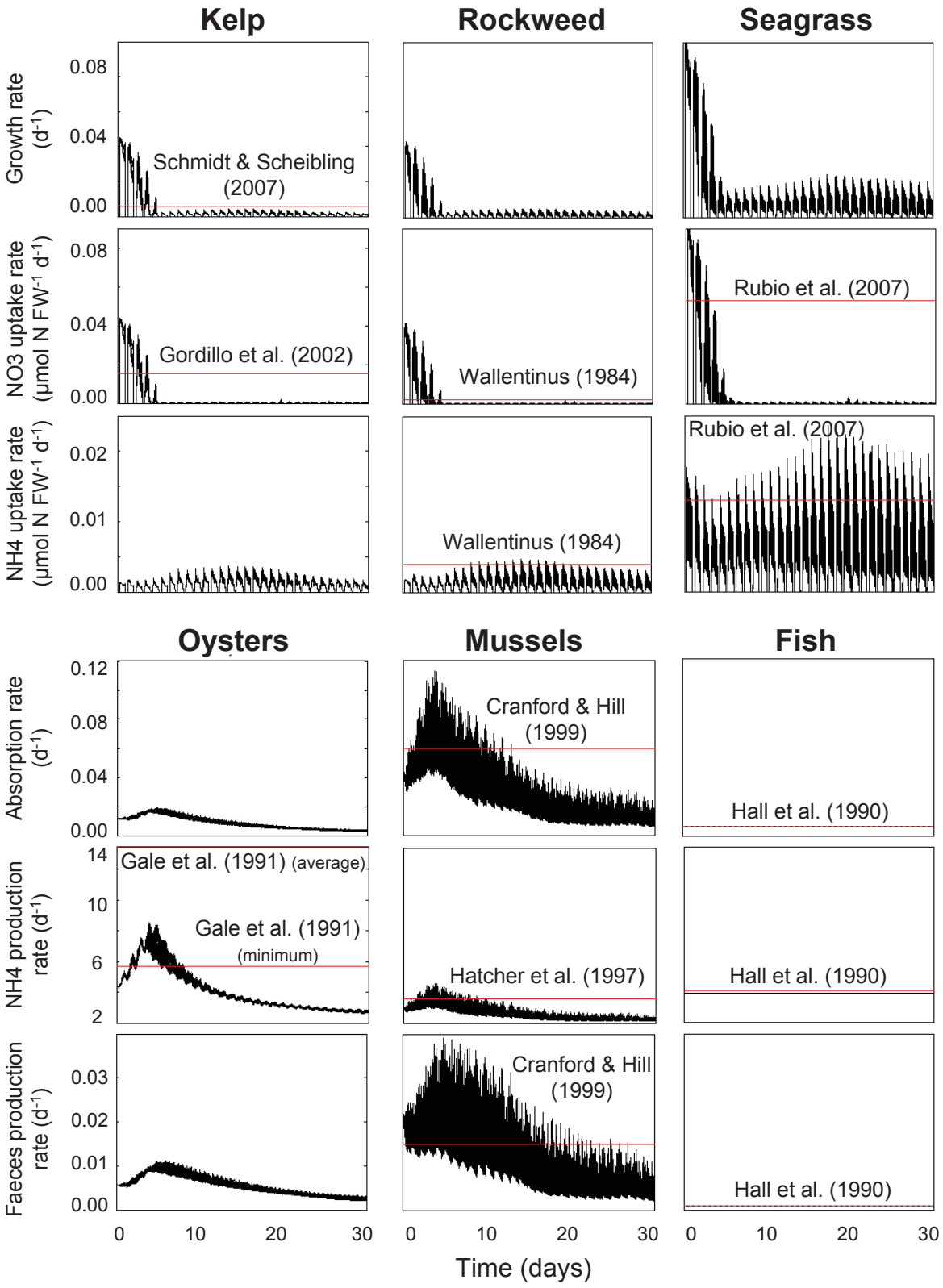

Figure 2-8. Black lines represent diagnostic physiological rates, modelled with the two-way (hybrid) model, for different macrobiota species (one line per super-individual). Red lines are comparable rates from the literature.

inside the oyster bed, but the far-field decrease in ammonia (Figure 2-3) was greater that the increase inside the oyster bed and therefore the total effect of oysters was a decrease in ammonia; (2 and 3) oysters and mussels were expected to increase large detritus, which they did inside the oyster reef and mussel farm, but again, the far-field decrease in large detritus was greater than the local increase. In retrospect, the results from these three mismatches make sense: the plume of phytoplankton-depleted water causes a trophic cascade of decreases in zooplankton, detritus and ultimately nutrients. These mismatches are, in fact, new hypotheses that may direct future research about the far-field effect of bivalve filter-feeding. There were 13 cases where no effects were expected but the model showed enhancing or decreasing effects (Figure 2-3).

Results from the one-way coupled model were unable to reproduce any of the expected spatial patterns. This emphasizes that two-way coupling is essential in shallow water applications.

2.4. Discussion

The goal of this study was to demonstrate that—in shallow environments—modelling macrobiota and planktonic ecosystem dynamics simultaneously, produces fundamentally different results than modelling them separately. Specifically, we tested the hypothesis that a two-way coupled model applied to a shallow coastal embayment with wild and farmed macrobiota species, will (a) significantly alter the planktonic food web structure, and (b) create spatial gradients in biomass of the macrobiota species.

2.4.1. Importance of Two-way Coupling of Macrobiota and Planktonic Ecosystem Variables in Coastal Ecosystem Models

2.4.1.1. Effects on Planktonic Ecosystem Variables

Results from our (two-way coupled) hybrid model showed that macrobiota can play a major role regulating the magnitude and spatial/temporal variability of the concentration of planktonic ecosystem tracers (i.e. nutrients, plankton and detritus) in coastal embayments (Figure 2-4 and Figure 2-5). This is consistent with findings of a fine-scale field survey in a coastal tropical embayment (Miyajima et al., 2007), where small-scale patches in chlorophyll and ammonia concentrations where detected over small patches of seagrass and coral reefs, respectively. Also Grant et al. (2008) and Ibarra (Chapter 3) have reported gradients in the concentration of phytoplankton caused by intense filter-feeding pressure from mussel farming.

Our modelling results also showed that aggregations of macrobiota can affect the nitrogen budget among the planktonic ecosystem tracers (Figure 2-7). A simulation from a one-way coupled version of our model—which can be interpreted as a planktonic ecosystem model running without macrobiota—resulted in higher concentrations of all the planktonic ecosystem variables, compared to the two-way coupled simulation (Figure 2-4 and Figure 2-5). In the two-way coupled model, the available nitrogen was shared among the macrobiota and the planktonic ecosystem variables, thus resulting in lower concentrations of all the planktonic ecosystem variables, and also in less nitrogen stored in the planktonic ecosystem tracers, compared to the simulation without macrobiota. Therefore, in shallow regions, planktonic ecosystem models that do not account the bilateral interactions between macrobiota and planktonic ecosystem variables, may overestimate the concentrations of all the planktonic ecosystem tracers.

2.4.1.2. Effects on Macrobiota Variables

Our hybrid model also showed that the gradients in tracer concentrations affect the physiology of macrobiota species, resulting in spatial gradients in their biomass. In other words, the spatial heterogeneity in planktonic ecosystem tracers caused by macrobiota also regulated the distribution of the macrobiota itself. Similar spatial gradients in growth and biomass have been observed in a mussel farm (Karayucel and Karayucel, 2000; Strohmeier et al., 2008).

Our modelling results also showed that two-way coupling of macrobiota and planktonic ecosystem variables is important in the estimation of the nitrogen budget among the macrobiota variables (Figure 2-7). A simulation from a one-way coupled version of our model—which in this case is interpreted as using the output of a planktonic ecosystem model to force a separate macrobiota model—resulted in higher concentrations of all macrobiota variables, compared to the two-way coupled simulation (Figure 2-4 and Figure 2-5). At the end of the one-way coupled simulation, the nitrogen stored in every macrobiota variable was higher than the results from the two-way coupled simulation. Therefore, macrobiota modelling studies should account for two-way interactions with planktonic ecosystem variables, and models that fail to do so may overestimate the concentrations of all macrobiota variables.

2.4.1.3. Effects on the Overall Mass-balance of the System

In shallow regions, modelling macrobiota and planktonic ecosystem dynamics separately (i.e. one-way coupling) generates results that are not mass-balanced. That is, the total nitrogen in the system spuriously increases over time (Figure 2-7C), due to the overestimation of both, macrobiota and planktonic ecosystem variables. For now, it is still a common practice to use the output of a planktonic ecosystem model to force food-web models representing the dynamics of higher-trophic macrobiota (i.e. one-way coupling; e.g. Cerco et al., 2010). However, there are increasingly more studies focusing efforts on the implementation of feedbacks from higher-trophic macrobiota to planktonic ecosystem dynamics (e.g. Steele and Ruzicka, 2011).

2.4.1.4. Implications for Food-web Stability and Long-term Ecosystem Predictions

In nature, two-way feedbacks have been found to be a fundamental requirement for the stability of complex food webs (Rooney et al., 2006; Neutel et al., 2007). It is not surprising that the stability of modelled food webs is also dependent on the ability of the model to represent two-way interactions among modelled species. Therefore, new trends in marine ecosystem modelling are calling for a more complete representation of the food web structure, by increasing the number of interacting components of the ecosystem, and feedback loops connecting them (Hannah et al., 2010). Also, researchers studying ecological networks are calling for metabolically-driven individual-based models that involve a large number of species (Ings et al., 2009).

2.4.1.5. Applications for Integrated Multi-Trophic Aquaculture

Generally speaking, all areas of aquaculture research, management and regulation should consider using spatially-explicit models that realistically couple the dynamics of aquacultured macrobiota with the planktonic ecosystem dynamics. However, there is an acute need for this type of modelling in Integrated Multi-Trophic Aquaculture (Barrington et al., 2009), where multiple species of different trophic levels are farmed in proximity of each other with the purpose of maximising yields while minimising environmental impacts. Quantitative and spatially-explicit information about planktonic ecosystem variables is key when deciding where and how far apart to rear one species with respect to the others (e.g. Reid et al., 2010). A recent study about the effect of bivalves on finfish farms (Navarrete-Mier et al., 2010) came under public criticism (Troell et al., 2011) because the authors neglected to consider the role of hydrodynamics, the impact of plumes of nutrients, and the response of primary producers. This is an example of how a sizable field survey (Navarrete-Mier et al., 2010)—without an appropriate model to fill in the gaps—arrives at conclusions that may or may not be correct, but that are certainly challengeable. End-to-end models that include hydrodynamics, planktonic ecosystem dynamics and

aquacultured macrobiota can be very useful in providing information to support or reject these types of research hypotheses.

2.4.2. Benefits of Hybrid Ecosystem Modelling

2.4.2.1. An Efficient Solution to Multi-species Integration

One challenge ahead is to develop modelling technologies that can handle the increased computational load demanded by modelling feedback loops among a large number of species in a 3-dimensional space. Here we argue that the hybrid approach may be the most appropriate approach to model a large number of species, by representing abundant and ubiquitous species with a grid-based model and rare species with an individual-based model.

In the hybrid model presented here, we represented six macrobiota species using the individual-based model, which required 1854 solutions of the ecosystem equations every time-step. Representing the same six species using a grid-based model would have required solving the ecosystem equations 84000 times every time step (i.e. number of cells × number of species, or 14000 × 6). Therefore the individual-based model only used 2.2% of the computations required to represent the same species with a grid-based model. On the other hand, we represented two abundant species (i.e. phytoplankton and zooplankton) using the grid-based model, which needed to solve the ecosystem equations 28000 times every time step. Representing abundant species using an individual-based model requires the addition of enough individuals to ensure that every grid cell has enough individuals to represent the species dynamics. Even if we only add 1 individual for every 100 m^3 of water, the individual-based model would have required to solve the ecosystem equations almost 4.5×10^6 times every time-step (i.e. number of cells × number of individuals per cell × number of species, or 14000 × 160 × 2). Therefore the grid-based model only used 0.6% of the computations required to represent the same two abundant species with the individual-based model.

Our hybrid ecosystem framework was thus able to represent the ecosystem dynamics using only 27% of the calculations needed by a grid-based model alone to represent the same ecosystem, or only 0.6% of the calculation needed by an individual-based model alone to represent the same ecosystem. The hybrid approach may be the most adequate approach to represent multiple species from across trophic levels, sizes and abundances.

2.4.2.2. A Hypothesis Testing Tool to Assess the Effect of Individuals on the Planktonic Ecosystem

Ecosystem models have been recognized as powerful tools to create and test hypotheses (Franks, 2009; Neuheimer et al., 2010). Eulerian models are adequate to test hypotheses of the effect of one tracer variable on the others (e.g. impact of zooplankton grazing on phytoplankton dynamics). In addition, individual-based models forced with the output of an Eulerian planktonic ecosystem model may be adequate to test hypotheses regarding the effect of tracer variables (e.g. phytoplankton concentration) on individual-based variables (e.g. larvae survival), especially when the research question focus on the processes such as transport over trophic dynamics. However, hypotheses regarding the effect of individual-based variables of macrobiota on planktonic ecosystem dynamics can only be tested using hybrid ecosystem models. Effectively, hybrid ecosystem models enable researchers to take results from laboratory experiments (e.g. filtration rate of fish larvae) and extrapolate them to an entire bay, to test whether they can explain the observed patterns.

Although the proposed framework is aimed to the development of models with high trophic resolution (i.e. many species or functional groups), it must be remembered that the increase of model complexity needs to be done gradually (Anderson, 2005) and with care of not surpassing the our ability to constrain the model with observations (Denman, 2003).

2.5. Conclusions

We presented a hybrid-ecosystem modelling framework, where ROMS simultaneously operates two ecosystem models: (1) a grid-based ecosystem model that represents planktonic ecosystem variables (i.e. nutrients, plankton and detritus) and (2) an individual-based ecosystem model that represents larger or higher-trophic level species (e.g. filter-feeders, macroalgae and fish). The hybrid framework allows for two-way interactions between the tracer- and individual-based models and therefore is strictly mass balanced.

We also applied the ROMS hybrid-ecosystem framework in an idealized embayment typical of Eastern Canada and found that—when accounting for two-way and mass-balanced interactions in shallow regions—the inclusion of wild and aquacultured macrobiota species significantly decreases the concentration of all planktonic ecosystem variables (i.e. plankton, nutrients and detritus) and all macrobiota variables (i.e. biomass of seagrass, macroalgae and bivalves). The two-way coupling also allows the creation of spatial gradients in biomass of the macrobiota species. Our findings suggest that future ecosystem modelling efforts in shallow coastal regions should account for macrobiota species (wild and/or aquacultured), using two-way and mass-balanced coupling.

Our results also showed that—in shallow coastal regions—two-way and spatially-explicit coupling are essential to reproduce planktonic ecosystem and macrobiota dynamics. However, one-way coupling between grid-based species and individual-based species may be sufficient to reproduce processes of interest in applications where the biomass of tracers is significantly larger than the biomass of individuals (e.g. fish larvae studies, when concentrations of larvae are too low to significantly affect concentrations of plankton). Although even in these cases two-way coupling may capture a new range of dynamics that may provide insight on the effect of fishing and climate change on fish populations (Travers et al. 2009).

The capabilities of the ROMS hybrid-ecosystem framework should be useful in the environmental management of any aquaculture operation (Henderson et al., 2001), particu-

larly in the design and management of Integrated Multi-Trophic Aquaculture. The hybrid ROMS can assist on the spatial planning of polyculture farms by estimating the production yields of the different aquacultured species, grown under different farm configurations. It can also be used to estimate the potential impact that the aquaculture species may have on the nearby wild macrobiota.

The ROMS hybrid-ecosystem framework is a 3-D, mass-balanced model optimized to efficiently represent interactions between physical, biological (lower- and higher-trophic levels) and anthropogenic processes in end-to-end models. But more importantly, the framework represents a path towards the unification of the previously separated disciplines of planktonic ecosystem, fisheries and aquaculture modelling (Travers et al., 2007; Cury et al., 2008; Moloney et al., 2011).

CHAPTER 3

Coupling 3-D Eulerian Bio-physics (ROMS) with Individual-based Shellfish Ecophysiology (SHELL-E): A Hybrid Model for Carrying Capacity and Environmental Impacts of Bivalve Aquaculture

3.1. Introduction

Bivalve aquaculture is growing exponentially worldwide, representing about 65% of total marine aquaculture production and about 11% of total seafood produced for human consumption (statistics for 2009; FAO, 2010). If this industry is to expand in a sustainable manner, it is imperative to understand and quantify (1) the effect of farmed bivalves on the environment, (2) the influence of environmental conditions on the production of bivalves, and (3) the relevant feedbacks between bivalves and the environment.

Following the expansion of bivalve aquaculture, the development of models that represent bivalve-environment interactions has also been growing rapidly during the last three decades (e.g. Incze et al., 1981; Fréchette et al., 1989; Dowd, 2003; Bacher and Gang-

[*] This chapter comprises a co-authored manuscript by D. A. Ibarra, K. Fennel, J. J. Cullen. The contribution of the author of this thesis to this manuscript includes the development of a shellfish ecophysiological model (SHELL-E), data analysis, and manuscript writing. K. Fennel provided some of the model forcing, and K. Fennel and J. J. Cullen contributed with guidance and multiple rounds of corrections.

nery, 2006; Grant et al., 2008; Grangeré et al., 2010). Although these models have diverse focuses and approaches, they all fall into two basic categories: (1) Eulerian or grid-based models, or (2) Lagrangian or particle-based models.

Eulerian or grid-based models track variables inside fixed volumes of space (i.e. boxes or grid cells). They are the model of choice to simulate variables that behave like tracers (e.g. temperature, phytoplankton concentration, etc.), where a single average value represents the state inside a whole box or grid cell (Lande and Lewis, 1989), and where exchanges among boxes or grid cells, along with changes within the box, are used to represent the dynamics everywhere within the gridded model domain. Eulerian models are by far the most commonly used models representing bivalve-environment interactions. The first models described the interactive influences of bivalve filtration and water currents on the concentration of phytoplankton in 1-D horizontal (Incze et al., 1981; Rosland et al., 2011) and vertical (Fréchette et al., 1989; Duarte et al., 2008) scenarios. Later models also included primary productivity and other lower-trophic level dynamics; however, a single box (i.e. 0-D model) was used to represent an entire bay (e.g. Dowd, 1997; Dame and Prins, 1998). Some newer studies use an individual growth model forced with environmental data (Bourles et al., 2009; Rosland et al., 2009). Meanwhile, the spatial resolution of other bivalve-environment models has increased over the years from 2-D box models (Grant et al., 2007; Troost et al., 2010), to 2-D models with fine grids (Duarte et al., 2003; Grant et al., 2008; Grangeré et al., 2010; Guyondet et al., 2010), to fine grids in 3-D (Marinov et al., 2007; Spillman et al., 2008; Leon et al., 2011, this study). These bivalve-environment models differ: for example, some estimate bivalve growth using Scope-For-Growth sub-models (SFG; Bayne et al., 1976), while others use Dynamic Energy Budget theory (DEB; Kooijman, 1986; 2000). However, all these models use the Eulerian framework, with domains divided in boxes or grid cells, and with variables representing the average state in each box or cell. Bivalves inside grid cells are also represented as an average concentration; however, unlike conventional Eulerian tracers (e.g. plankton concentration or temperature), the concentration of bivalves is not subject to transport by advection and turbulent diffusion processes. Moreover, if the Eulerian model is designed with many size-classes, each class would be defined with its own state vari-

able. For bivalves to grow from one size-class to the next one, each time-step some mass has to be subtracted from the smaller class and added to the larger class.

Lagrangian* or particle-based models track variables associated with sparsely distributed particles. Each particle usually represents a separate individual, thus particle-based models are often called individual-based models (IBMs; Grimm and Railsback, 2005). Commonly, 2-D and 3-D individual-based models are used to study larval dynamics (fish larvae: see review Miller 2007; bivalve larvae: North et al. 2008, 2010). The majority of these IBM models are forced with output from an Eulerian bio-physical model (i.e. one-way coupling). These IBM models allow the particles (each representing an individual larva) to "drift around", thereby experiencing different environmental conditions, like temperature, plankton concentration, etc. As each particle encounters different environmental conditions, the variables tracked for each particle (e.g. larval biomass or larval size) also evolve differently, depending on their surroundings. At the end of the simulation, the variables tracked for all particles are used to compute the properties of the entire system (e.g. total larval biomass, or larval abundance in a particular region). Therefore, system properties are said to "emerge" from the properties of the individual particles (Grimm and Railsback, 2005). For example, in an IBM with bivalves of different sizes, the model would track the size of each bivalve as it grows over time. Then, after the simulation is finished, the size of all the bivalves can be binned into size-classes to assess the evolution of size structure over time.

One-way coupled IBMs allow individuals to react to environmental variability, arguably better approximating reality than representing the system using a single bulk or average value (Woods and Onken, 1982; Lande and Lewis, 1989). However, it is important to emphasize that—although one-way coupled IBM models are very useful to assess the impact of the environment on individuals—the reverse is not possible. That is, the model structure of conventional one-way coupled IBM models does not allow individuals to in-

* The term Lagrangian applies only to particles drifting passively with local currents, and cannot be applied to particles than do not move or that move using swimming behaviour. Therefore, for the remainder of this study, we will not use the term Lagrangian to represent particle-based models.

fluence the variables of the Eulerian model in which they are embedded (e.g. larvae cannot change the concentration of phytoplankton).

In bivalve aquaculture, individual-based models have not been used extensively; however there are a few examples of their use in 0-D applications (e.g. Bacher and Gangnery, 2006). In addition, Duarte et al. (2010) used an IBM as a method for parameter optimization. That is, a model run is set up with hundreds of individual bivalves, each having physiological parameters randomly chosen within a permitted range. At the end of the simulation, comparisons of bivalve trajectories against observed bivalve growth allows the user to quickly select the model parameters that best reproduce the data. Ferreira et al. (2008) used output from a 3-D Eulerian bio-physical model to force growth of a modelled oyster and a modelled mussel in a few locations. The focus of the model was to evaluate the effect of the environment on bivalve growth; therefore the effects of bivalves on the environment were not resolved. Bivalve-environment feedbacks cannot be studied with this model configuration.

Here, we utilize a type of model referred to as an Eulerian/IBM hybrid (Chapter 2). Such hybrids simultaneously operate two models: an Eulerian model describes the dynamics of physical and planktonic ecosystem variables that are defined everywhere within a gridded domain (e.g. currents, temperature, nutrients, plankton, detritus etc.), while an IBM model describes the dynamics of variables only defined at discrete locations that are sparsely distributed within the domain (e.g. bivalve biomass). The Eulerian and IBM models run simultaneously and are two-way coupled, thus allowing Eulerian variables to modify IBM variables and vice-versa. Mass is exchanged among variables in the two models, and total mass is conserved in the system. This hybrid model allows (1) the environment to alter bivalve physiology, (2) bivalves to alter the environment, and (3) feedbacks between the two.

The objective of this study is to develop an Eulerian/IBM hybrid model capable of resolving spatially variable interactions and feedbacks between planktonic ecosystem vari-

ables and aquacultured bivalves, thereby enabling the assessment of carrying capacity and environmental impacts of bivalve aquaculture.

In this work we (1) describe the hybrid model, (2) assess model performance by comparing model results with available data, (3) estimate the carrying capacity for mussel aquaculture in a fjord in Eastern Canada, and (4) assess the sensitivity of the model to parameters and boundary conditions.

3.2. Materials and Methods

3.2.1. Model Overview

We implemented the shellfish ecophysiology model, SHELL-E, as part of the Regional Ocean Modeling System (ROMS), which is a state-of-the-art, open-source, 3-D ocean model (Haidvogel et al., 2008; http://myroms.org). ROMS is made of different modules that can be included or excluded in the executable file. Besides the hydrodynamic module, we also employed the sediment transport module (Warner et al., 2008), one of the lower-trophic biological modules (Fennel et al., 2006), and the individual-based biological module (Chapter 2). The first three modules (i.e. hydrodynamics, planktonic ecosystem and sediment transport) operate under an Eulerian or grid-based framework, where the model domain is discretized using a curvilinear, orthogonal and staggered Arakawa C-grid (Arakawa, 1966; Haidvogel et al., 2008). Beneath the water-column grid there is also a three-dimensional sediment bed grid, which is used to track sediment layering and bedload transport (Warner et al., 2008). The individual-based biological module operates in a particle-based framework (Chapter 2), where many particles can be inserted at discrete locations anywhere within the model domain. In this study, each particle represents a separate Culture Unit (CU), each containing a number of identical bivalves (Figure 3-1).

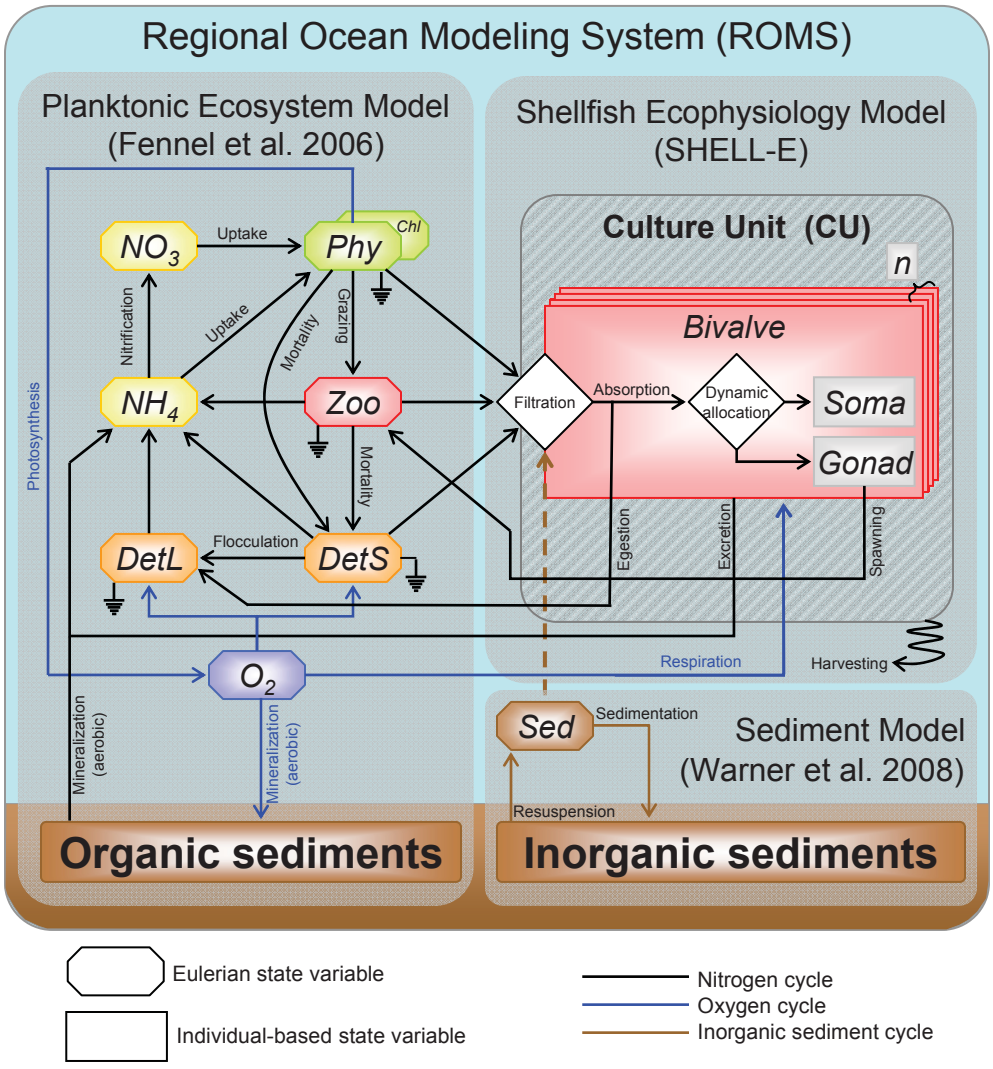

Figure 3-1. Diagram of the Eulerian/IBM hybrid model used in this study.

3.2.2. Hydrodynamic Model (ROMS)

ROMS is a 3-D, free-surface, terrain-following numerical ocean model that solves finite-difference approximations of the Reynolds-averaged Navier-Stokes equations using the hydrostatic and Boussinesq assumptions (Haidvogel et al., 2000; Shchepetkin and McWilliams, 2005). Here we only present relevant equations; see Chapter 2 for a complete description of the Eulerian/IBM hybrid modelling approach.

The time rate of change of any tracer, Ψ^j (e.g. salinity, phytoplankton, suspended sediments, etc.), is estimated using the following scalar transport equation (Chapter 2):

Eq. 3-1

$$\frac{\partial \Psi^j}{\partial t}(x,y,\sigma,t) = -u\frac{\partial \Psi^j}{\partial x} - v\frac{\partial \Psi^j}{\partial y} - \Theta\frac{\partial \Psi^j}{\partial \sigma} + \frac{\partial}{H_z \partial \sigma}\left(K_\Psi \frac{\partial \Psi^j}{H_z \partial \sigma} + v_\theta \frac{\partial \Psi^j}{H_z \partial \sigma}\right) + D_\Psi + C^j_{Eul} + C^j_{IBM}$$

The first three terms on the right hand side of the equation describe advection in the horizontal (x and y) and vertical (σ) directions, where σ is a dimensionless proportion of the water column depth, H_z (m). The fourth term describes vertical mixing and the fifth term (D_Ψ, mmol N m^{-3} s^{-1}) represents the horizontal diffusion terms, which vary depending on the settings chosen by the user (see Hedström, 2009). The sixth term (C^j_{Eul}, mmol N m^{-3} s^{-1}) represents the Eulerian source/sink terms. For planktonic ecosystem tracers, C^j_{Eul} is replaced with source/sink terms described in Fennel et al. (2006), and for sediment tracers, C^j_{Eul} is replaced with source/sink terms described in Warner et al. (2008). The last term, C^j_{IBM} (mmol N m^{-3} s^{-1}), represents the individual-based source/sink terms, and is replaced with equations Eq. 3-19 to Eq. 3-23, which are described in detail in section 3.2.6 below. All terms vary in space and time (x,y,σ,t) however, for simplicity, we omitted the spatial-temporal dependency in the terms on the right hand side of the equation. See Table 3-1 for a complete list of symbols and units.

Table 3-1 - List of variables, parameters and other symbols used in this chapter.

Symbol	Units	Value (Reference)	Description
(i) Coordinates and indices			
j	dimensionless	2-1	Eulerian scalar index
k	dimensionless	2-3	Culture Unit index
t	s (or d)	2-1	Time
x	m	2-1	Horizontal coordinate in the East-West direction
y	m	2-1	Horizontal coordinate in the North-South direction
σ	dimensionless	2-1	Vertical sigma coordinate
(ii) State variables			
• *Hydrodynamic model*			
Temp	°C	(1)	Local temperature
Salt	dimensionless	(1)	Local salinity
u	m s^{-1}	(1)	Mean component of the velocity in the x direction
v	m s^{-1}	(1)	Mean component of the velocity in the y direction
Θ	s^{-1}	(1)	Mean component of the velocity in the vertical (σ) direction
• *Planktonic ecosystem model*			
Chl	mg Chl m^{-3}	(Eq. 9 in 2)	Local concentration of chlorophyll
LDet	mmol N m^{-3}	(Eq. 12 in 2)	Local concentration of large detritus
NO3	mmol N m^{-3}	(Eq. 13 in 2)	Local concentration of nitrate
NH4	mmol N m^{-3}	(Eq. 14 in 2)	Local concentration of ammonium
Phy	mmol N m^{-3}	(Eq. 1 in 2)	Local concentration of phytoplankton
Oxy	mmol O_2 m^{-3}	(18)	Local concentration of oxygen
SDet	mmol N m^{-3}	(Eq. 11 in 2)	Local concentration of small detritus
Zoo	mmol N m^{-3}	(Eq. 10 in 2)	Local concentration of zooplankton
• *Sediment transport model*			
Sed	g m^{-3}	(Eq. 5 in 4)	Local concentration of inorganic sediments
• *Shellfish ecophysiology (SHELL-E) model*			
$Gonad_k$	mmol N ind^{-1}	Eq. 3-12	Reproductive biomass of an individual bivalve in Culture Unit k
$Soma_k$	mmol N ind^{-1}	Eq. 3-11	Structural biomass of an individual bivalve in Culture Unit k
n_k	ind	Eq. 3-17	Number of individual bivalves in Culture Unit k
(iii) Other ancillary and diagnostic variables and functions			
• *Hydrodynamic model*			
H_z	m	(1)	Thickness of the grid cell
• *Planktonic ecosystem model*			
I	W m^{-2}	(Eq. 5 in 2)	Photosynthetically available radiation
• *Shellfish ecophysiology (SHELL-E) model*			
○ *Bivalves*			
A_k	mmol N ind^{-1} d^{-1}	Eq. 3-3	Assimilation rate of an individual bivalve in Culture Unit k
B_k	mmol N ind^{-1}	Eq. 3-2	Biomass of an individual bivalve in Culture Unit k
F_k	m^3 ind^{-1} d^{-1}	Eq. 3-4	Filtration rate of an individual bivalve in Culture Unit k
$F_k^{\max}$	m^3 ind^{-1} d^{-1}	Eq. 3-4	Maximum filtration rate of an individual bivalve in Culture Unit k
Fae_k	mmol N ind^{-1} d^{-1}	Eq. 3-15	Faeces production rate of an individual bivalve in Culture Unit k
Food	mmol N m^{-3}	*Phy*+*Zoo*+*SDet*	Local concentration of food
$Harvest_k$	ind d^{-1}	Eq. 3-18	Number of individual bivalves removed from a Culture Unit in a time step through harvesting
$PsFae_k$	mmol N ind^{-1} d^{-1}	Eq. 3-16	Pseudofaeces production rate of an individual bivalve in Culture Unit k
$Spawning_k$	mmol N ind^{-1} d^{-1}	Eq. 3-14	Biomass of gametes expelled during reproduction by an individual bivalve in Culture Unit k

R_k	mmol N ind^{-1} d^{-1}	Eq. 3-10	Respiration rate of an individual bivalve in Culture Unit *k*
RE_k	dimensionless	Eq. 3-13	Reproductive effort (i.e. fraction of production allocated to reproduction) of an individual bivalve in Culture Unit *k*
$f_k(Temp)$	dimensionless	Eq. 3-6	Functional response of bivalve filtration to temperature
$f_k(Salt)$	dimensionless	Eq. 3-7	Functional response of bivalve filtration to salinity
$f_k(Food)$	dimensionless	Eq. 3-9	Functional response of bivalve filtration to food (i.e. plankton + zooplankton + detritus)
$f_k(Oxy)$	dimensionless	Eq. 3-8	Functional response of bivalve filtration to oxygen
(iv) Parameters			
• *Hydrodynamic model*			
K_ψ	m^2 s^{-1}	(1)	Eddy diffusivity coefficient
υ_θ	m^2 s^{-1}	(1)	Tracer kinematic diffusivity
• *Planktonic ecosystem model. Same as in Fennel et al. (2006), except for the parameters below.*			
K_P	(mmol N m^{-3}) ^{2}	(2)	Half-saturation concentration of phytoplankton ingestion by zooplankton
κ_{CDOM}	m^{-1}	(3)	Diffuse attenuation coefficient for downwelling PAR irradiance due to CDOM
κ_{TOTAL}	m^{-1}	(3)	Total diffuse attenuation coefficient for downwelling PAR irradiance
g_{max}	(mmol N m^{-3})$^{-1}$ d^{-1}	0.75 (21)	Maximum grazing rate of phytoplankton by zooplankton
n_{max}	d^{-1}	0.072 (21)	Phytoplankton mortality
m_P	d^{-1}	0.01 (21)	Maximum nitrification rate
θ_{max}	mg Chl (mg C)$^{-1}$	0.15 (21)	Maximum ratio of chlorophyll to phytoplankton C
• *Shellfish ecophysiology (SHELL-E) model*			
AE_P	dimensionless	0.9 (5)	Absorption efficiency of bivalves on phytoplankton
AE_D	dimensionless	0.2 (5)	Absorption efficiency of bivalves on small detritus
AE_Z	dimensionless	0.3 (6)	Absorption efficiency of bivalves on zooplankton
B_{Pub}	mmol N ind^{-1}	0.43 (7)	Bivalve biomass at puberty
B_{ref}	mmol N ind^{-1}	1 (Eq. 3-5)	Biomass of a reference bivalve
$F_{ref}^{\max}$	m^3 ind^{-1} d^{-1}	0.025 (21)	Filtration rate exhibited by a reference bivalve, B_{ref}, when evaluated in ideal environmental conditions
GT	dimensionless	0.44 (20)	Threshold fraction (i.e. *Gonad/B*) triggering spawning
K_{Temp}^{H}	(°C)$^{-1}$	0.1 (9)	Decreasing coefficient for limitation due to temperature at upper boundary
K_{Temp}^{L}	(°C)$^{-1}$	0.5 (9)	Decreasing coefficient for limitation due to temperature at lower boundary
K_{Salt}^{L}	(PSU)$^{-1}$	0.25 (10)	Decreasing coefficient for limitation due to salinity at lower boundary
K_{Oxy}^{L}	(mmol O_2 m^{-3})$^{-1}$	0.02 (12)	Decreasing coefficient for limitation due to oxygen at lower boundary
K_{Food}	mmol N m^{-3}	1 (6)	Half-saturation food concentration for bivalve filtration
K_{RE}	mmol N ind^{-1}	0.86 (11)	Half-saturation constant for reproductive effort, *RE*
NOQ	mol N (mol O_2)$^{-1}$	0.01 (17)	Nitrogen:oxygen quotient for bivalve respiration
Oxy_L	mmol O_2 m^{-3}	17.5 (12)	Lower limit of tolerance range for oxygen
R_m	d^{-1}	0.002 (21)	Weight-specific maintenance respiration rate of an individual bivalve
$Salt_L$	PSU	10 (10)	Lower limit of tolerance range for salinity
$Temp_H$	°C	25 (8)	Upper limit of tolerance range for temperature
$Temp_L$	°C	-4 (9)	Lower limit of tolerance range for temperature
β	dimensionless	0.12 (5)	Cost of growth coefficient of an individual bivalve
ε_P	dimensionless	1 (6)	Filtration efficiency of bivalves on phytoplankton
ε_D	dimensionless	0.5 (6)	Filtration efficiency of bivalves on small detritus
ε_Z	dimensionless	0.3 (6)	Filtration efficiency of bivalves on zooplankton
λ^{Nat}	d^{-1}	0.00137(19)	Natural mortality rate of bivalves in Culture Unit *k*

λ^{Harv}	d^{-1}	0.001 (15)	Harvesting rate
(v) Other			
Ψ^j	vary		State of the j^{th} Eulerian tracer (e.g. temperature, sediment concentration or phytoplankton concentration)
D_Ψ	vary		Horizontal diffusivity terms
C^j_{Eul}	vary		Eulerian source/sink terms for the j^{th} Eulerian scalar
C^j_{IBM}	vary		Individual-based source/sink terms for the j^{th} Eulerian scalar

1 Haidvogel et al. (2008)
2 Fennel et al. (2006)
3 See text in section 0
4 Warner et al. (2008)
5 Grant et al. (2008)
6 Guyondet et al. (2010)
7 Bayne et al. (1983)
8 Gonzales and Yevich (1976)
9 Calculated to yield less than 10% limitation at 0°C and 30% limitation at 15°C (Thompson 1984)
10 Calculated based on lethal salinity of 10 PSU and 10% limitation at 22.5 PSU (Almada-Villela 1984)
11 Calculated to yield a maximum mussel size of approximately 100 mm (Ibarra 2003)
12 Calculated to stop filtration at 17.5 mmol O_2 m^{-3} and to cause a 5% limitation at 175 mmol O_2 m^{-3} (Wang and Widdows, 1993)
13 Kooijman (2000)
14 Wallentinus (1984)
15 pers. comm. (J. Stairs, 2011)
16 Lotze et al. (1999)
17 Widdows and Johnson (1988)
18 Fennel et al. (in prep.)
19 Estimated so that, at the end of the one-year simulation, the final total biomass of bivalves in the embayment was the same as the initial total biomass.
20 Estimated from mussel meat yields (Smith, 2009), where maximum observed yields correspond to mussel with full gonad and minimum yields correspond to mussels with empty gonads.
21 Tuned

3.2.3. Planktonic Ecosystem Model

ROMS includes several planktonic or lower-trophic ecosystem models. In this study we used the Fennel et al. (2006) model, which has been described in detail elsewhere; here we present a brief summary. The planktonic model is a representation of the pelagic nitrogen cycle using six state variables (all with units of mmol N m^{-3}): phytoplankton (*Phy*), zooplankton (*Zoo*), nitrate (*NO*3), ammonium (*NH*4), small detritus (*SDet*), and large detritus (*LDet*). The model also tracks phytoplankton chlorophyll (*Chl*, mg Chl m^{-3}) and oxygen concentration (*Oxy*, mmol O_2 m^{-3}, Fennel et al. in preparation).

Phytoplankton nitrogen and chlorophyll are estimated separately from each other, thus allowing the nitrogen-to-chlorophyll ratio to change depending on the acclimation of phytoplankton to environmental conditions. Increases in both phytoplankton nitrogen and chlorophyll depend on the local concentration of ammonium and nitrate and the local photosynthetically available radiation (*I*, W m^{-2}), which is calculated at each grid cell depth using a variable attenuation coefficient (i.e. κ_{TOTAL} (m^{-1}), attenuation due to water plus attenuation due to chlorophyll). For this study, we also added attenuation due to coloured dissolved organic matter (CDOM), estimated using an empirical relationship between CDOM and salinity in Ship Harbour, Nova Scotia, Canada (κ_{CDOM} = (-0.0315·*salinity*) + 1.1429; Ibarra, 2003). Both, phytoplankton nitrogen and chlorophyll, are subject to grazing by zooplankton, sinking, flocculation into large detritus, and natural mortality. In this study we also added an individual-based loss term representing grazing by bivalves, which is explained in Section 3.2.6.

Zooplankton feeds on phytoplankton and excretes ammonium produced through basal metabolism and through a variable component proportional to the ingested phytoplankton. Zooplankton is also subject to natural mortality and, in this study, to filtration by bivalves (see Section 3.2.6).

The small detritus pool gains matter through zooplankton's "sloppy feeding" on phytoplankton and through mortalities of zooplankton and phytoplankton. The small detritus

loss terms include flocculation into aggregates, remineralisation into ammonium and sinking. We added consumption by bivalves (see Section 3.2.6).

Large detritus is formed by natural flocculation of phytoplankton and small detritus, and is lost by remineralisation into ammonium, and sinking. We also added a term representing gains due to bivalve faecal deposition (see Section 3.2.5.1.6).

Ammonium is lost due to uptake by phytoplankton and due to nitrification. The ammonium pool increases through the respiration of zooplankton, and through the remineralisation of small and large detritus. We added remineralization of ammonium associated with respiration of bivalves (see section 3.2.5.1.3). An additional production of ammonium occurs in the sediment as a result of benthic remineralisation. This process is included as a bottom boundary condition, where the flux of sinking phytoplankton, detritus and aggregates out of the bottommost grid box results immediately in a corresponding influx of ammonium at the sediment/water interface.

Nitrate is produced by the nitrification of ammonium, which occurs only in the dark and only in aerobic conditions. Nitrate decreases due to uptake by phytoplankton.

Oxygen dynamics are described in Fennel et al. (in preparation). Oxygen is exchanged between the atmosphere and the surface layer of the ocean depending on wind speed (Wanninkhof, 1992) and on the oxygen solubility in seawater, which is a function of temperature and salinity (Garcia and Gordon, 1992). In seawater, oxygen is produced via photosynthesis by phytoplankton and it is consumed by zooplankton respiration and by mineralization of detritus in the water column and of organic matter at the sea floor. We added a sink term due to respiration by bivalves (see section 3.2.5.1.3).

3.2.4. Sediment Transport Model

The sediment transport model (Warner et al., 2008) represents a three-dimensional sediment bed underneath the ocean layers. The sediment layers are initialized with specified

thickness, sediment-class distribution, porosity and age. The sediment classes are specified using fixed attributes of grain diameter, density, settling velocity, critical shear stress for erosion and an erodibility constant.

If sediment is eroded from the sediment bed and suspended in the water column, then it is transported by solving the advection-diffusion Eq. 3-1, where the term C^{j}_{Eul} is replaced by the source/sink terms shown in Equation 22 of Warner et al. (2008).

In this study, the transport model treats suspended sediments as being inorganic and not digestible by bivalves. Therefore, inorganic sediments filtered by bivalves are immediately returned to the water column as pseudofaeces (see section 3.2.5.1.7).

3.2.5. Shellfish Ecophysiology (SHELL-E) Model

Shellfish physiology and population dynamics are represented using a particle-based or individual-based framework (Chapter 2), where discrete Culture Units (k)—each containing a number (n_k, ind) of identical bivalves (B_k, mmol N ind^{-1})—are inserted anywhere within the model domain and then tracked throughout the model simulation. The total biomass of bivalves in a Culture Unit (mmol N) is defined as $n_k \times B_k$. Many Culture Units can coexist in the space of a single Eulerian grid cell.

Below we present functions that describe influences of environmental factors on the physiology of bivalves. However, the validity of these functions depends on the use of appropriate parameters, which are not always available. Please refer to Section 3.4.2. for a discussion on our choice of parameters. It should be noted that parameters and functions can vary for different model applications; therefore careful consideration and validation of functions and parameters is required for each particular application.

3.2.5.1. Growth of an Individual Bivalve

Our bivalve physiology model follows a classic approach described in Kremer and Nixon (1978), where key physiological rates are estimated as the product of a maximum rate and several dimensionless functions that impose the effect of environmental variables. This approach is extensively used in lower-trophic ecosystem models (e.g. Fasham et al., 1990; Sarmiento et al., 1993; Fennel et al., 2006) and is sometimes applied to bivalve-environment models (Fréchette et al., 1989; Dowd, 1997; 2005; Grant et al., 2008). Our model also implements two key aspects of the Dynamic Energy Budget theory (Kooijman, 1986; 2000), which is another approach that is gaining popularity in bivalve-environment models (Van der Veer et al., 2006; Maar et al., 2009; Rosland et al., 2009). The DEB theory is rooted in the assumption that feeding is proportional to body surface, while maintenance is proportional to the body volume (Kooijman, 1986; 2000). Therefore, in our model we imposed a surface-to-volume scaling between filtration and bivalve biomass by using a ⅔ exponent. Kooijman's DEB theory also assumes that the fraction of energy (or mass) allocated to reproductive tissue changes over time throughout the life history of an organism. Therefore, we implemented a dynamic mass allocation method to allow juvenile bivalves to mainly grow their structural biomass, while allowing adults to mainly grow their reproductive biomass (see section 3.2.5.1.4).

In our SHELL-E model, the time evolution of the biomass of an individual bivalve (i.e. growth), is defined by:

Eq. 3-2
$$\frac{\partial B_k}{\partial t} = (A_k - R_k) - Spawning_k$$

where B_k is bivalve biomass of an individual bivalve in Culture Unit k (mmol N ind^{-1}), the assimilation rate A_k (mmol N ind^{-1} d^{-1}) is the total amount of food assimilated into bivalve tissue by an individual bivalve per unit time, the respiration rate R_k (mmol N ind^{-1} d^{-1}) is the biomass of an individual bivalve lost due to catabolic processes, and $Spawning_k$ (mmol N ind^{-1} d^{-1}) is the loss term representing the gamete biomass expelled during re-

production by an individual bivalve in Culture Unit *k*. Note that, for simplicity, we omitted the spatial-temporal dependency (*x,y,σ,t*) in all variables.

3.2.5.1.1. Assimilation

The assimilation rate, which represents the biomass absorbed by an individual bivalve (after food filtration and ingestion), is estimated using the following equation:

Eq. 3-3 $$A_k = F_k \cdot \left[\left(\varepsilon_P \cdot AE_P \cdot Phy \right) + \left(\varepsilon_Z \cdot AE_Z \cdot Zoo \right) + \left(\varepsilon_D \cdot AE_D \cdot SDet \right) \right]$$

where the individual filtration rate F_k (m^3 ind^{-1} d^{-1}) is multiplied by the available food (phytoplankton, zooplankton and detritus) scaled by their respective filtration efficiencies (ε_P, ε_Z, and ε_D) and absorption efficiencies (AE_P, AE_Z and AE_D). This is to account for the fact that some food in the water is not retained by the filtering apparatus of the bivalve, and also some of the ingested food is not absorbed (i.e. incorporated into bivalve tissue) and is instead returned to the detrital pool in the form of faecal biodeposits (see sections 3.2.5.1.6 and 3.2.6). No organic material is incorporated in pseudofaeces (see Section 3.2.5.1.7). For details on the estimation of model parameters, see footnotes in Table 3-1.

3.2.5.1.2. Filtration

The individual filtration rate F_k, which represents the volume of water that an individual bivalve clears of particles per unit time, is estimated as follows:

Eq. 3-4 $$F_k = F_k^{\max} \cdot f_k(Temp) \cdot f_k(Salt) \cdot f_k(Oxy) \cdot f_k(Food)$$

where terms two to five are dimensionless limiting functions for temperature $f_k(Temp)$, salinity f_k ($Salt$), oxygen f_k (Oxy) and food particles $f_k(Food)$. The first term, $F_k^{\max}$ (m^3 ind^{-1} d^{-1}), represents the maximum filtration rate achievable by a bivalve of size B_k, and is estimated as follows:

Eq. 3-5

$$F_k^{\max} = F_{ref}^{\max} \cdot \left(\frac{B_k}{B_{ref}} \right)^{2/3}$$

where $F_{ref}^{\max}$ (m^3 ind^{-1} d^{-1}) is the filtration rate exhibited by a reference bivalve of biomass B_{ref} (usually 1 mmol N ind^{-1}), when evaluated in ideal environmental conditions (i.e. all the dimensionless limiting functions are equal to 1). The allometric exponent, ⅔, is in accordance with the surface-to-volume scaling proposed in the Dynamic Energy Budget theory (Kooijman, 1986; 2000).

We included limiting functions for all these environmental variables because these are the variables simulated by ROMS that have been shown to affect physiology in aquaculture bivalves (Gosling, 2003). However, depending on the application (e.g. species, geographical location, etc.), not all of these environmental variables may be important. Therefore, we included the ability to (1) generate diagnostic time-series for each limiting function, and (2) turn on/off each limitation. For each different application, test simulations can be run to assess which environmental limitations play an important role, and then one can turn off the limitations deemed unimportant. Moreover, because ROMS is open-source, the included limiting functions can be replaced for other more appropriate for a particular application.

3.2.5.1.2.1. Temperature Limitation

Temperature modulates the individual filtration rate through a sigmoid-type threshold equation, which is similar in form to the Type 3 threshold equation (Gentleman et al., 2003), typically used to describe the feeding response of zooplankton as a function of food concentration. We modified the sigmoid equation to include a species-specific tolerance range and a separate rate of decrease at the higher boundary (Eq. 3-6, Figure 3-2). Our equation has similar functionality as the 6-parameter Arrhenius-type equation used

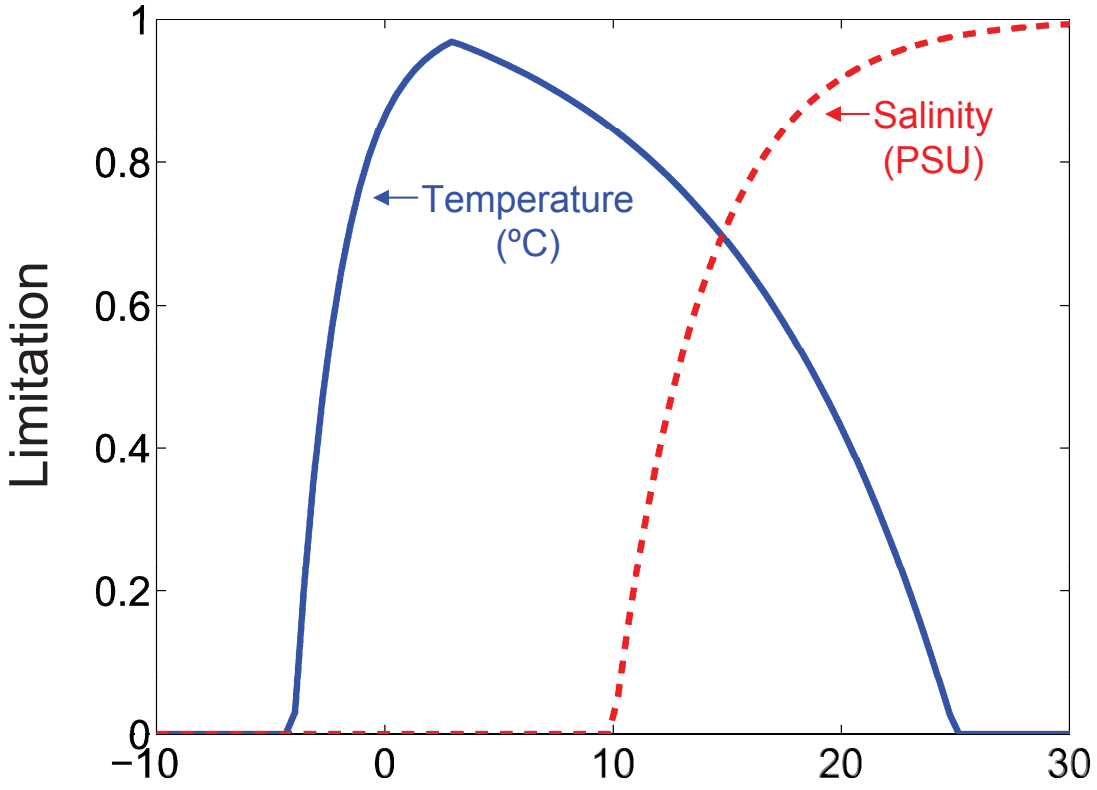

Figure 3-2. Illustration of the shape of the limiting functions for temperature (Eq. 3-6) and salinity (Eq. 3-7).

by Kooijman (2000), Van der Veer et al. (2006) and Bacher and Gangnery et al. (2006), however our equation only uses 4 parameters.

Eq. 3-6
$$f_k(Temp) = MIN\begin{cases} MAX\left\{0,\ 1-\exp\left[-K^L_{Temp}\cdot(Temp-Temp_L)\right]\right\} \\ MAX\left\{0,\ 1+\left(\dfrac{1-\exp(K^H_{Temp}\cdot Temp)}{\exp(K^H_{Temp}\cdot Temp_H)-1}\right)\right\} \end{cases}$$

where $Temp$ (°C) is local temperature, $Temp_L$ and $Temp_H$ (°C) are the lower and upper temperature limits of the tolerance range, and K^L_{Temp} and K^H_{Temp} (units: $(°C)^{-1}$) define the rate of decrease at the lower and upper boundaries, respectively. Note that in systems for which temperature never exceeds the upper limit, a simpler, 2 parameter equation is appropriate (e.g. see Section 3.2.5.1.2.2).

3.2.5.1.2.2. Salinity Limitation

We assumed that filtration rate is only limited when salinity is too low (e.g. Almada-Villela, 1984). Therefore we used a simpler sigmoid-type threshold equation:

Eq. 3-7
$$f_k(Salt) = MAX\left\{0,\ 1-\exp\left[-K^L_{Salt}\cdot(Salt-Salt_L)\right]\right\}$$

where $Salt$ (PSU) is local salinity, $Salt_L$ (PSU) is the salinity at which filtration shuts down (i.e. lower end of the tolerance range), and K^L_{Salt} (PSU^{-1}) defines the rate of decrease at the lower boundary (Figure 3-2).

3.2.5.1.2.3. Oxygen Limitation

Similar to salinity, low oxygen concentration limits the individual filtration rate (Wang and Widdows, 1993). Thus we implemented this limitation through a sigmoid-type threshold equation:

Eq. 3-8 $$f_k(Oxy) = MAX\left\{0,\ 1 - \exp\left[-K^L_{Oxy} \cdot (Oxy - Oxy_L)\right]\right\}$$

where *Oxy* (mmol O_2 m^{-3}) is local oxygen concentration, Oxy_L (mmol O_2 m^{-3}) is the oxygen concentration at which filtrations shuts down (i.e. lower limit of the tolerance range), and K^L_{Oxy} (units: (mmol O_2 m^{-3})$^{-1}$) defines the rate of decrease at the lower boundary.

3.2.5.1.2.4. Limitation due to Particle Concentration

Previous modelling studies (e.g. Dowd, 1997; Grant et al., 2007) proposed that the filtration rate of some bivalves is reduced at low concentrations of particles, and thus they implemented a Michaelis–Menten limitation of filtration dependent on the concentration of all food particles; in our case, *Phy* + *Zoo* + *SDet*:

Eq. 3-9 $$f_k(Food) = \frac{Phy + Zoo + SDet}{K_{Food} + Phy + Zoo + SDet}$$

where K_{Food} (mmol N m^{-3}) is the half-saturation concentration of food particles.

3.2.5.1.3. Respiration

The mass lost by an individual bivalve through respiration (R_k, mmol N ind^{-1} d^{-1}, second term on the right hand side of Eq. 3-2), is estimated using Eq. 3-10 below. The individual respiration rate includes a maintenance respiration rate, which depends solely on bivalve

biomass, and an active respiration rate representing losses directly related to feeding activity resulting in assimilation of food:

Eq. 3-10 $$R_k = (R_m \cdot B_k) + (\beta \cdot A_k)$$

where R_m (d^{-1}) is the weight-specific maintenance respiration rate, B_k is biomass of an individual bivalve (mmol N ind^{-1}) and β is the dimensionless cost of growth coefficient (Grant et al., 2007).

3.2.5.1.4. Dynamic Mass Allocation

After accounting for respiration, the remaining assimilated biomass is divided between soma and gonads. The allocation of mass between the two compartments is dynamic, changing through the life cycle of the bivalve. In juveniles, all available energy is allocated to the soma, and after puberty, an increasingly larger portion of the resources is allocated to reproduction. Finally, in large bivalves, almost all resources go to gonads and growth almost stops. The dynamic allocation of mass is described in the following two equations:

Eq. 3-11 $$\frac{\partial Soma_k}{\partial t} = (A_k - R_k) \cdot (1 - RE_k)$$

Eq. 3-12 $$\frac{\partial Gonad_k}{\partial t} = \left[(A_k - R_k) \cdot RE_k\right] - Spawning_k$$

where $Soma_k$ and $Gonad_k$ (mmol N ind^{-1}) are the bivalve structural and reproductive compartments, respectively. The first term on the right hand side of both equations, ($A_k - R_k$), is the Scope for Growth (SFG; Bayne et al., 1976) and represents the net rate of increase of biomass, either soma or reproductive products. The second term of both equations, ($1–RE_k$) and RE_k, respectively, are used to scale the SFG and define the dynamic

allocation. RE_k (dimensionless) is the reproductive effort, which is defined as the fraction of the total production that is allocated to reproduction, and is calculated as follows:

Eq. 3-13
$$RE_k = MAX\left(0, \frac{B_k - B_{Pub}}{K_{RE} + B_k - 2B_{Pub}}\right)$$

where B_{Pub} (mmol N ind^{-1}) is the bivalve biomass at puberty, and K_{RE} (mmol N ind^{-1}) is the half-saturation biomass for *RE*.

3.2.5.1.5. Spawning

Once a bivalve reaches puberty and starts allocating resources to reproduction, the gonad starts to grow. When the gonad weight reaches a threshold fraction of the total weight (*GT*, dimensionless), the entire gonad pool is emptied into the zooplankton pool in a process called spawning. The loss term $Spawning_k$ (mmol N ind^{-1} d^{-1}) represents the gonad biomass evacuated in one time-step and is calculated using the equation below:

Eq. 3-14
$$Spawning_k = \begin{cases} 0 & : \text{if } \frac{Gonad_k(t)}{B_k(t)} < GT \\ Gonad_k(t) & : \text{if } \frac{Gonad_k(t)}{B_k(t)} \geq GT \end{cases}$$

3.2.5.1.6. Faeces

The amount of undigested food that is evacuated as faeces (Fae_k, mmol N ind^{-1} d^{-1}) is calculated with the equation below:

Eq. 3-15
$$Fae_k = F_k \cdot \left\{ \left[\varepsilon_P \cdot (1 - AE_P) \cdot Phy\right] + \left[\varepsilon_Z \cdot (1 - AE_Z) \cdot Zoo\right] + \left[\varepsilon_D \cdot (1 - AE_D) \cdot SDet\right] \right\}$$

3.2.5.1.7. Pseudofaeces

In our model, inorganic suspended particles filtered by bivalves are not ingested. Instead they are immediately rejected back into the water-column as pseudofaeces ($PsFae_k$, mg m^{-3}) according the following equation:

Eq. 3-16 $$PsFae_k = F_k \cdot Sed$$

where *Sed* is the local concentration of suspended inorganic sediments (mg m^{-3}). Note that bivalves can incorporate algal cells and detritus into pseudofaeces, particularly when algal cells are toxic (e.g. Mafra et al., 2009). This process is not included in the current model formulation.

3.2.5.2. Population Dynamics

Following Bacher and Gangnery (2006), the time-rate of change of the number of identical bivalves in Culture Unit k (n_k, ind), is controlled by the natural mortality of bivalves, and by harvesting practices:

Eq. 3-17 $$\frac{\partial n_k}{\partial t} = (\lambda^{Nat} \cdot n_k) - Harvest_k$$

where λ^{Nat} is the natural mortality rate (d^{-1}), and $Harvest_k$ (ind d^{-1}) is the loss term describing the number of individuals in a Culture Unit removed from the system in one time step through harvesting. Harvesting is described below.

3.2.5.2.1. Harvesting

Every time step, a fraction of the bivalves in all Culture Units is harvested (i.e. removed from the system), as follows:

Eq. 3-18 $$Harvest_k = \lambda^{Harv} \cdot n_k$$

where λ^{Harv} is the harvesting rate (d^{-1}), which is calculated to be inverse of the time that bivalves spend in the farm. For example, in Ship Harbour mussels are harvested up to 3 years after they are seeded in the farm, therefore $\lambda^{Harv} = 1/(3\times365) = 0.0009\ d^{-1}$. Note that we implemented this harvesting function because it is a simple way to maintain a realistic total biomass of the aquaculture stock in the embayment. However, in reality, the harvesting process occurs differently, where farmers harvest a few entire culture units while leaving the rest intact. Future work should test whether a more realistic harvesting scheme would play an important role in the overall dynamics of the ecosystem.

3.2.6. Two-way Coupling of Planktonic and Shellfish Models

Perhaps the most significant advantage of an Eulerian/IBM hybrid model is its ability to represent feedbacks between bivalves and the surrounding environment. These feedbacks can be resolved because of the two-way coupling between the Eulerian planktonic ecosystem model and the individual-based bivalve physiology model, which allows for the simultaneous computations of (1) the effect of the environment on bivalves and (2) the effect of bivalves on the environment.

The effect that the environment exerts on bivalves is imposed through the dimensionless limiting functions in Eq. 3-4. On the other hand, the effect that the bivalves have on the environment is implemented through, C^j_{IBM}, the individual-based source/sink terms in Eq. 3-1. The C^j_{IBM} terms are different for every biological tracer, therefore we describe each separately in the sections below.

Phytoplankton concentration in a grid cell G is decreased by the sum of the filtration activity of all k Culture Units within the grid cell (i.e. $k \in G$).

Eq. 3-19 $$C_{IBM}^{Phy}(x_G, y_G, \sigma_G, t) = -\sum_{k \in G}\left(\frac{F_k(t) \cdot \varepsilon_P(t) \cdot n_k(t) \cdot Phy(x_G, y_G, \sigma_G, t)}{V(x_G, y_G, \sigma_G, t)}\right)$$

where V is the grid cell Volume (m^3). See Table 3-1 for other notation. Note that, for simplicity, we omitted the spatial and temporal dependencies (x_G, y_G, σ_G, t) in the equations below.

Similarly, zooplankton concentration in grid cell G is decreased by the sum of the filtration activity of all k Culture Units within the grid cell. However zooplankton is also increased when bivalves spawn.

Eq. 3-20 $$C_{IBM}^{Zoo} = -\sum_{k \in G}\left(\frac{F_k \cdot \varepsilon_Z \cdot n_k \cdot Zoo}{V}\right) + \sum_{k \in G}\left(\frac{Spawning_k \cdot n_k}{V}\right)$$

Small detritus in grid cell G is decreased by the sum of the filtration activity of all Culture Units within the grid cell.

Eq. 3-21 $$C_{IBM}^{SDet} = -\sum_{k \in G}\left(\frac{F_k \cdot \varepsilon_D \cdot n_k \cdot SDet}{V}\right)$$

Large detritus in grid cell G is increased with the production of faeces of bivalves of all Culture Units within the grid cell.

Eq. 3-22 $$C_{IBM}^{LDet} = \sum_{k \in G}\left(\frac{Fae_k \cdot n_k}{V}\right)$$

Ammonia in grid cell G is increased with excretion and mortality of bivalves of all Culture Units within the grid cell.

Eq. 3-23 $$C_{IBM}^{NH4} = \sum_{k \in G}\left(\frac{\left[R_k + (\lambda^{Nat} \cdot B_k)\right] \cdot n_k}{V}\right)$$

Oxygen in grid cell *G* is decreased due to respiration of bivalves of all Culture Units within the grid cell.

Eq. 3-24
$$C_{IBM}^{NH4} = \sum_{k \in G} \left(\frac{(R_k \cdot NOQ^{-1}) \cdot n_k}{V} \right)$$

where *NOQ* (units: mol N (mol O_2)$^{-1}$) is the Nitrogen:Oxygen quotient.

3.2.7. Model Application

We applied the SHELL-E model to Ship Harbour, Nova Scotia, Eastern Canada (Figure 3-3), which is an estuarine fjord with a mussel farm (see farm details in section 3.2.7.1). We compared model results with observations, however the modelling period (2004-2005) was different than the period of collection of the observations, because we did not have boundary forcing for the time when samples were collected (water samples: 1988-1992; CTD and currents: 2001; mussel size-distributions: 2001). Also, we compared our model results against published data from other sites in Atlantic Canada, including Mahone Bay and Bedford Basin, Nova Scotia (Cranford and Hill, 1999) and Trinity Bay, Newfoundland (Thompson, 1984). The application of the model encompassed six modelling experiments, which we briefly outline below.

Experiment 1 - Comparison against physical data. Using default parameters (Table 3-1), we ran the model to simulate two months (output at 15 min intervals) during a time of the year concurrent with our data of currents, temperature and salinity (see section 3.2.8.1). Only the hydrodynamic module was used for this run.

Experiment 2 - Comparison against biochemical and mussel physiology data. We ran the model to produce a one-year simulation (output at daily intervals) to compare model output against water samples collected from 1988 to 1992 for analysis of nutrients, chlorophyll, oxygen and particulate organic matter (see section 3.2.8.2) and against published

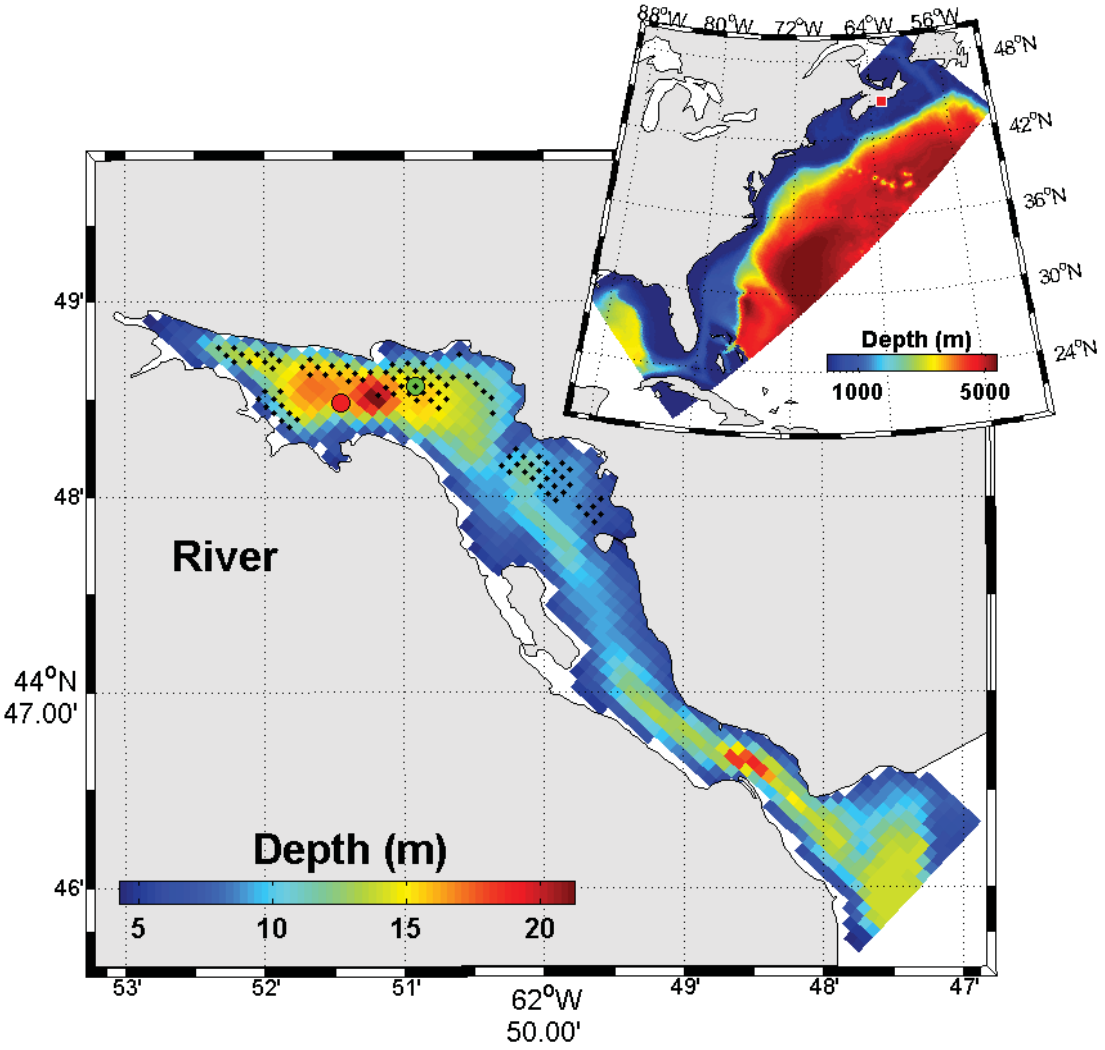

Figure 3-3. Upper-right corner shows bathymetry of the larger model domain (North-East North American shelf), which was used to force the open boundary of the smaller model domain (Ship Harbour, Eastern Canada), marked in the larger domain map with a red square. The main panel shows the bathymetry of the smaller model domain. The arrow marks the location of the river. The larger dots mark the stations where water samples (red) and mussel samples (green) were collected. The small black dots represent the Culture Units. Note that there are 4 Culture Units (on top of each other) occupying the middle of the water column, but this cannot be seen due to the perspective of this illustration.

rates of mussel physiology (Thompson, 1984; Cranford and Hill, 1999). We used default parameters (Table 3-1) and a mussel standing stock consistent with the stock reared at the time of collection of water samples (see section 3.2.7.1).

Experiment 3.- Comparison against mussel size-classes. We ran the model to produce a one-year simulation (output at daily intervals) to compare model output against the size-distributions of mussels collected in 2001 (see section 3.2.8.3). While all mussels in a Culture Unit are identical (same size), it is possible to create a size distribution by inserting many Culture Units (each of different size) in a single grid cell. At the end of the simulation, the size of all the mussels from all the Culture Units in the cell can be binned into size-classes to evaluate the resulting size-distribution after the one-year simulation.

We used default parameters (Table 3-1) and a mussel standing stock consistent with the stock reared during 2001. However, in the location where mussel samples were collected, we inserted multiple Culture Units, each initialized with a different initial biomass (i.e. initial size) so that the ensemble of Culture Units in that location would mimic the size-distribution of the mussel samples. Note that our notation should have an additional superscript denoting the size-class (e.g. B_k^d, A_k^d and R_k^d, where d is the size-class index). However, since the use of size classes is restricted to a small portion of our study, we opted to show a simplified notation where the size-class index is omitted.

Experiment 4 - Determination of carrying capacity. We ran 28 one-year simulations to estimate the harvest yield as a function of initial mussel density and mussel mortality (see details in section 3.2.10).

Experiment 5 - Analysis of model sensitivity to different parameters. We ran 55 one-year simulations using a low resolution grid (see section 3.2.7.2) to assess the effect of changes in the model parameters (see details in section 3.2.9).

Experiment 6 - Analysis of model sensitivity to boundary conditions. We ran three one-year simulations to assess the effect of changes in the boundary conditions (see details in section 3.2.9).

3.2.7.1. Study Site

Ship Harbour is a long (10 km) and narrow estuarine fjord, with a deeper inner basin with maximum depth of 27 m, and a shallow sill with an approximate depth of 7 m. The dominant source of fresh water is the Ship Harbour River (Figure 3-3), discharging an annual average of 18 m^3 s^{-1} (Gregory et al., 1993), and driving an estuarine circulation. Mean tides are 1.4 m and spring tides are 2.0 m (Gregory et al., 1993). At the seaward boundary, Ship Harbour is open to the North Atlantic.

Ship Harbour has one of the largest mussel farms in Nova Scotia (Aquaprime Mussel Ranch Ltd.). Blue mussels (*Mytilus edulis* and *M. trossolus*) are grown in mesh socks suspended from long-lines (Sénéchal et al., 2008). Juvenile mussels are seeded at an approximate size of 8 mm (i.e. B_k = 0.016 mmol N ind^{-1}), and they are harvested 3 years later at a approximate size of 75 mm or 10 mmol N ind^{-1} (John Stairs, pers comm.). At the time of collection of the water samples used in this study (1988 - 1992), the farm contained about 225 tons of mussels (wet weight with shell; Strain et al., 2002), and at the time of collection of the mussel size-distribution samples (2001) the farm had about 1000 tons of mussels (Ibarra, 2003).

3.2.7.2. Model Grids and Grid Nesting

We created two grids representing Ship Harbour. The high resolution grid (Figure 3-3) had 100 × 100 m grid cells and 10 sigma layers. The low resolution grid (not shown) had 700 × 700 m grid cells and 5 sigma layers. One-year simulations using the high resolution grid required about 1 day to run on 4 CPUs on our computer system (Linux cluster with 2.8 GHz Opteron processors), while the same simulation using the low resolution grid took about 15 minutes. We used the low resolution grid only for the analysis of sensitiv-

ity to model parameters (see section 3.2.9) and we used the high resolution grid for all other modelling experiments.

In both grids, the seaward open boundary was forced with output from a large meso-scale ROMS model for the North-East North American shelf (Figure 3-3), which has been described in detail in Fennel et al. (2008).

3.2.7.3. Forcing

Wind speed, air temperature, air pressure, relative humidity and rainfall rate from archive records (2004-2005) were obtained from the meteorological station in Shearwater Airport (http://www.meds-sdmm.dfo-mpo.gc.ca/isdm-gdsi/azmp-pmza/met/plot-graph-eng.asp?a=30), which is approximately 50 km from the study site. Short wave radiation was obtained from a Satlantic Land/Ocean Biogeochemical Observatory (LOBO; http://lobo.satlantic.com), about 55 km from the study site. The LOBO buoy was not operational during the time period of the modelling experiments, therefore we shifted in time the LOBO data, by subtracting 5 years from the time-stamps. We assumed that the dynamics in Ship Harbour are mainly driven by the seasonal signal of short wave radiation, and that daily variability is not as important.

The open boundary at the seaward end of Ship Harbour was forced with output from the WebTide tidal prediction model (Department of Fisheries and Oceans, Canada; http://www2.mar.dfo-mpo.gc.ca/science/ocean/coastal_hydrodynamics/WebTide/webtide.html) Also, the concentrations of all planktonic ecosystem variables entering the open boundary were forced using output from a meso-scale ROMS model described above.

Fresh water entering Ship Harbour through the river was simulated using a synthetic time-series created using data from Gregory et al. (1993). The concentration of the planktonic ecosystem tracers in the river's water was set to resemble a seasonal pattern (e.g. Dowd, 2005).

3.2.7.4. Initial Conditions

All physical and planktonic ecosystem variables were initialized with constant values over the entire domain. Modelling experiments began after a six-month model spin-up to allow physical and planktonic ecosystem variables to reach a distribution representative of the model dynamics. However, the individual-based variables (i.e. mussel soma, gonad and number of individuals) were reset at the beginning of the modelling experiment, to evaluate their evolution from a uniform condition.

3.2.8. Data Collection and Analysis

3.2.8.1. Physical Data

Temperature, salinity and current velocity were measured from September 19 to October 15 of 2001 using a CTD/current meter (2D-ACM, Falmouth Scientific, Inc.) moored at 4.5 m from the bottom Figure 3-3). Instrument deployment did not coincide with the period for which boundary forcing was available. That is, our model results correspond to a different year from the year when physical data were collected. Therefore, we restricted data/model comparison to seasonal means and did not attempt to explain short term variability.

3.2.8.2. Biological and Chemical Samples

Biological and chemical data were obtained from the BioChem database (DFO, 2005) and correspond to water samples collected in Ship Harbour (Figure 3-3) from 1988 to 1992. Data have been published elsewhere (Keizer et al., 1996; Strain, 2002); here we present only a brief description of their sample analysis. Ammonia and nitrates (i.e. nitrate + nitrite) were measured with autoanalyzer techniques (Strain, 2002), oxygen concentration was determined using a polarographic oxygen electrode (1991 survey) and Winkler titrations (1992 survey). Chlorophyll concentrations were determined using extracted fluorometry (Strickland and Parsons, 1968). Suspended particulate matter (SPM)

was estimated using preweighed filters and gravimetric analysis (Winneberger et al., 1963).

3.2.8.3. Size-distribution of Mussels

Mussels in Ship Harbour were sampled in September 2001 (Ibarra, 2003). At the time of collection, mussels from each of the three year classes were sampled from the lease shown in Figure 3-3. The length of individual mussels was measured and size-distributions for each year-class were calculated. See Appendix B for the equation to convert from mussel length into biomass.

3.2.9. Sensitivity Analysis

We assessed the sensitivity of our model to different model parameters and to boundary conditions. The sensitivity of individual-based variables (i.e. bivalve soma) and biological Eulerian variables (i.e. *Phy*, *Zoo*, *O2*, *NH4*, *NO3*, *SDet* and *LDet*) to all SHELL-E parameters was evaluated using 55 one-year model runs using the low resolution grid (see Section 3.2.7.2). First we ran a "standard" run using the default parameter values shown in Table 3-1. Then we ran two runs for each evaluated parameter, one where the standard parameter (P) was doubled and the other where it was halved. We estimated the sensitivity values, $S_{X|P}$ (dimensionless), using the following equation (Beres and Hawkins, 2001):

Eq. 3-25
$$S_{X|P} = \frac{\Delta X}{X} \cdot \left(\frac{\Delta P}{P} \right)^{-1}$$

where, for each of the variables mentioned above, X is the "standard" state, and ΔX is the difference of the states obtained with the doubled and halved parameters. $\Delta P = (P \times 2) - (P \div 2)$.

To assess the sensitivity to boundary conditions, we ran 3 one-year model runs using the high resolution grid (see Section 3.2.7.2). We ran the "standard" run using the default parameter values shown in Table 3-1. We also ran one model simulation where the values of the biological tracers at the boundary were doubled, and one simulation where the boundary values where halved.

3.2.10. Estimation of Carrying Capacity

In this study we evaluated the production carrying capacity, defined as the "optimized level of production" of aquacultured bivalves (McKindsey et al., 2006). The evaluation of bivalve production on the environment (i.e. ecological carrying capacity, McKindsey et al., 2006) is studied in detail in Chapter 4.

We ran 7 one-year long simulations using the high resolution grid, and using all the default parameters from Table 3-1. We ran each simulation with a different initial mussel density, ranging from 3 to 200 gdw m^{-3}. For each simulation we estimated the harvest yield, which was defined as the total mussel biomass at the end of the simulation minus the total biomass at the beginning of the simulation. The production carrying capacity was determined as the smallest initial mussel density that produced the highest harvest yield.

We observed that the estimated carrying capacity was dependant on the natural mortality. Therefore we repeated the procedure described above at natural mortalities of 0, 0.0001, 0.0005 and 0.001 d^{-1}.

3.3. Results

3.3.1. Hydrodynamics

We compared modelling results of temperature, salinity and current speed, against observations recorded with a CTD/current meter deployed in Ship Harbour in 2001 (Figure 3-4). Observed average current speeds in the East-West and North-South directions were 0.03 and 0.002 m s^{-1} higher than the modelled average speeds, respectively. Observed average temperature was the same as the model (15.40°C), but the observed average salinity was 0.1 PSU lower than the model. Considering that the model simulation corresponded to a different year from the observations (but same dates), the relatively small discrepancies between model and observations indicate that the model is reproducing the main hydrodynamic features of Ship Harbour. However, it is important to be aware that comparisons of histogram distributions (e.g. Figure 3-4) is not a very robust validation method because it cannot resolve difference in phase or in vertical structure.

3.3.2. Planktonic Ecosystem

Water-column planktonic ecosystem variables showed large spatial variability through Ship Harbour, as well as pronounced seasonal variability (Figure 3-5). The spring bloom caused the largest concentration of phytoplankton nitrogen, chlorophyll, oxygen and large detritus; while the lowest concentration of phytoplankton, chlorophyll, zooplankton and small detritus were seen in winter. Concentration of nitrate and large detritus were lowest in the summer. A detailed study on the planktonic ecosystem dynamics in Ship Harbour is presented in Chapter 4.

We compared observations from water samples collected from 1988 to 1992, against a one-year model simulation (Figure 3-6). Modelled phytoplankton nitrogen and chlorophyll concentrations showed seasonal variability with a very distinguishable spring bloom (peak of 4.2 mmol N m^{-3} or 17 mg Chl m^{-3}, see Figure 3-6) and a less distinguishable fall bloom (peak of 2 mmol N m^{-3} or 13 mg Chl m^{-3}). However the largest modelled

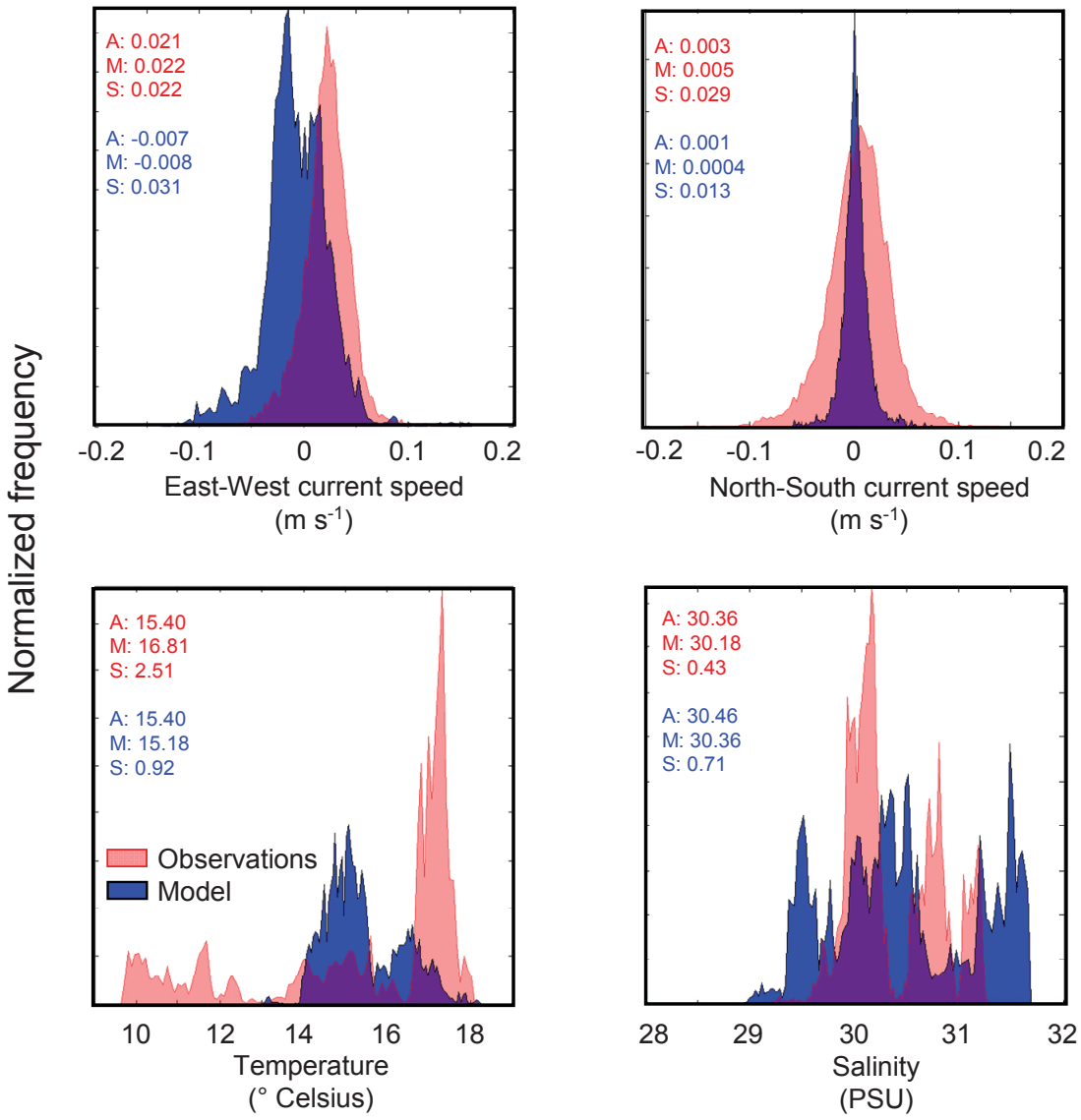

Figure 3-4. Comparison of hydrodynamic observations (red) against model results (blue). Histograms show the distribution of current speeds, temperature and salinity, recorded every 10 min at 4.5 m above the bottom, from September 19 to October 15 (n = 3605). Observations were made in 2001 (see location in Figure 3-3), however model results correspond to the same period in 2005, because the 2001 forcing was not available. Numbers are averages (A), medians (M) and standard deviations (S).

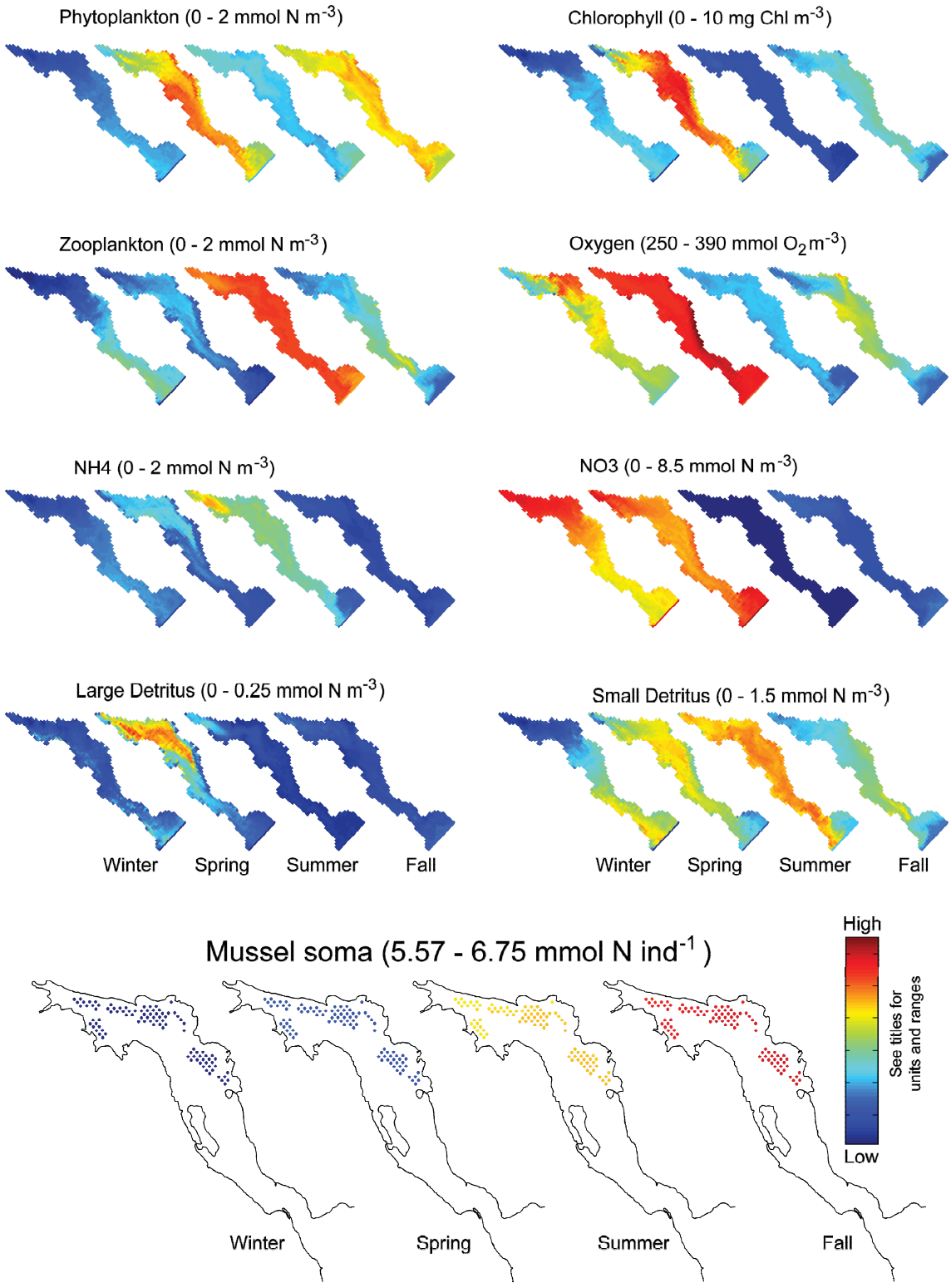

Figure 3-5. Four snapshots (winter, spring, summer and fall) of all Eulerian planktonic ecosystem state variables (coloured maps) and of the individual-based mussel soma (dotted maps) for Ship Harbour. All maps are top-views of the middle of the water column. The range and units of the colour-coding is the same among maps of the same variable, but different among variables (see parenthesis).

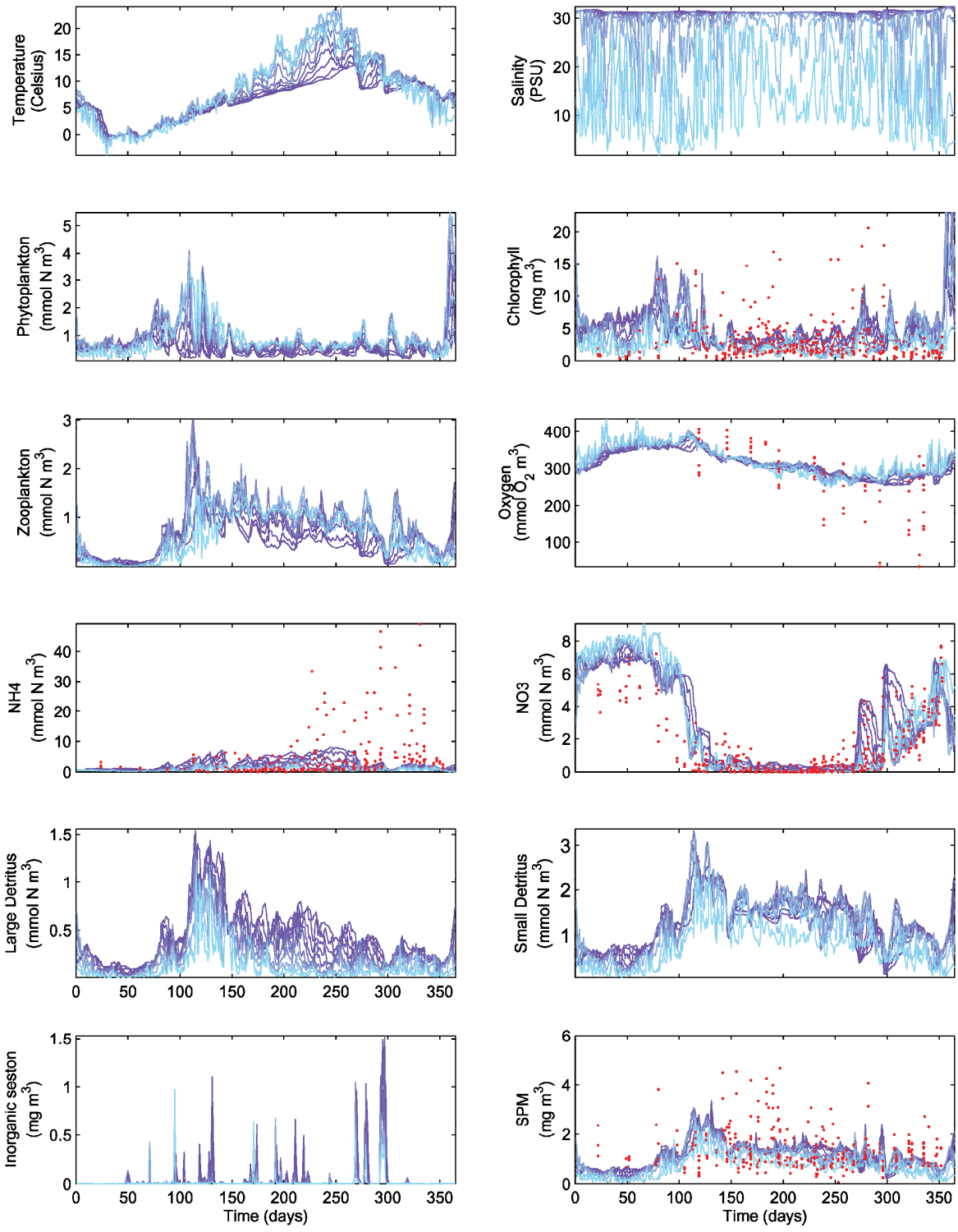

Figure 3-6. Comparison of biological and chemical observations from water samples (red dots) against model time-series from the same location (blue/purple lines; see collection location in Figure 3-2). Lighter blue lines correspond to shallower layers while darker purple lines correspond to deeper layers. Water samples were collected between 1988 and 1992 but model simulation is for 2005, because earlier forcing was not available.

concentrations occurred during late December (5.2 mmol N m^{-3} or 23 mg Chl m^{-3}). Both, phytoplankton nitrogen and chlorophyll, also showed periodic variability with a period of about 15 days, that is likely due to the spring-neap tidal cycle. Modelled chlorophyll is within the range of observations from water samples. However, the model did not reproduce very high peaks of chlorophyll seen sporadically during the summer. These peaks may be attributed to vertical migrations of phytoplankton (e.g. Hall and Paerl, 2011), resuspension of microalgae and detritus of macroalgae during wind events (e.g. MacIntyre and Cullen, 1996; Koh et al., 2006), or enhanced productivity associated with resuspension of sediments (e.g. Chen et al., 2010). We ran the model adding periodic discharges of nutrients at the location of the mussel processing plant (results not shown), but the bursts of nutrients were not enough to cause the observed chlorophyll spikes. Modelled chlorophyll also overestimated the observed concentration during late December to mid March. We speculate that the overestimation is because the model did not account for ice formation during winter months, which drastically reduces light penetration (Pegau and Zaneveld, 2000).

Modelled zooplankton was highest during late spring (4 mmol N m^{-3}) and lowest during the winter (0.5 mmol N m^{-3}). However, unlike phytoplankton, zooplankton remained relatively high during summer months. The zooplankton series also showed oscillation of approximately 15 days, likely due to the spring-neap tidal cycle.

Oxygen concentrations from both, water samples and model, showed highest concentrations when the water was coldest and lowest concentration when water was warmest, in accordance with oxygen solubility properties of seawater (Garcia and Gordon, 1992). However, the observations showed a much larger variability with depth, where lower concentrations were seen in deeper waters. At times, oxygen concentration in deeper waters was as low as 20 mmol O_2 m^{-3}; below the hypoxic threshold of 17.5 mmol O_2 m^{-3} (Wang and Widdows, 1993). The model did not reproduce the low oxygen concentration observed in deeper waters. This implies that there are sources of organic matter in Ship Harbour that are not accounted for by the model, and that lead to oxygen depletion. Also,

our model immediately remineralizes organic matter reaching the bottom, while in nature remineralization is spread out over seasons (Strain, 2002).

In both model and observations, ammonia was low in the winter (approximately 1 mmol N m^{-3}) and increased during the spring and summer as the water-column stratified (approximately 20 mmol N m^{-3} for the observations and 5 mmol N m^{-3} for the model). However the increase in ammonia concentration was much more pronounced in the observations (up to 48 mmol N m^{-3}) than in the model (up to 9 mmol N m^{-3}). Again, this suggests that there is a source of organic matter not accounted for in the model. Strain et al. (2002) were also puzzled by the high ammonia concentrations in Ship Harbour, which they could not explain by the presence of mussels alone.

Nitrate concentration in the model and the observations were high during the winter and late fall (up to 8 mmol N m^{-3}) and very low during the summer (0 to 0.25 mmol N m^{-3}). Strain et al. (2002) analysed nitrate-salinity relationships and concluded that nitrate in Ship Harbour likely comes from shelf water when the water column is mixed. Our model results are consistent with Strain et al. (2002) description of the nitrate dynamics in Ship Harbour.

The concentration of both, small and large detritus, follow similar patterns with highest concentration in late spring (1.5 and 3.2 mmol N m^{-3} for large and small detritus, respectively), intermediate concentration in the summer and early fall, and lowest concentration in the winter (0.1 and 0.9 mmol N m^{-3} for large and small detritus, respectively). Throughout the year, the concentration of small detritus was about double the concentration of large detritus. The modelled concentration of suspended inorganic particles showed sporadic spikes (maximum of 1.5 mg m^{-3}), consistent with resuspension of sediments during strong wind events. The concentration of suspended particulate matter (SPM; i.e. large detritus + small detritus + inorganic sediments + phytoplankton + zooplankton) predicted by the model was roughly within the range observed from the water samples. However the model could not reproduce some of the large spikes observed in the data. This is probably because the model did not account for resuspension of material

from the mussel socks, which is likely greater than resuspension at the bottom, because socks are closer to the surface where they can experience higher current speeds.

3.3.3. Mussel Physiology

We compared modelling results from the individual-based SHELL-E model against published physiological rates from different parts of Atlantic Canada (Thompson, 1984; Cranford and Hill, 1999). The modelled number of individuals in all Culture Units decreased exponentially (Figure 3-7); from 2 - 7 $\times$ 10^4 ind, to 1 - 4 $\times$ 10^4 ind) due to natural mortality and harvesting. Modelled soma (i.e. structural biomass of mussels) increased throughout the year (from 6.3 to approximately 6.8 mmol N ind^{-1}), however it increased more slowly after May. Modelled mussels at different locations grew at different rates. Although all mussels started the simulation with the same biomass, at the end of the one-year simulation there were differences in soma biomass of up to 0.5 mmol N ind^{-1}, with higher values in mussels in surface layers (Figure 3-5). In model runs with higher initial density this difference was 1.5 mmol N ind^{-1} (data not shown), including some mussels that did not gain any biomass during the one-year model simulation. Mussels in the surface layers appeared to grow faster than the rest, which is consistent with observation (J. Stairs, pers comm).

The shell length of modelled mussels was estimated diagnostically using an empirical relationship for Ship Harbour (Ibarra, 2003; see Appendix B). Because it was calculated from biomass, it followed the same pattern as the soma, where slower growth occurred during the winter months, and faster growth during the spring, particularly in mussels in surface layers.

The most notable pattern of the gonad state was the three spawning events. However, Guyondet et al. (2010) stated that it is common for mussels of the region to spawn 2 times per year. The discrepancy in numbers of spawning events per year may be attributed to the fact that mussels in our model spawn simply by reaching a soma/gonad threshold, while real mussels are known to spawn not only when their gonads are full, but also

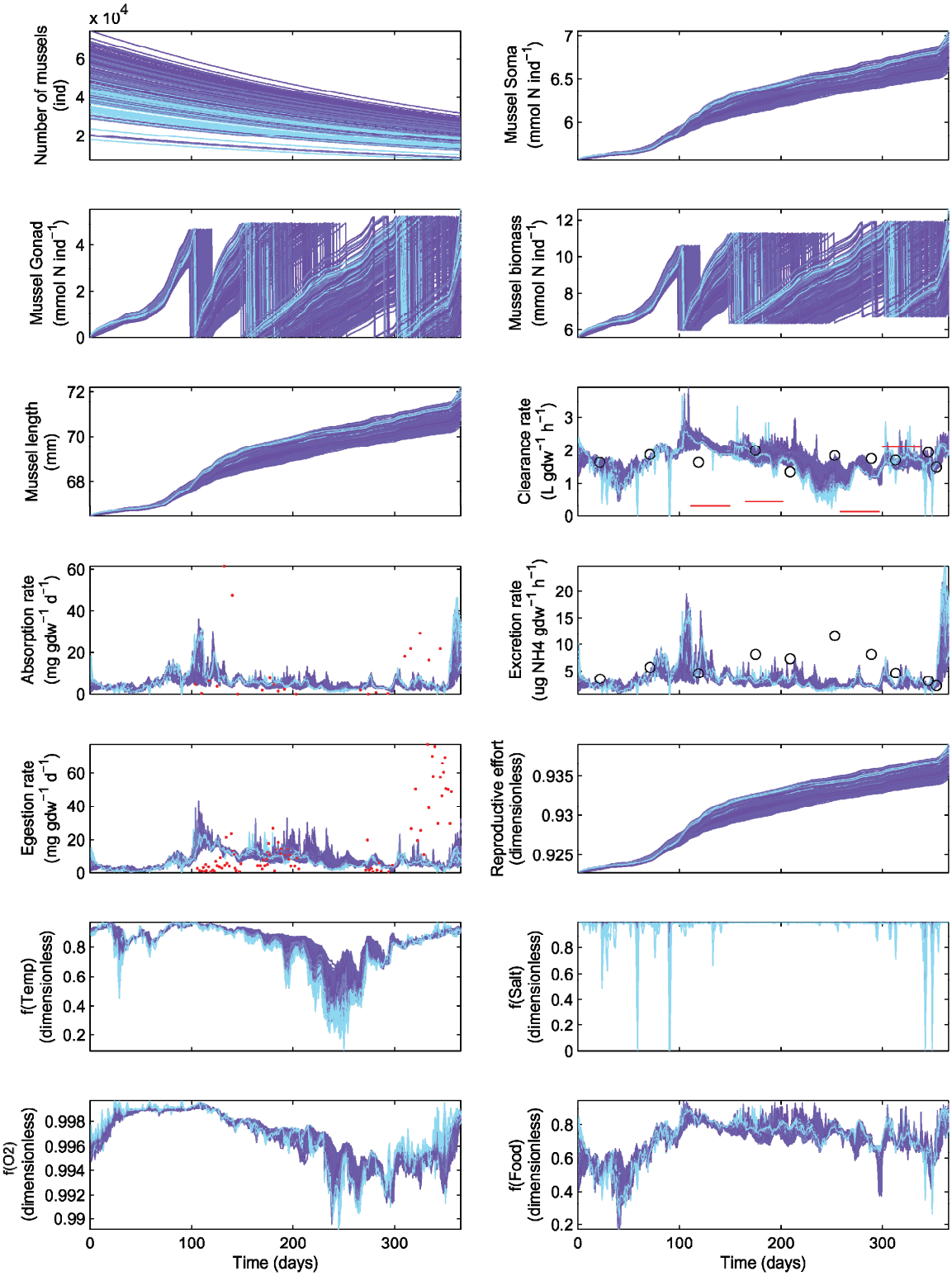

Figure 3-7. Comparison of results from the individual-based shellfish ecophysiology (SHELL-E) model (blue/purple time-series) against published physiological rates (black circles = Thomson 1984; red dots or lines = Cranford and Hill 1999). Lighter blue lines correspond to shallower layers while darker purple lines correspond to deeper layers.

when presented with a temperature cue (Gosling, 2003), which was not programmed in the modelled mussels. Like the soma, mussel gonads grew all year round (except during spawning events); however gonad growth was slower during the winter. Also, the gonads of mussels close to the surface grew faster and therefore, mussels close to the surface were usually the first to spawn. The total biomass of modelled mussels showed a large variability during the one-year simulation, mainly because of the spawning events, but also because of the spatial variability observed in soma growth among the modelled mussels.

Clearance rates varied throughout the one-year simulation showing both, low and high frequency variations. The bulk of the modelled clearance rates were between 0.5 and 2.8 L gdw^{-1} h^{-1} (i.e. 0.002 and 0.012 m^3 mmol N^{-1} d^{-1}), however there are some short moments where clearance rate in the surface layers was completely shut down because of low salinity. Also, there were some short peaks where clearance rates almost reached 4 L gdw^{-1} h^{-1}. (i.e. 0.017 m^3 mmol N^{-1} d^{-1}). One of the advantages of the SHELL-E model is its ability to separately track the different limitations modulating clearance rates. Therefore we can evaluate which environmental factor had the largest impact during different times of the year. Temperature played a large role in limiting filtration during months with hot water temperature, particularly in surface layers. However, during the rest of the year, food was the factor modulating clearance rates. Food limitation showed high frequency variations due to the tides (lowest during slack tides) and was responsible for the high frequency variability in clearance rates. Oxygen did not play an important role in our "standard" simulation, however in other model runs with high mussel densities, mussels depleted oxygen enough to cause a limitation as low as 0.4 (data not shown). Salinity only played a small role, where it limited filtration only for short periods of time and only in surface layers.

Modelled absorption rates were highest during blooms in the spring and late fall (approximately 40 mg gdw^{-1} d^{-1} or 0.6 mmol N ind^{-1} d^{-1}) and remained about 8 mg gdw^{-1} d^{-1} (or 0.1 mmol N ind^{-1} d^{-1}) for the rest of the year (see Appendix B for conversions). The variability in the absorption rate was within the range reported by Cranford and Hill

(1999), however they observed the highest rates only during the fall. Modelled excretion rates were also highest during blooms in the spring and late fall (approximately 20 μg N gdw^{-1} h^{-1} or 0.06 mmol N ind^{-1} d^{-1}) and remained about 3 μg N gdw^{-1} h^{-1} (or 0.01 mmol N ind^{-1} d^{-1}) for the rest of the year. The variability in excretion rates was within the range reported by Thompson (1984), however he observed the highest rates only during early fall, when water temperature was warmest. Time-series of both, absorption and excretion rates (Figure 3-7), showed variability consistent with the variability in the time-series in phytoplankton biomass (Figure 3-6).

Egestion rates were highest during the spring bloom (up to 40 mg gdw^{-1} d^{-1} or 0.4 mmol N ind^{-1} d^{-1}), however they remained relatively high during the summer. Unlike the rates of absorption and excretion, that closely resemble the time-series of phytoplankton, the rate of egestion depended more strongly on the local concentration of detritus and zooplankton. This is because mussels have lower absorption efficiencies for zooplankton and detritus, compared to the absorption efficiency for phytoplankton. Therefore, a large portion of the filtered zooplankton and detritus ends up egested as undigested faeces. Simulated egestion rates were within the range of rates measured in the field (Cranford and Hill, 1999). However, observed rates were highest in the fall when water temperature was the warmest.

The time series of reproductive effort resembled the series of soma and length, because both, soma and reproductive effort, are calculated diagnostically as a function the soma biomass. All mussels in the simulation were initialized to have the same initial size of 63 mm (1 gdw or 5.564 mmol N), which is the size of a "standard" adult mussel. This facilitates comparisons with physiological rates in the literature; however, because all mussels in the simulation were adults, the modelled reproductive effort shows only a slight increase (from 0.92 to 0.94) over the one-year simulation.

3.3.4. Mussel Growth and Size-distributions

We compared size-frequency distribution from mussels collected in 2001, against predicted size-distributions after a one-year model simulation (Figure 3-8). Comparing the modes of each distribution, we saw that mussels of the 2000 year-class grew in the model from 40 to 50 mm during the one-year simulation (i.e. from panel A to panel D, in Figure 3-8). Similarly, mussels of the 1999 year-class grew in the model from 60 to 65 mm (from panel B to panel E), and mussels of the 1998 year-class grew in the model from 65 to 70 mm (from panel C to panel F). Comparing sizes of mussels of the same age—that is, panel B with D, and panel C with E—we found that modelled growth of younger mussels was somewhat slower than the inferred from the measured differences between age classes (i.e. 10 mm yr^{-1} or from A to D, instead of 20 mm yr^{-1} or from A to B), while the modelled growth of older mussels (5 mm yr^{-1} or from B to E) was the same as the measured difference (from B to C). At the end of the experiment, the modelled variability in size of the 2000 and 1999 year-classes (panels D and E) was smaller than the observed variability of the measured counterparts at the beginning of the experiment (panels B and C). This is partially because the model does not account for the recruitment of seedlings from the spawning events, which accounted for the smaller size-classes in the initial (i.e. measured) distributions. Considering that the model was forced with atmospheric and boundary conditions from 2005, while mussels were sampled in 2001, we concluded that the model predicts mussel growth satisfactorily.

3.3.5. Sensitivity Analysis

We ran multiple one-year simulations to assess the sensitivity of model variables to changes in model parameters (Figure 3-9). The reference clearance rate parameter, $F_{ref}^{\max}$, was one of the most sensitive parameters affecting all assessed variables. Unfortunately, bivalves of the same species can exhibit large variations in estimated clearance rates (e.g. see Table 2 in Cranford and Hill 1999), partially due to differences in the techniques used to estimate of clearance rates (e.g. Cranford and Hill, 2001; Riisgard, 2001).

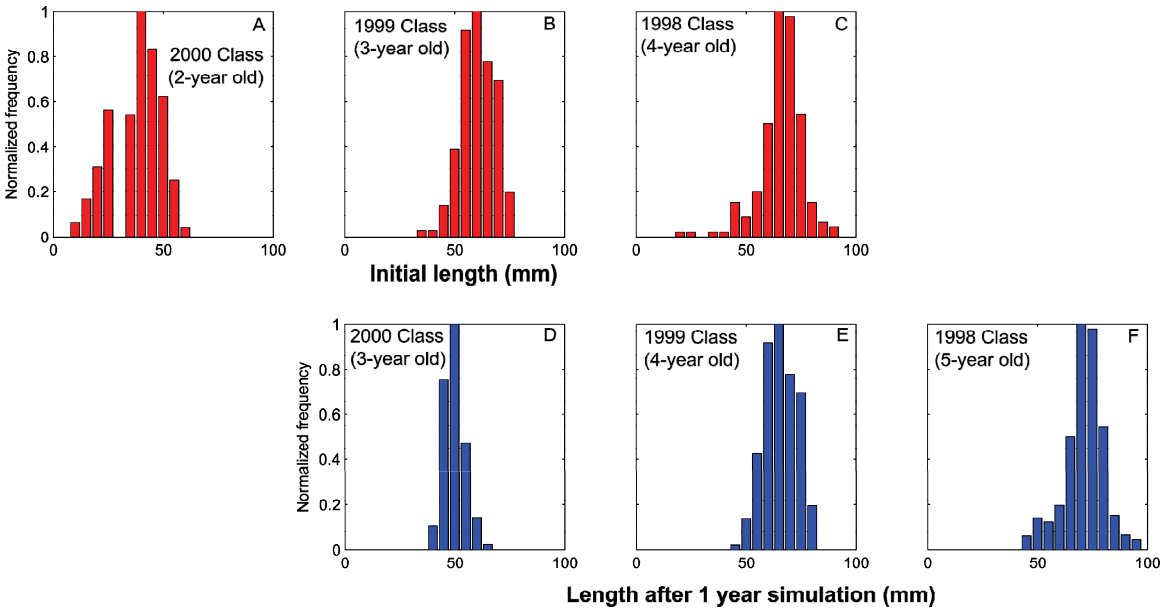

Figure 3-8. Histograms of size-distributions of mussels collected in Ship Harbour in 2001 from three year-classes (panels A, B and C). Note the seeding is done with 1-year old juvenile mussels purchased from a different site. Therefore, for clarity, we included in parentheses the age of mussels at harvest. These measured size-distributions were used to initialize the biomass of multiple Culture Units that were inserted at a single location corresponding to the location where the mussels were collected. After a one-year model simulation, the resulting size-distribution from the ensemble of Culture Units (panels D, E and F) can be compared against mussels of the same age from the initial distributions (i.e. compare D against B, and E against C).

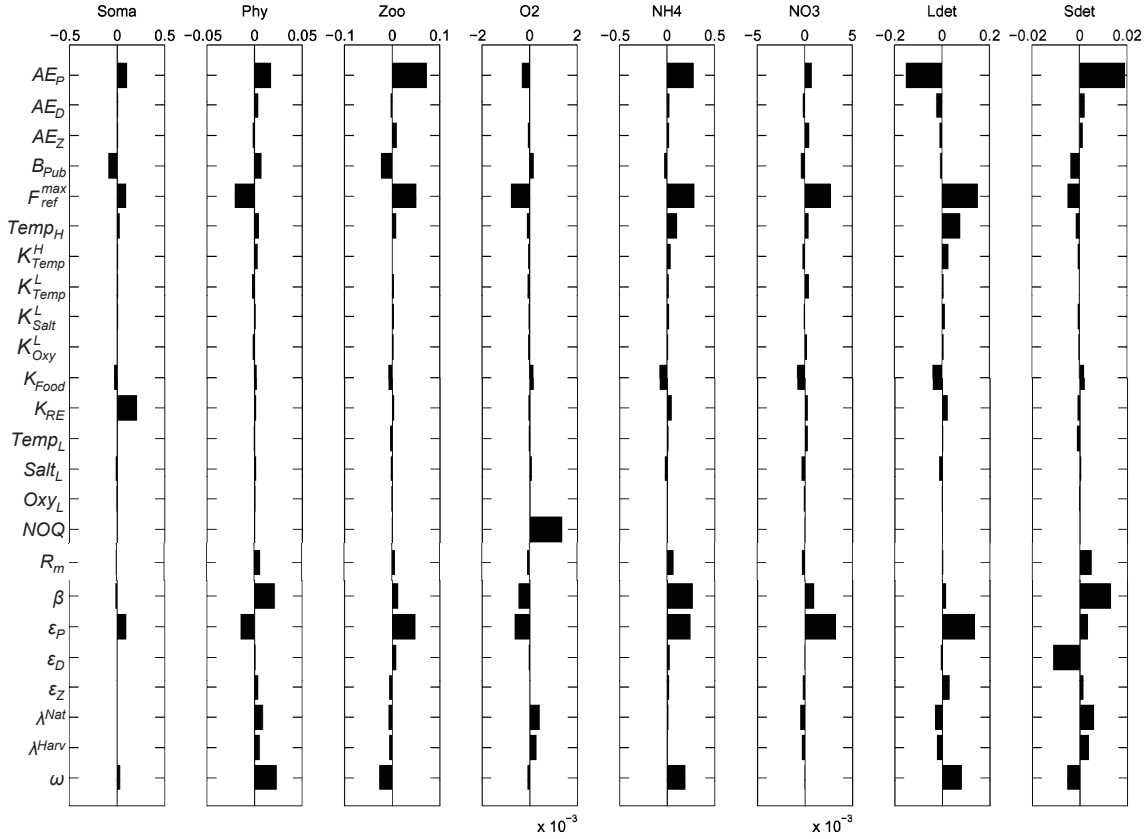

Figure 3-9. Sensitivity analysis: relative sensitivity of various model variables to changes in parameters of the SHELL-E model. A large positive sensitivity indicates that a small increase in the parameter causes a large increase in the outcome variable. Large negative sensitivities indicates that small parameter increases causes large decreases in the outcome variables. The magnitude of the sensitivity is comparable only within outcome variables.

The filtration and absorption efficiencies, ε_P and AE_P respectively, were also parameters that had relatively strong effects on all assessed variables. The cost of growth of an individual bivalve, β, had a large effect only on the Eulerian variables, and the threshold fraction triggering spawning, ω, had a large effect on all Eulerian variables except for oxygen and nitrate concentration. Some parameters only had a large effect on one variable. Namely, the filtration efficiency for detritus, ε_D , had an impact only on the concentration of small detritus; the Nitrogen:Oxygen quotient, NOQ, had an effect only on the concentration of oxygen; and the half-saturation constant for reproductive effort, K_{RE}, had an effect only on mussel soma. It should be recognized that comparison of the sensitivities of variables to changes in different parameters is complicated by the fact that changing each parameter value by a factor of two does not ensure that each change has the same relationship to uncertainty in the value of that parameter, either due to biological factors or inherent uncertainty in the formulation of the function.

The analysis of sensitivity of variables to the boundary forcing (Figure 3-10) showed that an increase of oxygen concentration at the boundary results in a increase in oxygen in areas close to the boundary, but that the effect diminishes with distance from the boundary to an almost unchanged state at the opposite end of the fjord. Similar patterns were seen with small and large detritus. However, phytoplankton and chlorophyll showed the opposite; an increase at the seaward boundary resulted in a strong decrease in phytoplankton and chlorophyll in the inner basin. The increase in phytoplankton at the boundary promotes an increase in growth of the mussels. Then, the increase in mussel biomass triggers a feedback resulting in a local decrease of phytoplankton in the inner basin, which is where most of the mussels are farmed. Also, the strong decrease in phytoplankton in the inner basin results in a decrease in nutrient uptake, which may explain the strong increase in nitrate in the inner basin.

3.3.6. Carrying Capacity

We estimated the production carrying capacity for farmed mussels in Ship Harbour using multiple one-year simulations of the hybrid model to determine the relationship of har-

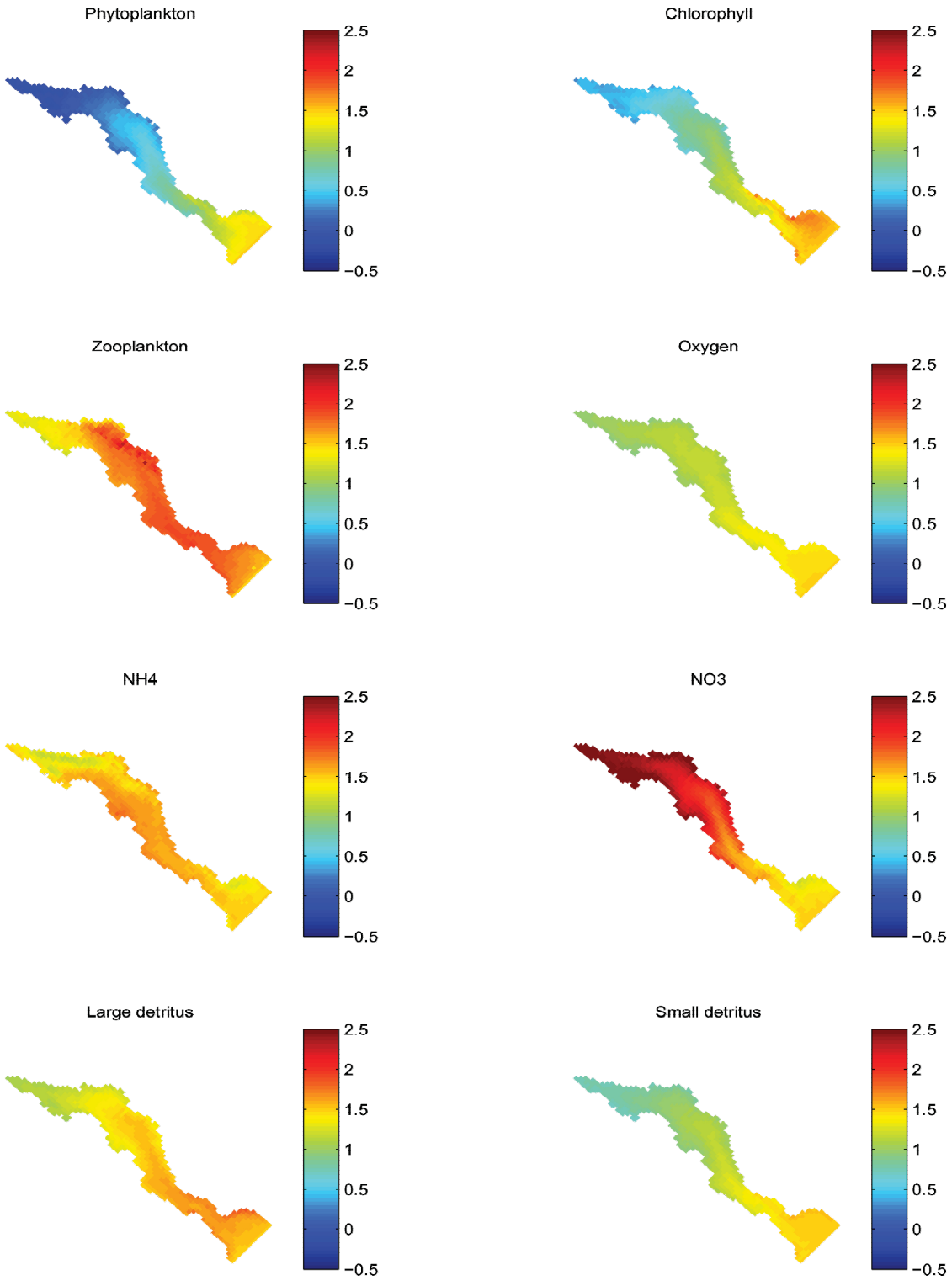

Figure 3-10. Sensitivity analysis: sensitivity of various modeled variables to changes in the forcing at the seaward boundary. Positive numbers indicate an increase in the assessed variable as a response to an increase of the boundary forcing. Negative numbers indicate a decrease in the variable as a response to an increase in the boundary forcing. Units in all the panels are dimensionless.

vested yield as a function of initial seeding density* and natural mortality (Figure 3-11). For any given natural mortality, at low initial seeding densities, the harvested yield increases substantially with small increases in initial density. However at intermediate seeding densities, mussels become food limited, thus small increases in initial density translate into minimal or null increases in yield. Finally, at high initial seeding densities, food limitation is so strong that mussels in the centre of the lease do not get enough food to offset their catabolic metabolism (Eq. 3-2) and natural mortality (Eq. 3-17), so the Culture Units start losing weight. Therefore, the harvested yield at high seeding densities actually decreases compared to the yield estimated at intermediate seeding densities. The production carrying capacity of the system is the optimized level of production (McKindsey et al., 2006), which is usually reached when seeding at an intermediate seeding density. Farmers seeding mussels at a lower density than the optimal density are underutilizing their resources, while farmers seeding above the optimal seeding density are overexploiting their resources, wasting seeding effort, and ultimately not harvesting as much as with a smaller initial density.

For Ship Harbour, we estimate that the carrying capacity should be achieved at mussel seeding densities of approximately 60 gdw m^{-3} (for a natural mortality of 0.001 d^{-1}), yielding a harvest of about 400 tons of mussels per year. The current seeding density in Ship Harbour is about 33 gdw m^{-3} (Ibarra, 2003) suggesting that aquaculture activities in Ship Harbour have not reached their carrying capacity. However, we do not advise to increase their seeding densities on the basis of this prediction alone, because of uncertainties associated with our estimation of the natural mortality rate of mussels. This parameter has to be accurately estimated before the model can provide a more reliable estimate of the carrying capacity for Ship Harbour. Testing of the model predictions would then focus on the other assumptions of the model.

* Note that the mussel densities (units: mmol N m^{-3}) reported in this study reflect the bivalve biomass divided by the volume of the mussel lease. Other studies used as a reference the volume of the entire inner basin of the fjord (e.g. Strain et al. 2002).

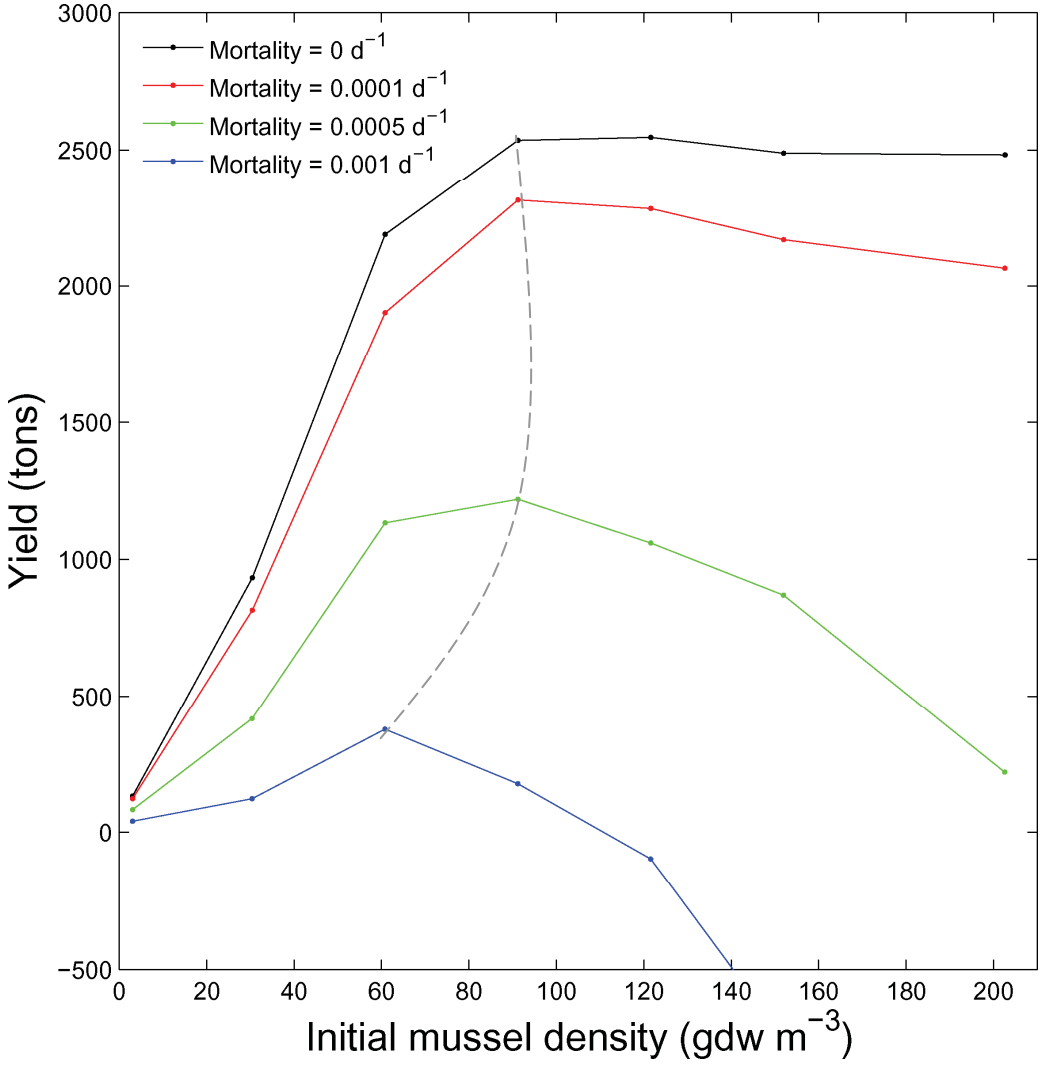

Figure 3-11. Estimation of carrying capacity for a mussel farm in Ship Harbour. Each density-yield curve was generated using multiple one-year simulations of the Eulerian/IBM hybrid model, and each curve depicts the relationship between initial seeding density and harvested yield under one of four scenarios with different natural mortalities. For each curve, the carrying capacity is estimated as the point of the curve with the maximum yield. The grey dashed line connects the maximum yields of all four mortality scenarios.

Our results also show that natural mortality plays an important role in the estimation of harvest yield, where higher mortalities translate into lower yields. However, the more significant result is that the shape of the density-yield curves changes with increasing mortality. That is, the harvest yield at high initial densities decreases very rapidly in scenarios with high mortality; sometimes to the point where the harvests is less than the initial seeding (i.e. negative yield). The main implication of this change in shape of the density-yield curves is that the maximum yield (i.e. carrying capacity) shifts towards smaller initial densities at higher natural mortalities. In our lower-mortality simulations, a five-fold increase in natural mortality (from 0.0001 to 0.0005 d^{-1}) did not change the estimated maximum yield (90 gdw m^{-3}). However in our higher mortality simulations, a doubling of the natural mortality (from 0.0005 to 0.001 d^{-1}) resulted in a 33% decrease in yield (from 90 to 60 gdw m^{-3}). Our results emphasize the importance of considering natural mortality when attempting to estimate the carrying capacity of a farm. Although there are a few studies investigating the effect of natural mortality on bivalve standing stock (e.g. Bald et al., 2009), we are unaware of any study assessing the effect of natural mortality on the estimated carrying capacity.

3.4. Discussion

3.4.1. Hybrid (Eulerian/IBM) Ecosystem Modelling

The Eulerian/IBM modelling system presented in this study simultaneously represented planktonic ecosystem and bivalve ecophysiology processes in a 3-D spatially-explicit context. Many bivalve-environment models assume a negligible effect of local primary production (e.g. Incze et al., 1981; Bacher et al., 2003). That is, the local concentration of phytoplankton only depends on the balance between material entering the model domain (via forcing through an open boundary) and material filtered by the bivalves. These models cannot resolve feedbacks between bivalve physiology and phytoplankton dynamics, which are thought to be important in applications where the residence time of water within the domain is comparable to the doubling time of phytoplankton (Pilditch et al.,

2001). The application of bivalve-environment models neglecting primary production should be restricted to lease-scale applications (e.g. Ibarra, 2003).

Our hybrid modelling system can assess feedbacks between bivalves and the environment because the model explicitly represents both water column environmental variables and bivalve physiological variables. The effect of the environment on bivalves was imposed via environmental limiting functions (e.g. $f_k(Temp)$, $f_k(Salt)$, $f_k(Oxy)$, etc.). Through these functions, environmental variables modulate the physiological rates that regulate bivalve growth. As bivalve physiology changes, the impact of bivalves on environmental variables also changes, allowing for feedbacks acting at different time and space scales. In our study, it appears that mussel filtration caused a decrease in the concentration of available food at the head of the estuary (Figure 3-5, panels at the top).

The simultaneous simulation of planktonic ecosystem and bivalve physiology processes allowed us to assess relationships that are essential for the sustainable management of aquaculture operations. For example, our results showed that the relationship between initial seeding density and final harvest yield, which is the basis of the estimation of carrying capacity, depends on natural mortality. Many bivalve-environment models designed to estimate carrying capacity do not account for bivalve mortality (e.g. Incze et al., 1981; Sarà and Mazzola, 2004; Grant et al., 2007; Filgueira et al., 2010). Other carrying capacity models do take bivalve mortality into consideration (e.g. Dame and Prins, 1998; Duarte et al., 2003; Guyondet et al., 2010); however, these studies do not investigate the effect of mortality on the estimation of carrying capacity.

Another common type of bivalve-environment models does include primary productivity and other lower-trophic level process, but at the expense of spatial resolution. These are ecosystem box models, where an entire bay is represented with a single box (i.e. 0-D models; e.g. Dowd, 1997; Dame and Prins, 1998; Rosland et al., 2009) or with a few boxes (i.e. coarse 2-D models; e.g. Grant et al., 2007; Troost et al., 2010). These models assume that the contents of the box are completely mixed, thus bivalves have access to all the food within a box. In reality, food is usually not distributed homogeneously within a

bay. Physical process such as solar heating of surface waters and freshwater runoff can produce water stratification, and biological process such as the filtration by bivalves can produce gradients in the distribution of phytoplankton (Ibarra, 2003; Grant et al., 2008). The differences between a fine-scale 3-D model and a coarse 2-D model was briefly studied by Guyondet et al. (2010). They compared results from their 3-D model for the Grande-Entrée lagoon (Iles-de-la-Madeleine, Québec, Canada) against results from a 2-D multiple-box model for the same region (Grant et al., 2007). The coarse 2-D model predicted a reduction in the concentration of phytoplankton of 15%, and a reduction of bivalve growth of 11%, as a result of a doubling in bivalve biomass. The fine-scale 3-D model predicted a 2.6% reduction in phytoplankton and a 3.5% reduction in bivalve growth as a result of the same doubling in bivalve biomass; however there were other differences between the two models apart from their spatial resolution. Spillman et al. (2008) also developed a fine-scale 3-D model and argued that—compared to coarse 1-D or 2-D models—their model predicted lower concentrations of food (and higher waste) in grid cells closest to their modeled bivalves; however, bay-averaged concentrations of food and nutrients remained relatively unaffected.

As we mentioned before, there are other advanced bivalve-environment models that coupled physical-biological and bivalve physiology models, and that are spatially resolved by using fine scale grids in 2-D (Duarte et al., 2003; Grant et al., 2008; Grangeré et al., 2010; Guyondet et al., 2010) and fine grids in 3-D (Spillman et al., 2008; Leon et al., 2011). All these are Eulerian or grid-based models and therefore they all have to represent the bivalve biomass in each grid cell as an average concentration. State variables in Eulerian models must be defined in all grid cells within the model domain; hence, equations must be solved for each variable and for each grid cell. This is the main disadvantage of Eulerian models, where only a limited number of variables can be added (e.g. additional bivalve species, or size-classes, or physiological state variables) before the model slows down beyond practical limits. Therefore, Eulerian models with many grid cells (i.e. 3-D) may be limited to use simple physiological models, while Eulerian models using many bivalve physiological variables (e.g. *soma*, *gonad*, $f_k(Temp)$, $f_k(Salt)$, $f_k(Oxy)$, etc.) may be limited to use 2-D domains with fewer grid cells.

Our model is an Eulerian/IBM hybrid, which means that bivalves are represented using sparsely distributed particles. Adding particle-based variables also increases the length of time required to finish a simulation, however the increase in time depends on the amount of particles, and not on the number of grid cells. Therefore, the Eulerian portion of the hybrid model can be 3-D and with many grid cells, while the IBM portion of the model can track many variables, without compromising the speed of the model (see Chapter 2). The particle-based portion of our Eulerian/IBM hybrid model tracks 3 prognostic and 17 diagnostic variables (see Table 3-1). While the prognostic variables (i.e. $Soma_k$, $Gonad_k$, n_k,) allow the model to represent complex physiological processes, like spawning events—the diagnostic variables (e.g. A_k, R_k, F_k, RE_k, $f_k(Temp)$, $f_k(Salt)$, $f_k(Oxy)$, etc.) provide information crucial to the testing of the model (Franks, 2009) and valuable for the application of the model in site selection and farm management. The ability of Eulerian/IBM hybrid models to employ many particle-based variables makes them an ideal candidate to simulate ecosystems with multiple species and/or polyculture farms (e.g. Chapter 2), and to simulate scenarios with multiple size-classes in each grid cell (e.g. this study).

Our results also showed that cultured bivalves can have a significant effect on the planktonic ecosystem variability and nutrient cycling of the system. However, the effect of aquacultured bivalves on the environment in Ship Harbour is studied in detail elsewhere (Chapter 4).

3.4.2. Choice of Model Parameters

A disadvantage of all numerical models is that they can produce results even when supplied with non-sense parameters. Since the validity of the model results depends on the validity of the chosen of parameters, it is essential to validate the chosen parameters—for each particular application—by comparing model results against data. Data-model comparisons should include the main model results (i.e. prognostic variables), but also ancillary results (i.e. diagnostic variables) that should include modelled estimates of physio-

logical rates that are directly comparable against results from laboratory and field experiments (Franks, 2009). See Section 3.4.3 for a discussion of the data-model comparisons in this study.

Ideally, modellers should choose functions and parameters estimated from physiological experiments conducted on the same species, and under the same environmental conditions, as the model application. Unfortunately, ideal parameters are rarely available, thus modellers are often forced to improvise and use less appropriate parameters, often in simplified functions, and sometimes even to use parameters arising from educated guesses. Therefore, it is critical that modellers disclose their assumptions and point out their limitations.

In this study, the limitation of filtration by temperature was regulated by parameters that we chose from a study from Newfoundland (Thompson, 1984). These parameters imposed a reduction in the modelled filtration rate of up to 80% in the summer. We cannot verify if this temperature effect on filtration indeed occurred. However, based on anecdotal information from mussel farmers, we think that mussels in Eastern Canada are stressed during the weeks of hottest temperatures. But this limitation due to high temperature may be restricted to populations of mussels acclimated to cold water, since some population of mussels in Italy have been shown to exhibit normal filtration rates at temperatures above 25ºC (Schulte, 1975).

Also, the limitation of filtration by salinity was mediated through parameters we chose from a study assessing the impact of salinity on shell growth (Almada-Villela, 1984). We assumed that a decrease in shell growth reflects a decrease in filtration, but this may not be the case. The sporadic, yet pronounced, decreases in filtration due to low salinity in our modelled results (Figure 3-7) are the results of our choice of parameters and we do not have any way to verify if this phenomenon indeed happens in Ship Harbour. However, this can be seen as a new hypothesis that needs field data to be tested, with results being used to improve the parameterization. Overall, the effect of salinity on our modelled results was minimal and limited only to the mussels closest to the surface.

3.4.3. Comparison of Model Results against Data

Data-model comparisons showed that our model predicts planktonic ecosystem variables and bivalve physiology variables within ranges observed in the field (Figure 3-6 and Figure 3-7). However, due to restricted availability of forcing, our model results correspond to a different time from the time of collection of the observations. Also, some observations (from Cranford and Hill, 1999 and Thompson, 1984) were collected from different embayments than the modelled study site. This lack of concomitance limits the ability of the data to reject the model (Franks, 2009). That is, it is difficult to separate how much of the differences between the model results and observations are due to spatial and temporal differences, and how much is due to inadequacies of the model, or errors in our assumptions. However, even with these limited abilities, the available data provided a frame of reference that allowed us to constrain the model, and to evaluate the overall range of the modelled output. Nevertheless, it is important to confront the model against data collected in the same place and time as model results to be able to assess the model in more detail—particularly its ability to reproduce short term variations in planktonic ecosystem variability.

3.5. Conclusions

We developed an Eulerian/IBM hybrid modelling system capable of simultaneously representing feedbacks between planktonic ecosystem variables and bivalve ecophysiology processes. The Eulerian part of the modelling system was used to represent grid-based processes such as phytoplankton photosynthesis, grazing by zooplankton, uptake of nutrients and mineralization of detritus; while the IBM part of the modelling system represented bivalve ecophysiological processes, e.g., bivalve filtration, absorption, excretion, egestion and mortality. The simultaneous and combined simulation of these grid- and particle-based processes allowed us to assess (1) the effect of the environment on cultured

bivalves, (2) the effects of bivalves on the environment, and most importantly (3) feedbacks between the two.

The hybrid modelling system used in this study facilitates the implementation of numerous prognostic and diagnostic ecophysiological variables that make this model a versatile tool for aquaculture management. In this work we estimated the carrying capacity of a mussel farm in Ship Harbour, and we emphasized that carrying capacity is sensitive to the natural mortality of bivalves, a parameter that needs to be estimated accurately to produce precise estimations of the carrying capacity of a system. The 3-D hybrid model used in this work exemplifies the applicability of models with high spatial-resolution that also have high complexity in the number of processes represented by the model. However, these complex models must be carefully set up with appropriate parameters and rigorously tested against data before their use in operational decision making.

The hybrid model presented in this study is part of the Regional Ocean Modeling System (ROMS), which is an ocean model that has been widely used in applications ranging from effects of climate change (Wang et al., 2008), to larval connectivity (North et al., 2008; Rasmussen et al., 2009), to data assimilation from autonomous underwater vehicles (Chao et al., 2008), and is recognized as state-of-the-art ocean model by the oceanographic community. The use of ROMS for an aquaculture application is a step towards narrowing the gap between fundamental and applied sciences. It is beneficial for the aquaculture community because it adds sound tools to its repertoire, and it is also beneficial for the ocean modelling community because it makes modelling techniques more main-stream and promotes the wide use of these oceanographic tools.

CHAPTER 4

Impacts of Bivalve Aquaculture on the Spatial Distribution of Phytoplankton

4.1. Introduction

Bivalve aquaculture is growing exponentially world-wide (FAO, 2010). Therefore, the ability to measure and predict bivalve-induced changes in water quality, particularly the concentration and spatial distribution of phytoplankton, is essential to foster a sustainable and profitable shellfish aquaculture industry (Grangeré et al., 2010) and to preserve the functioning of coastal ecosystems (Worm et al., 2002).

Our current understanding of the effect of bivalves on phytoplankton is that dense aggregations of bivalves, through filter-feeding, decrease the local concentration of phytoplankton, as shown inside long-line farms (Grange and Cole, 1997; Ogilvie et al., 2000; Pilditch et al., 2001; Cranford et al., 2008; Grant et al., 2008; Guyondet et al., 2010), raft farms (Cabanas et al., 1979; Heasman et al., 1998), natural mussel beds (Prins and Smaal, 1994; Prins et al., 1996; Smaal and Zurburg, 1997), oyster reefs (Nelson et al., 2004) and beds of native (Nakamura and Kerciku, 2000) and invasive bivalves (Ackerman et al., 2001) in freshwater lakes. In addition, it is well documented that the waste products of bivalves locally increase the concentration of nutrients, particularly ammonia (e.g. Baudinet et al., 1990; Dame et al., 1991; Cranford et al., 2007; Jansen et al., 2011). However, the impact of this bivalve-mediated fertilization on the concentration and spatial distribution of phytoplankton has not been fully resolved. Mesocosm experiments with and

[*] This chapter comprises a co-authored manuscript by D. A. Ibarra, K. Fennel, J. J. Cullen. The contribution of the author of this thesis to this manuscript includes data collection and analysis, and manuscript writing. K. Fennel provided some of the model forcing, and K. Fennel and J. J. Cullen contributed with guidance and multiple rounds of corrections.

without bivalves showed that ammonia generated by bivalves may increase the growth rate of phytoplankton (Pietros and Rice, 2003). Also, field studies in mussel beds (Asmus and Asmus, 1991; Prins and Smaal, 1994) and long-line farms (Jansen et al., 2011) showed that—during nutrient-limited conditions*—the nitrogen released by the bivalves as waste exceeded the nitrogen consumed as phytoplankton. Therefore, many have suggested that during nutrient-limited conditions the bivalve-mediated fertilization has the potential to enhance phytoplankton primary production (Asmus and Asmus, 1991; Jansen et al., 2011), and perhaps even to increase phytoplankton biomass (Baudinet et al., 1990). However, Newell et al. (2004) debated that, due to burial of biodeposits and denitrification, bivalves ultimately reduce system-level phytoplankton production and biomass. Also, Prins and Small (1994) stated that bivalve grazing is an effective 'top-down' control that maintains a low phytoplankton biomass even during periods of nutrient enrichment, arguing that filter-feeders merely cause a higher turnover of phytoplankton. The key ecological question still remains: During nutrient-limited conditions, do bivalves decrease or increase phytoplankton biomass?

In this study, we argue that bivalves simultaneously do both, decrease and increase phytoplankton biomass, however they do so in separate locations. That is, bivalves decrease phytoplankton inside the farm, while increasing it outside the farm. To be clear and rigorous, we stated our argument in the form of a working hypothesis:

(A) *Throughout the year, filter-feeding by aquacultured bivalves causes a localized decrease in phytoplankton production and biomass inside the farm; but also,* (B) *during nutrient-limited and light-replete conditions, bivalve-mediated fertilization causes a localized increase in phytoplankton production and biomass outside, but close to, the bivalve farm.*

* In this study, "nutrient-limited" refers to conditions where the concentration of ammonium and nitrate is low enough to depress the growth rate of phytoplankton. In other words, it refers to conditions where the nutrient limitation term (Equation 2 in Fennel et al. 2006) is significantly less than 1.

Note that this hypothesis proposes localized increases and decreases in phytoplankton biomass. When averaging phytoplankton biomass over the whole embayment and over a whole year, we expect a net decrease of phytoplankton due to the presence of bivalves. However, it is the local concentration of plankton, nutrients and other biological variables, that is of interest for farm management (e.g. Waite et al., 2005) and for the assessment of the impacts of bivalves on other species (e.g. D'Amours et al., 2008). Therefore, in this study we focus on the distribution of phytoplankton at fine spatial and temporal scales.

To test the hypothesis above, first we have to use the hypothesis to predict patterns in the distribution of phytoplankton biomass in embayments with bivalve aquaculture. Then, to test the hypothesis, we can use field surveys and modelling experiments to see if we can find the predicted patterns. However, before we outline the predictions, it is important to define some spatial regions within embayments with bivalve aquaculture: the "inside-farm" region is defined as the space occupied by the aquacultured bivalves (Figure 4-1); the "beside-farm" region is the space surrounding the farm[*]; and the "far-field" region is the area away from the farm, but adjacent to the beside-farm region. The spatial patterns predicted by the hypothesis are illustrated in Figure 4-1 and outlined below:

From part (A) of the hypothesis, we expect to find—throughout the year—the minimum concentration of phytoplankton in the inside-farm region.

From part (B) of the hypothesis, we also expect to find—during nutrient-limited and light-replete conditions—the maximum concentration of phytoplankton in the beside-farm region, while finding an intermediate phytoplankton concentration in the far-field region.

As mentioned above, there many studies showing an inside-farm decrease in phytoplankton (e.g. Ogilvie et al., 2000; Guyondet et al., 2010), thus supporting the part of the hy-

[*] For the purpose of this study, we arbitrarily defined the width of the beside-farm region to be one farm length.

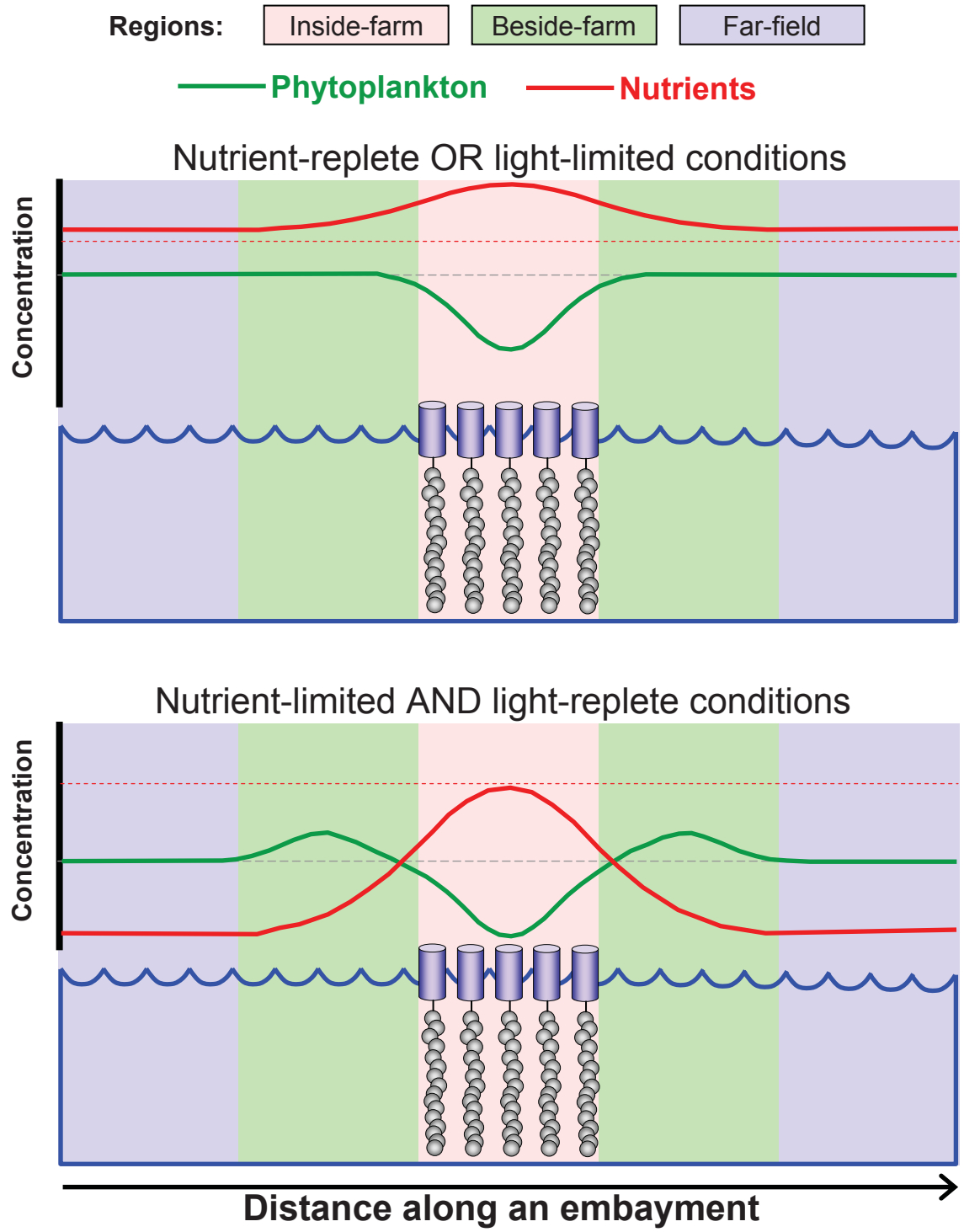

Figure 4-1. Diagram illustrating the different regions within an embayment with a bivalve farm. The minimum concentration of phytoplankton is expected to occur in the inside-farm region. However, during nutrient-limited and light-replete conditions, phytoplankton production is expected to increase around the farm, causing a halo of increased phytoplankton in the beside-farm region. Short red dashes represent the threshold between nutrient-limited and nutrient-replete conditions. Long gray dashes represent the concentration of phytoplankton in the absence of bivalves.

pothesis about decreased phytoplankton due to filter-feeding (i.e. part A). However, to the best of our knowledge, there is only one study showing an increase in phytoplankton biomass beside an aggregation of bivalves (Nakamura and Kerciku, 2000); thus supporting the part of the hypothesis about increased phytoplankton biomass due to bivalve-mediated fertilization (i.e. part B). However, the study by Nakamura and Kerciku (2000) was conducted in a lake with natural populations of bivalves. It is unknown whether bivalve-mediated fertilization can cause local increases of phytoplankton in coastal environments, which generally experience stronger currents than lakes, and which are the main arenas for the development of bivalve aquaculture.

To test the hypothesis above, we surveyed the spatial distribution of chlorophyll in an embayment with a bivalve farm during a time of the year characterized by nutrient-limited and light replete conditions (Platt et al., 1972). Like many other field studies of phytoplankton in bivalve farms (e.g. Fréchette et al., 1991; Pilditch et al., 2001; Dowd, 2003; Cranford et al., 2008; Grant et al., 2008), we used a combination of water samples and an *in situ* fluorometer to assess the spatial distribution of chlorophyll. However, unlike previous studies, we also used measurements from an *in situ* absorption meter, as a secondary (and independent) proxy for chlorophyll concentration (see instrument details in Section 4.2.2). The intention of our survey was to determine if distributions of chlorophyll were consistent with predictions from parts A and B of our hypothesis (see above). However, we could not be certain that the observed patterns were caused by the proposed mechanisms because we lacked appropriate controls (i.e. embayments without bivalves) and replicates (i.e. other embayments with bivalves), and even then there may be little validity in the notion of replicate embayments. Therefore, we used a 3-D hydrodynamic model coupled to a plankton ecosystem model and to a bivalve ecophysiology model (Chapter 3) to (1) predict patterns of phytoplankton distribution that could be compared to our measurements, thus increasing confidence that our observations could be caused by the proposed mechanisms; and to (2) run simulations with and without bivalves to isolate the effect that bivalves have on the concentration of phytoplankton and other biochemical variables.

There are many models representing interactions between bivalves and their surrounding environment. Many of these models are spatially-explicit, that is, the ecosystem model is coupled to a hydrodynamic model that divides the embayment into a fine grid in two dimensions (i.e. 2-D models; e.g. Duarte et al., 2003; Grant et al., 2008; Grangeré et al., 2010; Guyondet et al., 2010) or in three dimensions (i.e. 3-D models; e.g. Marinov et al., 2007; Spillman et al., 2008; Leon et al., 2011). However, many recent models represent an entire embayment using a single box (i.e. 0-D models; e.g. Grangeré et al., 2009; Byron et al., 2011). We wanted to explore if 0-D models could reproduce the embayment-averaged properties of the system, despite their inability to reproduce the fine scale gradients produced by bivalve farms. Therefore, we developed a 0-D version of our 3-D model to compare runs of the two models using the same physiological parameters and forcing, thus isolating the differences due to the spatial simplification of the 0-D model.

In this work, we (1) measured chlorophyll along a fjord in Eastern Canada during nutrient-limited and light-replete conditions; (2) reproduced the observed patterns using a 3-D model; (3) used the 3-D model to infer what mechanisms caused the patterns observed in the data and the model; (4) used the 3-D model to determine the effects of bivalve aquaculture on other planktonic ecosystem variables in the fjord; (5) compared results from the 3-D and 0-D models to assess whether the spatial gradients caused by the bivalve farm affect the predictive ability of 0-D models.

4.2. Materials and Methods

4.2.1. Study Site

Ship Harbour is a 10 km-long estuarine fjord in the Eastern shore of Nova Scotia, Canada (Figure 4-2). A shallow sill at a depth of approximately 7 m divides the fjord into an inner and an outer basin, both with maximum depths of approximately 25 m. The inner basin hosts one of the largest mussel farms in the province (Aquaprime Mussel Ranch Ltd.), where blue mussels (*Mytilus edulis* and *M. trossolus*) are grown in mesh socks suspended

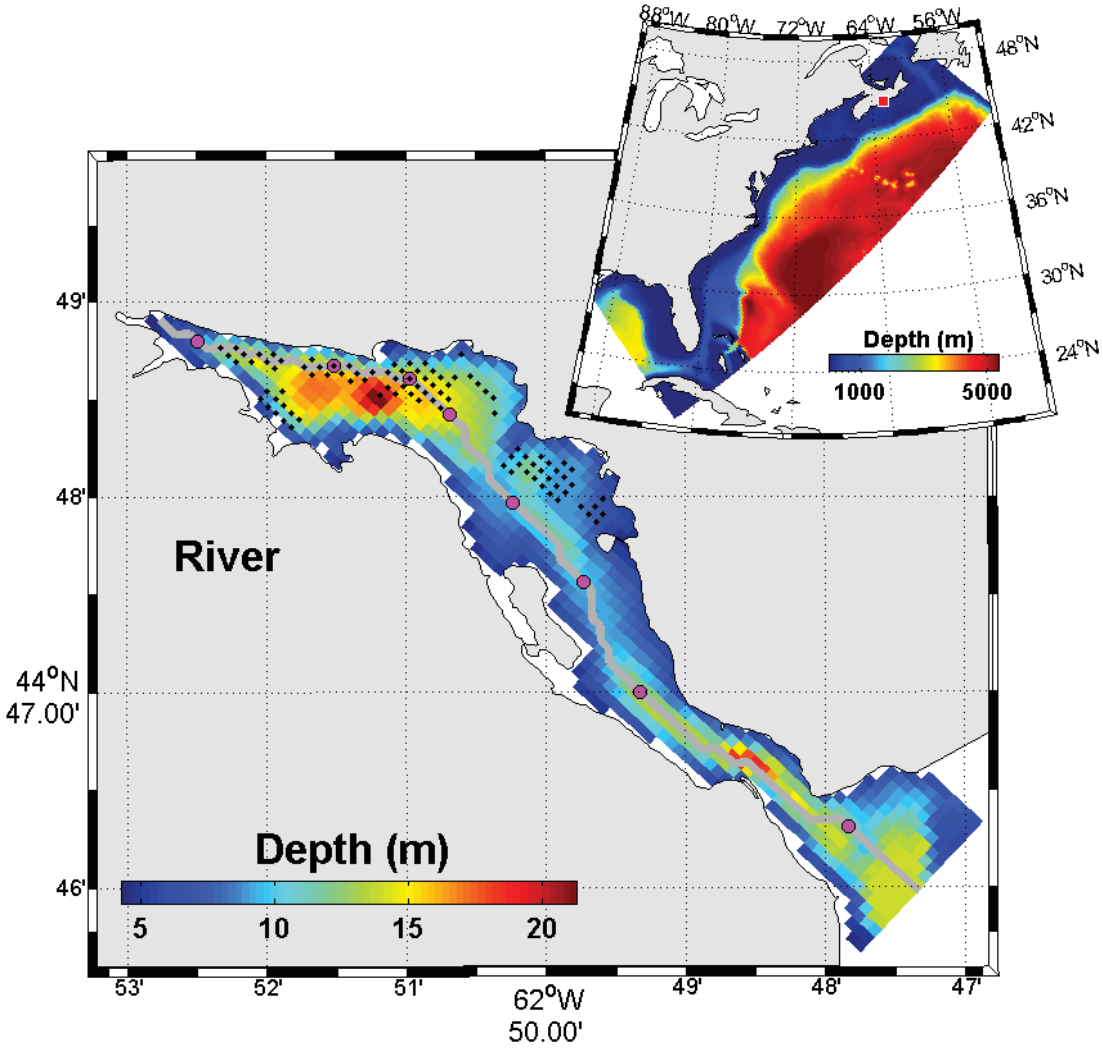

Figure 4-2. Upper-right corner shows bathymetry of the larger model domain (North-East North American shelf), which was used to force the open boundary of the smaller model domain, marked with a red square in the larger domain map. The main panel shows the bathymetry of the smaller model domain (Ship Harbour, Eastern Canada). The arrow marks the location of the river. The larger magenta dots mark the sampling stations, and the small black dots represent the Culture Units. Note that there are 4 Culture Units (on top of each other) occupying the middle of the water column, but this cannot be seen due to the perspective of this illustration. The gray transect line marks the location of the data presented in subsequent figures.

from long-lines (Sénéchal et al., 2008). At the time of this experiment, the farm had a stock of about 1000 tons of mussels (J. Stairs, pers. comm.). More information about Ship Harbour can be found in Gregory et al. (1993), Strain et al. (2002) and Ibarra (2003).

4.2.2. Data Collection and Analysis of Water Samples

During 5 days and nights (9 to 14 September, 2006), we conducted 18 transects along Ship Harbour (Figure 4-2). At every sampling station along the transect we cast an oceanographic sonde equipped with a chlorophyll fluorometer (ECO-FL3, WET Labs Inc.) and an absorption/attenuation meter (ac-s, WET Labs Inc.). At some of the sampling stations we also collected water samples. Sampling depths were chosen after visualizing output from the sonde to ensure water collection at prominent features of fluorescence and absorption. Additional water samples were collected at the surface and at approximately the middle of the water column, which was the depth where mussels were thought to have the greatest impact on the concentration of phytoplankton. Water samples were transported to shore within 2 h of collection, where triplicate aliquots (70 ml) were filtered through a Whatman GF/F glass fibre filter, and preserved in 10 ml of pre-chilled 90% acetone. The concentration of chlorophyll-a was later determined from the extracted samples using the Welschmeyer fluorometric method (Welschmeyer, 1994).

In situ fluorescence was measured in volts, but units were subsequently converted to mg Chl m^{-3} using a linear regression between *in situ* fluorescence and extracted chlorophyll concentration from the water samples (Figure 4-3).

Absorption spectra (400 - 758 nm) from the absorption meter were used to estimate a second proxy of chlorophyll using the method of Davis et al. (1997). Briefly, digital counts from the absorption meter were converted to engineering units (m^{-1}) by referencing them to clean Nanopure water counts, and by dividing by the pathlength of the instrument. Then absorption at the red peak of chlorophyll, $a(676)$ (i.e., absorption coefficient at 676 nm), was baseline-corrected using a linear interpolation between $a(633)$ and

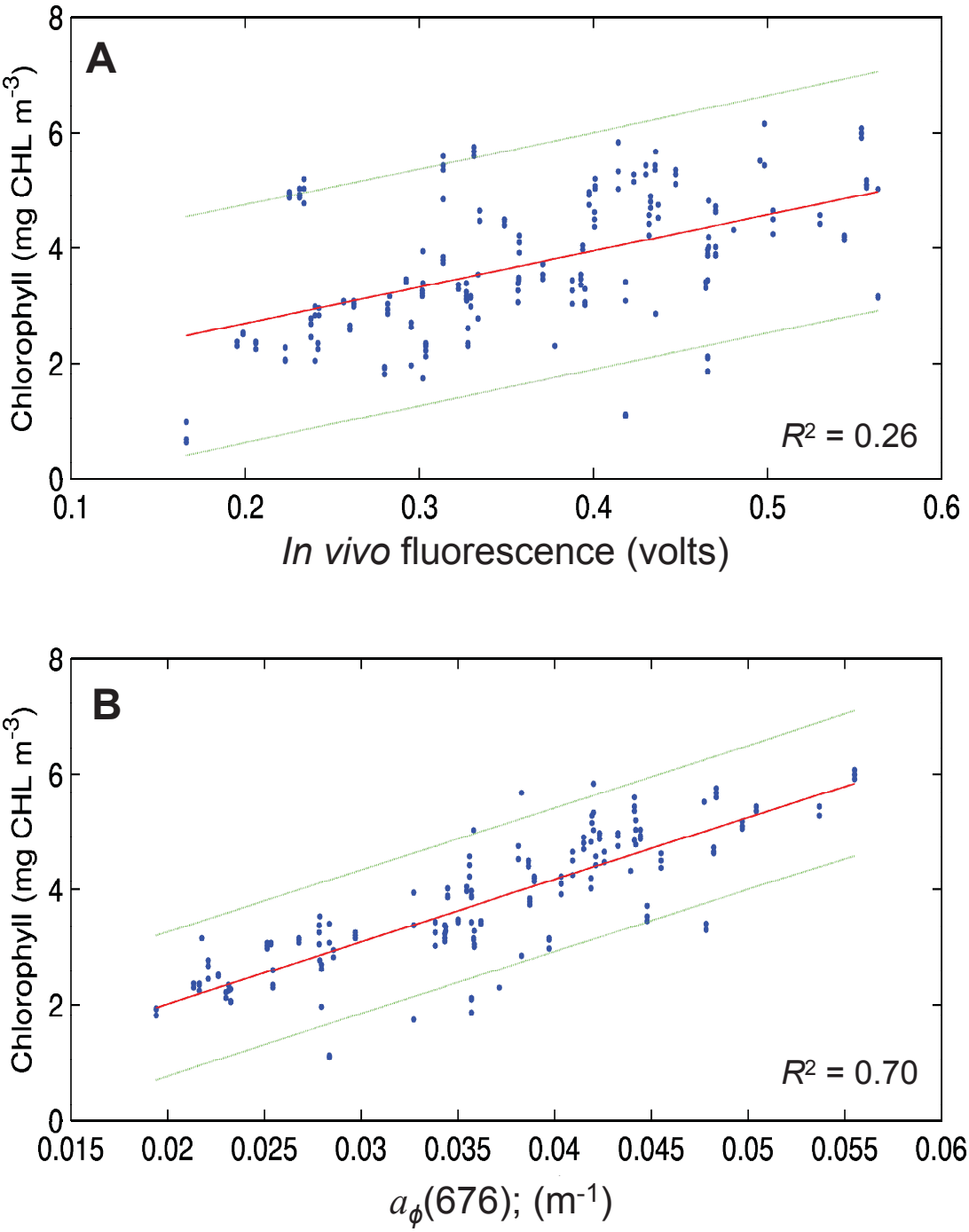

Figure 4-3. Calibration of instruments onboard the profiling sonde. Upper panel show the linear regression between *in situ* fluorescence and extracted chlorophyll from water samples ($R^2 = 0.26$, $p < 0.001$, $n = 204$). Lower panel shows the linear regression between baseline-corrected absorption at 676 nm, $a_\phi(676)$, and extracted chlorophyll nm ($R^2 = 0.70$, $p < 0.001$, $n = 178$). Green lines are 95% confidence intervals. Both regressions were calculated using 68 water samples (dots show each triplicate aliquot).

a(698). This corrected absorption was converted to mg Chl m^{-3} using a linear regression with extracted chlorophyll concentration from the water samples (Figure 4-3). We also compared the slope of this regression (units: m^2 mg^{-1}), which is an estimate of the specific absorption coefficient of phytoplankton (cf. Bricaud et al., 1995), to published observations.

4.2.3. 3-D Physical-biological Coupled Model

We used the Regional Ocean Modeling System (ROMS), which is a state-of-the-art, open-source, 3-D ocean modelling system (Haidvogel et al. 2008; www.myroms.org). Details of the application of ROMS to Ship Harbour, as well as its validation against a multi-year dataset of water samples, can be found in Chapter 3. Here we only present a summary.

ROMS is made of different modules that can be included or excluded. For this study, we used the hydrodynamic module (Haidvogel et al. 2008), one of the planktonic ecosystem modules (Fennel et al. 2006), and the individual-based biological module (Chapter 2) in combination with a shellfish ecophysiology module (Chapter 3). The hydrodynamic module of ROMS is an Eulerian, 3-D, sigma-coordinate, free-surface, terrain-following numerical hydrodynamic model that solves finite-difference approximations of the Reynolds-averaged Navier-Stokes equations using the hydrostatic and Boussinesq assumptions (Haidvogel et al., 2000; Shchepetkin and McWilliams, 2005; Haidvogel et al., 2008).

The planktonic ecosystem module (Fennel et al. 2006) describes the pelagic nitrogen cycle using six state variables: phytoplankton (*Phy*), zooplankton (*Zoo*), nitrate (*NO3*), ammonium (*NH4*), small detritus (*SDet*), and large detritus (*LDet*), all quantified in units of mmol N m^{-3}. The planktonic ecosystem model also tracks phytoplankton chlorophyll (*Chl*, mg Chl m^{-3}) and oxygen concentration (*Oxy*, mmol O_2 m^{-3}, Fennel et al. in preparation), and it has a simplified benthic component that immediately remineralizes (into ammonium) any organic matter reaching the bottom.

The shellfish ecophysiology model (SHELL-E; Chapter 3) describes shellfish physiology and population dynamics using an individual-based framework (Chapter 2). The model tracks the state of many discrete Culture Units (k)—each containing a number (n_k, ind) of identical bivalves (B_k, mmol N ind^{-1}). The total biomass of bivalves in a Culture Unit is defined as $n_k \times B_k$. Bivalve biomass is divided in reproductive and structural tissues (i.e. gonad and soma), and the model represents several physiological processes such as particle filtration, absorption, respiration, excretion, defecation, spawning, natural mortality and harvesting. Comparisons between model results and data from Ship Harbour, as well as discussion about the validity of the used parameters, are presented elsewhere (Chapter 3).

We ran three experiments using a high resolution grid made of 100 × 100 m cells and 10 evenly spaced vertical layers (Figure 4-2). Unless otherwise indicated, forcing and initial conditions were the same as in Chapter 3. Summarizing, forcing at the seaward open boundary was obtained from the output of a large meso-scale ROMS model for the North-East North American shelf (NENA; Figure 4-2) and from the WebTide tidal prediction model; atmospheric forcing was obtained from a meteorological station nearby; and freshwater entering Ship Harbour through the river was simulated using a synthetic time-series created using data from Gregory et al. (1993). The concentration of the planktonic ecosystem tracers in the river's fresh water was set to resemble a seasonal pattern (e.g. Dowd, 2005). All physical and planktonic ecosystem variables were initialized with constant values over the entire domain, followed by a model spin up to allow physical and planktonic ecosystem variables to reach a distribution representative of the model dynamics (see details below).

Experiment 1 - Comparison against bio-optical data. Using default parameters (Table 3-1), we ran ROMS/SHELL-E to simulate two weeks (output at 30 min intervals) during the time of the year of the survey, but for the year of 2005, because the NENA boundary forcing for 2006 was not available. The model was spun up for 2 weeks prior to the beginning of the experiment.

Experiment 2 - Effect of mussel density on planktonic ecosystem variables. We ran four 1-year simulations (output at 1 day intervals) for the year of 2005. For the four model simulations, we used all the default parameters (Table 3-1) with the exception of bivalve concentration*, which were 0, 15, 33.5 and 67 mmol N m^{-3}, respectively. Note that at the time of sampling (i.e. 2006), bivalve concentration was 33.5 mmol N m^{-3} (Ibarra, 2003). Therefore, the simulations represent a scenario with the current density (33.5 mmol N m^{-3}), scenarios with double and half the current density (15 and 67 mmol N m^{-3}, respectively), and a control without mussels. Simulations were spun up for 6 months prior to the beginning of the experiment. After all simulations were completed, the year-averaged concentration of every planktonic ecosystem variable was computed, and the effect of bivalves on each planktonic ecosystem variable was estimated by subtracting the year-average of each treatment run (i.e. bivalve concentrations of 15, 33.5 or 67 mmol N m^{-3}) from the year-average of the control run without bivalves.

Experiment 3 - Comparison of 0-D and 3-D models. We ran the 3-D ROMS/SHELL-E model using the same configuration of Experiment 1, with the exception of the planktonic ecosystem forcing at the seaward open boundary, where we used a constant concentration for all planktonic ecosystem variables to facilitate the comparison with the 0-D model. The constant values of the planktonic ecosystem variables were *Phy* = 0.7, *Zoo* = 1, *SDet* = 1.5, *LDet* = 0.5, *NO3* = 0.5 and *NH4* = 0.5; all in units of mmol N m^{-3}.

4.2.4. 0-D Biological Model

To assess if a 0-D model can accurately predict the bay-averaged properties of a system despite its inability to represent spatially-resolved patterns, we needed to compare results from two models, one 0-D and the other 3-D, which were otherwise identical to each other. Therefore, we created a 0-D version of the 3-D ROMS/SHELL-E model (see Appendix C). The 0-D model utilizes a single box to describe the planktonic ecosystem dy-

* The concentration of bivalves in each Eulerian grid cell was estimated as the biomass of the Culture Unit (i.e. $n_k \times B_k$) divided by the volume of the grid cell.

namics averaged over the entire embayment. The transport dynamics are reduced to a single parameter (i.e. flushing rate; d^{-1}) governing the exchange rate between the embayment and the open ocean waters. In this study, we assumed that the concentration of all planktonic variables in the open ocean remain constant throughout the simulation (values shown above), thus allowing us to estimate a steady-state solution for the concentration of all variables inside the embayment.

To compare the 0-D model against the 3-D ROMS/SHELL-E model, we used the 3-D model (i.e. Experiment 3) to compute the average bivalve concentration and the average filtration rate, which are quantities required as parameters for the 0-D model. After running the 3-D and 0-D models with the exact same initial conditions, parameters and open boundary forcing, we calculated the bay-averaged concentrations of all the variables of the 3-D model (at every time-step) and we compared them against the output of the 0-D model.

4.3. Results

4.3.1. Comparison of Bio-optical Proxies and Chlorophyll from Water Samples

We used two independent instruments onboard a profiling sonde to assess the concentration of chlorophyll in Ship Harbour: (1) a chlorophyll fluorometer and (2) an absorption meter. We also used measurements of extracted chlorophyll from water samples to calibrate the bio-optical instruments. The calibration consisted of linear regressions between extracted chlorophyll from the water samples and co-occurring measurements of *in vivo* fluorescence ($R^2 = 0.26$, $p < 0.001$, $n = 204$, Figure 4-3A) and baseline-corrected absorption at 676 nm ($a_\phi(676)$, $R^2 = 0.70$, $p < 0.001$, $n = 178$, Figure 4-3B); the latter was a better predictor of chlorophyll than the former (i.e. higher R^2). Measurements of *in situ* stimulated fluorescence are subject to non-photochemical quenching during conditions of bright light, which causes a decrease in the observed fluorescence in surface layers during the day (Cullen and Lewis, 1995). Fluorescence profiles conducted during the day were

subject to some degree of non-photochemical quenching and thus exhibited lower fluorescence signal than the profiles conducted at night, which were not subject non-photochemical quenching (data not shown). This is the main reason why the coefficient of determination of the regression between extracted chlorophyll and fluorescence was relatively poor. Also, this is why the standard deviation of the fluorescence-derived chlorophyll (Figure 4-4B) is higher than the standard deviation of the absorption-derived chlorophyll (Figure 4-4D).

Measurements of *in situ* absorption can be influenced by light absorbing substances other than chlorophyll, like coloured dissolved organic matter (CDOM) and non-algal suspended particles (Kirk, 1994; Mobley, 1994). However, CDOM absorption decreases exponentially with wavelength and at 676 nm is small compared to the shorter wavelengths. Also, the baseline correction method (Davis et al., 1997) further minimizes the effect of CDOM and other non-algal substances. In Ship Harbour, high concentration of CDOM can be found in the freshwater discharged by the river (Ibarra, 2003), however river flow was minimal during the experiment, thus CDOM close to the surface was not a problem in our dataset. However, CDOM can also be produced in the sediments (Shank et al., 2005). To minimize the risk of detecting CDOM or resuspended sediments, we tried to stop our instrument profiles a couple of meters away from the bottom. However, some of the observed high absorption close to the bottom (Figure 4-4C) may be the result on high CDOM or resuspended particles. Measuring a second proxy for chlorophyll is a good practice to avoid arriving at incorrect ecological conclusions due to biases on the relationship between chlorophyll and any proxy.

From the slope of linear regression between $a_\phi(676)$ and chlorophyll [$a_\phi(676) = (0.007 \times Chl) + 0.015$; $R^2 = 0.7$], we estimated the specific absorption of phytoplankton, $a_\phi^*(676)$ [m^2 (mg Chl)$^{-1}$], which is related to the dominant cell size of natural phytoplankton communities (Ciotti et al., 2002). The $a_\phi^*(676)$ found in Ship Harbour during the experiment (0.007 m^2 mg^{-1}) was consistent with the specific absorption of phytoplankton of about 100 μm (i.e. microplankton; 0.007 to 0.01 m^2 mg^{-1}; Ciotti et al. 2002). Realistic values for the slope of the regression reinforce the interpretation that the baseline-corrected red peak

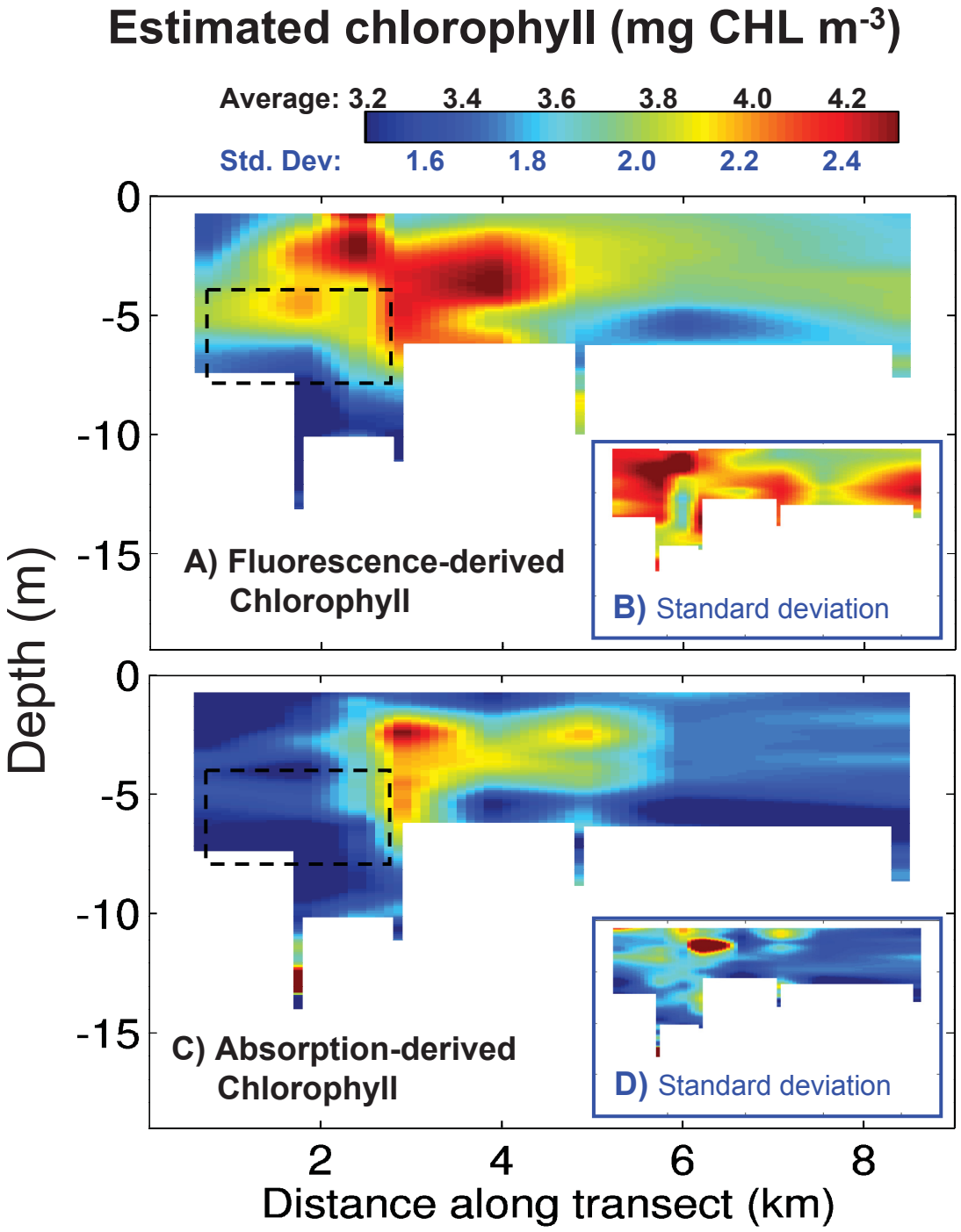

Figure 4-4. Bioptically-derived chlorophyll concentration, averaged over the 5 days of the experiment, along the transect line shown in Figure 4 2. The average chlorophyll concentration was estimated from 132 profiles using two independent instruments: an chlorophyll fluorometer (panel A) and an *in situ* absorption meter (panel C). The small inserts (panels B and C) are the standard deviation of the data shown in their respective larger panels. The dotted squares mark the region occupied by aquacultured mussels. The main chlorophyll feature shows a phytoplankton bloom beside the farm.

of the absorption coefficient is a useful measure of chlorophyll concentration. Notably, it is not sensitive to non-photochemical quenching, as is chlorophyll fluorescence.

4.3.2. Measured and Modelled Chlorophyll Concentration

From the 132 profiles conducted, over 5 days and nights, along Ship Harbour (see Figure 4-2 for details on the location of the transect line), we calculated two independent estimates of the average concentration of chlorophyll, based on fluorescence and absorption (Figure 4-4, panels A and C). Both estimates showed the lowest concentrations of chlorophyll (i.e. ~ 3.2 mg Chl m^{-3}) in the section of the transect occupied by aquacultured mussels (i.e. inside-farm region). Also, both estimates showed the highest concentrations of chlorophyll (i.e. ~ 4.5 mg Chl m^{-3}) in a region immediately beside the farmed mussels (i.e. beside-farm region); this apparent beside-farm bloom extended about 2 km away from the mussel farm. The concentration of chlorophyll close to the mouth of the fjord was approximately 3.5 to 3.7 mg Chl m^{-3}, somewhere in between the lowest inside-farm and the highest beside-farm concentrations. Our observations are consistent with the expected spatial distribution of phytoplankton biomass (i.e. inside-farm minima and beside-farm maxima) and thus support our hypothesis (see 4.1 Introduction). One discrepancy between the two methods used to estimate chlorophyll was that, using the fluorescence method, a relatively high estimated concentration of chlorophyll was shown in the surface layers above the region occupied by mussels (Figure 4-4A) , which was not evident in the estimates derived from absorption (Figure 4-4C). Examination of the possible causes of this discrepancy, such as influences of excreted nutrients on the physiology of phytoplankton and hence fluorescence yield, are beyond the scope of this study.

The depletion of chlorophyll inside the mussel farm, and the chlorophyll bloom beside the region with farmed mussels, were also reproduced using the ROMS/SHELL-E 3-D model (Figure 4-5). Although the magnitude and the horizontal location of the modelled bloom resemble that of the measured bloom, the modelled bloom occurred mainly in the surface layers. However this discrepancy may be because we used forcing from 2005 to force the model (forcing from 2006 was unavailable), thus two storms that occurred dur-

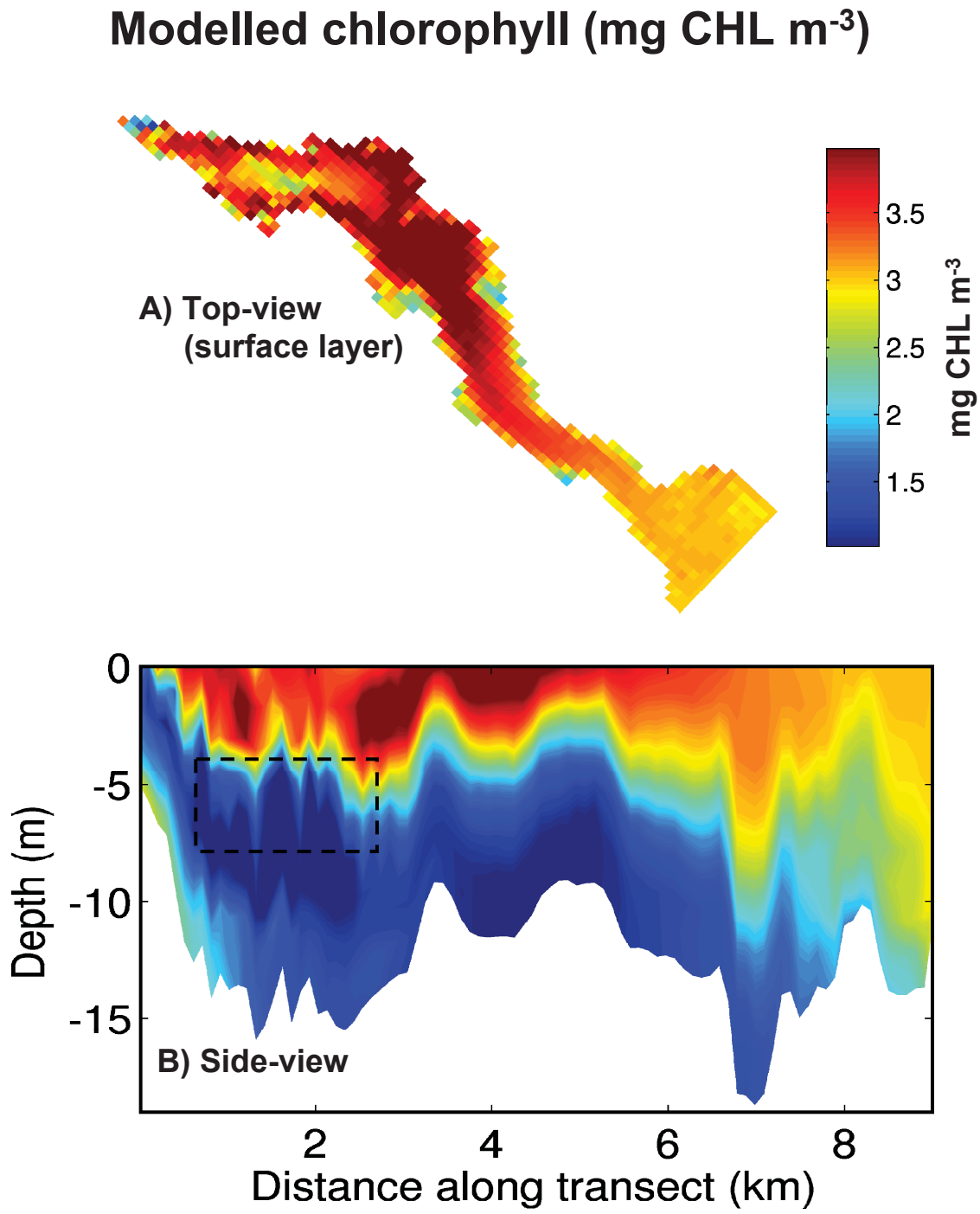

Figure 4-5. Modelled chlorophyll concentration. Panels show the average chlorophyll concentration estimated from a 5 days simulation using ROMS/SHELL-E, a 3-D hydrodynamic model coupled to a planktonic ecosystem model and to a bivalve ecophysiology model. Panel A is top view (surface layer), panel B is a side-view along the transect line shown in Figure 4-2. The dotted squares mark the region occupied by aquacultured mussels. The higher modelled chlorophyll concentrations occurred beside the aquaculture farm.

ing the 5-day experiment were not represented in the forcing. We speculate that these storms mixed the bloom deeper into the water column.

4.3.3. Impacts of Mussel Aquaculture on the Concentration of Chlorophyll

To estimate the effect of mussels on the concentration of chlorophyll, we subtracted a control model run without mussels from three treatment model runs with mussels at the current concentration (33.5 mmol N m^{-3}), half of the current concentration (15 mmol N m^{-3}) and double the current concentration (67 mmol N m^{-3}; Figure 4-6). We found that the modelled concentration of chlorophyll was reduced in the region occupied by the mussel farm (i.e. inside-farm region). The reduction of chlorophyll within the farm was observed at all times throughout the year, however the reduction was stronger during the spring and fall blooms (approx. -7 mg Chl m^{-3}, corresponding to 75%), and less intense during the summer months (approx. -1 mg Chl m^{-3}, corresponding to -50%). Also, the concentration of chlorophyll within the farm was more reduced in model runs with higher mussels concentrations (Figure 4-6). The low concentrations of chlorophyll inside the mussel farm are consistent with phytoplankton depletion by the filter-feeding activity of mussels, and with findings of others studying the impact of bivalve filter-feeding on phytoplankton (e.g. Fréchette et al., 1989; Pilditch et al., 2001; Ibarra, 2003; Grant et al., 2008; Cugier et al., 2010).

We also found in our model results that during half of the year (late spring to early winter), bivalves caused an increase in the concentration of chlorophyll around the farm (about 1 to 2 mg Chl m^{-3}). The halo extended several kilometres outside the farm, sometimes reaching the mouth of the fjord (Figure 4-6). This halo of enhanced chlorophyll was strongest close to the edge of the mussel farm (up to +8 mg Chl m^{-3} during some extreme events during the spring bloom). The enhancement of chlorophyll beside the farm was more pronounced in model runs with higher mussel concentrations. Also, in all model runs, the halo of enhanced chlorophyll was strongest during the spring bloom, and absent from January to late March. During these winter months, the chlorophyll-depleted water

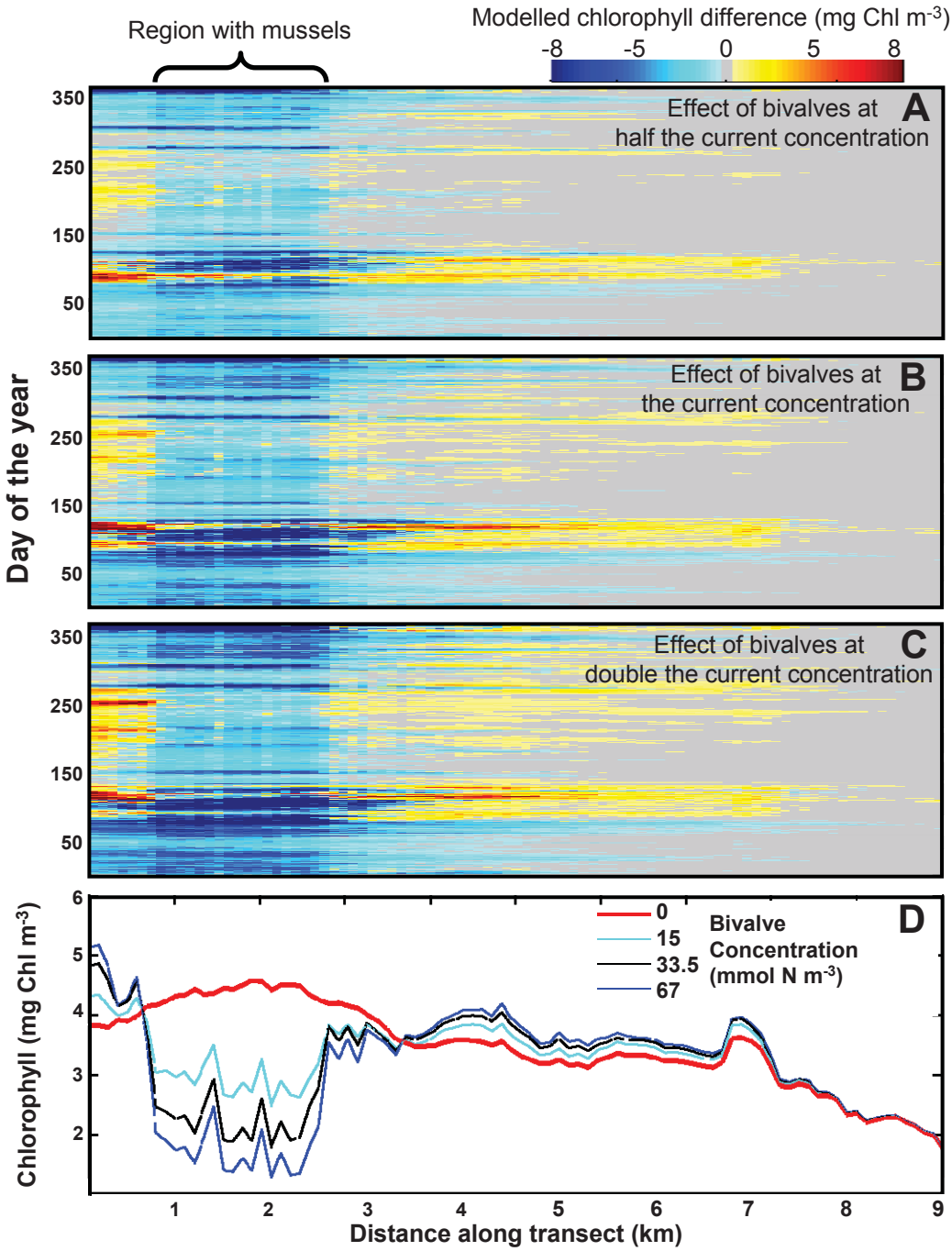

Figure 4-6. Effect of aquacultured bivalves on chlorophyll. Panels A, B and C show time-series of modelled chlorophyll difference along the transect line (see Figure 4-2) and the middle of the water column. Modelled chlorophyll difference was calculated by subtracting a control run without mussels from treatment runs with bivalve concentrations of 15 (panel A), 33.5 (panel B) or 67 mmol N m^{-3} (panel C). In all cases, chlorophyll was reduced in the region inside the mussel farm; however, from April to October (i.e. day 90 to 275), chlorophyll was enhanced in a region around the farm. Panel D shows the concentration of chlorophyll along the transect line, averaged between days 90 and 275, which the period when the system is nutrient limited (see Figure 4-7) and when the beside-farm enhancement of chlorophyll occurs.

inside farm produced a plume that extended several kilometres outside the farm, sometimes reaching the mouth of the fjord.

The gradient in chlorophyll between inside and beside the farm was steepest during the spring bloom (~10 mg Chl m^{-3} over 2 km; Figure 4-6B) because chlorophyll beside the farm was the most enhanced at the same times when the chlorophyll inside the farm was the most depleted. The gradient in chlorophyll difference between inside and beside the farm was also steeper in model runs with higher mussel concentrations. For example, during the summer, the chlorophyll difference between inside and beside the farm (i.e. 2 km apart) was 2 mg Chl m^{-3} in the simulation with half the current mussel concentration, 4 mg Chl m^{-3} in the simulation at the current mussel concentration, and about 6 mg Chl m^{-3} in the simulation with double the current mussel concentration.

During the half of the year when the halos of enhanced chlorophyll occurred, the average concentration of chlorophyll, for the run at the current mussel concentration (i.e. 33.5 mmol N m^{-3}), was reduced approximately 44% inside the farm, while it was increased about 8% in the area beside the farm (Figure 4-6C). The length of the plume of enhanced chlorophyll was approximately 4 km. Model runs with different mussel concentrations showed differences in the magnitude of the reduction in chlorophyll inside the farm, and in the enhancement of chlorophyll beside the farm. However, the spatial location of the regions of chlorophyll depletion and enhancement remained unchanged in all model runs. That is, model simulations with mussels crossed over the simulation without mussels (i.e. switching from chlorophyll enhancement to chlorophyll depletion), at the exact same location in the three simulations with different mussel densities.

In the ecosystem model used by the ROMS model (i.e. Fennel et al. 2006), phytoplankton production is estimated as the product of (1) the light- and temperature-limited growth rate (d^{-1}), (2) the dimensionless nutrient limitation, and (3) the local concentration of phytoplankton (mmol N m^{-3}). We calculate each of these three terms, as well as their product (i.e. phytoplankton production), to understand the processes that cause the development of the halo of enhanced chlorophyll (Figure 4-7). We found that Ship Harbour

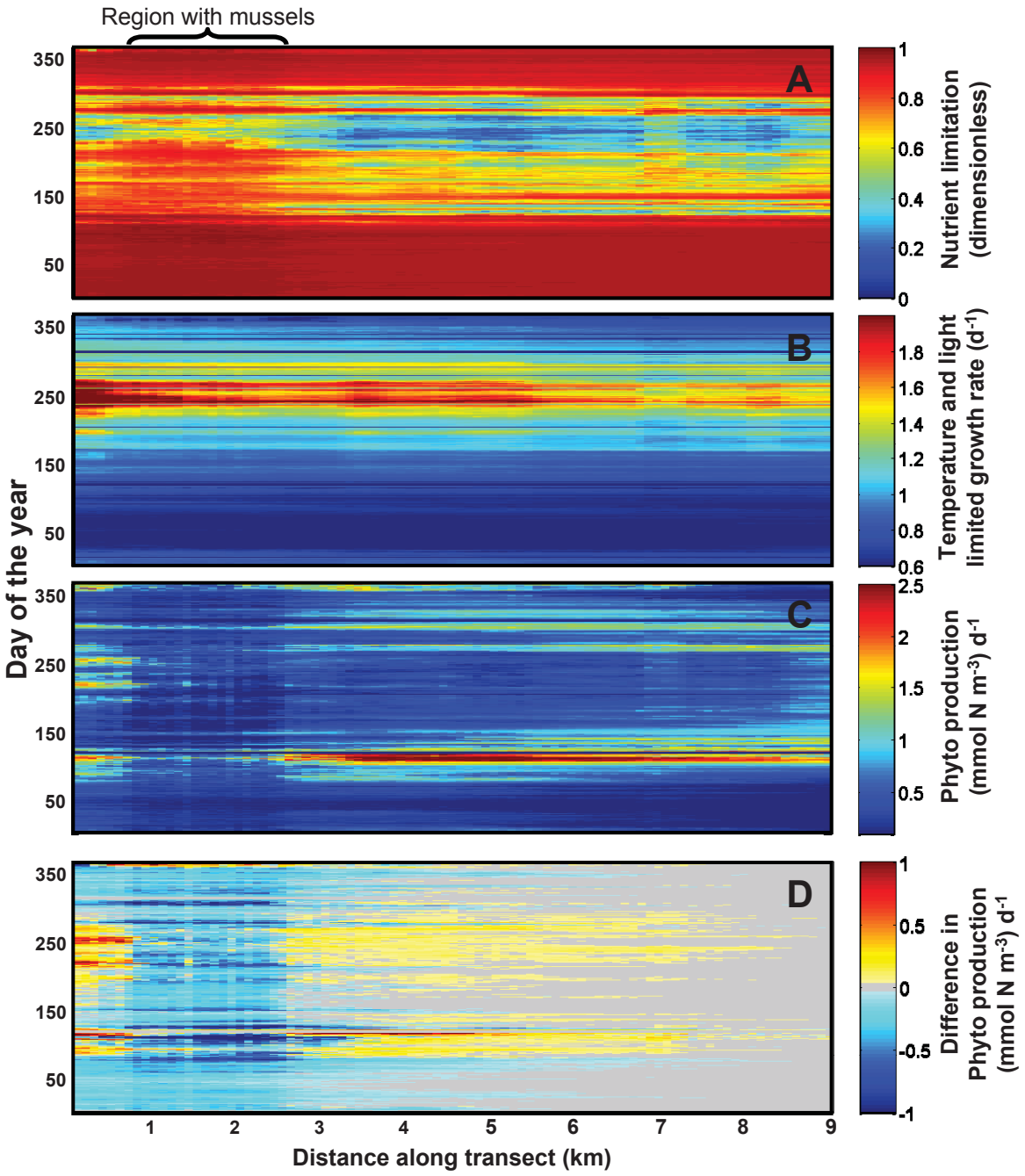

Figure 4-7. Modelled time-series along the transect line (middle of water column) of (A) phytoplankton nutrient limitation, (B) temperature- and light-limited phytoplankton growth, and (C) phytoplankton production, which was calculated by multiplying panel A by panel B, and by the phytoplankton standing concentration (not shown). Panel D shows the difference in phytoplankton production, which was calculated by subtracting the phytoplankton production from the model run using the current bivalve concentration (i.e. panel C), minus the production from a run without mussels (not shown).

follows a phytoplankton growth cycle typical of the North Atlantic (Riley, 1946; Platt, 1971). During the winter and late fall there is an abundance of nutrients thus relieving phytoplankton of any nutrient limitation (i.e. the nutrient limitation term is close to 1); however light is limiting, hence phytoplankton production is relatively low during those dark and cold months (Figure 4-7C). High primary production mainly occurs during two small windows in the spring and early fall (i.e. spring and fall blooms, respectively), which are times with high nutrients and high light. In the absence of aquacultured mussels, low primary productivity occurs during the bright summer months because the low nutrient concentration limits growth. However, in the case with aquacultured mussels, the waste products of mussels relieve the nutrient limitation inside and around the mussel farm (Figure 4-7A). Inside the mussel farm, the concentration of phytoplankton is kept low by bivalve filter-feeding, therefore the surplus of nutrients cannot be used. However, beside the mussel farm—where the phytoplankton stock is not reduced by mussel filtration—phytoplankton production is enhanced due to the increased concentration of nutrients produced as the wastes of the mussel farm. It is important to emphasise that currently our ROMS/SHELL-E model immediately remineralizes organic matter reaching the bottom thus not allowing for a lagged remineralization, which would further increase the local concentration of nutrients during the summer and thus further enhancing primary production beside the farm.

In Figure 4-7D, we subtracted the phytoplankton production from a control model run without mussels from the production from a treatment run with mussels. We found that mussels decreased primary production inside the mussel farm throughout the year (by 0.2 to 0.5 (mmol N m^{-3}) d^{-1} during the summer and by up to 1 (mmol N m^{-3}) d^{-1} during the spring bloom)—because of the local decrease in the phytoplankton standing stock, due to bivalve filter-feeding. However we also found that mussels increase primary productivity beside the lease during months with abundant light (by ~0.2 (mmol N m^{-3}) d^{-1} during the summer and by up to 1 (mmol N m^{-3}) d^{-1} in the spring bloom). Therefore we concluded that the halos of enhanced chlorophyll shown in Figure 4-4, are a result of halos of enhanced phytoplankton production caused by the increased nutrient concentration from mussel wastes, during the months of abundant light but limited nutrients. Our modelling

results support our hypothesis. Again, if our model would allow for a lagged remineralization of biodeposits, we would expect an even stronger pattern with higher concentration of phytoplankton in the halo.

4.3.4. Impacts of Mussel Aquaculture on other Planktonic Ecosystem Variables

To understand the effect of mussels on phytoplankton, we also looked at the effect of mussels on the concentration and spatial distribution of all other planktonic ecosystem variables. We calculated the year-averaged concentration of each planktonic ecosystem variable for a control model run without mussels, and we subtracted it from the year-averages of three treatment model runs with mussel concentrations of 15, 33.5 and 67 mmol N m^{-3} (Figure 4-8).

Mussels locally reduced phytoplankton nitrogen and chlorophyll in the area inside and in close proximity of the farm (Figure 4-8). However, mussels also caused a slight increase in the year-averaged concentrations of phytoplankton and chlorophyll, evaluated at mid depth, in regions outside the boundaries of the farm that extended all the way to the mouth of the fjord. The maximum depletion of phytoplankton and chlorophyll occurred in the middle of the largest mussel lease (i.e. 63% depletion of phytoplankton nitrogen, or 92% depletion of chlorophyll, for the simulation at the current mussel density). The maximum enhancement of phytoplankton and chlorophyll occurred outside, but close to, the mussel leases (i.e. 28% enhancement of phytoplankton nitrogen, or 63% enhancement of chlorophyll, for the simulation at the current mussel density); however the enhancement decreased with distance from the mussel leases. The value of the mean, minimum and maximum percent changes of phytoplankton and chlorophyll were dependent on the concentration of aquacultured mussels. However the spatial location of the minimum depletion and maximum enhancement did not appear to be dependent on the concentration of farmed mussels. That is, the region of the domain experiencing depletion or enhancement of phytoplankton remained approximately the same in the three simulations, despite their different mussel densities. What changed between the simulations was the degree by which phytoplankton was depleted or enhanced. When evaluating the entire domain for

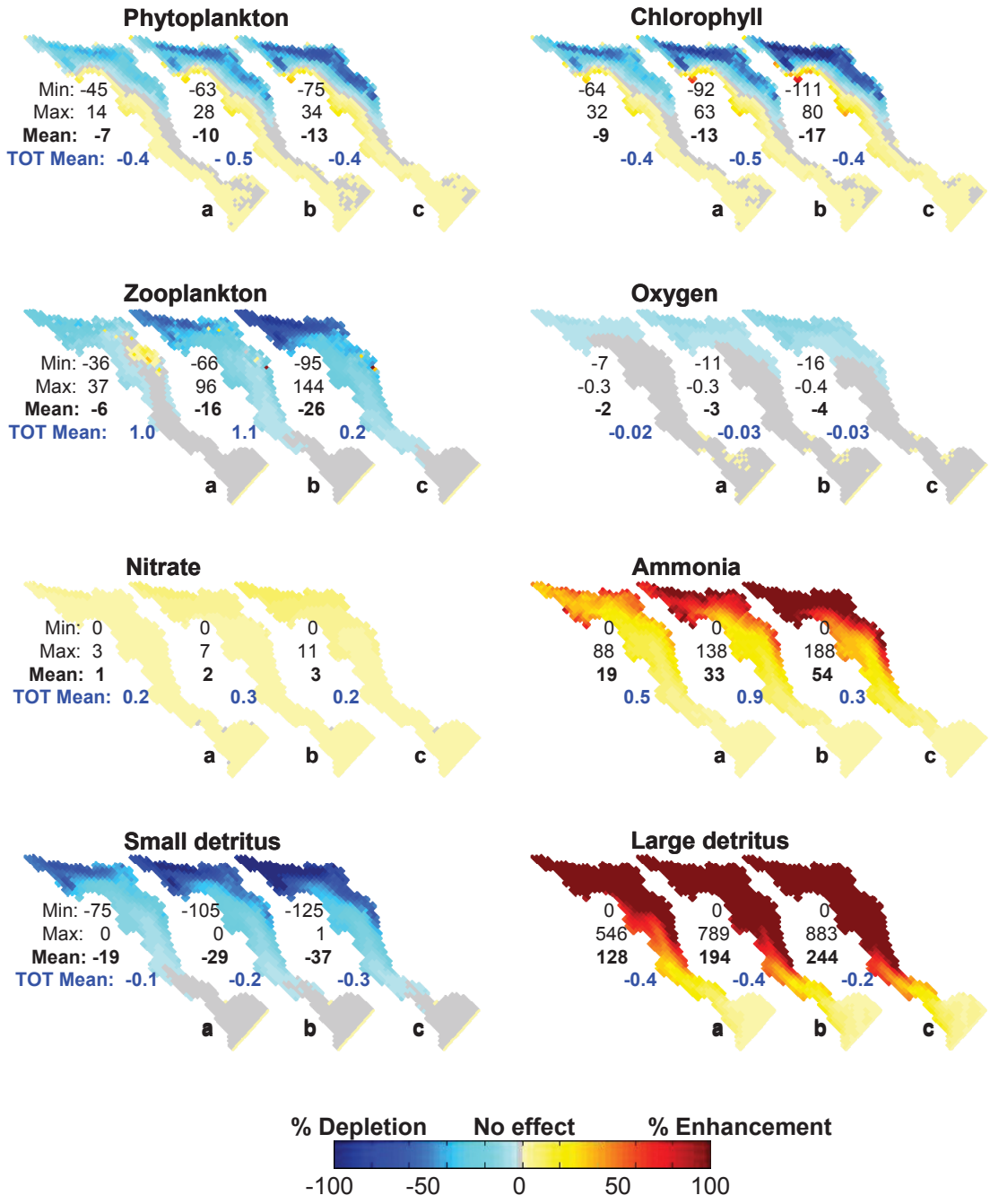

Figure 4-8. Effect of bivalve concentration on planktonic ecosystem variables. Each map of Ship Harbour (middle of the water column) represents the percentage difference calculated by subtracting the year-averaged results of a control model run without bivalves, from one of the treatment model runs with bivalves at half of the current concentration (a; 15 mmol N m^{-3}), bivalves at the current concentration (b; 33.5 mmol N m^{-3}), and bivalves at double the current concentration (c; 67 mmol N m^{-3}). Negative values (blue and cyan) indicate percent decrease in tracers due to the effect of mussels, while positive values (yellow and red) indicate percent increase. Min, max and mean numbers are the minimum, maximum and means of the data shown in each map (middle of the water column), respectively. Tot mean values are the mean of the entire domain.

the entire year, mussels decreased phytoplankton nitrogen and chlorophyll only by a small 0.5% (Figure 4-8).

Mussels had a similar effect on zooplankton and small detritus in the middle of the water column. Both zooplankton and small detritus were depleted by mussels, yielding the greatest depletion in the middle of the largest mussel lease (see metrics in Figure 4-8). The percentage of depletion of zooplankton and small detritus decreased with distance from the mussels to the point of negligible effect close to the mouth of the fjord. Both, the intensity of the maximum depletion and the length of plume of depleted water, were dependent on the concentration of aquacultured mussels. When evaluating the entire domain for the entire year, mussels increase zooplankton by 1.1% but decreased small detritus by 0.2% (Figure 4-8).

Oxygen in the middle of the water column was slightly depleted due to mussel respiration. However, the effect of mussels on oxygen was only restricted to an area inside the mussel leases and a small distance away from them (Figure 4-8). Nitrate was slightly enhanced by the presences of aquacultured mussels, presumably because of the decreased uptake caused by the depletion of phytoplankton. The enhancement of nitrate, although small, was highest inside the mussel leases and lower everywhere else. When evaluating the entire domain for the entire year, mussels decreased oxygen by 0.03% and increased nitrate by 0.3% (Figure 4-8).

Mussels had a large increasing effect on the concentration of both, ammonia and large detritus in the middle of the water column (see metrics in Figure 4-8). The concentration of ammonia and large detritus were greatly enhanced close to the mussels and the enhancement effect decreased with distance from the mussels. However, the enhancing effect extended all the way to the mouth of the embayment. The magnitude of the enhancement in ammonia and large detritus was directly related to the concentration of aquacultured mussels. In the entire domain (average for the entire year), mussels increased ammonia by 0.09%, but decrease large detritus by 0.4% (Figure 4-8), showing

that the effect of mussel on the water column variables depends on the scale of assessment.

4.3.5. Comparison of 3-D Model vs. 0-D Model

In the previous sections we emphasized that aquacultured bivalves produced strong gradients in the spatial distribution of planktonic ecosystem variables. However, number of bivalve-environment models are 0-D (e.g. Dowd, 1997; Rosland et al., 2009; Byron et al., 2011). That is, they represent an entire embayment using a single box, hence disregarding any spatial variability, and only representing temporal changes in the average state of the system. In order to assess the effect of this spatial simplification on the predictive capabilities of 0-D models, we constructed a 0-D version of the 3-D ROMS/SHELL-E model used in this study (see Appendix C for details). First we ran the 3-D model for 10 days using constant boundary conditions. Then we used the output from the 3-D model to compute parameters required by the 0-D model (i.e. average bivalve filtration rate and average phytoplankton growth rate). Finally, we ran the 0-D model and compared its output against the results from the 3-D model. We did this comparison on model runs with and without mussels (Figure 4-9).

When comparing results from the simulations without mussels, we found that the results from the 0-D model were very close to the 3-D model. The 3-D model showed semidiurnal tidally-driven oscillations that the 0-D model could not reproduce because of its simplified flushing scheme. However, the magnitude of most variables modelled with the 0-D model were remarkably close to those of the 3-D model. After the 10-day simulation, the largest discrepancies were on the concentrations of phytoplankton and ammonia (7% and 12%, respectively), but even those discrepancies were not very large.

On the contrary, when comparing the 0-D and 3-D results from the simulations with mussels, we found large differences. After a 10-day simulation, large detritus predicted with 3-D model was 44% higher than the predicted with the 0-D model, and small detritus predicted with the 0-D model was 22% higher than the predicted with the 3-D model. For all

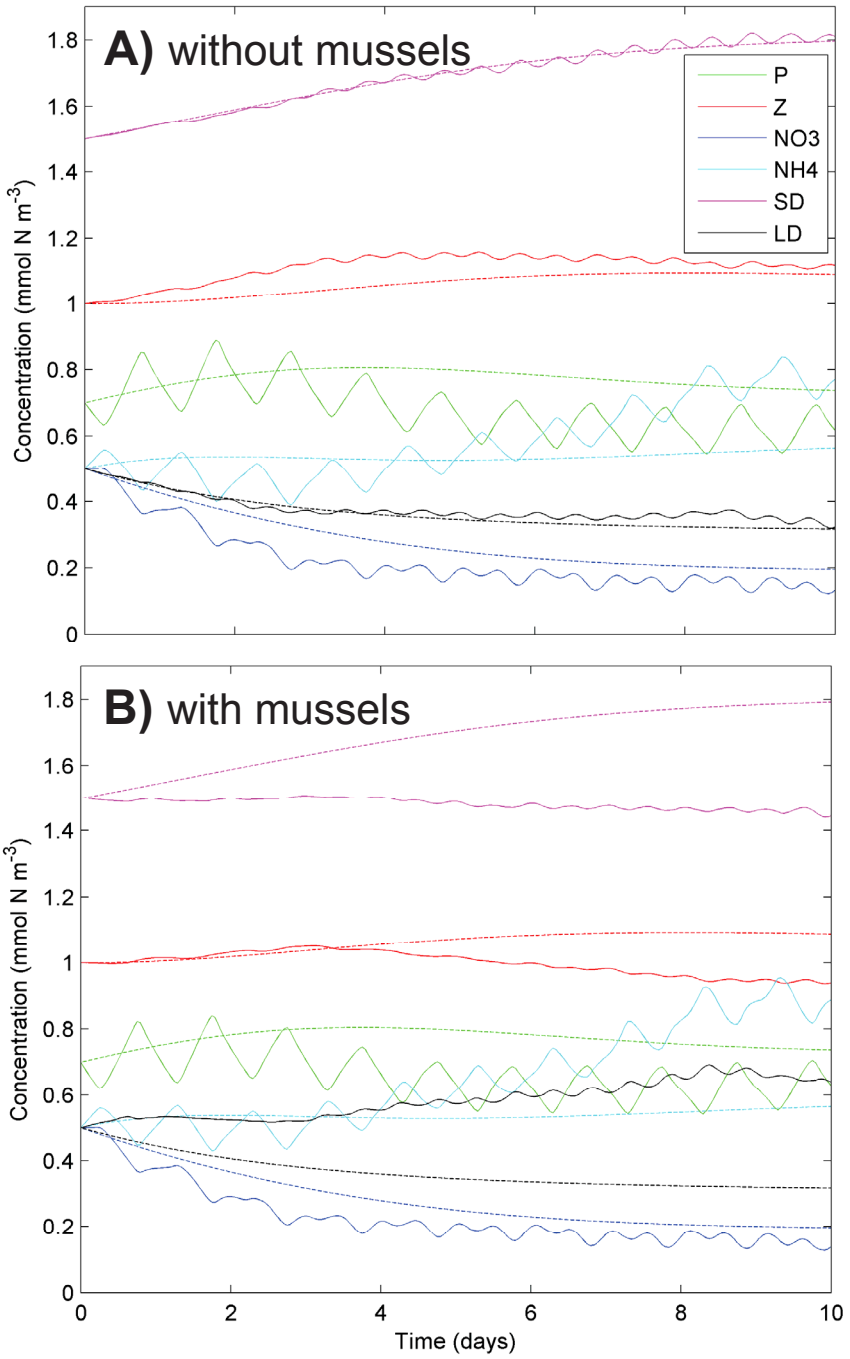

Figure 4-9. Comparison between the steady-state 0-D model (dashed lines) and the 3-D ROMS/SHELL-E model averaged over the entire embayment (solid lines). Different colors represent different planktonic ecosystem variables (see legend). Panel A show results from a run without mussels, while panel B shows results from a run with mussels at the current concentration.

other variables, the difference between the results of the 0-D and 3-D models with mussels were larger than the differences between the simulations without mussels. We concluded that the spatial gradients produced by sessile sources or sinks (e.g. mussel filtration or mussel excretion) can have a significant effect on the average state of the system. In these cases, 0-D models cannot resolve the average dynamics of the system and a 2-D or 3-D model is needed to adequately represent the system. However, multi-box models (e.g. Dowd, 2005; Grant et al., 2007) could be a computationally economic alternative to adequately represent systems with bivalve aquaculture.

4.4. Discussion

4.4.1. Impacts of Bivalve Aquaculture on the Spatial Distribution of Phytoplankton

In this study we found that bivalves locally reduced the concentration of phytoplankton inside the farm, but also—during nutrient-limited and light-replete months—enhanced the concentration of phytoplankton beside the farm. Many field studies measuring phytoplankton proxies have found results consistent with a decrease of phytoplankton biomass inside bivalves farms using long-lines (e.g. Rosenberg and Loo, 1983; Fréchette et al., 1991; Grange and Cole, 1997; Ogilvie et al., 2000; Pilditch et al., 2001; Coffin, 2003; Dowd, 2003; Ibarra, 2003; Grant et al., 2008; Strohmeier et al., 2008), farms using rafts (e.g. Cabanas et al., 1979; Heasman et al., 1998), and also inside naturally occurring mussel beds (e.g. Asmus and Asmus, 1991; Dame et al., 1991; Prins et al., 1996; Smaal and Haas, 1997). The depletion of phytoplankton inside farms has also been predicted using models that include hydrodynamics, bivalve filtration and phytoplankton production (e.g. Dowd, 2003; Grant et al., 2008; Cugier et al., 2010; Guyondet et al., 2010), and also with models that included hydrodynamics and bivalve filtration, but did not include phytoplankton production (e.g. Pouvreau et al., 2000; Pilditch et al., 2001; Ibarra, 2003).

The localized increase in phytoplankton biomass due to an enrichment of nutrients caused by bivalve wastes (i.e. excretion and remineralization of bio-deposits) has had far less

attention than the decrease of phytoplankton due to bivalve grazing. After measuring phytoplankton and nutrient fluxes in mussel farms (e.g. Baudinet et al., 1990; Jansen et al., 2011) and in natural mussel beds (e.g. Asmus and Asmus, 1991), the authors hypothesized that the nutrients from the wastes of bivalves had the potential to promote primary productivity, potentially offsetting bivalve filter-feeding, and thus resulting in a net increase in phytoplankton in the system. However, Prins and Small (1994) later concluded that bivalve filter-feeding keeps the phytoplankton biomass low, thus minimizing its ability to uptake nutrients, and thus rendering bivalve-rich system as net sinks of phytoplankton. Since then, the conclusion of Prins and Small (1994) has gained popularity, thus most researchers consider coastal ecosystems with dense aggregations of bivalves as systems controlled by top-down processes (i.e. filter-feeding) and net sinks of phytoplankton (e.g. Newell et al. 2004). Our model showed that for the system as a whole, mussels are of course a sink for phytoplankton. However, local increases are generated, and these merit careful consideration.

The main limitation of the work done in the early 1990's (Baudinet et al., 1990; Asmus and Asmus, 1991; Prins and Smaal, 1994) is that, when doing their nutrient budget calculations, the entire bay had to be considered as a single uniformly-mixed box. The 0-D approach used by these authors cannot resolve the spatial variability within the system; therefore the authors could not assess a scenario where phytoplankton biomass is decreased inside a farm or bivalve bed, but increased somewhere else within the embayment. With the development of spatially-explicit 2-D and 3-D models, researchers were able to assess the spatial distribution of phytoplankton in embayments with bivalve aquaculture; however, the emphasis was made on the depletion of plankton by filter-feeding. In one case (i.e. Cugier et al., 2010), results from a 2-D model of an embayment with bivalves actually showed an outside-farm increase in phytoplankton; yet this finding was overlooked. However, Cugier et al. (2010) did emphasize the importance of the feedback between bivalve waste production and phytoplankton growth on the increase of phytoplankton production during nutrient-limited conditions.

In the introduction we presented the working hypothesis that, besides decreasing phytoplankton biomass inside the farm, bivalves also increase phytoplankton beside the farm during conditions of limited nutrients but plentiful light. To our knowledge, our study is the first to provide observations and modelling results that support this hypothesis in a marine environment with aquacultured bivalves. However there is one other study, conducted in a freshwater lake, showing a chlorophyll decrease over a natural bivalve bed, follow by an increase in chlorophyll some distance away from the bed (Nakamura and Kerciku, 2000). In our study, the observed and modelled beside-farm enhancement of chlorophyll were higher than the reported by Nakamura and Kerciku (2000), which is likely because the farmed bivalves are kept at a higher concentrations that in natural beds.

On larger scales, the impact of bivalve filtration on phytoplankton has been described as the balance of residence time, filtration turnover rates and primary production rates (Dame and Prins, 1998; Gibbs, 2007). However, the localized effect of bivalves on phytoplankton is also of importance. Our results show how bivalves can locally enhance phytoplankton biomass during nutrient-limited conditions (i.e. in agreement with Asmus and Asmus, 1991; Jansen et al., 2011), while at the same time causing a system-wide decrease in phytoplankton biomass (i.e. in agreement with Prins and Smaal, 1994; Newell et al., 2004). This is an example of how spatially-explicit models can help resolve conundrums that cannot be solved by 0-D models. However, even within fine resolution models, it is hard to determine what is an appropriate spatial resolution; for example, Rosland et al. (2011) used grid cells of a few meters, much finer than the cell size used in this study. One advantage of ROMS is that it can handle nested grids of different resolutions, and also it can handle different cell sizes within one grid (i.e. finer cells in areas of interest), however we did not used this functionality in this study.

4.4.2. Mechanisms Responsible for the Beside-farm Increase of Phytoplankton

In this study, we also investigated the mechanisms responsible for the beside-farm enhancement of phytoplankton biomass. We found that—during months with sufficient light but limited nutrients—ammonia from bivalve excretion and remineralization of bi-

valve faeces and pseudofaeces, relieves phytoplankton from nutrient limitation in areas inside and around bivalve farms. The alleviation of nutrient limitation enhances primary productivity beside bivalve farms. However, inside the farm, the intense filter-feeding pressure maintains phytoplankton biomass low, minimizing the uptake of the available nutrients, and thus maintaining a low primary productivity inside the farm. The mechanisms responsible for the beside-farm enhancement of phytoplankton biomass imply that, during nutrient-limited conditions, phytoplankton beside bivalve farms grow using nitrogen that was fixed or deposited by the bivalves during times of food abundance and then slow-released throughout times of nutrient scarcity. In other words, bivalve farms may act as bio-capacitors that accumulate nitrogen directly in their tissues and indirectly in their biodeposits, during the spring and fall blooms, and then slow-release it throughout the year, effectively subsiding primary productivity beside the farm during times with bright light but low nutrient concentrations. The indirect effect, where organic matter produced during the spring bloom is accumulated into the biodeposit pool and subsequently remineralized and slow-released as nutrients, has been identified as an important mechanism to continue primary production during nutrient-limited conditions (Dowd, 2005; Cugier et al., 2010). We argue that the same happens with the nitrogen fixed in bivalve tissue (i.e. direct effect), which is then slow-released as metabolic by-products of maintenance metabolism ($R_m \times B_k \times n_k \times V^{-1}$ = 0.072 mmol N m^{-3} d^{-1}; evaluated for an average cell in day 250, see equations, parameters and figures in Chapter 3) and through the decomposition of mussels that died due to natural mortality ($\lambda_{nat} \times B_k \times n_k \times V^{-1}$ = 0.049 mmol N m^{-3} d^{-1}). The ammonium released as a result of growth-related metabolism ($\beta \times A_k \times n_k \times V^{-1}$ = 0.029 mmol N m^{-3} d^{-1}) is somewhat smaller than the other two sources because there is little food at time of the year (late summer). Also note the ammonium released through this last term (i.e. growth-related metabolism) is not "time-lagged"; that is, it is a result of food ingested shortly before the ammonium release.

Unfortunately, we could not fully test the bio-capacitor hypothesis because our model instantaneously remineralizes organic matter reaching the bottom. Therefore, our results only reflect the effect of the slow-release of ammonium through bivalve maintenance metabolism (i.e. direct bio-capacitor effect). Future work should quantitatively explore the

impact of the time lag between the deposition of bivalve faeces and pseudofaeces and their remineralization (i.e. indirect bio-capacitor effect). For alternative benthic-pelagic coupling schemes, see Soetaert et al. (2000).

4.4.3. Ecological Significance of the Beside-farm Increase of Phytoplankton

The near-field enhancement effect of bivalve farms and natural bivalve beds may play a significant ecological role in temperate ecosystems. Our measurements showed a maximum concentration of chlorophyll beside the mussel farm that was about 1 mg Chl m^{-3} higher than the far-field concentration. Although, this represents an increase of about 28% in chlorophyll, it still is a small increase compared to the main features of phytoplankton variability in the system (i.e. 15 mg Chl m^{-3} during the spring bloom; Strain 2002). However, in Chapter 3, we presented data from water samples showing spikes of up to 18 mg Chl m^{-3} in a station beside a mussel lease during the summer (Figure 3-6). We speculate that these chlorophyll spikes may be a result of resuspension of benthic microalgae, or vertical migrations of pelagic phytoplankton. However these processes cannot be reproduced by our model in its current configuration.

Regardless of the magnitude of the increase in chlorophyll in the beside-farm region, we argue that its ecological significance lies on the timing of this event. Nutrient-limited conditions occur during warm summer months, which are characterized by highest abundance and diversity of benthic invertebrates and demersal fish (Schmidt and Scheibling, 2007). Because the increased phytoplankton productivity associated with the relief of nutrient limitation occurs during this biologically active time of the year, the enhancement of primary productivity may propagate up the food chain, effectively increasing secondary and tertiary production in regions adjacent to bivalve farms and natural beds (e.g. D'Amours et al., 2008). Also, the relief of nutrient limitation beside the farm may benefit other primary producers besides phytoplankton—like seagrass (e.g. Wall et al., 2008) and macroalgae (e.g. in integrated aquaculture; Chopin et al., 2001). However, it is important to emphasize that bivalves simply rearrange the available nitrogen in the system, causing

enrichments that are localized in space and lagged in time (i.e. bivalves do not make nitrogen, so their effect on the inlet as a whole is as a net sink for nitrogen).

4.4.4. Potential Implications of the Spatial Gradients Caused by Bivalves

We found that bivalve farms may cause pronounced spatial gradients in the concentration of phytoplankton, not only by reducing the concentration inside the farm, but also by increasing the concentration beside the farm. The strong gradients in phytoplankton concentration have been shown to generate strong gradients in bivalve growth resulting in larger bivalves at the edge of bivalve farms (e.g. Waite et al., 2005; Strohmeier et al., 2008). Modelling studies attempting to predict the spatial gradients in phytoplankton concentration or in bivalve growth should include a planktonic ecosystem sub-model (Grant et al., 2008) and should include feedbacks between bivalve waste production and phytoplankton production (Cugier et al., 2010). Models not including these processes may have to "tweak" model parameters (e.g. bivalve filtration or bivalve absorption rate) to abnormally high values, to be able to reproduce observations; which is a bad modelling practice (Franks, 2009).

The restoration of natural bivalve beds (e.g. Pietros and Rice, 2003) or the development of bivalve farms (e.g. Rice, 2001) have been proposed as strategies to increase water clarity. Our results indicate that this strategy should work well in very eutrophic systems. However, if the system experiences nutrient-limited conditions during times of the year, the increase in water clarity may be restricted to areas inside bivalve farms or beds; but also, in cases with high-density bivalve farms, water clarity may actually decrease in regions outside the farm. Therefore, projects attempting to improve water clarity through bivalve filtration should consider the use a spatially-explicit 2-D or 3-D model to prevent undesired results.

4.4.5. Comparison of the 3-D and 0-D Bivalve-environment Models

In this study we compared a 3-D physical/planktonic ecosystem/bivalve ecophysiology model and a 0-D version of the 3-D model. We specifically built the 0-D model, with minimal physics but with the same ecosystem equations as the 3-D model, to be able to isolate the effect of spatial resolution on the model outcome. Guyondet et al. (2010) compared output of a fine-grid model against a coarse-box model applied to the same region and for the same time; however the equations of the two models were different, thus it was impossible to separate differences due to spatial resolution from the differences due to the distinct model formulations.

Our modelling results showed that 3-D and 0-D models produced very similar results in the absence of bivalves. However, when bivalves were added, the results from the 3-D and 0-D were different. This means that the presence of bivalves creates spatial gradients that modify the average state of the systems, in ways that 0-D models cannot reproduce. However, 0-D bivalve-environment models are still commonly used (e.g. Grangeré et al., 2009; Byron et al., 2011), and most of these studies have shown fairly good agreement between modelled and observed variables. Thus we think it is possible to counteract the effect of bivalve-induced spatial gradients by 'tuning' the ecophysiological parameters of 0-D bivalve-environment models. However—using the 'wrong' parameters to obtain the 'right' result—produces misleading insight about the system and is overall a bad modelling practice (e.g. Franks, 2009). In addition, when 0-D bivalve-environment models are used in an inverse configuration (i.e. where the objective of the model is to estimate model parameters from the observations), the resulting parameters are likely to be wrong. Also, 0-D models may have to be 'tuned' again after small changes in the system, like the addition of a second farm, thus making them less applicable for management. Therefore, 0-D bivalve-environment models may not be very useful for management or research applications that depend on the quantitative analysis of model results. However, multi-box models (e.g. Chapelle et al., 2000; Dowd, 2005; Grant et al., 2007) may provide a computationally economic alternative that may be used to estimate the average state of systems with bivalve aquaculture.

4.5. Conclusions

In this study we provided conclusive evidence supporting our hypothesis that aquaculture bivalves not only decrease phytoplankton biomass inside the farm, but also increase phytoplankton beside the farm during conditions of limited nutrients but adequate light. We observed an inside-farm chlorophyll minima and a beside-farm chlorophyll maxima, and we reproduced this observations using ROMS/SHELL-E, a 3-D physical/planktonic ecosystem/bivalve ecophysiology coupled model. We also determined that the inside-farm chlorophyll minima was caused by bivalve filter-feeding, while the beside-farm maxima were a result of bivalve-mediated fertilization caused by the farm wastes, which enhanced primary productivity during nutrient-limited and light-replete conditions (i.e. late spring to late fall). We also found that bivalve farms act as bio-capacitors effectively subsidizing primary productivity with ammonium released (via maintenance excretion and natural mortality) during times with low concentrations of nutrients, potentially having ecosystem-wide effects by enhancing nearby seagrass and macroalgae. Our results showed that the effect of bivalves on the spatial distribution of phytoplankton are complex, non-linear, and require spatially-explicit 2-D or 3-D models to be adequately resolved.

As bivalve aquaculture continues its exponential growth throughout the most complex and dynamic regions of the world (i.e. coastal environments), it is increasingly more important to employ state-of-the-art ocean models and bio-optical instruments, to assist ecosystem management and to prevent a decline of the functions and services of these coastal ecosystems.

CHAPTER 5

Conclusions

5.1. Weaving Marine Ecosystems from End to End

It is a common practice in experimental ecology, and perhaps in science in general, to isolate successively smaller parts of nature for its detailed study. As Kremer and Nixon (1978) pointed out, this reductionism is implicit in a large and growing literature dedicated to the study of physiological and ecological responses of organisms under controlled laboratory conditions, and controlled field experiments. The aim of many of these studies is to generate insights about the role of these organisms in their ecosystems. However, it is very difficult to intuitively deduce the role of these organisms in hydrodynamic and complex ecosystems with many feedback controls. Therefore, researchers have used numerical simulation models to propagate the effect of these organism-level responses to entire ecosystems. For example, Eppley and Thomas (1969) estimated the growth rate of some species of marine phytoplankton in a controlled laboratory experiment, then Fasham et al. (1990) used these growth rates (and others, Eppley, 1972) to estimate the role of phytoplankton in oceanic mixed layer ecosystems.

While models are inherently reductionist because they can never include all the complexity of the "real world", one may argue that modellers follow an approach reversed to the reductionist approach used by experimental scientists. That is, the building blocks of models are the findings from controlled experiments, which are then pieced together into successively larger and more comprehensive models. While most modellers strive to use the simplest model that reproduces the observed data, the scientific questions confronting scientists are increasingly more complex, and thus there is a trend towards developing holistic models, which out of necessity are increasingly more complex and comprehensive models (Arhonditsis et al., 2008). However, as we explain below, overly complex

and over-parameterized models can surpass our ability to constrain them properly with observations and may not necessarily increase insight or predictability. As suggested by Anderson (2005), the increase of model complexity needs to be done gradually and with a "healthy dose of scepticism regarding model outcomes."

While ecosystem models are also becoming increasingly more complex, differences in scientific questions have resulted in two distinct modelling paths. When interested in biogeochemical cycles, models tend to increase in complexity by coupling planktonic ecosystem models to hydrodynamic and particle dynamics models (e.g. Fasham et al., 1990). On the other hand, when interested in marine resource management, models have tended to increase in complexity by increasing the number of species in the model (e.g. Ecopath; Christensen and Walters, 2004). Until a few years ago, computational constraints forced a choice between including high spatial resolution and hydrodynamic realism, or including a high trophic resolution (i.e. many species or functional groups). However, it is increasingly more evident that ecosystem models need both, spatial/hydrodynamic realism and trophic realism (Moloney et al., 2011). In nature, feedback loops among multiple trophic levels are a fundamental requirement for the stability of complex food webs (Rooney et al., 2006; Neutel et al., 2007). It makes sense to think that the same feedback loops are a fundamental requirement for the stability of modelled food webs (Hannah et al., 2010). Therefore, the goal ahead is to develop broadly applicable hydrodynamic modelling frameworks (e.g. Biogeochemical Ocean General Circulation Models; Friedrichs et al., 2009), capable of representing interactions of species from end to end of the trophic spectrum (Travers et al., 2007; Fennel, 2008; Fulton, 2010; Moloney et al., 2011).

Two foreseeable challenges on the road to develop end-to-end models are: (1) how to deal with the increased model complexity? and (2) how to deal with the increased computing demand? The first challenge regards the observation that, in complex models, the increased number of parameters can surpass our ability to constrain them properly from observations (i.e. unjustifiable degrees of freedom; Denman, 2003; McDonald and Urban, 2010). That is, increases in model complexity tend to produce a better model fit to calibration data; however, beyond a certain level of complexity the benefits of adding pa-

rameters are diminished because the risk of overfitting becomes greater (Myung, 2000; McDonald and Urban, 2010). On the other hand, removing parameters indiscriminately is also dangerous and it has been argued that modellers should not omit biological complexity unless it had been demonstrated (empirically and/or mathematically) that it is safe to do so (Flynn, 2005). Therefore, the increase in model complexity should be guided by the increase in the number of observational data sets that can be used to validate the model parameters. However, the risk of overfitting is only one problem of model complexity, another problem regards the observation that when models become too complex, the model "payoff" starts to decrease (Grimm et al., 2005), likely because the modeller has to spend too much time figuring out what is the model doing, thus leaving less time to use the model to solve scientific questions. This later problem may be solved by following a "community approach", where many modellers share the task of developing and validating different parts of the modelling framework, and where exchanges of information among developers, users and modellers in-training are accomplished via online discussion boards and wikis (e.g. www.ecopath.org and www.myroms.org). Other examples of community models are the models targeted to specific regions, like those developed by multinational European groups (e.g. COHERENS and ERSEM). In community-supported models, the total time invested to model development and validation (i.e. the sum of the time investment from all community members) can be much greater than the time investment of a single modeller or a single modelling laboratory. Therefore, if the main limitation of model "payoff" is the time investment for model development and validation, then the community approach is the only plausible alternative to tackle the increasing demands for model complexity. However, users of complex models (same as any other model) still need to validate model parameters and still need to understand the model assumptions and limitations, and achieving these requirements is not necessarily any easier under a "community approach".

The problem of increased computing demand is discussed in the next section.

5.2. Hybrid (Eulerian/IBM) Modelling Framework

Modelling a large number of state variables in a Eulerian 3-D space demands a lot of computing resources. In shallow coastal applications—where the grid cells must be about 100 m apart and where the model time step must be in the order of a few seconds—modelling a large number of state variables truly exceeds the limits of even today's high-performance computer clusters. In this thesis, to overcome this computer limitation, a hybrid (Eulerian/Individual-based) modelling framework was developed (Chapter 2). In this hybrid framework, tracer-like variables that occur everywhere within the model domain (e.g. temperature or phytoplankton concentration) are specified using a grid-based or Eulerian framework, while variables that only occur in a few places within the domain (e.g. biomass of aquacultured mussels) are specified using a particle-based framework. In an example shown in Chapter 2, the hybrid framework was able to represent the ecosystem dynamics using only 27% of the calculations needed by a grid-based model alone, or only 0.6% of the calculations needed by an individual-based model alone. However, in this thesis the hybrid model was applied to examples with only a few species; far less than conventional food web models. Although a reasonable starting point, the hybrid approach still needs to be applied to a true multispecies ecosystem, in 3D space, to verify the claim of optimal performance.

Hybrid models were first developed almost 30 years ago to study phytoplankton dynamics (Woods and Onken, 1982) and have also been used to study zooplankton dynamics (Batchelder et al., 2002). However, these models were not widely used, perhaps because plankton is ubiquitous and needs to be specified more or less everywhere within the model domain, therefore these hybrid models require more computing resources, than a grid-based model would, to represent the same variables. Also, Lande and Lewis (1989) showed that plankton dynamics computed with an individual-based model were very similar to results from an equivalent Eulerian or grid-based model, thus concluding that the increased computing demand was not worth it. However, a different story emerges from hybrid models that utilize their individual-based capabilities to study macrobiota species that are only found in a few grid cells. Here not only the computing efficiency of

the model is greatly increased, but also the individual-based approach is better suited to represent the life-history of macrobiota species.

The main limitation of hybrid models is that they require coding the ecophysiology models directly inside the code of an ocean circulation model, which are usually written in a language foreign to ecologists (i.e. Fortran). However, ecology is a field used to interdisciplinary work. For example, the newest generation of ecologists are now very fluent in R (www.r-project.org), a statistical software initially developed by statisticians for statisticians, but that is now increasingly used in ecological studies. Nonetheless, to promote a wide use of hybrid ecosystem models, it is key to demonstrate their applicability and to lay out their usefulness. The message of this thesis is that—in the ocean—all phenomena of ecological interest occur within a fluid environment that is non-intuitive for us terrestrial-minded beings. Therefore, studying these phenomena within a hydrodynamic framework is likely to produce new insights about marine ecosystems. Ocean circulation models are a natural platform where these ecological processes can be represented, and thus the implementation of these hydrodynamic tools in ecological research should be fostered.

5.3. Interactions Between Macrobiota and its Physical-planktonic Environment

In this thesis, it was shown that—in shallow costal regions—macrobiota species, like macroalgae and bivalves, can have a large influence in the concentration and spatial distribution of planktonic ecosystem variables like the plankton, nutrients and detritus. It was also shown that the resulting persistent gradients in the concentration of the planktonic variables can in turn affect the physiology of macrobiota, representing feedbacks that can regulate the spatial distribution of macrobiota biomass.

The interactions between macrobiota and planktonic variables are complex, non-linear, and sometimes non-intuitive. Here, a hydrodynamic model coupled to a planktonic ecosystem model and several macrobiota ecophysiology models was able to reproduce most of the expected patterns, like bivalves locally decreasing phytoplankton, or fish wastes enhancing nearby macroalgae (Chapter 2, Figure 2-3). However, the model also produced other patterns that were not expected, such as oysters decreasing ammonia and large detritus. In Chapter 3, one of those non-expected results (i.e. mussels locally increasing nearby phytoplankton) was studied in detail. It was found that the waste products of mussels (i.e. ammonium) cause a localized increase in phytoplankton production and biomass in areas outside, but nearby, mussel farms during nutrient-limited and light-replete conditions. In this thesis, 67 studies researching the influence of bivalves on phytoplankton were reviewed. Form those 67 studies, the localized increase in phytoplankton due to bivalve wastes was only briefly mentioned as a possibility in 3 studies, and actually measured in only one study. This is an example about how patterns that are not intuitively expected can be lost in the data and modelling results. Unfortunately, in hydrodynamically complex systems like shallow coastal regions, even subtle feedbacks can cause patterns that escape intuition, but that are ecologically relevant. This emphasises (1) the need for hydrodynamic models capable of resolving feedbacks among macrobiota and planktonic variables, and (2) the need to look at the model results without any 'tuning' (i.e. all parameters set to their default, or best guess, value[*]). Unexpected model results can be caused by human mistake in the model formulation or parameterization, but they can also be evidence of a pattern that is escaping our intuition and that deserves further investigation.

Macrobiota species increase the temporal and spatial variability of the planktonic ecosystem variables—particularly in shallow coastal ecosystems. This is shown in the data and modelling results presented throughout this thesis (e.g. Figure 2-4, Figure 3-6 and Figure 4-4), but also in data and modelling results from most of the studies conducted in shallow regions that were reviewed here. This high temporal and spatial variability probably has a

[*] After the first inspection of model results using the default or best guess values, the parameters can still be fine tuned to improve model predictions.

large influence in all organisms living in these shallow regions, but certainly, it has a huge influence on the research efforts attempting to depict ecosystem dynamics in these systems. One approach to produce scientific insight in these highly variable regions is to use mechanistic numerical models like the one used in this thesis. However, as shown in Chapter 2, these models must integrate macrobiota and planktonic ecosystem variables using a two-way coupling approach that allows bidirectional transfers of mass; thus conserving the mass-balance of the system. Also, as shown in Chapter 4, these models must be spatially-explicit (i.e. 2-D or 3-D) because in these shallow regions macrofauna often produces persistent gradients in the spatial distribution of the planktonic variables. Box models (i.e. 0-D) that assume a uniform distribution of all variables throughout the model domain cannot reproduce the average state of systems showing persistent and/or strong spatial gradients of any variable. In summary, in applications where the modelling objective is to resolve spatial interactions between macrobiota and the planktonic ecosystem, it is essential to use coupled hydrodynamic-biological models that are spatially-explicit and with ecosystem components are two-way coupled.

Understanding the interactions between macrobiota and its physical-planktonic environment is of special interest in the management of any activity taking place in coastal regions, particularly aquaculture. As shown Chapter 3, calculations essential to the management of bivalve farms, such as the estimation of the carrying capacity of the system, involves simulations that depend on the appropriate representation of subtle feedbacks between spatially-heterogeneous variables. As shown in Chapter 2, these simulations are of particular importance in systems where many species are farmed simultaneously (i.e. Integrated Multi-Trophic Aquaculture). In theory, growing multiple species simultaneously maximizes growth and minimizes wastes. However, in practice, it is key to place each farmed species in an appropriate location in relation to the other species given the hydrodynamic environment, and this is very hard to do without a spatially-explicit hydrodynamic-ecosystem model that bilaterally integrates planktonic variables and macrobiota variables. Finally, as pointed out earlier, this requires an optimized hybrid modelling framework capable of handling both, grid-based and particle-based, biological variables.

5.4. Future Work

In Chapter 2, interactions among macrobiota and planktonic species were assessed in a synthetic embayment. Future work should attempt to assess these interactions in a real embayment where the spatial distribution of macrofauna has been appropriately surveyed. Also, the ecophysiological models in this chapter are simplistic because they were developed with the intention to demonstrate the effect of macrobiota on planktonic variables over a short time period. Applications needing longer simulations or that need a more in-depth assessment of interactions between species, may require to formulate more realistic ecophysiological models. An example of a more realistic ecophysiological model was presented in Chapter 3 (i.e. SHELL-E).

The limiting functions used in the ecophysiology models presented in this thesis (i.e. Chapters 2 and 3) need to be better assessed and validated either by using targeted laboratory experiments, or by confronting model results (including diagnostic variables, Franks, 2009) against observational data from different locations and environments. Also, many of the parameters used in this thesis came from studies conducted in a different region from the study region, or for a different species, or measuring different rates that the ones modelled in this study. While often modellers are forced to improvise by adapting results from studies that are not ideal for the model application, efforts should be made to expand our library of parameters. This process should be guided by close interactions between modellers and experimental physiologists and ecologists (Flynn, 2005).

The planktonic ecosystem model used in this thesis assumes an immediate remineralization of organic matter reaching the ocean bottom (Fennel et al., 2006). Future work should attempt to implement a time lag in this remineralization, preferably controlled by temperature and oxygen concentration. An even more ambitious remineralization scheme could also attempt to replace the small and large detritus variables (i.e. *SDet* and *LDet*) for 2 sediment size classes from the Warner et al. (2008) sediment model, thus allowing the new detritus variables to be resuspended back to the water column during times of

high current velocity. These modifications to time-lag the process of remineralization of organic particles should improve the data-model comparisons of Chapters 3 and 4 (particularly ammonia). But also, this modifications would allow the testing of the full biocapacitor hypothesis presented in Chapter 4. Under the current configuration, the model can only test the part of the hypothesis related to bivalve excretion and mortality, and cannot test for the impact of a time-lag in the remineralization of biodeposits.

The SHELL-E model (Chapter 3) may be improved by adding a new "gut" state variable, that would hold nitrogen ingested but awaiting to be absorbed and incorporated into bivalve soma or gonad. This new state variable should improve estimates of the bivalve "meat yield", which is the ratio of bivalve meat to whole weight, and an index routinely monitored by bivalve farmers. Also, the new "gut" variable may improve estimates of bivalve filtration rates if filtration is made a function of "gut fullness" (Duarte et al., 2010).

Finally, in Chapter 4 it was shown that bivalve-mediated fertilization locally enhances phytoplankton biomass outside a mussel farm in Ship Harbour. Also, while mussels had a system-wide depletion effect on phytoplankton, the local increase of phytoplankton near the farm ameliorates this system-wide depletion effect. Future work should investigate if this phenomenon occurs in other embayments with bivalve aquaculture in temperate regions.

In this thesis, a new modelling framework was developed to study multi-species ecological interactions in hydrodynamic coastal ecosystems. Here, this modelling framework was used to test hypotheses and to develop insight. However, the use of this framework for quantitative prediction of marine ecosystem dynamics will depend on the validation of functions and parameters and assessment of the accuracy of the model predictions. These are essential next steps.

APPENDIX A

Individual-based Module

The IBM module allows the insertion and tracking of individual groups of organisms within the model domain. To accomplish this, we built the IBM module as an extension of the existing "floats module" of ROMS, which enables the insertion of inert particles that can be tracked through the model domain. When the IBM module is "turned on", inert floats are treated as individual organisms by (1) activating additional code that allows floats to carry on ecophysiological processes, (2) reading additional biological parameters from the floats input file, and (3) printing additional biological variables and parameters in the floats output file. Future improvements on the float tracking algorithms in ROMS are immediately usable by the IBM module.

Super-individuals: The individual-based biology module tracks groups formed by many identical individuals, herein referred to as super-individuals (Scheffer et al., 1995). The initial number of organisms in the super-individual is specified by the user, and can decrease or increase using population dynamics equations. However, super-individuals cannot divide into multiple super-individuals of smaller size. Many super-individuals of different species, life-stages, and/or size-classes can co-exist in a single grid cell, and the total number of super-individuals in the model domain is unlimited.

Inputs: Super-individuals are inserted using an input text file. Each row in the input file represents a super-individual and contains: (1) x, y and z insertion coordinates; (2) time of insertion, which allows seeding or recruitment events throughout the model run; (3) initial number of organisms forming the super-individual; (4) initial-conditions for all other state variables of the ecophysiological models; (5) parameters of the ecophysiological

model; (6) integers indicating species and life-stage and (7) integers specifying which transport, behavioural and ecophysiological models to use.

Physical transport: ROMS estimates the trajectory followed by floats (or super-individuals) using one of three algorithms: (1) 3-D Lagrangian, where floats can move solely according to local advection and diffusion; (2) isobaric, where floats are restricted to move along planes of constant pressure; or (3) geopotential, where floats are restricted to move along planes of constant depth. We added one more option, (4) static or sessile, in which floats are not transported by ocean currents and therefore remain in the location where they were inserted.

Behavioural transport: We allotted space to include behavioural models to allow super-individuals to move independently of ocean currents via swimming or buoyancy changes. For now, we have only included the simplest case, which denotes no behaviour. However, note that the isobaric, geopotential and static options for physical transport yield trajectories that may deviate from a purely Lagrangian transport; therefore implying an implicitly behaviour of floats or super-individuals.

Ecophysiology: The module currently has five models. The first four (Fig. 1) are generic models to simulate the ecophysiology of different functional groups (i.e. generic macroalgae, seagrass, filter-feeders and aquacultured fish). The fifth is an advanced model to simulate Shellfish Ecophysiology (SHELL·E), which is described in detail in Chapter 3. Other physiological and population dynamics models can be easily coupled.

General approach: At each time-step, the IBM module loops over all super-individuals. For each super-individual, the module: (1) identifies the 3-D location of the super-individual and reads the concentration of all tracers (e.g. temperature, phytoplankton, etc.) in the containing grid cell; (2) identifies which ecophysiology model to use and selects it; (3) applies the selected ecophysiology model and local tracers to estimate physiological rates of one individual in the super-individual; (4) uses the individual physiological rates to grow or catabolically consume each individual in the super-individual; (5)

used the selected ecophysiology model to update the number of organisms forming the super-individual using mortality and/or recruitment rates; and (6) uses the individual physiological rates estimated in step (3) and the updated super-individual size, to estimate the production or consumption of local tracers by the super-individual. At the end of the time-step, the tracer concentrations in each grid cell reflect the cumulative effect of all super-individuals in each cell. The dynamics of the entire ecosystem are computed post-simulation using the recorded model output.

Outputs: The interface generates one NetCDF file containing (1) time-series of each of the 12 state variables for each super-individual; (2) time-series of all biological and physical tracers (e.g. phytoplankton, salinity, etc.) at the location of each super-individual; (3) initial-conditions and parameters for each super-individual, and (4) biological and physical parameters for the ROMS run.

Conditionals: During each time step, the IBM module estimates the production or consumption of biological tracers in each cell containing individuals. In the reactions where tracers decrease due to filter-feeding, there is the potential for the filtration capacity of the individuals to exceed the volume of the cell containing them, causing ROMS to crash. The following condition must be fulfilled:

Eq. A-1
$$dt < \frac{V(x,y,x,t)}{\sum_{s} n_s(x,y,z,t) \cdot F_s(x,y,z,t)}$$

This condition may be easily met in most cases. However, in applications using very high grid resolution (hence very small cell volume) and with large congregations of individuals (i.e. large n_s), the time step dt may be constrained by the above (biological) condition rather than by the (physical) condition to resolve gravity waves.

APPENDIX B

Conversions Used in Chapter 3

5.4.1. Biomass (mmol N, gdw, gww)

To convert the mussel biomass from units of gram dry weight of soft tissue (gdw) to mmol N, and to grams wet weight of whole mussels (gww), we assume that dried soft tissues contain 7.79% of nitrogen (Smaal and Vonck, 1997), and that dried tissue weight is 7.5% of the total wet weight (Ibarra, 2003), then:

Eq. B-1 1 gdw = 5.564 mmol N

Eq. B-2 1 gww = 0.075 gdw

5.4.2. Length vs. Weight

We used a relationship estimated using mussels from Ship Harbour (Ibarra 2003).

Eq. B-3 $$W = 0.0001 \times L^{2.8714}$$

were W is mussel wet weight (gww) and L is length (mm).

5.4.3. Absorption Rate

To convert absorption rate in units of mmol N ind^{-1} d^{-1} (i.e. A_k) into units of mg gdw^{-1} d^{-1} (i.e. $\widetilde{A}_k$), we follow the following conversion:

Eq. B-4 $$\widetilde{A}_k = \frac{(A_k \cdot 14) + (A_k \cdot NC \cdot 12)}{B_k \cdot 0.18}$$

where 14 and 12 are the molar masses (g mol^{-1} or mg $mmol^{-1}$) of nitrogen and carbon, respectively. The term ($B_k \cdot 0.18$) is the bivalve biomass in units of gdw ind^{-1}, and *NC* is the nitrogen-to-carbon ratio of the absorbed food. Here we assumed *NC* = 10 mmol C $(mmol\ N)^{-1}$. Note the mg in the units of $\widetilde{A}_k$ refer to mg of C plus mg of N.

5.4.4. Excretion Rate

To convert modelled excretion rates (or respiration rate) in units of mmol N ind^{-1} d^{-1} (i.e. R_k) into units typically used in the literature of µg N gdw^{-1} h^{-1} (i.e. $\widetilde{R}_k$), we follow the following conversion:

Eq. B-5
$$\widetilde{R}_k = \frac{R_k \cdot 14 \cdot 1000 \cdot 24^{-1}}{B_k \cdot 0.18}$$

5.4.5. Egestion Rate

To convert egestion rate (or faeces production rate) in units of mmol N ind^{-1} d^{-1} (i.e. Fae_k) into units of µg gdw^{-1} h^{-1} (i.e. $\overline{Fae}_k$), we follow the following conversion:

Eq. B-6
$$\overline{Fae}_k = \frac{\left(Fae_k \cdot 14\right) + \left(Fae_k \cdot NC \cdot 12\right)}{B_k \cdot 0.18}$$

APPENDIX C

Description and Equations of the 0-D Ecosystem Model

The following ecosystem model is a simplification of the 3-D ecosystem model presented in Fennel et al. (1996) and the bivalve ecophysiology model, SHELL-E, presented in Chapter 3. In this model, the planktonic ecosystem dynamics in an embayment are represented with a single box (i.e. 0-D model), where exchanges in and out of the box are represented with a single parameter, χ (d^{-1}), denoting the flushing rate of the embayment. The time rate of change of phytoplankton is given by:

Eq. C-1

$$\frac{\partial Phy}{\partial t} = \mu(L_{NO3} + L_{NH4})Phy - gL_P Zoo - m_p Phy - \tau(SDet + Phy)Phy - w_P \frac{Phy}{z} - F\varepsilon_P Phy + \chi(Phy_0 - Phy)$$

where μ (d^{-1}) is the maximum growth at a given temperature and irradiance; g (units: (mmol N m^{-3})$^{-1}$ d^{-1}) is the maximum grazing rate of phytoplankton by zooplankton; m_P (d^{-1}) is the phytoplankton mortality; τ (units: (mmol N m^{-3})$^{-1}$ d^{-1}) is the aggregation parameter representing the flocculation of phytoplankton into large detritus; w_P (m d^{-1}) is the sinking velocity of phytoplankton; F (d^{-1}) is the clearance rate of the entire bivalve community in the embayment; ε_P (dimensionless) is the filtration efficiency of bivalves on phytoplankton, and Phy_0 is the constant concentration of phytoplankton outside of the embayment. The phytoplankton growth limitations due to the concentration of nitrate, L_{NO3} (dimensionless), and ammonium, L_{NH4} (dimensionless), are described below:

Eq. C-2
$$L_{NO3} = \frac{NO3}{K_{NO3} + NO3} \cdot \frac{1}{1 + \left(NH4 / K_{NH4}\right)}$$

Eq. C-3
$$L_{NH4} = \frac{NH4}{K_{NH4} + NH4}$$

where K_{NO3} and K_{NH4} (both with units of mmol N m^{-3}) are the half-saturation concentration for uptake of nitrate and ammonium, respectively.

The limitation for phytoplankton grazing by zooplankton, L_P (dimensionless), is described below:

Eq. C-4
$$L_P = \frac{Phy^2}{K_P + Phy^2}$$

where K_P (mmol N m^{-3}) is the half-saturation concentration of phytoplankton ingestion by zooplankton.

The time rate of change zooplankton and detrital pools are described are described by:

Eq. C-5
$$\frac{\partial Zoo}{\partial t} = gL_P \beta Zoo - l_{BM} Zoo - l_E L_P \beta Zoo - m_Z Zoo^2 - F\varepsilon_Z Zoo + \chi(Zoo_0 - Zoo)$$

Eq. C-6
$$\frac{\partial SDet}{\partial t} = gL_P(1-\beta)Zoo + m_Z Zoo^2 + m_P Phy - \tau\left(SDet + Phy\right)SDet - r_{SD} SDet - w_{SD}\frac{SDet}{z} - F\varepsilon_D SDet + \chi(SDet_0 - SDet)$$

Eq. C-7

$$\frac{\partial LDet}{\partial t} = \tau\left(SDet + Phy\right)^2 - r_{LD}LDet - w_{LD}\frac{LDet}{z} + F\varepsilon_P(1-\alpha_P)Phy + F\varepsilon_Z(1-\alpha_Z)Zoo + F\varepsilon_D(1-\alpha_D)SDet + \chi(LDet_0 - LDet)$$

where β (dimensionless) is the assimilation efficiency of zooplankton on phytoplankton; l_{BM} (d^{-1}) is the excretion rate of zooplankton due to basal metabolism; l_E (d^{-1}) is the maximum rate of assimilation-related excretion; m_Z (d^{-1}) is the zooplankton mortality rate; ε_Z and ε_D (dimensionless) are the filtration efficiencies of bivalves on zooplankton and small detritus, respectively; Zoo_0, $SDet_0$ and $LDet_0$ are the constant concentrations of zooplankton, small detritus and large detritus outside of the embayment, respectively; r_{SD} (d^{-1}) and r_{LD} (d^{-1}) are the remineralization rates of small and large detritus, respectively; w_{SD} and w_{LD} (m d^{-1}) are the sinking rates of small and large detritus, respectively; α_P, α_Z and α_D (dimensionless) are the absorption efficiencies of bivalves on phytoplankton, zooplankton and small detritus, respectively; and z (m) is the depth of box, which represents the average depth of the embayment.

The time rate of chance of the concentration of nitrate and ammonium are defined by:

Eq. C-8

$$\frac{\partial NO3}{\partial t} = -\mu L_{NO3}Phy + nNH4 + \chi(NO3_0 - NO3)$$

Eq. C-9

$$\frac{\partial NH4}{\partial t} = -\mu L_{NH4}Phy - nNH4 + l_{BM}Zoo + l_E L_P \beta Zoo + r_{SD}SDet + r_{LD}LDet + w_P\frac{Phy}{z} + w_{SD}\frac{SDet}{z} + w_{LD}\frac{LDet}{z} + R_m B + l_B F\varepsilon_P\alpha_P Phy + l_B F\varepsilon_Z\alpha_Z Zoo + l_B F\varepsilon_D\alpha_D SDet + m_B B + \chi(NH4_0 - NH4)$$

where n (d^{-1}) is the nitrification rate; R_m (d^{-1}) is the weight-specific maintenance respiration rate of bivalves; l_B (dimensionless) is the cost of growth coefficient for bivalves; m_B (d^{-1}) is the mortality rate for bivalves; and $NO3_0$ and $NH4_0$ are the constant concentrations of nitrate and ammonia outside of the embayment, respectively.

Finally, the time rate of change of the concentration of bivalves inside the embayment is defined as follows:

Eq. C-10

$$\frac{\partial B}{\partial t} = F\varepsilon_P\alpha_P Phy + F\varepsilon_Z\alpha_Z Zoo + F\varepsilon_D\alpha_D SDet - R_m B - l_B F\varepsilon_P\alpha_P Phy - l_B F\varepsilon_Z\alpha_Z Zoo - l_B F\varepsilon_D\alpha_D SDet - m_B B$$

Bibliography

Abreu, M.H., Varela, D.A., Henriquez, L., Villarroel, A., Yarish, C., Sousa-Pinto, I., Buschmann, A.H. (2009) Traditional vs. integrated multi-trophic aquaculture of *Gracilaria chilensis* C. J. Bird, J. McLachlan & E. C. Oliveira: productivity and physiological performance. *Aquaculture*, 293(3-4):211-220.

Ackerman, J.D., Loewen, M.R., Hamblin, P.F. (2001) Benthic-pelagic coupling over a zebra mussel reef in western Lake Erie. *Limnology and Oceanography*, 46(4):892-904.

Almada-Villela, P.C. (1984) The effects of reduced salinity on the shell growth of small *Mytilus edulis*. *Journal of the Marine Biological Association of the United Kingdom*, 64:171-182.

Anderson, T.R. (2005) Plankton functional type modelling: running before we can walk? *Journal of Plankton Research*, 27(11):1073-1081.

Apostolaki, E.T., Marba, N., Holmer, M., Karakassis, I. (2009) Fish farming enhances biomass and nutrient loss in *Posidonia oceanica* (L.) Delile. *Estuarine Coastal and Shelf Science*, 81(3):390-400.

Arakawa, A. (1966) Computational design for long-term numerical integration of the equations of fluid motion: two-dimensional incompressible flow. Part I. *Journal of Computational Physics*, 1(1):119-143.

Arhonditsis, G.B., Papantou, D., Zhang, W.T., Perhar, G., Massos, E., Shi, M.L. (2008) Bayesian calibration of mechanistic aquatic biogeochemical models and benefits for environmental management. *Journal of Marine Systems*, 73(1-2):8-30.

Asmus, R.M., Asmus, H. (1991) Mussel beds: limiting or promoting phytoplankton? *Journal of Experimental Marine Biology and Ecology*, 148(2):215-232.

Awaji, T., Imasato, N., Kunishi, H. (1980) Tidal exchange through a strait: a numerical experiment using a simple model basin. *Journal of Physical Oceanography*, 10:1499-1508.

Bacher, C., Gangnery, A. (2006) Use of dynamic energy budget and individual based models to simulate the dynamics of cultivated oyster populations. *Journal of Sea Research*, 56(2):140-155.

Bacher, C., Grant, J., Hawkins, A.J.S., Fang, J., Zhu, M., Besnard, M. (2003) Modelling the effect of food depletion on scallop growth in Sungo Bay (China). *Aquatic Living Resources*, 16:10-24.

Bald, J., Sinquin, A., Borja, A., Caill-Milly, N., Duclercq, B., Dang, C., de Montaudouin, X. (2009) A system dynamics model for the management of the Manila clam, *Ruditapes philippinarum* (Adams and Reeve, 1850) in the Bay of Arcachon (France). *Ecological Modelling*, 220(21):2828-2837.

Baretta-Bekker, J.G., Baretta, J.W., Ebenhoh, W. (1997) Microbial dynamics in the marine ecosystem model ERSEM II with decoupled carbon assimilation and nutrient uptake. *Journal of Sea Research*, 38(3-4):195-211.

Barrington, K., Chopin, T., Robinson, S. (2009) Integrated multi-trophic aquaculture (IMTA) in marine temperate waters. In: Soto, D. (ed) Integrated mariculture - A global review, Vol 529. FAO Fisheries and Aquaculture Technical Paper. Rome, Italy. p. 7-46.

Batchelder, H.P., Edwards, C.A., Powell, T.M. (2002) Individual-based models of copepod populations in coastal upwelling regions: implications of physiologically and environmentally influenced diel vertical migration on demographic success and nearshore retention. *Progress in Oceanography*, 53(2-4):307-334.

Batchelor, G.K. (2000) An introduction to fluid dynamics. Cambridge University Press, 615 pp.

Baudinet, D., Alliot, E., Berland, B., Grenz, C., Plante-Cuny, M.R., Plante, R., Salen-Picard, C. (1990) Incidence of mussel culture on biogeochemical fluxes at the sediment-water interface. *Hydrobiologia*, 207(1):187-196.

Bayne, B.L., Bayne, C.J., Carefoot, T.C., Thompson, R.J. (1976) The physiological ecology of *Mytilus californianus* Conrad. *Oecologia*, 22(3):229-250.

Bayne, B.L., Salkeld, P.N., Worrall, C.M. (1983) Reproductive effort and value in different populations of the marine mussel, *Mytilus edulis* L. *Oecologia*, 59(1):18-26.

Beres, D.L., Hawkins, D.M. (2001) Plackett-Burman techniques for sensitivity analysis of many-parametered models. *Ecological Modelling*, 141(1-3):171-183.

Beverton, R.J.H., Holt, S.J. (1957) On the dynamics of exploited fish populations. *UK Ministry of Agriculture, Fisheries and Food, Fishery Invest, Ser II*, 19:533.

Bissett, W.P., Walsh, J.J., Dieterle, D.A., Carder, K.L. (1999) Carbon cycling in the upper waters of the Sargasso Sea: I. Numerical simulation of differential carbon and nitrogen fluxes. *Deep-Sea Research Part I-Oceanographic Research Papers*, 46(2):205-269.

Boucher, G., Boucherrodoni, R. (1988) In situ measurements of respiratory metabolism and nitrogen fluxes at the interface of oyster beds. *Marine Ecology-Progress Series*, 44(3):229-238.

Bourles, Y., Alunno-Bruscia, M., Pouvreau, S., Tollu, G., Leguay, D., Arnaud, C., Goulletquer, P., Kooijman, S. (2009) Modelling growth and reproduction of the Pacific oyster *Crassostrea gigas*: advances in the oyster-DEB model through application to a coastal pond. *Journal of Sea Research*, 62(2-3):62-71.

Bricaud, A., Babin, M., Morel, A., Claustre, H. (1995) Variability in the chlorophyll-specific absorption coefficients of natural phytoplankton: Analysis and parameterization. *J Geophys Res*, 100(C7):13321–13332.

Brigolin, D., Dal Maschio, G., Rampazzo, F., Giani, M., Pastres, R. (2009) An individual-based population dynamic model for estimating biomass yield and nutrient fluxes through an off-shore mussel (*Mytilus galloprovincialis*) farm. *Estuarine Coastal and Shelf Science*, 82(3):365-376.

Bryan, K. (1969) A numerical method for the study of the circulation of the world ocean. *Journal of Computational Physics*, 4(3):347-376.

Budgell, W.P. (2005) Numerical simulation of ice-ocean variability in the Barents Sea region. *Ocean Dynamics*, 55(3):370-387.

Buneman, O., Barnes, C.W., Green, J.C., Nielsen, D.E. (1980) Principles and capabilities of a 3-D, E-M particle simulations. *Journal of Computational Physics*, 38(1):1-44.

Byron, C., Link, J., Costa-Pierce, B., Bengtson, D. (2011) Calculating ecological carrying capacity of shellfish aquaculture using mass-balance modeling: Narragansett Bay, Rhode Island. *Ecological Modelling*, 222(10):1743-1755.

Cabanas, J.M., González, J.J., Mariño, J., Pérez, A., Román, G. (1979) Estudio del mejillón y de su epifauna en los cultivos flotantes de la Ría de Arosa. III. Observaciones previas sobre la retención de partículas y la biodeposición de una batea. *Boletin del Instituto Español de Oceanografía*, 5:45–50.

Carmona, R., Kraemer, G.P., Yarish, C. (2006) Exploring northeast american and asian species of *Porphyra* for use in an integrated finfish-algal aquaculture system. *Aquaculture*, 252(1):54-65.

Carver, C.E.A., Mallet, A.L. (1990) Estimating the carrying-capacity of a coastal inlet for mussel culture. *Aquaculture*, 88(1):39-53.

Cerco, C.F., Tillman, D., Hagy, J.D. (2010) Coupling and comparing a spatially- and temporally-detailed eutrophication model with an ecosystem network model: an initial application to Chesapeake Bay. *Environmental Modelling & Software*, 25(4):562-572.

Chang, Y.J., Sun, C.L., Chen, Y., Zhang, Y.Y., Yeh, S.Z. (2010) Incorporating climate changes into population dynamic modelling: an individual-based modelling approach for lobster. *Canadian Journal of Fisheries and Aquatic Sciences*, 68(1):122-136.

Chao, Y., Li, Z.J., Farrara, J.D., Moline, M.A., Schofield, O.M.E., Majumdar, S.J. (2008) Synergistic applications of autonomous underwater vehicles and regional ocean modeling system in coastal ocean forecasting. *Limnology and Oceanography*, 53(5):2251-2263.

Chapelle, A., Menesguen, A., Deslous-Paoli, J.M., Souchu, P., Mazouni, N., Vaquer, A., Millet, B. (2000) Modelling nitrogen, primary production and oxygen in a Mediterranean lagoon. Impact of oysters farming and inputs from the watershed. *Ecological Modelling*, 127(2-3):161-181.

Chen, Z., Hu, C., Muller-Karger, F.E., Luther, M.E. (2010) Short-term variability of suspended sediment and phytoplankton in Tampa Bay, Florida: observations from a coastal oceanographic tower and ocean color satellites. *Estuarine, Coastal and Shelf Science*, 89(1):62-72.

Chopin, T., Buschmann, A.H., Halling, C., Troell, M., Kautsky, N., Neori, A., Kraemer, G.P., Zertuche-Gonzalez, J.A., Yarish, C., Neefus, C. (2001) Integrating seaweeds into marine aquaculture systems: a key toward sustainability. *Journal of Phycology*, 37(6):975-986.

Christensen, V., Walters, C.J. (2004) Ecopath with Ecosim: methods, capabilities and limitations. *Ecological Modelling*, 172(2-4):109-139.

Ciotti, A.M., Lewis, M.R., Cullen, J.J. (2002) Assessment of the relationships between dominant cell size in natural phytoplankton communities and the spectral shape of the absorption coefficient. *Limnology and Oceanography*, 47(2):404-417.

Coffin, D. (2003) An estimation of the carrying capacity of a commercial mussel farm in Newfoundland. M.Sc. Thesis, Memorial University of Newfoundland, 182 pp.

Cranford, P.J., Hill, P.S. (1999) Seasonal variation in food utilization by the suspension-feeding bivalve molluscs *Mytilus edulis* and *Placopecten magellanicus*. *Marine Ecology-Progress Series*, 190:223-239.

Cranford, P.J., Hill, P.S. (2001) Evaluating the 'reliability' of filtration rate measurements in bivalves. *Marine Ecology-Progress Series*, 215:303-305.

Cranford, P.J., Li, W., Strand, O., Strohmeier, T. (2008) Phytoplankton depletion by mussel aquaculture: high resolution mapping, ecosystem modeling, and potential indicators of ecological carrying capacity. *ICES CM*, H12:1-5.

Cranford, P.J., Strain, P.M., Dowd, M., Hargrave, B.T., Grant, J., Archambault, M.C. (2007) Influence of mussel aquaculture on nitrogen dynamics in a nutrient enriched coastal embayment. *Marine Ecology-Progress Series*, 347:61-78.

Cromey, C.J., Nickell, T.D., Black, K.D. (2002) DEPOMOD - modelling the deposition and biological effects of waste solids from marine cage farms. *Aquaculture*, 214(1-4):211-239.

Cromey, C.J., Nickell, T.D., Treasurer, J., Black, K.D., Inall, M. (2009) Modelling the impact of cod (*Gadus morhua* L) farming in the marine environment-CODMOD. *Aquaculture*, 289(1-2):42-53.

Cugier, P., Struski, C., Blanchard, M., Mazurié, J., Pouvreau, S., Olivier, F., Trigui, J.R., Thiébaut, E. (2010) Assessing the role of benthic filter feeders on phytoplankton production in a shellfish farming site: Mont Saint Michel Bay, France. *Journal of Marine Systems*, 82(1-2):21-34.

Cullen, J.J., Lewis, M.R. (1995) Biological processes and optical measurements near the sea-surface: some issues relevant to remote sensing. *Journal of Geophysical Research*, 100(13):255–213.

Cury, P.M., Shin, Y.J., Planque, B., Durant, J.M., Fromentin, J.M., Kramer-Schadt, S., Stenseth, N.C., Travers, M., Grimm, V. (2008) Ecosystem oceanography for global change in fisheries. *Trends in Ecology & Evolution*, 23(6):338-346.

D'Amours, O., Archambault, P., McKindsey, C.W., Johnson, L.E. (2008) Local enhancement of epibenthic macrofauna by aquaculture activities. *Marine Ecology-Progress Series*, 371:73-84.

Dame, R., Dankers, N., Prins, T., Jongsma, H., Smaal, A. (1991) The influence of mussel beds on nutrients in the Western Wadden Sea and Eastern Scheldt estuaries. *Estuaries and Coasts*, 14(2):130-138.

Dame, R.F., Prins, T.C. (1998) Bivalve carrying capacity in coastal ecosystems. *Aquatic Ecology*, 31(4):409-421.

Davis, R.F., Moore, C.C., Zaneveld, J.R.V., Napp, J.M. (1997) Reducing the effects of fouling on chlorophyll estimates derived from long-term deployments of optical instruments. *Journal of Geophysical Research*, 102:5851-5855.

Denman, K.L. (2003) Modelling planktonic ecosystems: parameterizing complexity. *Progress in Oceanography*, 57(3-4):429-452.

Dennison, W.C., Alberte, R.S. (1982) Photosynthetic responses of *Zostera marina* L. (eelgrass) to in situ manipulations of light intensity. *Oecologia*, 55(2):137-144.

DeYoung, B., Heath, M., Werner, F., Chai, F., Megrey, B., Monfray, P. (2004) Challenges of modeling ocean basin ecosystems. *Science*, 304(5676):1463-1466.

DFO (2005) BioChem: database of biological and chemical oceanographic data. Version 8. Department of Fisheries and Oceans, Canada. http://www.meds-sdmm.dfo-mpo.gc.ca/biochem/biochem-eng.htm.

Dowd, M. (1997) On predicting the growth of cultured bivalves. *Ecological Modelling*, 104(2-3):113-131.

Dowd, M. (2003) Seston dynamics in a tidal inlet with shellfish aquaculture: a model study using tracer equations. *Estuarine, Coastal and Shelf Science*, 57(3):523-537.

Dowd, M. (2005) A bio-physical coastal ecosystem model for assessing environmental effects of marine bivalve aquaculture. *Ecological Modelling*, 183(2-3):323-346.

Duarte, P., Fernández-Reiriz, M.J., Filgueira, R., Labarta, U. (2010) Modelling mussel growth in ecosystems with low suspended matter loads. *Journal of Sea Research*, 64(3):273-286.

Duarte, P., Labarta, U., Fernandez-Reiriz, M.J. (2008) Modelling local food depletion effects in mussel rafts of Galician Rias. *Aquaculture*, 274(2-4):300-312.

Duarte, P., Meneses, R., Hawkins, A.J.S., Zhu, M., Fang, J., Grant, J. (2003) Mathematical modelling to assess the carrying capacity for multi-species culture within coastal waters. *Ecological Modelling*, 168(1-2):109-143.

Eppley, R.W. (1972) Temperature and phytoplankton growth in the sea. *Fishery Bulletin*, 70(4):1063-1085.

Eppley, R.W., Thomas, W.H. (1969) Comparison of the half-saturation constants for growth and nitrate uptake of marine phytoplankton. *Journal of Phycology*, 5(4):375-379.

FAO (2010) The state of world fisheries and aquaculture 2010. United Nations Food and Agriculture Program, Rome, 197 pp. http://www.fao.org/docrep/013/i1820e/i1820e.pdf

Fasham, M.J.R., Ducklow, H.W., McKelvie, S.M. (1990) A nitrogen-based model of plankton dynamics in the oceanic mixed layer. *Journal of Marine Research*, 48(3):591-639.

Fennel, K., Wilkin, J., Levin, J., Moisan, J., O'Reilly, J., Haidvogel, D. (2006) Nitrogen cycling in the Middle Atlantic Bight: results from a three-dimensional model and implications for the North Atlantic nitrogen budget. *Global Biogeochemical Cycles*, 20(3):GB3007.

Fennel, K., Wilkin, J., Previdi, M., Najjar, R. (2008) Denitrification effects on air-sea CO_2 flux in the coastal ocean: simulations for the northwest North Atlantic. *Geophysical Research Letters*, 35:L24608.

Fennel, W. (2008) Towards bridging biogeochemical and fish-production models. *Journal of Marine Systems*, 71(1-2):171-194.

Ferreira, J.G., Hawkins, A.J.S., Monteiro, P., Moore, H. (2008) Integrated assessment of ecosystem-scale carrying capacity in shellfish growing areas. *Aquaculture*, 275(1-4):138-151.

Filgueira, R., Grant, J., Strand, Asplin, L., Aure, J. (2010) A simulation model of carrying capacity for mussel culture in a Norwegian fjord: role of induced upwelling. *Aquaculture*, 308:20-27.

Flynn, K.J. (2005) Castles built on sand: dysfunctionality in plankton models and the inadequacy of dialogue between biologists and modellers. *Journal of Plankton Research*, 27(12):1205.

Forster, R.M., Luning, K. (1996) Photosynthetic response of *Laminaria digitata* to ultraviolet A and B radiation. *Scientia Marina*, 60:65-71.

Franks, P.J.S. (2009) Planktonic ecosystem models: perplexing parameterizations and a failure to fail. *Journal of Plankton Research*, 31(11):1299-1306.

Fréchette, M., Booth, D.A., Myrand, B., Bérard, H. (1991) Variability and transport of organic seston near a mussel aquaculture site. *ICES Marine Science Symposia*, 192:24-32.

Fréchette, M., Butman, C.A., Geyer, W.R. (1989) The importance of boundary-layer flows in supplying phytoplankton to the benthic suspension feeder, *Mytilus edulis* L. *Limnology and Oceanography*, 34(1):19-36.

Friedrichs, M.A.M., Carr, M.E., Barber, R.T., Scardi, M., Antoine, D., Armstrong, R.A., Asanuma, I., Behrenfeld, M.J. (2009) Assessing the uncertainties of model estimates of primary productivity in the tropical Pacific Ocean. *Journal of Marine Systems*, 76(1-2):113-133.

Fulton, E.A. (2010) Approaches to end-to-end ecosystem models. *Journal of Marine Systems*, 81(1-2):171-183.

Garcia, H.E., Gordon, L.I. (1992) Oxygen solubility in seawater: better fitting equations. *Limnology and Oceanography*:1307-1312.

Gentleman, W., Leising, A., Frost, B., Strom, S., Murray, J. (2003) Functional responses for zooplankton feeding on multiple resources: a review of assumptions and biological dynamics. *Deep Sea Research-Part II-Topical Studies in Oceanography*, 50(22):2847-2876.

Gevaert, F., Janquin, M.A., Davoult, D. (2008) Biometrics in *Laminaria digitata*: a useful tool to assess biomass, carbon and nitrogen contents. *Journal of Sea Research*, 60(3):215-219.

Gibbs, M.T. (2007) Sustainability performance indicators for suspended bivalve aquaculture activities. *Ecological indicators*, 7(1):94-107.

Gonzalez, J.G., Yevich, P. (1976) Responses of an estuarine population of the blue mussel *Mytilus edulis* to heated water from a steam generating plant. *Marine Biology*, 34(2):177-189.

Gordillo, F.J.L., Dring, M.J., Savidge, G. (2002) Nitrate and phosphate uptake characteristics of three species of brown algae cultured at low salinity. *Marine Ecology-Progress Series*, 234:111-118.

Gosling, E.M. (2003) Bivalve molluscs: biology, ecology and culture. Fishing News Books, 443 pp.

Grange, K., Cole, R. (1997) Mussel farming impacts. *Aquaculture Update*, 19:1-3.

Grangeré, K., Lefebvre, S., Bacher, C., Cugier, P., Ménesguen, A. (2010) Modelling the spatial heterogeneity of ecological processes in an intertidal estuarine bay: dynamic interactions between bivalves and phytoplankton. *Marine Ecology-Progress Series*, 415:141-158.

Grangeré, K., Menesguen, A., Lefebvre, S., Bacher, C., Pouvreau, S. (2009) Modelling the influence of environmental factors on the physiological status of the Pacific oyster *Crassostrea gigas* in an estuarine embayment; The Baie des Veys (France). *Journal of Sea Research*, 62(2-3):147-158.

Grant, J., Bacher, C., Cranford, P.J., Guyondet, T., Carreau, M. (2008) A spatially explicit ecosystem model of seston depletion in dense mussel culture. *Journal of Marine Systems*, 73(1-2):155-168.

Grant, J., Cranford, P., Hargrave, B., Carreau, M., Schofield, B., Armsworthy, S., Burdett-Coutts, V., Ibarra, D. (2005) A model of aquaculture biodeposition for multiple estuaries and field validation at blue mussel (*Mytilus edulis*) culture sites in eastern Canada. *Canadian Journal of Fisheries and Aquatic Sciences*, 62(6):1271-1285.

Grant, J., Curran, K.J., Guyondet, T.L., Tita, G., Bacher, C., Koutitonsky, V., Dowd, M. (2007) A box model of carrying capacity for suspended mussel aquaculture in Lagune de la Grande-Entree, Iles-de-la-Madeleine, Quebec. *Ecological Modelling*, 200(1-2):193-206.

Gregory, D., Canada. Dept. of, F., Oceans. Scotia-Fundy Region, P., Chemical Sciences, B., Bedford Institute of, O. (1993) Oceanographic, geographic and hydrological parameters of Scotia-Fundy and southern Gulf of St. Lawrence inlets. Bedford Institute of Oceanography; Department of Fisheries and Oceans, Scotia-Fundy Region, Physical and Chemical Sciences Branch, 248 pp.

Grimm, V. (1999) Ten years of individual-based modelling in ecology: what have we learned and what could we learn in the future? *Ecological Modelling*, 115(2):129-148.

Grimm, V., Railsback, S.F. (2005) Individual-based modeling and ecology. Princeton Univercity Press, 428 pp.

Grimm, V., Revilla, E., Berger, U., Jeltsch, F., Mooij, W.M., Railsback, S.F., Thulke, H.H., Weiner, J., Wiegand, T., DeAngelis, D.L. (2005) Pattern-oriented modeling of agent-based complex systems: lessons from ecology. *Science*, 310(5750):987.

Grizzle, R.E., Greene, J.K., Coen, L.D. (2008) Seston removal by natural and constructed intertidal eastern oyster (*Crassostrea virginica*) reefs: a comparison with previous laboratory studies, and the value of in situ methods. *Estuaries and Coasts*, 31(6):1208-1220.

Guarini, J.M., Blanchard, G.F., Bacher, C., Gros, P., Riera, P., Richard, P., Gouleau, D., Galois, R., Prou, J., Sauriau, P.G. (1998) Dynamics of spatial patterns of microphytobenthic biomass: inferences from a geostatistical analysis of two comprehensive surveys in Marennes-Oleron bay (France). *Marine Ecology-Progress Series*, 166:131-141.

Guyondet, T., Roy, S., Koutitonsky, V.G., Grant, J., Tita, G. (2010) Integrating multiple spatial scales in the carrying capacity assessment of a coastal ecosystem for bivalve aquaculture. *Journal of Sea Research*, 64(3):341-359.

Guzzetta, G., Ajelli, M., Yang, Z.H., Merler, S., Furlanello, C., Kirschner, D. (2011) Modeling socio-demography to capture tuberculosis transmission dynamics in a low burden setting. *Journal of Theoretical Biology*, 289:197-205.

Haidvogel, D.B., Arango, H., Budgell, W.P., Cornuelle, B.D., Curchitser, E., Di Lorenzo, E., Fennel, K., Geyer, W.R., Hermann, A.J., Lanerolle, L., Levin, J., McWilliams, J.C., Miller, A.J., Moore, A.M., Powell, T.M., Shchepetkin, A.F., Sherwood, C.R., Signell, R.P., Warner, J.C., Wilkin, J. (2008) Ocean forecasting in terrain-following coordinates: formulation and skill assessment of the Regional Ocean Modeling System. *Journal of Computational Physics*, 227(7):3595-3624.

Haidvogel, D.B., Arango, H.G., Hedström, K., Beckmann, A., Malanotte-Rizzoli, P., Shchepetkin, A.F. (2000) Model evaluation experiments in the North Atlantic Basin: simulations in nonlinear terrain-following coordinates. *Dynamics of Atmospheres and Oceans*, 32(3-4):239-281.

Hall, N.S., Paerl, H.W. (2011) Vertical migration patterns of phytoflagellates in relation to light and nutrient availability in a shallow, microtidal estuary. *Marine Ecology-Progress Series*, 425:1-19.

Hall, P.O.J., Anderson, L.G., Holby, O., Kollberg, S., Samuelsson, M.O. (1990) Chemical fluxes and mass balances in a marine cage farm. 1. Carbon. *Marine Ecology-Progress Series*, 61(1-2):61-73.

Hall, P.O.J., Holby, O., Kollberg, S., Samuelsson, M.O. (1992) Chemical fluxes and mass balances in a marine cage farm. 4. Nitrogen. *Marine Ecology-Progress Series*, 89(1):81-91.

Hannah, C., Vezina, A., St John, M. (2010) The case for marine ecosystem models of intermediate complexity. *Progress in Oceanography*, 84(1-2):121-128.

Harlin, M.M., Craigie, J.S. (1978) Nitrate uptake by *Laminaria longicruris* (Phaeophyceae). *Journal of Phycology*, 14(4):464-467.

Haslett, S.K. (2008) Coastal systems. Routledge, 216 pp.

Heasman, K.G., Pitcher, G.C., McQuaid, C.D., Hecht, T. (1998) Shellfish mariculture in the Benguela system: raft culture of *Mytilus galloprovincialis* and the effect of rope spacing on food extraction, growth rate, production, and condition of mussels. *Journal of Shellfish Research*, 17:33-40.

Hedström, K. (2009) Technical Manual for a Coupled Sea-Ice/Ocean Circulation Model (Version 3). U.S. Department of the Interior Minerals Management Service, Anchorage, Alaska, 159 pp.
https://www.myroms.org/wiki/index.php/File:Manual_2010.pdf

Henderson, A., Gamito, S., Karakassis, I., Pederson, P., Smaal, A. (2001) Use of hydrodynamic and benthic models for managing environmental impacts of marine aquaculture. *Journal of Applied Ichthyology*, 17(4):163-172.

Hess, K.W. (1976) 3-dimensional numerical-model of estuary circulation and salinity in Narragansett Bay. *Estuarine and Coastal Marine Science*, 4(3):325-338.

Holmer, M., Argyrou, M., Dalsgaard, T., Danovaro, R., Diaz-Almela, E., Duarte, C.M., Frederiksen, M., Grau, A., Karakassis, I., Marbà, N. (2008) Effects of fish farm waste on *Posidonia oceanica* meadows: synthesis and provision of monitoring and management tools. *Marine Pollution Bulletin*, 56(9):1618-1629.

Huse, G., Fiksen, O. (2010) Modelling encounter rates and distribution of mobile predators and prey. *Progress in Oceanography*, 84(1-2):93-104.

Huston, M., DeAngelis, D., Post, W. (1988) New computer models unify ecological theory. *BioScience*, 38(10):682-691.

Ibarra, D.A. (2003) Estimation of seston depletion by cultured mussels (*Mytilus* spp.) using measurements of diffuse attenuation of solar irradiance from optical moorings. M.Sc. Thesis, Dalhousie University, 126 pp.

Incze, L.S., Lutz, R.A., True, E. (1981) Modeling carrying capacities for bivalve molluscs in open, suspended-culture systems. *Journal of the World Mariculture Society*, 12:143-155.

Ings, T.C., Montoya, J.M., Bascompte, J., Bluthgen, N., Brown, L., Dormann, C.F., Edwards, F., Figueroa, D., Jacob, U., Jones, J.I., Lauridsen, R.B., Ledger, M.E., Lewis, H.M., Olesen, J.M., van Veen, F.J.F., Warren, P.H., Woodward, G. (2009) Ecological networks - beyond food webs. *Journal of Animal Ecology*, 78(1):253-269.

Jansen, H.M., Strand, Ø., Strohmeier, T., Krogness, C., Verdegem, M., Smaal, A. (2011) Seasonal variability in nutrient regeneration by mussel *Mytilus edulis* rope culture in oligotrophic systems. *Marine Ecology-Progress Series*, 431:137-149.

Jennings, S., Melin, F., Blanchard, J.L., Forster, R.M., Dulvy, N.K., Wilson, R.W. (2008) Global-scale predictions of community and ecosystem properties from simple ecological theory. *Proceedings of the Royal Society B: Biological Sciences*, 275(1641):1375-1383.

Kadanoff, L.P. (2000) Statistical physics: statics, dynamics and renormalization. World Scientific, 483 pp.

Karayucel, S., Karayucel, I. (2000) The effect of environmental factors, depth and position on the growth and mortality of raft-cultured blue mussels (*Mytilus edulis* L.). *Aquaculture Research*, 31(12):893-899.

Keizer, P.D., Milligan, T.G., Rao, D.V.S., Strain, P.M., Bugden, G. (1996) Phytoplankton monitoring program: Nova Scotia component - 1989 to 1994. *Canadian Technical Report of Fisheries and Aquatic Sciences/Rapport Technique Canadien des Sciences Halieutiques et Aquatiques*, 2136:74.

Kelly, J.R., Volpe, J.R. (2007) Native eelgrass (*Zostera marina* L.) survival and growth adjacent to non-native oysters (*Crassostrea gigas* Thunberg) in the Strait of Georgia, British Columbia. *Botanica Marina*, 50(3):143-150.

Kindall, J.L., Muller, L.I., Clark, J.D., Lupardus, J.L., Murrow, J.L. (2011) Population Viability Analysis to Identify Management Priorities for Reintroduced Elk in the Cumberland Mountains, Tennessee. *Journal of Wildlife Management*, 75(8):1745-1752.

Kirk, J.T.O. (1994) Light and photosynthesis in aquatic ecosystems. Cambridge University Press, 509 pp.

Koh, C.H., Khim, J.S., Araki, H., Yamanishi, H., Mogi, H., Koga, K. (2006) Tidal resuspension of microphytobenthic chlorophyll a in a Nanaura mudflat, Saga, Ariake Sea, Japan: flood-ebb and spring-neap variations. *Marine Ecology-Progress Series*, 312:85-100.

Kohlmeier, C., Ebenhöh, W. (2007) Modelling the ecosystem dynamics and nutrient cycling of the Spiekeroog back barrier system with a coupled Euler-Lagrange model on the base of ERSEM. *Ecological Modelling*, 202(3-4):297-310.

Kooijman, S.A.L.M. (1986) Energy budgets can explain body size relations. *Journal of Theoretical Biology*, 121(3):269-282.

Kooijman, S.A.L.M. (2000) Dynamic energy and mass budgets in biological systems. Cambridge University Press, 424 pp.

Korb, R.E., Gerard, V.A. (2000) Nitrogen assimilation characteristics of polar seaweeds from differing nutrient environments. *Marine Ecology-Progress Series*, 198:83-92.

Kremer, J.N., Nixon, S.W. (1978) A coastal marine ecosystem: simulation and analysis. Springer, 217 pp.

Lande, R., Lewis, M.R. (1989) Models of photoadaptation and photosynthesis by algal cells in a turbulent mixed layer. *Deep-Sea Research Part A: Oceanographic Research Papers*, 36(8):1161-1175.

Langdon, C.J., Newell, R.I.E. (1990) Utilization of detritus and bacteria as food sources by two bivalve suspension-feeders, the oyster *Crassostrea virginica* and the mussel *Geukensia demissa*. *Marine Ecology-Progress Series*, 58(3):299-310.

Larkum, A.W.D., Orth, R.J., Duarte, C.M. (2006) Seagrasses: biology, ecology, and conservation. Springer, 691 pp.

Latour, R.J., Brush, M.J., Bonzek, C.F. (2003) Toward ecosystem-based fisheries management. *Fisheries*, 28(9):10-22.

Leon, L.F., Smith, R.E.H., Hipsey, M.R., Bocaniov, S.A., Higgins, S.N., Hecky, R.E., Antenucci, J.P., Imberger, J.A., Guildford, S.J. (2011) Application of a 3D hydrodynamic-biological model for seasonal and spatial dynamics of water quality and phytoplankton in Lake Erie. *Journal of Great Lakes Research*, 37:41-53.

Libralato, S., Solidoro, C. (2009) Bridging biogeochemical and food web models for an end-to-end representation of marine ecosystem dynamics: the Venice lagoon case study. *Ecological Modelling*, 220(21):2960-2971.

Lima, I.D., Doney, S.C. (2004) A three-dimensional, multinutrient, and size-structured ecosystem model for the North Atlantic. *Global Biogeochemical Cycles*, 18(3):GB3019.

Lonsdale, D.J., Cerrato, R.M., Holland, R., Mass, A., Holt, L., Schaffner, R.A., Pan, J., Caron, D.A. (2009) Influence of suspension-feeding bivalves on the pelagic food webs of shallow, coastal embayments. *Aquatic Biology*, 6(1-3):263-279.

Lotze, H.K., Schramm, W., Schories, D., Worm, B. (1999) Control of macroalgal blooms at early developmental stages: *Pilayella littoralis* versus *Enteromorpha* spp. *Oecologia*, 119(1):46-54.

Maar, M., Bolding, K., Petersen, J.K., Hansen, J.L.S., Timmermann, K. (2009) Local effects of blue mussels around turbine foundations in an ecosystem model of Nysted off-shore wind farm, Denmark. *Journal of Sea Research*, 62(2-3):159-174.

MacIntyre, H.L., Cullen, J.J. (1996) Primary production by suspended and benthic microalgae in a turbid estuary: time-scales of variability in San Antonio Bay, Texas. *Marine Ecology-Progress Series*, 145(1-3):245-268.

Madec, G. (2008) NEMO ocean engine. Note du Pole de modélisation, Institut Pierre-Simon Laplace (IPSL) No. 27, ISSN No.1288-1619, France, 322 pp. http://www.nemo-ocean.eu/content/download/15482/73217/file/NEMO_book_v3_3.pdf

Mafra, L.L., Bricelj, V.M., Ouellette, C., Leger, C., Bates, S.S. (2009) Mechanisms contributing to low domoic acid uptake by oysters feeding on *Pseudo-nitzschia* cells. I. Filtration and pseudofeces production. *Aquatic Biology*, 6(1-3):201-212.

Mann, K.H. (1973) Seaweeds - Their productivity and strategy for growth. *Science*, 182(4116):975-981.

Marbà, N., Holmer, M., Gacia, E., Barron, C. (2006) Seagrass beds and coastal biogeochemistry. In: Larkum, A.W.D., Orth, R.J., Duarte, C.M. (eds) Seagrasses: biology, ecology, and conservation. Springer. Dordrecht, The Netherlands. p. 135-157.

Marinov, D., Galbiati, L., Giordani, G., Viaroli, P., Norro, A., Bencivelli, S., ZaldÃ-var, J.M. (2007) An integrated modelling approach for the management of clam farming in coastal lagoons. *Aquaculture*, 269(1-4):306-320.

McDonald, C.P., Urban, N.R. (2010) Using a model selection criterion to identify appropriate complexity in aquatic biogeochemical models. *Ecological Modelling*, 221(3):428-432.

McKindsey, C.W., Lecuona, M., Huot, M., Weise, A.M. (2009) Biodeposit production and benthic loading by farmed mussels and associated tunicate epifauna in Prince Edward Island. *Aquaculture*, 295(1-2):44-51.

McKindsey, C.W., Thetmeyer, H., Landry, T., Silvert, W. (2006) Review of recent carrying capacity models for bivalve culture and recommendations for research and management. *Aquaculture*, 261(2):451-462.

Miller, T.J. (2007) Contribution of individual-based coupled physical-biological models to understanding recruitment in marine fish populations. *Marine Ecology-Progress Series*, 347:127-138.

Miyajima, T., Tanaka, Y., Koike, I., Yamano, H., Kayanne, H. (2007) Evaluation of spatial correlation between nutrient exchange rates and benthic biota in a reef-flat ecosystem by GIS-assisted flow-tracking. *Journal of Oceanography*, 63(4):643-659.

Mobley, C.D. (1994) Light and water: radiative transfer in natural waters. Academic Press, 592 pp.

Moloney, C.L., St John, M.A., Denman, K.L., Karl, D.M., Koster, F.W., Sundby, S., Wilson, R.P. (2011) Weaving marine food webs from end to end under global change. *Journal of Marine Systems*, 84(3-4):106-116.

Myung, I.J. (2000) The Importance of Complexity in Model Selection. *Journal of Mathematical Psychology*, 44(1):190-204.

Nakamura, Y., Kerciku, F. (2000) Effects of filter-feeding bivalves on the distribution of water quality and nutrient cycling in a eutrophic coastal lagoon. *Journal of Marine Systems*, 26(2):209-221.

Navarrete-Mier, F., Sanz-Lazaro, C., Marin, A. (2010) Does bivalve mollusc polyculture reduce marine fin fish farming environmental impact? *Aquaculture*, 306(1-4):101-107.

Nelson, K.A., Leonard, L.A., Posey, M.H., Alphin, T.D., Mallin, M.A. (2004) Using transplanted oyster (*Crassostrea virginica*) beds to improve water quality in small tidal creeks: a pilot study. *Journal of Experimental Marine Biology and Ecology*, 298(2):347-368.

Neuheimer, A.B., Gentleman, W.C., Pepin, P., Head, E.J.H. (2010) How to build and use individual-based models (IBMs) as hypothesis testing tools. *Journal of Marine Systems*, 81(1-2):122-133.

Neutel, A.M., Heesterbeek, J.A.P., van de Koppel, J., Hoenderboom, G., Vos, A., Kaldeway, C., Berendse, F., de Ruiter, P.C. (2007) Reconciling complexity with stability in naturally assembling food webs. *Nature*, 449(7162):599-602.

Newell, R.I.E. (1988) Ecological changes in Chesapeake Bay: are they the result of overharvesting the eastern oyster, *Crassostrea virginica*? In: Lynch, M.P., Krome, E.C. (eds) Understanding the estuary: advances in Chesapeake Bay research, proceedings of a conference 29-31 March 1988. Chesapeake Research Consortium Publication 129 (available at www.vims.edu/GreyLit/crc129.pdf). Baltimore, Maryland. p. 536–546.

Newell, R.I.E., Fisher, T.R., Holyoke, R.R., Cornwell, J.C. (2004) Influence of eastern oysters on nitrogen and phosphorus regeneration in Chesapeake Bay, USA. In: Dame, R., Olenin, S. (eds) The comparative roles of suspension-feeders in ecosystems, NATO Science Series: IV - Earth and Environmental Sciences. Kluwer Academic Publishers. Dordrecht, The Netherlands. p. 93-120.

Nguyen, N., Drogoul, A., Auger, P. (2008) Methodological steps and issues when deriving individual based-models from equation-based models: a case study in population dynamics. In: Bui, T.D., Ho, T.V., Ha, Q.T. (eds) Intelligent agents and multi-agent systems, proceedings, Lecture notes in artificial intelligence. Hanoi, Vietnam. p. 295-306.

Nielsen, S.L., Sand-Jensen, K. (1990) Allometric scaling of maximal photosynthetic growth-rate to surface volume ratio. *Limnology and Oceanography*, 35(1):177-181.

Nobre, A.M., Ferreira, J.G., Nunes, J.P., Yan, X.J., Bricker, S., Corner, R., Groom, S., Gu, H.F., Hawkins, A.J.S., Hutson, R., Lan, D.Z., Silva, J., Pascoe, P., Telfer, T., Zhang, X.L., Zhu, M.Y. (2010) Assessment of coastal management options by means of multilayered ecosystem models. *Estuarine Coastal and Shelf Science*, 87(1):43-62.

North, E.W., King, D.M., Xu, J., Hood, R.R., Newell, R.I.E., Paynter, K., Kellogg, M.L., Liddel, M.K., Boesch, D.F. (2010) Linking optimization and ecological models in a decision support tool for oyster restoration and management. *Ecological Applications*, 20(3):851-866.

North, E.W., Schlag, Z., Hood, R.R., Li, M., Zhong, L., Gross, T., Kennedy, V.S. (2008) Vertical swimming behavior influences the dispersal of simulated oyster larvae in a coupled particle-tracking and hydrodynamic model of Chesapeake Bay. *Marine Ecology-Progress Series*, 359:99-115.

Nunes, J.P., Ferreira, J.G., Gazeau, F., Lencart-Silva, J., Zhang, X.L., Zhu, M.Y., Fang, J.G. (2003) A model for sustainable management of shellfish polyculture in coastal bays. *Aquaculture*, 219(1-4):257-277.

Ogilvie, S.C., Ross, A.H., Schiel, D.R. (2000) Phytoplankton biomass associated with mussel farms in Beatrix Bay, New Zealand. *Aquaculture*, 181(1-2):71-80.

Peckol, P., Harlin, M.M., Krumscheid, P. (1988) Physiological and population ecology of intertidal and subtidal *Ascophyllum nodosum* (Phaeophyta). *Journal of Phycology*, 24(2):192-198.

Pedersen, M.F., Borum, J. (1997) Nutrient control of estuarine macroalgae: growth strategy and the balance between nitrogen requirements and uptake. *Marine Ecology-Progress Series*, 161:155-163.

Pegau, W.S., Zaneveld, J.R.V. (2000) Field measurements of in-ice radiance. *Cold Regions Science and Technology*, 31(1):33-46.

Pietros, J.M., Rice, M.A. (2003) The impacts of aquacultured oysters, *Crassostrea virginica* (Gmelin, 1791) on water column nitrogen and sedimentation: results of a mesocosm study. *Aquaculture*, 220(1-4):407-422.

Pikitch, E.K., Santora, C., Babcock, E.A., Bakun, A., Bonfil, R., Conover, D.O., Dayton, P., Doukakis, P., Fluharty, D., Heneman, B., Houde, E.D., Link, J., Livingston, P.A., Mangel, M., McAllister, M.K., Pope, J., Sainsbury, K.J. (2004) Ecosystem-based fishery management. *Science*, 305(5682):346-347.

Pilditch, C.A., Grant, J., Bryan, K.R. (2001) Seston supply to sea scallops (*Placopecten magellanicus*) in suspended culture. *Canadian Journal of Fisheries and Aquatic Sciences*, 58(2):241-253.

Platt, T. (1971) Annual production by phytoplankton in St. Margaret's Bay, Nova Scotia. *Journal Du Conseil International pour l'exploration de la Mer*, 33(3):324-333.

Platt, T., Prakash, A., Irwin, B. (1972) Phytoplankton, nutrients and flushing of inlets on the coast of Nova Scotia. *Le Naturaliste Canadien*, 99(4):253-261.

Politikos, D.V., Triantafyllou, G., Petihakis, G., Tsiaras, K., Somarakis, S., Ito, S.I., Megrey, B.A. (2011) Application of a bioenergetics growth model for European anchovy (*Engraulis encrasicolus*) linked with a lower trophic level ecosystem model. *Hydrobiologia*, 670(1):141-163.

Pouvreau, S., Bacher, C., Héral, M. (2000) Ecophysiological model of growth and reproduction of the black pearl oyster, *Pinctada margaritifera*: potential applications for pearl farming in French Polynesia. *Aquaculture*, 186(1-2):117-144.

Powell, E.N., Hofmann, E.E., Klinck, J.M., Ray, S.M. (1992) Modeling oyster populations. I: A commentary on filtration rate. Is faster always better? *Journal of Shellfish Research*, 11:387-398.

Powell, T.M., Lewis, C.V.W., Curchitser, E.N., Haidvogel, D.B., Hermann, A.J., Dobbins, E.L. (2006) Results from a three-dimensional, nested biological-physical model of the California Current System and comparisons with statistics from satellite imagery. *Journal of Geophysical Research-Oceans*, 111(C7):C07018.

Prins, T.C., Smaal, A.C. (1994) The role of the blue mussel *Mytilus edulis* in the cycling of nutrients in the Oosterschelde estuary (The Netherlands). *Hydrobiologia*, 282(1):413-429.

Prins, T.C., Smaal, A.C., Dankers, N., Pouwer, A.J. (1996) Filtration and resuspension of particulate matter and phytoplankton on an intertidal mussel bed in the Oosterschelde estuary (SW Netherlands). *Marine Ecology-Progress Series*, 142:121-134.

Rasmussen, L.L., Cornuelle, B.D., Levin, L.A., Largier, J.L., Di Lorenzo, E. (2009) Effects of small-scale features and local wind forcing on tracer dispersion and estimates of population connectivity in a regional scale circulation model. *Journal of Geophysical Research-Oceans*, 114:C01012.

Reid, G.K., Liutkus, M., Bennett, A., Robinson, S.M.C., MacDonald, B., Page, F. (2010) Absorption efficiency of blue mussels (*Mytilus edulis* and *M. trossulus*) feeding on Atlantic salmon (*Salmo salar*) feed and fecal particulates: implications for integrated multi-trophic aquaculture. *Aquaculture*, 299(1-4):165-169.

Rice, M.A. (2001) Environmental impacts of shellfish aquaculture: filter feeding to control eutrophication. In: Tlusty, M., Bengtson, D., Halvorson, H.O., Oktay, S., Pearce, J., Rheault, R.B. (eds) Marine aquaculture and the environment: a meeting for stakeholders in the Northeast. Cape Cod Printing, Inc. Boston, USA. p. 77-86.

Riisgard, H.U. (2001) On measurement of filtration rates in bivalves-the stony road to reliable data: review and interpretation. *Marine Ecology-Progress Series*, 211:275-291.

Riley, G.A. (1946) Factors controlling phytoplankton populations on Georges Bank. *Journal of Marine Research*, 6(1):54-73.

Rodehutscord, M., Pfeffer, E. (1999) Maintenance requirement for digestible energy and efficiency of utilisation of digestible energy for retention in rainbow trout, *Oncorhynchus mykiss*. *Aquaculture*, 179(1-4):95-107.

Romero, J., Lee, K.S., Pérez, M., Mateo, M.A., Alcoverro, T. (2006) Nutrient dynamics in seagrass ecosystems. In: Larkum, A.W.D., Orth, R.J., Duarte, C.M. (eds) Seagrasses: Biology, Ecology and Conservation. Springer. Dordrecht, The Netherlands. p. 227-254.

Rooney, N., McCann, K., Gellner, G., Moore, J.C. (2006) Structural asymmetry and the stability of diverse food webs. *Nature*, 442(7100):265-269.

Rosenberg, R., Loo, L.O. (1983) Energy-flow in a *Mytilus edulis* culture in western Sweden. *Aquaculture*, 35(2):151-161.

Rosland, R., Bacher, C., Strand, Å., Aure, J., Strohmeier, T. (2011) Modelling growth variability in longline mussel farms as a function of stocking density and farm design. *Journal of Sea Research*, 66(4):318-330.

Rosland, R., Strand, Ø., Alunno-Bruscia, M., Bacher, C., Strohmeier, T. (2009) Applying Dynamic Energy Budget (DEB) theory to simulate growth and bio-energetics of blue mussels under low seston conditions. *Journal of Sea Research*, 62(2-3):49-61.

Sanderson, J.C., Cromey, C.J., Dring, M.J., Kelly, M.S. (2008) Distribution of nutrients for seaweed cultivation around salmon cages at farm sites in north-west Scotland. *Aquaculture*, 278(1-4):60-68.

Sarà, G., Mazzola, A. (2004) The carrying capacity for Mediterranean bivalve suspension feeders: evidence from analysis of food availability and hydrodynamics and their integration into a local model. *Ecological Modelling*, 179(3):281-296.

Sarmiento, J.L., Slater, R.D., Fasham, M.J.R., Ducklow, H.W., Toggweiler, J.R., Evans, G.T. (1993) A seasonal 3-dimensional ecosystem model for nitrogen cycling in the North-Altlantic euphotic zone. *Global Biogeochemical Cycles*, 7(2):417-450.

Saunders, M.I., Metaxas, A., Filgueira, R. (2010) Implications of warming temperatures for population outbreaks of a nonindigenous species (*Membranipora membranacea*, Bryozoa) in rocky subtidal ecosystems. *Limnology and Oceanography*, 55(4):1627-1642.

Scheffer, M., Baveco, J.M., Deangelis, D.L., Rose, K.A., Vannes, E.H. (1995) Super-individuals a simple solution for modelling large populations on an individual basis. *Ecological Modelling*, 80(2-3):161-170.

Schmidt, A.L., Coll, M., Romanuk, T.N., Lotze, H.K. (2011) Ecosystem structure and services in eelgrass *Zostera marina* and rockweed *Ascophyllum nodosum* habitats. *Marine Ecology-Progress Series*, 437:51-68.

Schmidt, A.L., Scheibling, R.E. (2007) Effects of native and invasive macroalgal canopies on composition and abundance of mobile benthic macrofauna and turf-forming algae. *Journal of Experimental Marine Biology and Ecology*, 341(1):110-130.

Schulte, E.H. (1975) Influence of algal concentration and temperature on the filtration rate of *Mytilus edulis*. *Marine Biology*, 30(4):331-341.

Seiwell, H.R. (1938) Use of non-conservative properties of sea water to physical oceanographical problems. *Nature*, 142:164-165.

Sénéchal, J., Grant, J., Archambault, M.C. (2008) Experimental manipulation of suspended culture socks: growth and behavior of juvenile mussels (*Mytilus* spp.). *Journal of Shellfish Research*, 27(4):811-826.

Shank, G.C., Zepp, R.G., Whitehead, R.F., Moran, M.A. (2005) Variations in the spectral properties of freshwater and estuarine CDOM caused by partitioning onto river and estuarine sediments. *Estuarine, Coastal and Shelf Science*, 65(1-2):289-301.

Shchepetkin, A.F., McWilliams, J.C. (2005) The regional oceanic modeling system (ROMS): a split-explicit, free-surface, topography-following-coordinate oceanic model. *Ocean Modelling*, 9(4):347-404.

Sheng, J., Zhao, J., Zhai, L. (2009) Examination of circulation, dispersion, and connectivity in Lunenburg Bay of Nova Scotia using a nested-grid circulation model. *Journal of Marine Systems*, 77(3):350-365.

Shin, Y.J., Cury, P. (2004) Using an individual-based model of fish assemblages to study the response of size spectra to changes in fishing. *Canadian Journal of Fisheries and Aquatic Sciences*, 61(3):414-431.

Shin, Y.J., Travers, M., Maury, O. (2010) Coupling low and high trophic levels models: Towards a pathways-orientated approach for end-to-end models. *Progress in Oceanography*, 84(1-2):105-112.

Short, F.T., Burdick, D.M., Kaldy Iii, J.E. (1995) Mesocosm experiments quantify the effects of eutrophication on eelgrass, *Zostera marina*. *Limnology and Oceanography*, 40(4):740-749.

Smaal, A.C., Haas, H.A. (1997) Seston dynamics and food availability on mussel and cockle Beds. *Estuarine, Coastal and Shelf Science*, 45(2):247-259.

Smaal, A.C., Vonck, A. (1997) Seasonal variation in C, N and P budgets and tissue composition of the mussel *Mytilus edulis*. *Marine Ecology-Progress Series*, 153:167-179.

Smaal, A.C., Zurburg, W. (1997) The uptake and release of suspended and dissolved material by oysters and mussels in Marennes-Oleron Bay. *Aquatic Living Resources*, 10(01):23-30.

Smith, D.W., Horne, A.J. (1988) Experimental measurement of resource competition between planktonic microalgae and macroalgae (seaweeds) in mesocosms simulating the San Francisco Bay-Estuary, California. *Hydrobiologia*, 159(3):259-268.

Smith, G. (2009) P E I Mussel Monitoring Program. 2009 Report. Technical Report # 243. Prince Edward Island Department of Fisheries and Aquaculture and Rural Development. 91 pp. http://www.gov.pe.ca/photos/original/MMR_2009.pdf

Soetaert, K., Middelburg, J.J., Herman, P.M.J., Buis, K. (2000) On the coupling of benthic and pelagic biogeochemical models. *Earth-Science Reviews*, 51(1-4):173-201.

Soto, D., Aguilar-Manjarrez, J., Hishamunda, N. (eds) (2008) Building an ecosystem approach to aquaculture. FAO/Universitat de les Illes Balears Expert Workshop. 7–11 May 2007, Palma de Mallorca, Spain., Vol 14. FAO Fisheries and Aquaculture Proceedings, Rome. 221 pp.

Spillman, C.M., Hamilton, D.P., Hipsey, M.R., Imberger, J. (2008) A spatially resolved model of seasonal variations in phytoplankton and clam (*Tapes philippinarum*) biomass in Barbamarco Lagoon, Italy. *Estuarine, Coastal and Shelf Science*, 79(2):187-203.

Steele, J.H., Ruzicka, J.J. (2011) Constructing end-to-end models using ECOPATH data. *Journal of Marine Systems*, 87:227-238.

Strain, P.M. (2002) Nutrient Dynamics in Ship Harbour, Nova Scotia. *Atmosphere-Ocean*, 40(1):45-58.

Strickland, J.D.H., Parsons, T.R. (1968) A practical handbook of seawater analysis, Bulletin 167. Fisheries Research Board of Canada, 311 pp.

Strohmeier, T., Duinker, A., Strand, Ø., Aure, J. (2008) Temporal and spatial variation in food availability and meat ratio in a longline mussel farm (*Mytilus edulis*). *Aquaculture*, 276(1-4):83-90.

Thompson, K.R., Kelley, D.E., Sturley, D., Topliss, B., Leal, R. (1998) Nearshore circulation and synthetic aperture radar: an exploratory study. *International Journal of Remote Sensing*, 19(6):1161-1178.

Thompson, R.J. (1984) The reproductive cycle and physiological ecology of the mussel *Mytilus edulis* in a subarctic, non-estuarine environment. *Marine Biology*, 79(3):277-288.

Thompson, W.A., Vertinsk.I, Krebs, J.R. (1974) Survival value of flocking in birds - simulation model. *Journal of Animal Ecology*, 43(3):785-820.

Thursby, G.B., Harlin, M.M. (1984) Interaction of leaves and roots of *Ruppia maritima* in the uptake of phosphate, ammonia and nitrate. *Marine Biology*, 83(1):61-67.

Trancoso, A.R., Saraiva, S., Fernandes, L., Pina, P., Leitao, P., Neves, R. (2005) Modelling macroalgae using a 3D hydrodynamic-ecological model in a shallow, temperate estuary. *Ecological Modelling*, 187(2-3):232-246.

Travers, M., Shin, Y.J., Jennings, S., Cury, P. (2007) Towards end-to-end models for investigating the effects of climate and fishing in marine ecosystems. *Progress in Oceanography*, 75(4):751-770.

Travers, M., Shin, Y.J., Jennings, S., Machu, E., Huggett, J.A., Field, J.G., Cury, P.M. (2009) Two-way coupling versus one-way forcing of plankton and fish models to predict ecosystem changes in the Benguela. *Ecological Modelling*, 220(21):3089-3099.

Troell, M., Chopin, T., Reid, G., Robinson, S., Sara, G. (2011) Letter to the editor. *Aquaculture*, 313(1-4):171-172.

Troost, T.A., Wijsman, J.W.M., Saraiva, S., Freitas, V. (2010) Modelling shellfish growth with dynamic energy budget models: an application for cockles and mussels in the Oosterschelde (southwest Netherlands). *Philosophical Transactions of the Royal Society B-Biological Sciences*, 365(1557):3567-3577.

USDA (2008) Composition of foods raw, processed, prepared. USDA National Nutrient Database for Standard Reference, Release 21. Beltsville, Maryland. 39 pp. http://www.nal.usda.gov/fnic/foodcomp/Data/SR21/sr21_doc.pdf

Van der Veer, H.W., Cardoso, J.F.M.F., Van der Meer, J. (2006) The estimation of DEB parameters for various Northeast Atlantic bivalve species. *Journal of Sea Research*, 56(2):107-124.

Waite, L., Grant, J., Davidson, J. (2005) Bay-scale spatial growth variation of mussels *Mytilus edulis* in suspended culture, Prince Edward Island, Canada. *Marine Ecology-Progress Series*, 297:157-167.

Wall, C.C., Peterson, B.J., Gobler, C.J. (2008) Facilitation of seagrass *Zostera marina* productivity by suspension-feeding bivalves. *Marine Ecology-Progress Series*, 357:165-174.

Wallentinus, I. (1984) Comparisons of nutrient uptake rates for Baltic macroalgae with different thallus morphologies. *Marine Biology*, 80(2):215-225.

Wang, S.Y., McGrath, R., Hanafin, J., Lynch, P., Semmler, T., Nolan, P. (2008) The impact of climate change on storm surges over Irish waters. *Ocean Modelling*, 25(1-2):83-94.

Wang, W.X., Widdows, J. (1993) Metabolic responses of the common mussel *Mytilus edulis* to hypoxia and anoxia. *Marine Ecology-Progress Series*, 95:205-205.

Wanninkhof, R. (1992) Relationship between wind speed and gas exchange. *Journal of Geophysical Research*, 97(25):7373–7382.

Warner, J.C., Sherwood, C.R., Signell, R.P., Harris, C.K., Arango, H.G. (2008) Development of a three-dimensional, regional, coupled wave, current, and sediment-transport model. *Computers and Geosciences*, 34(10):1284-1306.

Welschmeyer, N.A. (1994) Fluorometric analysis of chlorophyll *a* in the presence of chlorophyll *b* and pheopigments. *Limnology and Oceanography*, 39(8):1985-1992.

Werner, F.E., Quinlan, J.A., Lough, R.G., Lynch, D.R. (2001) Spatially-explicit individual based modeling of marine populations: a review of the advances in the 1990s. *Sarsia*, 86(6):411-421.

Widdows, J., Johnson, D. (1988) Physiological energetics of *Mytilus edulis*: scope for growth. *Marine Ecology-Progress Series*, 46(1):113-121.

Winneberger, J.H., Austin, J.H., Klett, C.A. (1963) Membrane filter weight determinations. *Journal (Water Pollution Control Federation)*, 35(6):807-813.

Woods, J.D., Onken, R. (1982) Diurnal variation and primary production in the ocean - preliminary results of a Lagrangian ensemble model. *Journal of Plankton Research*, 4(3):735-756.

Worm, B., Lotze, H.K., Hillebrand, H., Sommer, U. (2002) Consumer versus resource control of species diversity and ecosystem functioning. *Nature*, 417:848-851.

Yahel, G., Post, A.F., Fabricius, K., Marie, D., Vaulot, D., Genin, A. (1998) Phytoplankton distribution and grazing near coral reefs. *Limnology and Oceanography*, 43(4):551-563.

Zimmerman, R.C., Smith, R.D., Alberte, R.S. (1987) Is growth of eelgrass nitrogen limited? A numerical simulation of the effects of light and nitrogen on the growth dynamics of *Zostera marina*. *Marine Ecology-Progress Series*, 41(2):167-176.